Chapter 4: Result and Discussions

This chapter deals with the results and discussion section. Accordingly, it is categorized into two units. First unit deals with the result and discussion of the experimental investigations, and then second unit describes the results and discussion part pertaining to the model formulation and numerical simulation analysis.

In the experimental investigations, the effect of gasifier-engine operating parameters is quite significant on the performance and emission of the engine. In this section, the impact of gasification equivalence ratio, engine compression ratio, engine load, biomass blend percentage on the dual fuel mode engine performance and exhaust emissions (NOx, CO_2, HC, and CO) are investigated. Additionally, this chapter also investigates the economic feasibility of the SBP-briquette plant and subsequently uses this briquette to produce producer gas in a downdraft gasifier, which is then used in a VCR dual fuel engine to investigate its combustion, performance, and exhaust characteristics. In this context, a brief overview of gasifier-engine coupled experimental results has been revealed in the following sections. Moreover, the simulation results of SI-engine fuelled with producer gas and propane blend are also discussed.

The first five subsections of the first unit deals with the results obtained from the experimental investigations. First subsection focuses on comparative performance and optimisation analysis of biomass gasification of Briquette, Mahua wood, and Coconut shell with CI-engine integrations.

Second subsection in the experimental section analyses the importance of co-gasification. This section is further categorised into two sub-parts. First sub-part describes the results of biomass (Mahua wood + Sawdust briquette) co-gasification, and second sub-part focuses on

experimental work on the downdraft gasifier using different blend percentages of (coal-mahua biomass) under variable operating condition integrated with dual fuel IC engine.

Third subsection shifts the experimental work of co-gasification to waste triple feed-material (coal + briquette + mahua wood) blends using downdraft gasifier integrated with dual fuel diesel engine: An RSM-based comparative parametric optimization.

Fourth subsection concludes the comparative performance and optimization analysis of coal gasification, biomass gasification, and co-gasification of equi-blends of feed materials using neat diesel and dual fuel CI engine.

Fifth subsection of the experimental work employs economic viability of the small-scale briquette manufacturing plant in order to promote waste-to-fuel conversion through sugarcane bagasse pith briquette, and subsequently its application in heating and power generation in gasification-engine system. This unit also discusses economic viability of gasification-engine system.

Finally, the Second unit of the results and discussion part deals with the comprehensive quasi-dimensional thermodynamic numerical modelling and simulation analysis of the SI engine fuelled with peach biomass-based producer gas and propane blend.

(A) Experimental analysis

This section deals with the experimental investigations of economic feasibility of biomass and waste-to-fuel conversion through gasification technology integrated with internal combustion engine.

4.1 Comparative performance and Optimization analysis of biomass gasification-CI engine.

4.1.1 *Introduction*

Restoring a healthy environment and meeting the nation's expanding energy demand requires an uninterrupted renewable energy supply with efficient technology. One of the most effective technologies for producing gaseous fuel and subsequent electricity is the gasification of waste biomass. But the seasonal interruption of biomass waste availability creates a discontinuity in power production in the Gasifier-Engine-Genset system. Also, the different types and quantities of biomass in rural areas vary from location to location, producing different producer gas (PG) qualities. Thus, there is a need to identify its potential. Therefore, this study aims to analyze how the PG production from the gasification of Mahua wood, Sawdust briquette, and Coconut-shell affects dual-fuelled mode engine performance. To do this, Gasifier-engine experiment was conducted with operating parameters of engine brake power (BP) and compression ratio (CR) at a favorable gasification equivalence ratio (GER). Response Surface Methodology (RSM) was applied to predict optimal operating parameters for maximum engine performance and minimum emissions. RSM resulted in the optimum setting of 16.04-16.34 CR and 2.78-3.20 kW BP for maximum efficiency and diesel saving (DS). The briquette-PG-based DF engine offers maximum Brake thermal efficiency (BTE) of 25%. However, 24% BTE of coconut shell based-PG DF engine offers 57.83% maximum DS. And, respective optimum output responses were found to be 0.3223kg/kWh Brake specific diesel consumption (BSDC), 0.0636 % vol. CO, 16.73 ppm HC, 1.51%vol. CO_2, and 8.19 ppm NOx. In summary, these biomass gasifications with engine integration have the potential to replace diesel with the lowest possible exhaust emissions.

In order to utilize biomass waste easy to handle, the thermochemical process is an efficient technology for converting gaseous, liquid, and charcoal fuel components. Pyrolysis of biomass can be a source of liquid fuels [160]. However, among pyrolysis and gasification thermochemical processes, gasification has better biomass conversion efficiency [161]. The gasification process occurs when PG is produced in the gasifier. In this process, the biomass is converted through various thermochemical reaction stages, such as drying (<200 °C), thermal decomposition or pyrolysis (200−500°C), reduction (650−900°C), and partial oxidation/combustion (800−1200 °C) [12]. The details of the gasification process are shown in Figure 4.1.1.

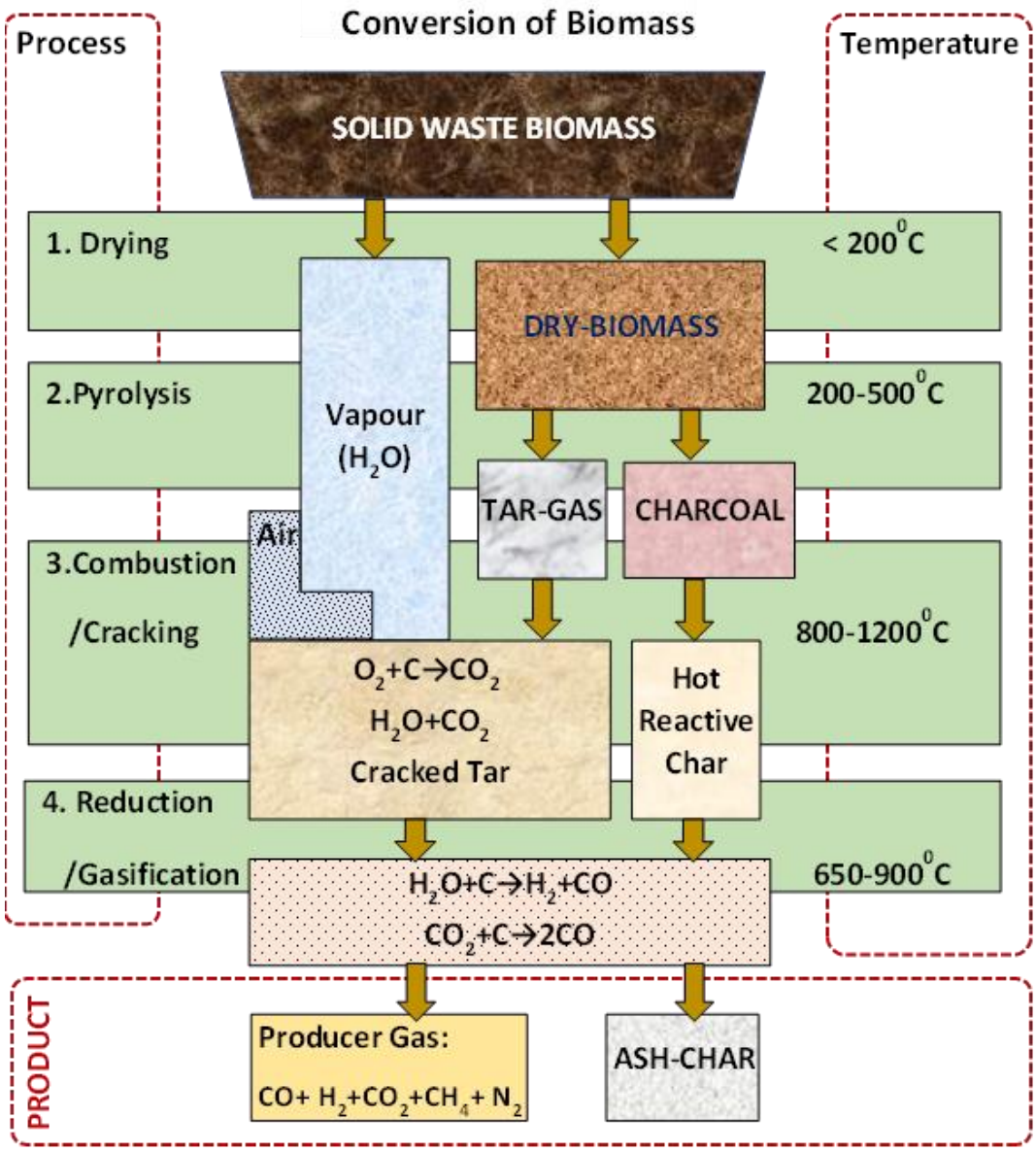

Figure 4.1.1. Schematic diagram of an air-downdraft fixed bed gasification system

Under the above context, the present study chose waste biomass gasifier feed material such as mahua tree (Madhuca Indica), coconut shell, and sawdust briquette. So far as feed material availability for gasification is concerned, the availability of mahua tree waste collection is associated with the forest (seasonal as branch falls in summer) directly and wood industries. In India, the total area of mahua tree cultivation was approximately 62500 hectares in 2013 [162], [163]. Whereas sawdust is generated from wood processing industries, the collection of sawdust briquettes could be sufficiently obtained from briquette manufacturer industries. India

produces around 18.91 million tonnes of sawdust annually; after utilization, there are 5.5 million tonnes of surplus sawdust [164].

Similarly, the Coconut fruit can be found throughout the year, primarily harvested in summer; however, its cultivation belongs to the coastal area. Once the coconut peeled out, after extraction of water and endosperm/ copra, the coconut shell is being discarded as waste material [17]. The largest production of coconut shells belongs to Indonesia. However, India produced around 10.5 million tonnes of coconut shells in 2012 [165]. Thus, alternatively utilizing these gasifier feed materials (Mahua wood waste, sawdust briquette, and coconut shell), the gasification process can be sustained throughout the year with the IC engine coupled for electricity generation. Further, an investigation is entailed to certain difficulties in DDG, as it varies with the nature of feedstocks, like gasifier temperature elevation, variation in product concentration, overall gasification efficiency, and subsequent engine efficiency [28]. Consequentially, it won't be easy to control the gasification process for individual feed material in an auto-thermal DDG. Thus, there is a need for a gasifier with fuel-flexible accessibility.

Within this context and respective research gap, the novelty of the present work is associated with the conduction of experimental investigations on downdraft gasifier with diesel engine integration in order to compare overall performance to evaluate the feasibility of gasification and power generation with various feedstock types in a single automated self-controlling device. In reviewing the previous work in the literature, there are numerous studies reported using producer gas in DF mode engines with or without the application of optimization implementation. However, it was observed that cumulative and comparative performance is absent among different feedstock gasification with increasing the performance and minimizing the emissions of a DF engine run with diesel and PG blended fuel. The details of recent progress PG based on the previous optimization applied work to the present work are mentioned in Table 4.1.1. In the Table, except for two who compared the multiple feedstocks, most of the work is

with single feedstock. Hence, it must be a study of cumulative comparison among various feed materials at the same operating conditions. However, there have successfully applied the RSM optimization tool. Moreover, in review, no work has been found that has studied the cumulative investigation over Mahua-Sawdust briquette-coconut shell-based PG generation and utilization in DF mode diesel engines. The RSM optimizer tool has an average of 95% desirability as a significant value to confirm the reliability of the model value with the experiment [166].

Hence to bridge this gap, in the present investigation, RSM based Design expert software has been applied to optimize the operating parameters of the air downdraft Gasifier-CI engine performance with Mahua-Briquette-Coconut shell-based PG for finding the best response of performance and emission limits. The investigation deals with two operating parameters: CI engine BP and compression ratio at favorable GER. RSM has been used for optimum values to maximize the engine BTE, diesel saving and minimize the BSDC, engine exhaust of CO, CO_2, HC, and NOx. Finally, the result of the study concludes that all three-gasifier feedstock material has significant potential to generate engine power under optimum operating conditions and can provide a better exploration and valorization of alternate waste biomass to solve the seasonal and unavailability of feeding materials. Thus, no prior research exists on exploring agricultural biomass potential, optimizing DF engine performance and emissions using RSM in the potential region, incorporating this research with good novelty.

Table 4.1.1. Comparison between previous and present work.

Feed material	Experiment on	Optimization tool	Optimization variable	Ref.
Rice husk, Coconut shell, Rubber shell-based PG and Diesel	CI-Engine	RSM	Engine Load and CR	[166]
Coir pith, Rice husk, Rubber wood, Coconut shell and Rubber seed kernel shell PG and diesel	CI-Engine	RSM	Calorific value and load	[82]
Babool wood PG and Biodiesel	CI-Engine	RSM	Engine load, pilot fuel injection timing and pressure	[167]
Biodiesel and PG	CI-Engine	RSM	Load, CR, Injection timing	[168]
Babul wood PG and diesel	CI-Engine	RSM	blending ratios, CR, and Injection timing	[169]
Diesel and cocoa pod husk-PG	CI-Engine	RSM	Brake power and Compression ratio	[170]
Coal PG and Diesel	CI-Engine	RSM	Gasification ER, engine load and CR	[35]
Present Work				
Mahua-Saw dust-Briquette-Coconut shell PG and diesel	CI-Engine	RSM	Gasification ER, Engine CR and Brake power	**Not yet**

4.1.2 Properties and preparations of fuels

Gasification converts biomass to producer gas through drying, pyrolysis, oxidation, and reduction [171, 172]. In the present work, PG was produced from Briquette, Mahua wood, and Coconut shell using a 14kW downdraft biomass gasifier. This PG is used as a secondary fuel in this experimental analysis. A small amount of diesel fuel is always needed in DF mode

because gaseous fuel won't ignite under the prevailing pressure and temperature [173]. The governor mechanism regulates the amount of fuel injected to get the desired power. Figure 4.1.2 shows the properties of the feed materials used in the experiment, and all were based on a dry basis. Table 4.1.2 lists the different physical and chemical properties of diesel, briquette, mahua wood, and coconut shell.

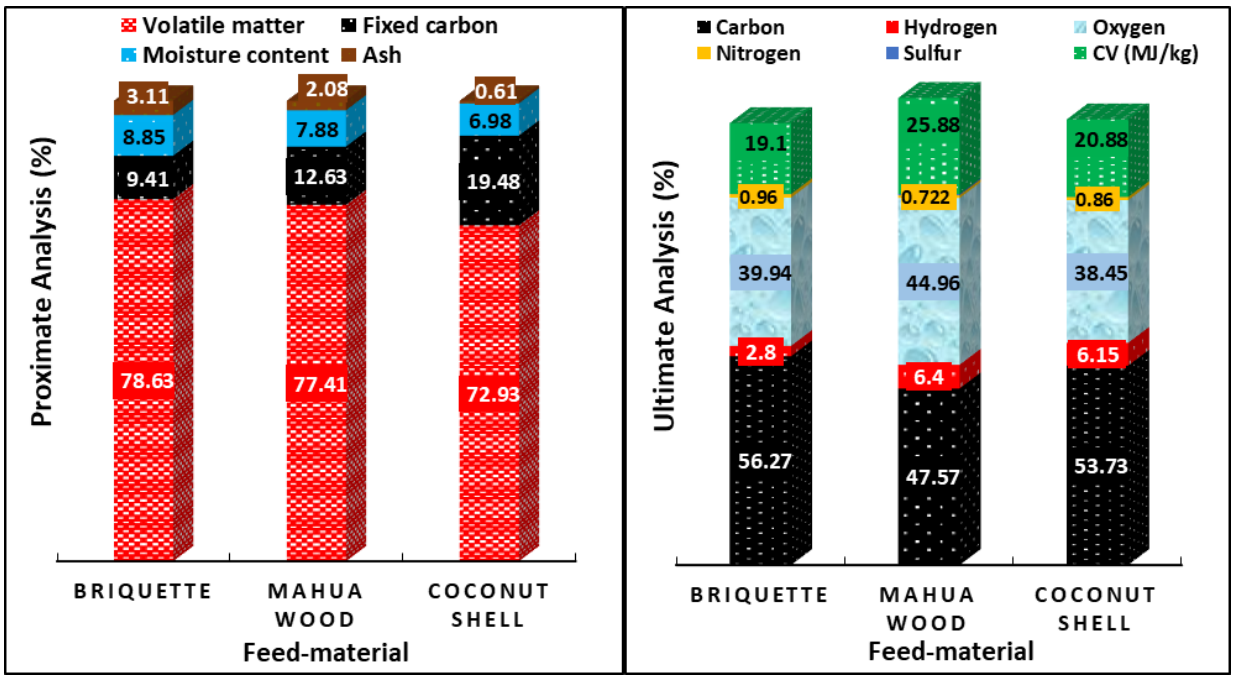

Figure 4.1.2. Properties of feed materials used in experimentation in terms of wt% dry basis.

Table 4.1.2. Physical and chemical properties of tested fuels [174-177]

Test Properties	Diesel fuel	Briquette	Mahua wood	Coconut shell
Lower heating value (MJ/kg)	45.9	19.1	25.88	20.88
Density (kg/m^3)	815	900-1000	468.27±1.8	702.10
Moisture content (wt%)	-	8.85	7.88	6.98
Sulfur content (wt%)	0.22	0.03	0.34	0.02

Test Properties	Diesel fuel	Briquette	Mahua wood	Coconut shell
Ash content (wt%)	0.0055	3.11	2.08	0.61
Carbon hydrogen ratio	6.82	20.09	7.43	8.73
Stoichiometric air-fuel ratio	14.92	4.40	4.43	5.11
Cellulose (wt%)	-	43.6	37.92±0.13	36.13
Hemicellulose (wt%)	-	27.4	27.33±0.13	20.36
Lignin (wt%)	-	29.0	14.20±0.11	32.33

4.1.3 Experimental results using gasifier

The experiments were conducted in a downdraft gasifier-diesel engine coupling, the detailed specification is presented in Tables 3.1.1 and 3.1.2 (material & methodology). In order to obtain enhanced quality of PG, several gasification parameters need to be observed and regulated. These variables may include the amount of fuel consumed, the air fuel ratio, the temperature profile inside the gasifier, the volume of products produced, char and tar release, PG composition and its calorific value, energy loss calculation, the efficiency of the gasification process, etc. During the gasification process, the various feedstocks were consumed as fuel at a rate of 6 kg/h, and air-gasification was held at 0.43 GER. The maximum gasification temperature was around 600^{o}C at the inner surface of the gasifier shell near the oxidation zone. Figure 4.1.3 shows the variation of the average temperature of (T1 and T2) drying, (T3) pyrolysis, (T4) oxidation/combustion, (T5) reduction zone and (T6) grate of the downdraft gasifier with six thermocouple positions installed at different locations along the gasification reaction zones for three different feedstocks.

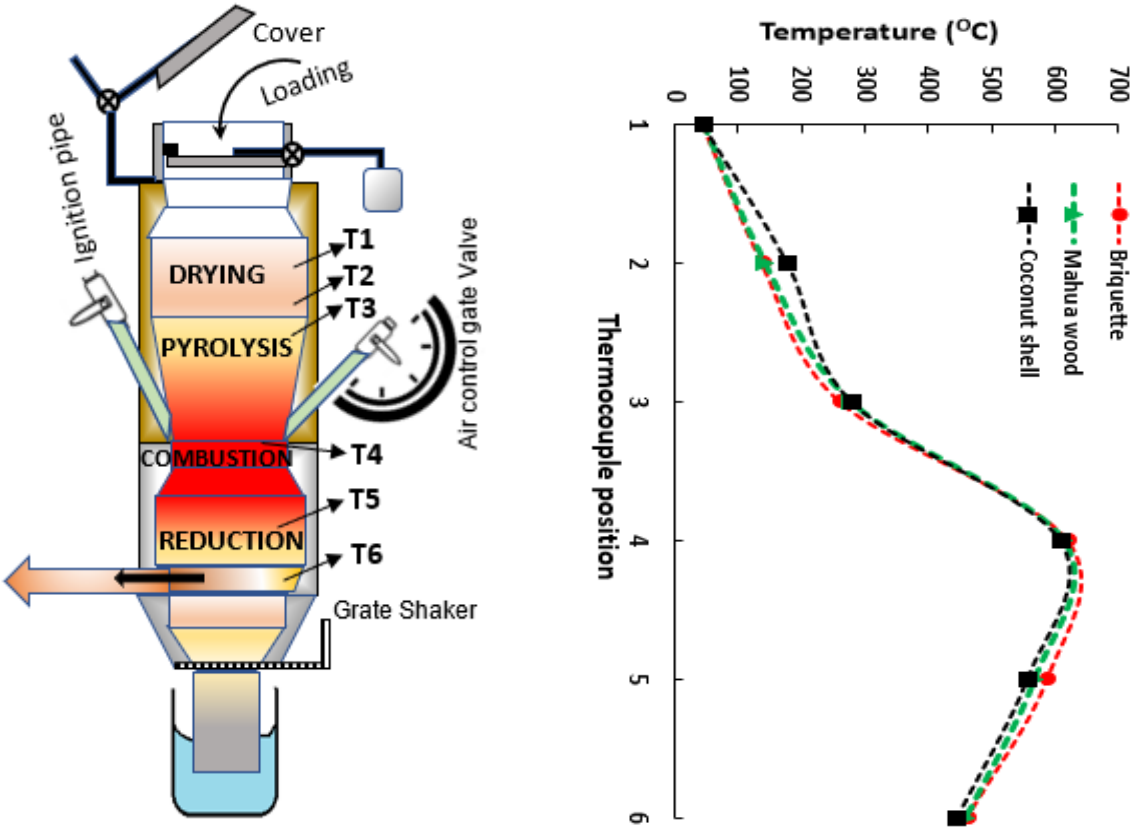

Figure 4.1.3. Temperature profile at the inner surface of gasifier shell for different biomass feedstock.

The energy-mass allocation method was adopted to calculate the energy share percentage during the gasification process, including energy input, output, and losses. The energy inputs typically include the energy content of the feedstock, the heat required for the gasification reactions, and the energy used for process operations such as preheating, drying, and feeding. The energy outputs comprise the energy content of the PG, the sensible heat in the PG, whereas unaccounted energy losses are the balancing of total heat, which includes losses through radiation, conduction, or convection. After gasification, the char quantity was found to be 17.9kg, 18.6kg, and 15.0kg for briquette, mahua wood, and coconut shell, respectively (Table 4.1.3). Also, the gasification characteristics in terms of PG composition, LHV, and gasification efficiency for three biomasses are shown in Table 4.1.3. The gasification efficiency is defined

by the ratio of the total amount of lower heating value of the gas to the lower heating value of the fuel as mentioned in equation 4.1.1.

$$\eta = \frac{\text{LHVof gas (MJ/Nm}^3) \times \text{gasyield (Nm}^3/\text{kg})}{\text{LHVof fuel (MJ/kg)}} \times 100\% \quad (4.1.1)$$

As gasification efficiency highly depends on feedstock quality and gasification operating parameters. In this view, the gasification efficiency for different biomass gasification was found to be 32.02%, 38.42%, and 64.65% for briquette, mahua wood, and coconut shell, respectively.

Table 4.1.3. Experimental results of gas composition and gasification characteristics

Particular	**Briquette**	**Mahua wood**	**Coconut shell**
Producer gas composition			
CO	18.6	22.16	21%
H_2	12.0	17.55	20%
CO_2	14.0	11.89	13%
CH_4	-	3.07	< 3%
N_2	55.4	45.33	50%
PG calorific value (MJ/Nm^3)	2.447	3.978	5.4
Gasification Air-fuel ratio	1.892	1.90	2.19
Gasification efficiency %	32.02	38.42	64.65
After gasification- Residual CV (MJ/kg)	9.27	12.56	6.2
Mass analysis			
Feedstock Input (kg)	40	40	40
Residual left (kg)	17.9	18.6	15.0

4.1.4 Energy balance in the gasifier

The performance of the gasifier may be measured by the quality of the PG in terms of heating value. Gas yield, Lower heating value, Cold gas efficiency (CGE), and energy distribution are the essential criteria for the analysis of gasification performance [172]. Gas yield mainly depends on the producer gas flow rate to the feedstock consumption rate [178]. In the current experiment, the gas yield observed was 2.5 Nm^3/kg of biomass. CGE is the ratio of the heat energy contained in the producer gas to the heat energy contained in the raw biomass [179]. Figure 4.1.4 shows the Sankey diagram for the energy distribution in the downdraft gasifier. The values have been calculated based on the energy-mass allocation method. In the present experiment, the feed material intake was 40 kg. Accordingly, based on the LHV of feed materials (Table-4.1.2), the total energy content of feed materials was calculated as 764MJ, 1035.2MJ, and 835.2MJ for briquette, mahua wood, and coconut shell, respectively, as shown in Figure 4.1.4. According to reports, 20% of the LHV of the fuels is typically utilized for sensible heat contribution during gasification [180]. Consequently, the sensible heat share has been allocated for respective feedstock gasification. Using gas yield-energy allocation and the heating values of various materials (Table-4.1.3), the total PG-energy content was calculated as 244.7 MJ, 397.72 MJ, and 540 MJ for briquette, mahua wood, and coconut shell, respectively. Table 4.1.3 shows the residual mass left after gasification and the respective CV content for residual energy evaluation. Thus, using the residual mass-energy allocation technique, the energy of residual with tar content was determined as 168.03 MJ, 235.74 MJ, and 95.1 MJ for briquette, mahua wood, and coconut shell, respectively. The rest percentages of the energy balance are considered unaccountable energy losses, which include losses from minor gas leakages, circumference of temperature sensors, gasifier lid, and different pipe joints. This value was found to be 3.97 % -25.99 % for respective biomasses.

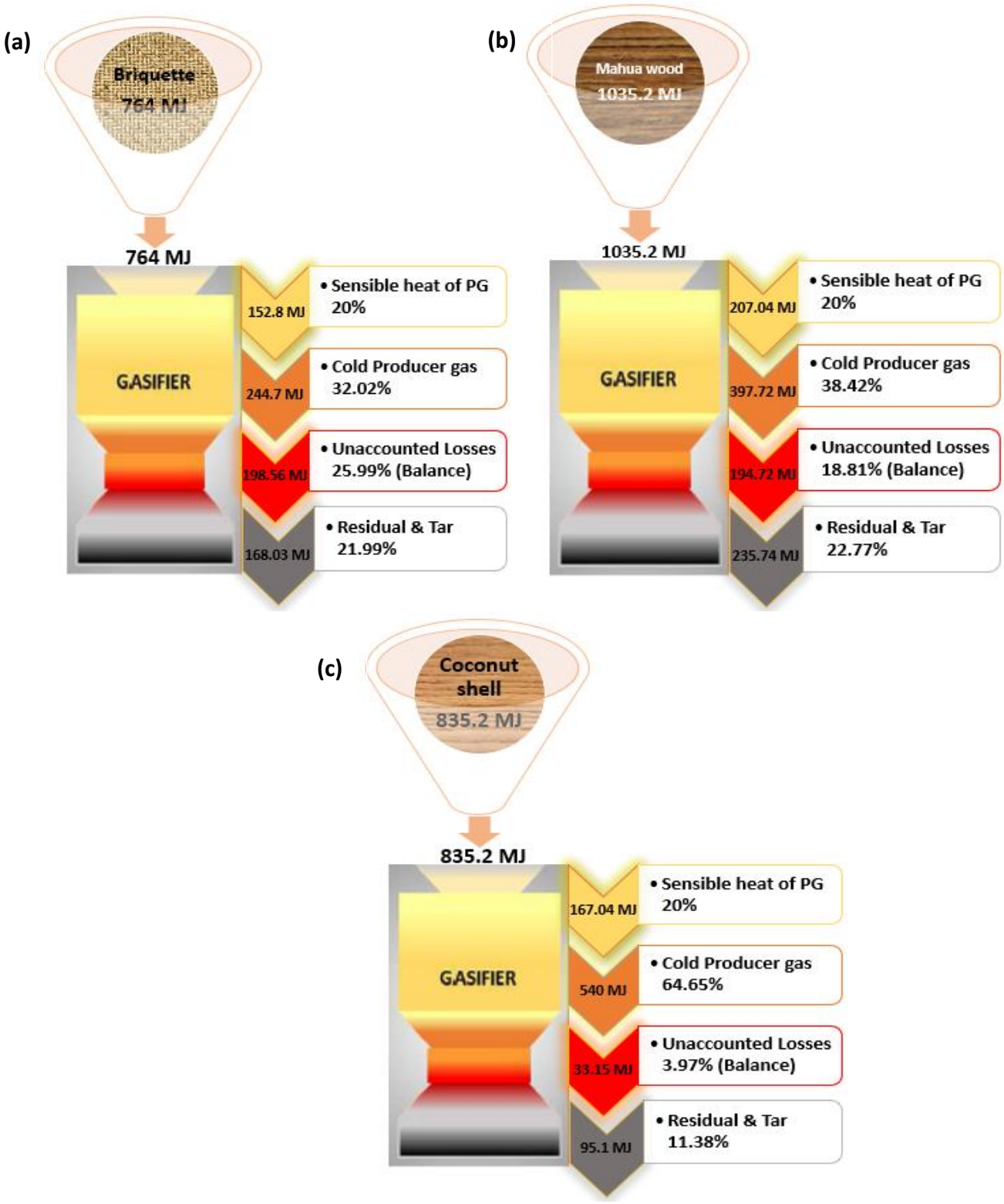

Figure 4.1.4. Sankey diagram representing energy distribution in gasifier using (a) Briquette (b) Mahua wood (c) Coconut shell as a feed-material

4.1.5 Model analysis and Interpretation

The primary model utilized in the investigation is statistically assessed by the ANOVA, which revealed that the quadratic model is best suited for all seven output responses (BSDC, BTE, Diesel saving, CO, HC, CO_2, and NO_x) for every three feed-materials (Briquette, Mahua wood, Coconut shell). Tables 4.1.4 and 4.1.5 show the ANOVA and fit statistics results of performance and emission responses, respectively, for the quadratic model. The Table also includes the F-value and p-value for numerical data that are needed to validate any model [35]. F-values of the model are higher in all cases, indicating the model is significant. All p-values lie < 0.05 indicating the model is significant. The model used to calculate BSDC, BTE, Diesel saving, CO, CO_2, HC, and NOx was evaluated using statistical indices including standard deviation, mean, R^2, Adj-R^2, Pred-R^2, and Adq-R^2. Good models have low standard deviations. Tables 4.1.4 and 4.1.5 also show that the response standard deviation varied from 0.0177 to 31.87, demonstrating that the model is well-fitted for optimization. Mean responses are also tabulated for each feedstock condition. Tables reveal that R^2 is high (0.6713-0.9989), confirming that the generated quadratic model fits the data and illustrates its accuracy. Adj-R^2, which is always $\leq R^2$, shows response variability based on model significance. Adj-R^2 values represent the variance of design parameters used to develop the selected model, whereas Pred-R^2 values indicate the variation of data not utilized in model determination. PG from briquette had Adj-R^2 values of 0.9960, 0.9014, 0.9634, 0.9780, 0.9777, 0.9632, and 0.7921 for BSDC, BTE, Diesel saving, CO, HC, CO_2, and NO_x, whereas PG from mahua wood had values of 0.9980, 0.9076, 0.5983, 0.9733, 0.9444, 0.9720, and 0.8210. Moreover, PG from coconut shell also yielded Adj-R^2 values of 0.9931, 0.9112, 0.9244, 0.9390, 0.9851, 0.9377, and 0.8878 for the responses. For the suitable quadratic model in CCD RSM, the difference between Adj-R^2 and Pred-R^2 must be approximately 0.20 [181]. For model selection, the signal-to-noise ratio, i.e., Adequate precision, should be > 4 [182]. In the present work, all response statistics for the

three feed materials are > 4. Hence, the model selected for this work is appropriate for the investigation being carried out.

The predicted and actual values for the seven responses for the DF engine that was operating with PG from Briquette, Mahua wood, and Coconut shell are depicted in Figure 4.1.1S as attached in the Appendix. It provides convincing assurance that the selected model is suitable for forecasting the performance characteristics of a DF engine utilizing PG from the specified feed materials since it demonstrates that the predicted values are closely related to actual values [158]. Plots make it easy to interpret two-factor interactions. A perturbation plot is used to determine how each input process parameter affects response outputs and which input variable is more significant. If the slope of the plot is steep, it indicates that the parameter under consideration has a greater impact on the response. On the other hand, if the plot is flat, it indicates that the considered parameter has the least impact on the response [183]. The graphs of the perturbation plot for the seven responses for the DF engine that was operating with PG from Briquette, Mahua wood, and Coconut shell are shown in Figure 4.1.2S, as attached in the Appendix. The ANOVA and perturbation plots analysis interpret that CR and BP affect response parameters. From the perturbation plots, Engine brake power significantly affects BSDC and BTE responses from the deviation point. Parameter B (Engine BP) has the steepest slope of emission parameters CO, and HC, making it more responsive. This is because when engine brake power enhances, fuel delivery to the engine increases, which raises the combustion temperature inside the cylinder and increases CO emissions owing to incomplete combustion due to oxygen shortages. The quadratic model predicts response variables using actual equations. The following quadratic equations from 4.1.2 to 4.1.8 were found adequate for predicting seven responses: BSDC, BTE, DS, CO, HC, CO_2, and NO_x for the three specified feedstocks (Briquette, Mahua wood, and Coconut shell).

Table 4.1.4. ANOVA and fit statistics of performance responses

	BTE			BSDC			Diesel saving		
	Briq.	*Mahua*	*CS*	*Briq.*	*Mahua*	*CS*	*Briq.*	*Mahua*	*CS*
Model									
F-value	550.55	1118.33	787.08	21.12	22.61	23.56	58.96	9.19	27.91
P-value	<0.0001	<0.0001	<0.0001	0.0010	0.0008	0.0007	<0.0001	0.0067	0.0004
Std. Deviation	0.6110	0.2826	0.7620	0.4457	0.4741	0.6097	2.32	7.14	2.63
Mean	15.00	9.59	12.63	1.07	1.25	1.45	32.74	35.51	47.71
R^2	0.9978	0.9989	0.9943	0.9462	0.9496	0.9515	0.9801	0.6713	0.9588
Adjusted R^2	0.9960	0.9980	0.9931	0.9014	0.9076	0.9112	0.9634	0.5983	0.9244
Predicted R^2	0.9918	0.9939	0.9902	0.8110	0.8191	0.8124	0.9023	0.5063	0.7674
Adequate Precision	57.7099	84.7190	63.2674	12.4066	11.5889	11.9294	25.4223	7.7143	16.1506

Table 4.1.5. ANOVA and fit statistics of emission responses

	CO			**HC**			**CO_2**			**NO_x**		
	Briquette	*Mahua*	*Coconut shell*	*Briquette*	*Mahua*	*Coconut shell*	*Briquette*	*Mahua*	*Coconut shell*	*Briquette*	*Mahua*	*Coconut shell*
Model F-value	98.58	81.14	57.47	97.48	38.38	146.70	58.57	77.34	34.13	9.38	26.22	30.02
P-value	<0.0001	<0.0001	<0.0001	<0.0001	0.0002	<0.0001	<0.0001	<0.0001	0.0002	<0.0001	0.0002	0.0001
Std. Deviation	0.0177	0.0120	0.0796	6.16	4.52	7.94	0.0706	0.0547	0.1694	3.29	31.87	4.39
Mean	0.1717	0.0850	0.4642	50.08	25.67	91.83	1.71	1.68	2.91	13.17	114.08	22.92
R^2	0.9880	0.9854	0.9557	0.9878	0.9697	0.9919	0.9799	0.9847	0.9660	0.8866	0.8535	0.9184
Adjusted R^2	0.9780	0.9733	0.9390	0.9777	0.9444	0.9851	0.9632	0.9720	0.9377	0.7921	0.8210	0.8878
Predicted R^2	0.9280	0.9369	0.8924	0.9384	0.8948	0.9560	0.9068	0.9216	0.8509	0.2299	0.7370	0.7988
Adequate Precision	27.3962	22.511	21.6545	24.4891	15.5013	36.5933	20.8872	27.6152	18.9049	8.8133	14.2941	17.2715

$CO_{Briquette}$ (%vol.) = +3.34739 -0.409453*CR +0.133565*BP -0.019882*CR*BP +0.013750 *CR^2 +0.035101 BP^2

CO_{Mahua} (%vol.) = +1.49119 -0.139359*CR -0.176582*BP +0.003252*CR*BP +0.003750* CR^2 +0.019493*BP^2

$CO_{Coconut\ shell}$ (%vol.) = +4.26377 -0.199168*CR -1.45122*BP +0.071257*CR*BP (4.1.2)

$HC_{Briquette}$ (ppm) = -656.50813+81.95057*CR -20.05960*BP -3.23221*CR*BP -2.1250*CR^2 +13.24128*BP^2

HC_{Mahua} (ppm) = -57.61683 +15.31798*CR -56.78125*BP +1.40986*CR*BP -0.500000*CR^2 +5.51662*BP^2

$HC_{Coconut\ shell}$ (ppm) = -1952.22756 +296.10781*CR -341.05201*BP +15.87953*CR*BP -10.00*CR^2 +6.70273*BP^2 (4.1.3)

$CO_{2\ Briquette}$ (%vol.) = +30.17593 -3.80181*CR +0.584476*BP -0.027935*CR*BP +0.1250*CR^2 -0.053125* BP^2

$CO_{2\ Mahua}$ (%vol.) = +11.99989 -1.46687*CR +0.941161*BP - 0.019206*CR*BP +0.050*CR^2 -0.209504*BP^2

$CO_{2\ Coconut\ shell}$ (%vol.) = -76.76689 +9.60689*CR -3.35097*BP +0.220646*CR*BP -0.287500*CR^2 -0.238839*BP^2 (4.1.4)

$NO_{x\ Briquette}$ (ppm) = +245.44454 -30.01833*CR +16.07159*BP -1.72850*CR*BP +1.00*CR^2 +2.57106*BP^2

$NO_{x\ Mahua}$ (ppm) = -516.19509 +31.87500*CR +51.24836*BP

$NO_{x\ Coconut\ shell}$ (ppm) = +75.94777 -3.53950*CR -126.82962*BP +7.70406*CR*BP (4.1.5)

$BTE_{Briquette}$ (%) = +52.73690 -6.09721*CR+14.30062*BP -0.098047*CR*BP +0.174887CR^2 -1.48376*BP^2

BTE_{Mahua} (%) = +91.34151 -10.92683*CR +5.70028*BP +0.085943*CR*BP +0.325850*CR^2 -0.620371*BP^2

$BTE_{Coconut\ shell}$ (%) = -6.58882 +0.390660*CR +7.28882*BP (4.1.6)

$BSDC_{Briquette}$ (kg/kWh) = -4.97115 +1.45881*CR -5.87106*BP +0.162889*CR*BP -0.056154*CR^2 +0.648458*BP^2

$BSDC_{Mahua}$ (kg/kWh) = +21.45384 -2.01197*CR -3.67534*BP +0.013893*CR*BP +0.057914*CR^2 +0.715997*BP^2

BSDC $_{Coconut\ shell}$ (kg/kWh) =	+50.43473 -5.36975*CR -4.31489*BP -0.010624*CR*BP +0.158617*CR² +0.933378*BP²	(4.1.7)
Diesel saving $_{Briquette}$ (%) =	+1055.50318-137.73675*CR +63.50692*BP - 2.65160*CR*BP +4.51409*CR² -4.67693*BP²	
Diesel saving $_{Mahua}$ (%) =	+85.40276 -2.20095*CR -7.23049*BP	
Diesel saving $_{Coconut\ shell}$ (%) =	-1670.93975 +198.06712*CR +15.63855*BP +0.318235*CR *BP -5.74503*CR² -4.68628*BP²	(4.1.8)

4.1.6 Response surface investigation

4.1.6.1 Brake-specific diesel consumption with engine CR and BP

BSDC is the amount of fuel consumed for each unit of brake power per hour. It indicates the efficiency with which the engine develops the power from the fuel. Figure 4.1.5 shows the variation of BSDC of the engine with respect to BP and CR. The BSDC shows a decreasing trend with the engine BP during DF mode operation. This was due to the enhanced combustion at higher BP or load [85]. Further, results suggested that there was a very slight decrease in BSDC with CR. In the present work, at 18 CR and 3.3kW BP minimum BSDC calculated for briquette was 0.2213 kg/kWhr, for mahua wood was 0.3059 kg/kWhr, and for coconut shell, this value was 0.2132 kg/kWhr. In a similar line, other authors obtained the BSDC as 0.302 kg/kWhr [184] and 0.39 kg/kWhr [85]. BSDC generally relies on the calorific value of PG and its used fraction.

4.1.6.2 BTE with engine CR and BP

The fluctuation of BTE of the engine while it was run on dual fuel mode (diesel-PG) with regard to engine brake power and varied CRs for the chosen biomass feed-material (Briquette, Mahua wood, Coconut shell) are illustrated as shown in Figure 4.1.6 (a)-(c). The engine's BTE increases as the engine BP increases. This is due to the rich premixing of the fuel with producer

gas at enhanced load and temperature conditions leading to a better combustion rate of the mixture. From the experiment, it was observed that the BTE of a DF engine run with producer gas from Briquette, Mahua wood, and Coconut shell was 25.34% at CR 16, 17.12%, and 24.09% at CR 18, BP 3.3 kW, respectively. According to the experimental trends, briquette showed the highest BTE as compared to other feedstocks. However, in the case of biomass gasification, other authors obtained a BTE of 25.8% [82], 21.61% [85], and 19% [89].

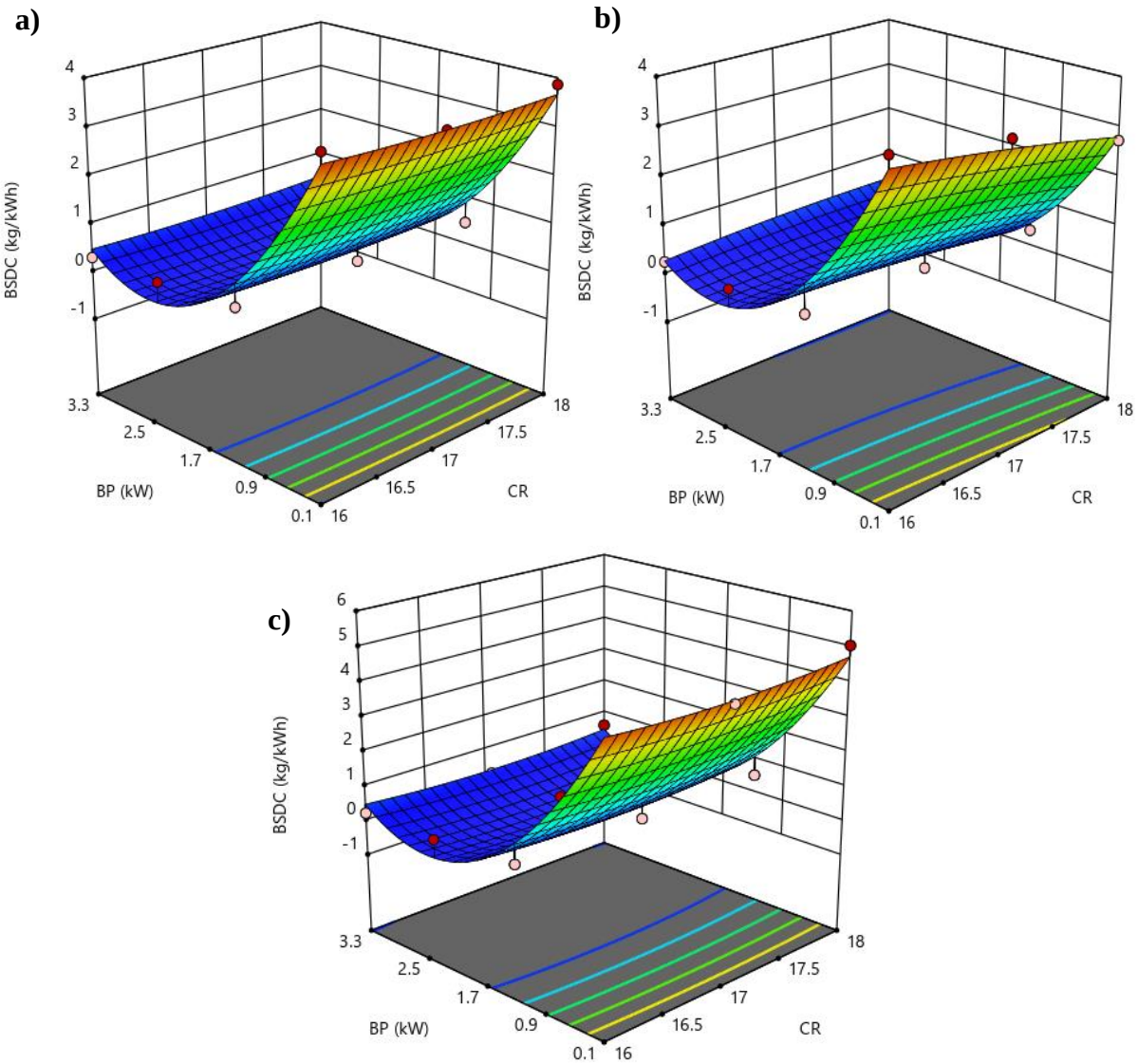

Figure 4.1.5. Variation of BSDC with engine CR and Brake power using (a) Briquette (b) Mahua wood (c) Coconut shell as a feed-material

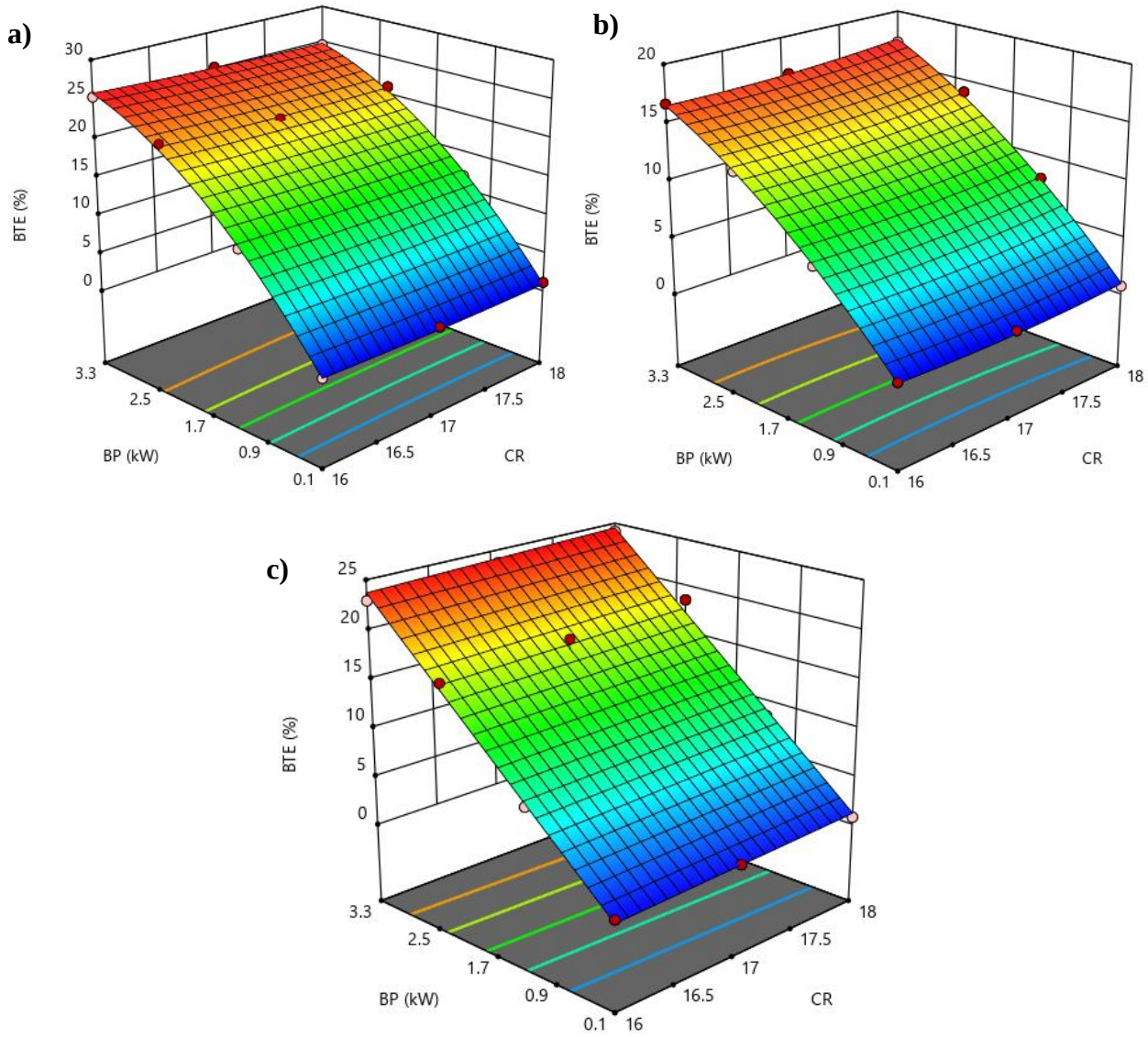

Figure 4.1.6. Variation of BTE with engine CR and Brake power using (a) Briquette, (b) Mahua wood, (c) Coconut shell as a feed-material

4.1.6.3 Diesel saving with engine CR and BP

The reduction of diesel fuel consumption is the main objective of DF engine application. Therefore, one of the technical criteria that need to be looked into is diesel saving. Figure 4.1.7(a)-(c) illustrates the diesel savings for a DF engine employing coconut shell, mahua wood, and PG from briquettes as feedstock. The maximum diesel saving of 57.83% was observed for a CI engine fuelled with PG of coconut shells at 2.3 kW CR 17. This is due to the increased CV of PG gas produced from coconut shells, which is 5.4 MJ/Nm^3, and its improved

combustion efficiency, which results in higher diesel-saving percentages [17]. The amount of diesel savings reduces when the CV of the PG reduces. Mahua wood was used as the feedstock at CR 16 and 0.1 kW, resulting in a diesel saving of 52.5%, whereas briquette usage resulted in the lowest diesel saving, 50.92%. Figures 4.1.7(a)-(c) show that the amount of diesel saved increases with an increase in compression ratio because higher CR results in improved combustion efficiency, which raises the amount of diesel saved for producing the necessary power. Likewise, other authors had achieved a maximum diesel saving of 58.18% [85], 65% [185], and 49.05% [35].

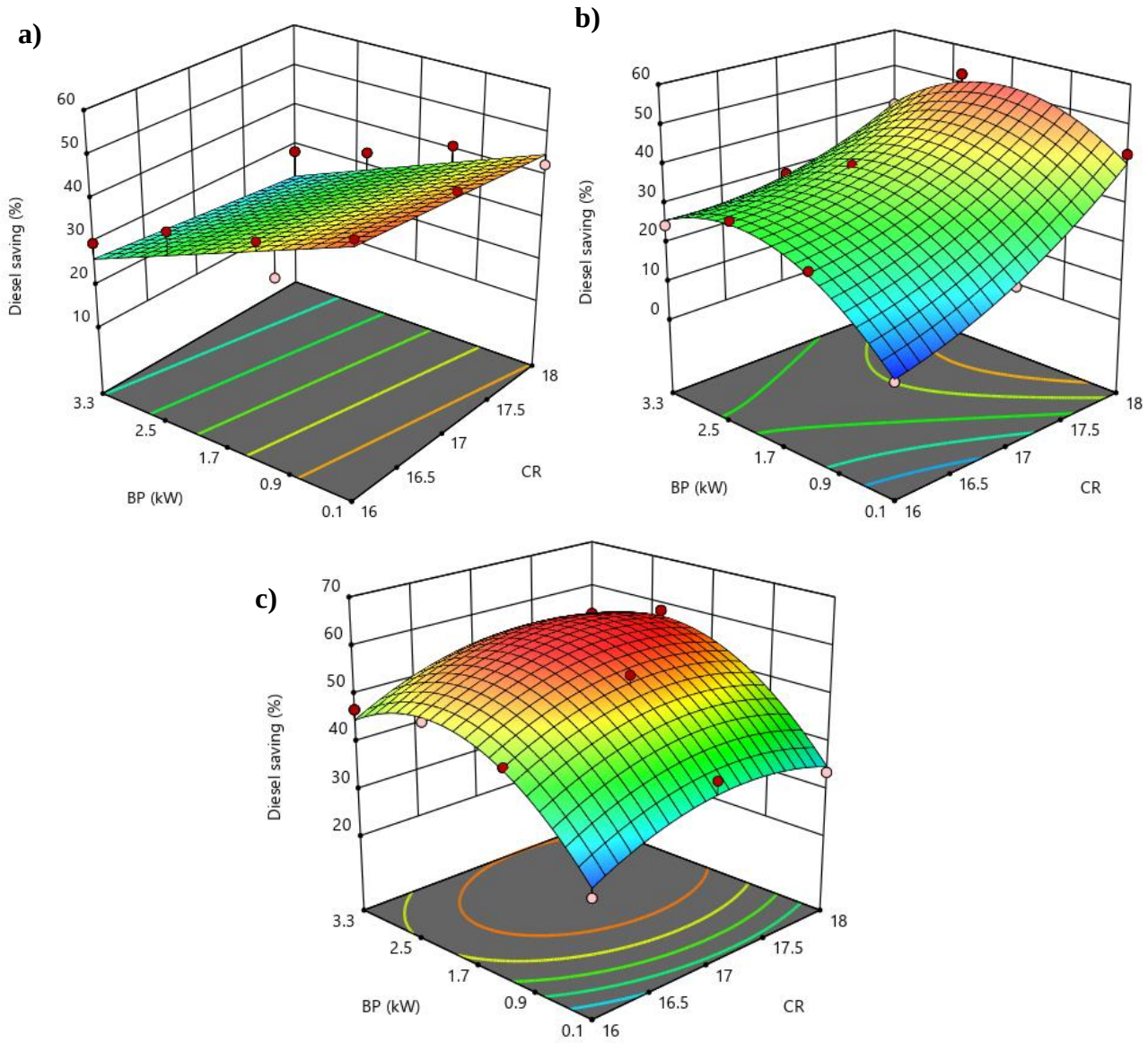

Figure 4.1.7. Variation of Diesel saving with engine CR and Brake power using (a) Briquette, (b) Mahua wood, (c) Coconut shell as a feed-material

4.1.6.1 CO emissions with engine CR and BP

The primary reason for the CO emission is incomplete combustion and lack of oxygen molecule during the expansion stroke. Figure 4.1.8 (a)-(c) shows the variation of CO emissions produced by a DF engine running on diesel and PG from briquette, mahua wood, and coconut shell with engine CR and BP. According to the data, it has been determined that there is a correlation between an increase in the calorific value of the PG and a corresponding increase in the amount of CO emission. At a higher BP and CR, CO emissions decreased. This may be due to the less oxygen in PG may prevent complete combustion. As the load increases, more air-fuel mixture is introduced into the engine cylinder, favouring complete combustion and reducing CO emissions. Mahua wood exhibits the lowest CO emissions trend out of the three feedstocks, with values ranging from 0.02-0.18% by volume, as can be shown in Figure 4.1.8(b). This is due to the fact that the mahua wood-derived PG has the lowest diesel replacement possible, and the addition of the PG-air mixture to the cylinder of the engine highers the amount of oxygen that is necessary for the combustion process to be finished. Therefore, a lower concentration of CO emission can be interpreted as evidence of complete combustion. According to Figure 11(a) and (b), the CO emissions of briquette and coconut shell each range from 0.05 to 0.4% by vol. and from 0.09-1.04% by vol. As can be seen from Figures 4.1.8(a) through 4.1.8(c), the highest levels of CO emission are recorded at lower CR values. This is because there is not enough air present in the cylinder to support complete combustion when the CR is low. Because of this, the cylinder volume decreases, and with it, the amount of air that can be admitted, ultimately resulting in incomplete combustion [35, 178].

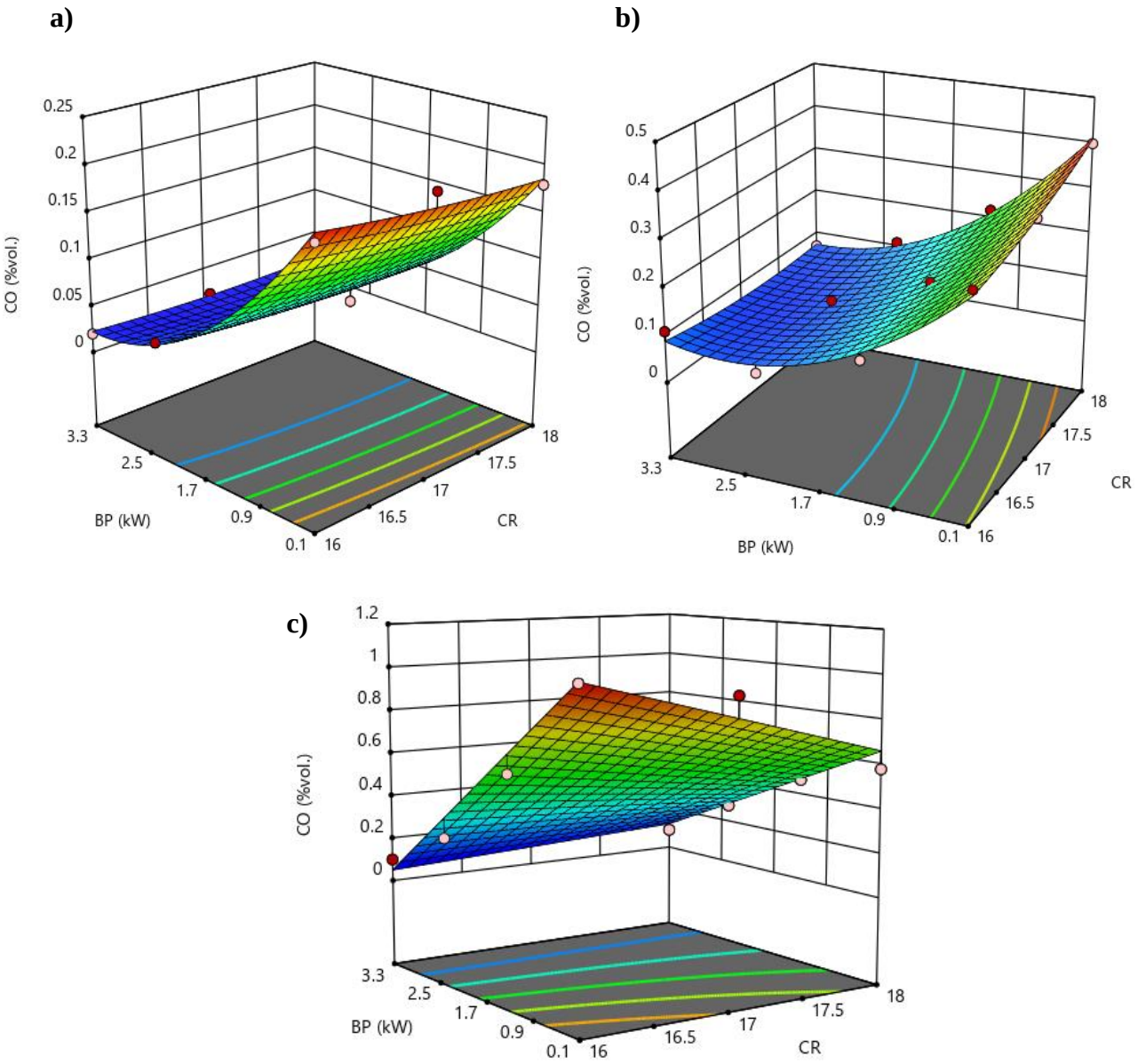

Figure 4.1.8. Variation of CO emissions with engine CR and Brake power using (a) Briquette, (b) Mahua wood, (c) Coconut shell as a feed-material.

4.1.6.2 HC emissions with engine CR and BP

The incomplete combustion of the carbon-containing fuel results in the production of hydrocarbon emissions. The number of hydrocarbons found in an engine's exhaust gases is one of the most critical factors in determining the quality of the combustion process that takes place

inside the engine. The reduced availability of carbon atoms, the shorter quenching distance, and the rapid flame speed of hydrogen were the reasons that contributed to the reduction in the emission of hydrocarbons. The fluctuation in hydrocarbon emissions produced by a DF engine that uses PG from Briquette, mahua wood, and coconut shell as secondary fuel is illustrated in Figure 4.1.9 (a)-(c) and depicted under a variety of BP and CR conditions. When the CR of an engine is higher, the pressure and temperature inside the cylinder are higher. This causes the emissions of HC to be higher. In addition, the heat that must be produced to generate the same power level is higher for the PG with the higher CV. Because of this, a greater quantity of PG is needed to produce the same amount of power, which increases emissions. The highest 223 ppm HC emission at CR16 was observed while using a coconut shell as a PG. An increase in CR from 16 to 18 reduced average HC emissions of around 42% for coconut shell and 6.25% for briquette, while an increase of 30.76% for mahua wood. Moreover, the HC emissions reduced significantly as BP increased from 0.1kW to 3.3kW in DF mode operation. This might be due to better combustion at higher brake power or load [186].

4.1.6.3 CO_2 emissions with engine CR and BP

Since CO_2 emissions are the main contributor to global warming, they are detrimental to the environment. If the injected fuel has a high CO_2 percentage or contains little methane, CO_2 emissions from DF engines are found to be substantial. Additionally, the complete burning of the fuel results in the generation of CO_2 due to the enhanced oxidation of carbon in the presence of sufficient oxygen and higher in-cylinder temperatures. Figure 4.1.10(a)-(c) illustrates the relationship between engine CR and BP regarding the content of CO2 available in the engine exhaust gas. The introduction of PG in the DF mode CI engine increases CO_2 emission with BP, reaching the maximum at 1.2 kW and then decreasing. Because CO and CO_2 are also constituents of producer gas, the combustion of either of these substances results in increased

CO_2 emissions. At CR18, 0.1 kW, and CR 16, 3.3 kW, respectively, the minimum and maximum CO_2 contents for Briquette-powered producer gas are recorded to be 1.2 and 2.3% by volume. At the same CR and engine BP, the minimum CO_2 emissions occur using mahua wood and coconut shell, respectively. The maximum and minimum values of CO_2 for mahua wood are 2.2 and 1.1 %vol. respectively, and for the coconut shell, the values are 3.8 and 1.5 %vol. respectively. According to the experimental findings, as engine CR increases, the magnitude of CO_2 emissions increases. This was due to the better combustion of fuel mixtures at enhanced CR conditions [187].

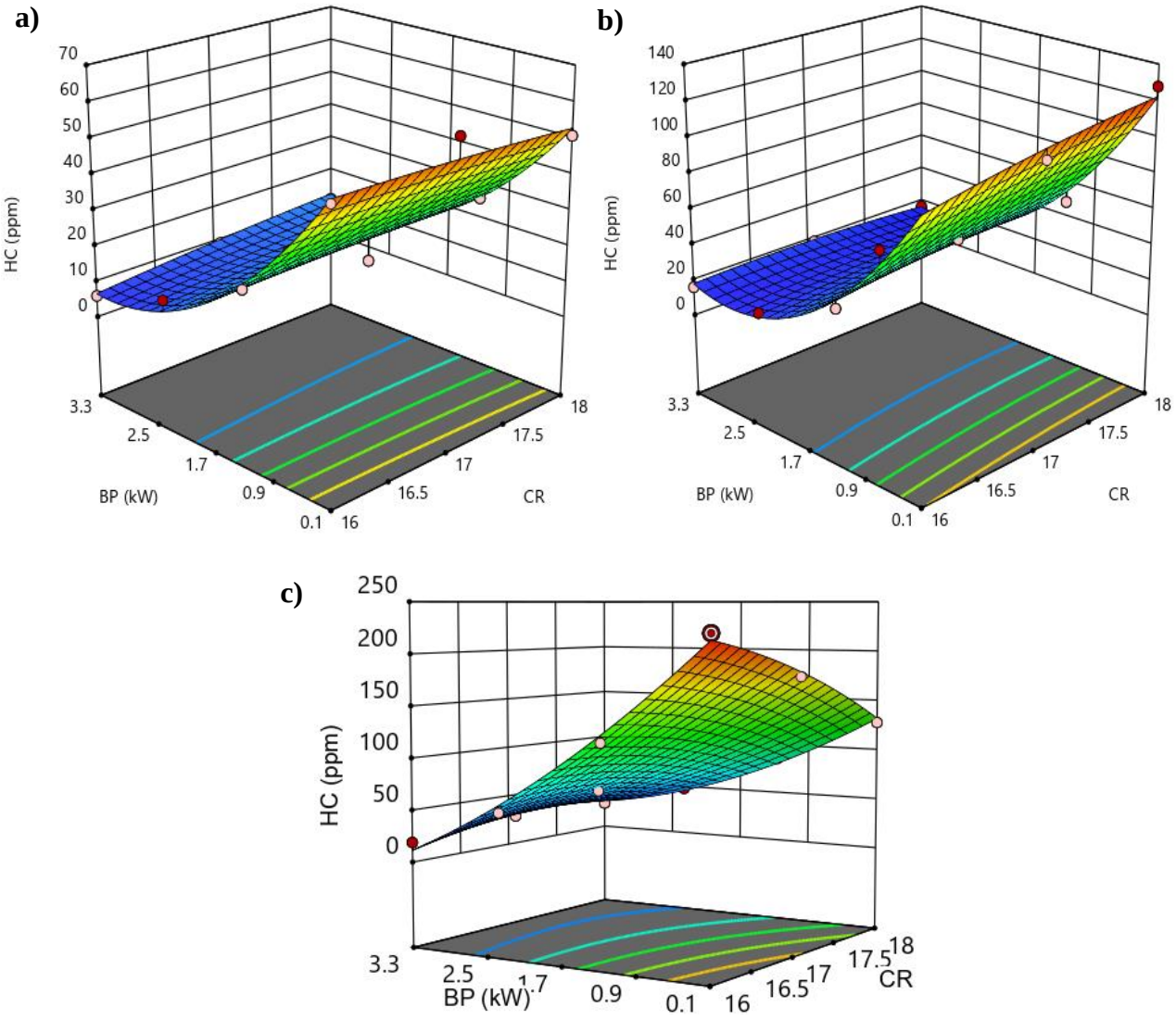

Figure 4.1.9. Variation of HC emissions with engine CR and Brake power using (a) Briquette (b) Mahua wood (c) Coconut shell as a feed-material.

4.1.6.4 NO_X emissions with engine CR and BP

NOx emission depends on the availability of nitrogen and oxygen, gas temperature, and residence time. Figure 4.1.11(a)-(c) shows how the BP and engine CR affect the amount of NOx that is emitted by a diesel engine operating in DF mode and using Briquette, Mahua wood, and Coconut shell as secondary fuel. The generation of nitrogen oxides is aided by conditions in which there is a high concentration of oxygen and a high temperature in the air-fuel mixture. It has been noticed from the figure that as the CR increases, the magnitudes of NOx emission increases for all three biomasses. This occurred as a result of more fuel being fed under a higher CR, which increased the pressure and temperature within the cylinder of the engine, so making the combustion mechanism more efficient. In the dual fuel approach, the range of NOx emission for briquette is 6-31 ppm, while the range for mahua wood is between 40-220 ppm, and the range for coconut shell is between 6-56 ppm, as shown in Figure 14(a)- (c). However, other authors reported NO_x emissions in DF mode as 80 ppm [81] and 173 ppm [85].

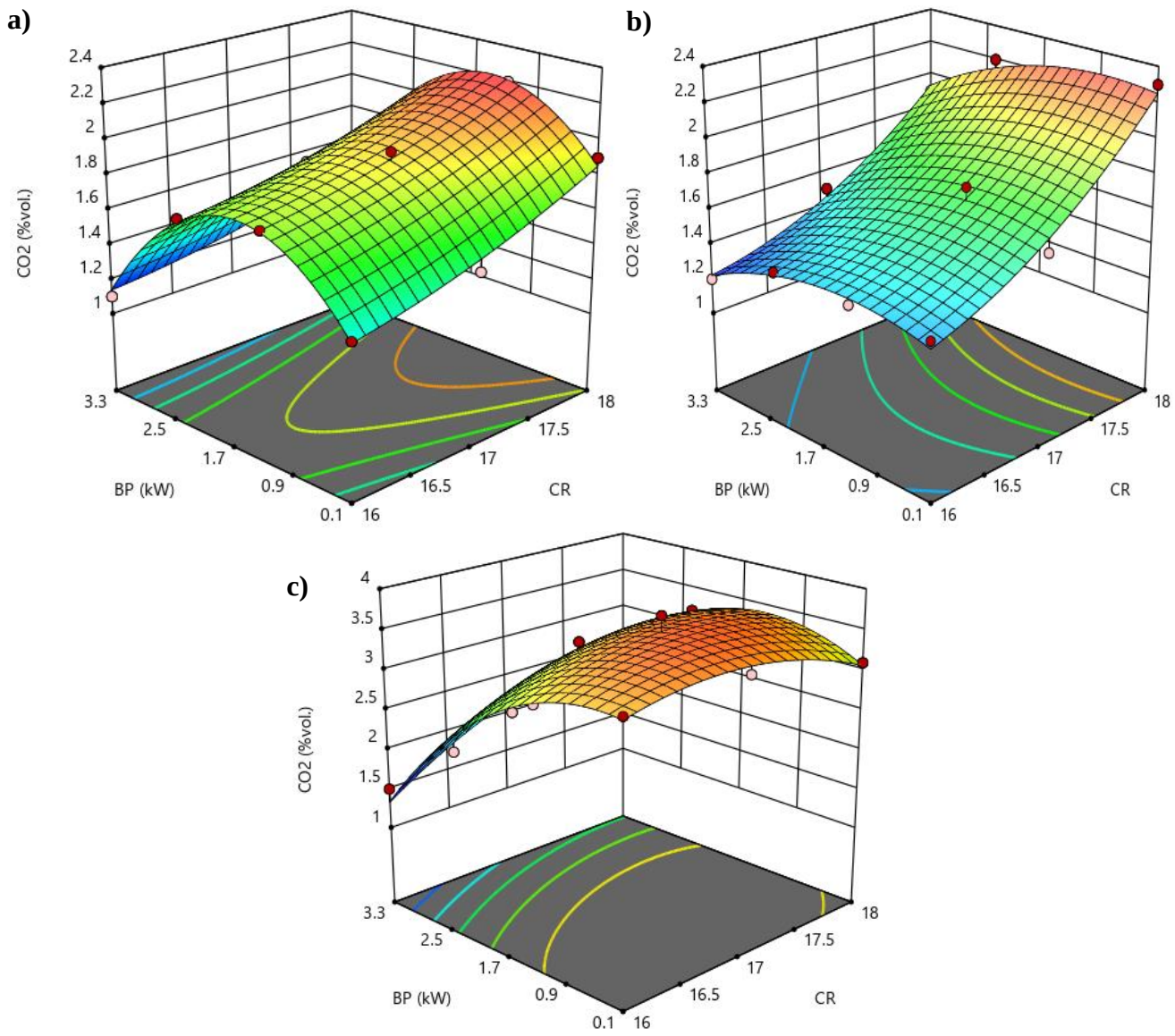

Figure 4.1.10. Variation of CO_2 emissions with engine CR and Brake power using (a) Briquette, (b) Mahua wood, (c) Coconut shell as a feed-material

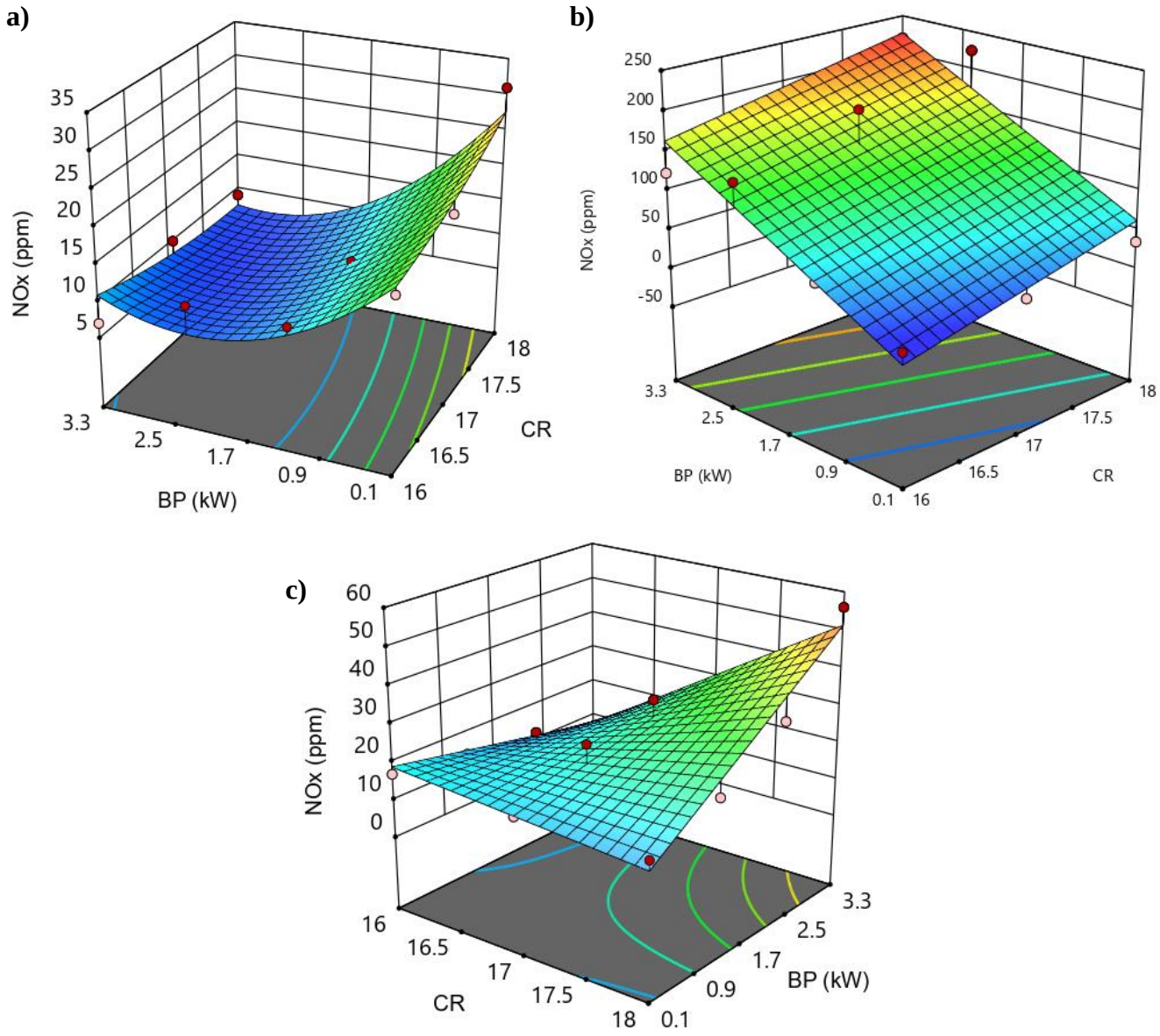

Figure 4.1.11. Variation of NO_x emissions with engine CR and Brake power using (a) Briquette, (b) Mahua wood, (c) Coconut shell as a feed-material

4.1.7 *Optimisation*

When inspecting an experiment with multiple responses, optimization is one of the most effective procedures that must be taken [188]. From the experimental trial results, it has been determined that the impacts of CR and BP on the magnitudes of BSDC, BTE, DS, CO, HC, CO_2, and NO_x conflict with one another. Thus, it is essential to optimize CR and BP to maximize engine performance and limit exhaust emissions. Figure 4.1.12 shows the optimization plot depicting how the different experimental settings affect the predicted responses for a stored model. Figure 4.1.12(a) shows that the optimum solution for the briquette-derived PG-based DF engine was procured at 16.34 CR and 2.78 kW BP. The corresponding optimum performance values were procured as 0.036 kg/kWh BSDC, 23.64% BTE and 30.07 % Diesel saving, and the CO, HC, CO_2, and NOx emissions were observed as 0.067 % by volume, 14.95 ppm, 1.374 % by volume, and 7.97 ppm respectively. Figure 4.1.12(b)-(c) also shows the optimal solution plots of input and response parameters for mahua wood and coconut shell. Similarly, the optimum values for a Mahua wood PG-operated DF engine are BSDC 0.4905 kg/kWh, BTE 16.52 %, DS 28.86 %, CO 0.0227 %vol., HC 6.609 ppm, CO_2 1.1402 %vol., and NOx 128.08 ppm respectively. Moreover, Coconut shell derived PG has an optimum value of BSDC 0.3223 kg/kWh, BTE 22.52 %, DS 46.33 %, CO 0.0636 %vol., HC 16.738 ppm, CO_2 1.512 %vol., and NOx 8.190 ppm respectively. The overall desirability of Briquette, Mahua wood, and Coconut shell is calculated to be 0.85, 0.76, and 0.91, respectively.

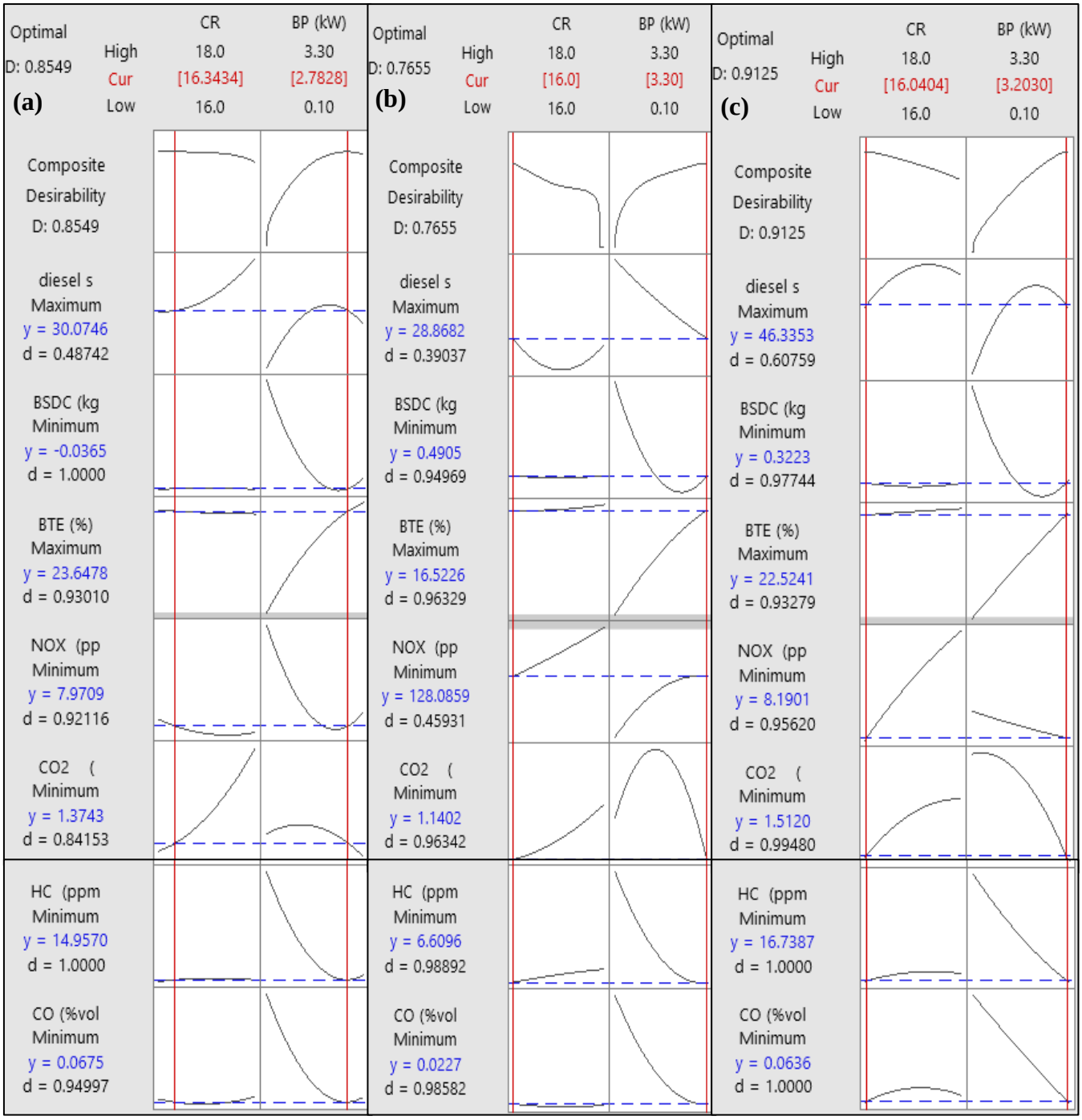

Figure 4.1.12. Cumulative Optimisation plots for (a) Briquette, (b) Mahua, (c) Coconut shell

4.1.8 Desirability plots and validation

Desirability function optimization is a popular method. How close the lower and upper limits are to the real optimum determines desirability. Desirable spans between 0 and 1, with 0

representing an undesirable configuration for the selected response and 1 representing the ideal case. It can be seen from Figures 4.1.13 that the coconut shell-based PG DF engine operation has the maximum cumulative desirability value of 0.91. The related desirability functions for output response variables- BSDC, BTE, Diesel saving, CO, HC, CO_2, and NOx are 0.96, 0.96, 0.40, 1, 1, 1, and 0.92, respectively. This information can be found in Figure 4.1.13(c). The cumulative desirability plot for the input variables and output responses for Briquette and Mahua wood be seen in Figures 4.1.13(a) and (b), respectively. The combined desirability for Briquette, Mahua wood, and Coconut shell is 0.85, 0.71, and 0.91, which is an excellent dependability metric since all values are closer to 1 than they are to any other number.

After determining the optimal values of the input variables by using multi-objective optimization, the subsequent step is to verify the optimal values and validate the performance and emission parameters of the dual fuel engine using the optimized results as input variables. This step follows the previous step of determining the optimum levels of the input variables. Another series of experiments were carried out with the same experimental setup, and the output response was recorded after each one. The experiments were designed so that the optimal input values could be used. Nevertheless, instrumental and human errors cause uncertainty in the experiment's measured values while conducting the experiment. To consolidate the experiment readings, a Gaussian uncertainty analysis is done [189]. Table 4.1.6 lists the uncertainties of different output responses during an experiment. Inaccuracies that are systematic and precise, such as those that occur when using research tools to collect data or when rounding off mistakes occur during data observation, can be the root source of these uncertainties. The expected outcomes are correct because the deviations do not constitute a statistically significant difference. In addition, an error analysis is performed to determine whether the RSM model can accurately predict the responses between the experimental and the predicted values of the RSM model of responses [190]. This is performed in order to determine

whether or not the RSM model accurately predicts the responses. Moreover, (Appendix A4) lists the calculations encountered during uncertainty analysis.

Table 4.1.7 shows the minimum and maximum errors for the Briquette-derived DF engine are 0.63% and 6.6%. When Mahua wood was applied, maximum and minimum RSM predicted, and experimental error was 0.90 and 4.54%, respectively. Experiments on a DF engine driven with coconut shell PG indicated 1.32 and 5% errors, respectively. The Table shows that predicted and experimental values are closely related. The RSM-developed model can predict performance and engine exhaust emissions to determine the optimum magnitudes for test experiments.

Table 4.1.6. Uncertainties of output parameters

Output parameter	**Measuring range**	**Accuracy**	**Uncertainty (%)**
BTE %	–	± 5	± 0.5
Diesel saving %	–	± 0.1	± 0.2
Fuel properties			
CO	0 – 10 vol. %	± 0.1 volume %	± 0.1
CO_2	0 – 20 vol. %	± 0.3 volume %	± 0.2
HC	0 – 2000 ppm	± 10 ppm	± 0.2
NO_x	0 – 5000 ppm	± 20 ppm	± 0.5

Table 4.1.7. Validation between RSM based result and respective experiment

Response	***RSM predicted result***			***Experimental result***			***% Error***		
	Briquette	***Mahua***	***Coconut***	***Briq.***	***Mahua***	***Coconut***	***Briq.***	***Mahua***	***Coconut***
Inputs:CR, BP(kW)	*CR: 16.34* *BP: 2.78*	*CR: 16* *BP: 3.30*	*CR: 16.04* *BP: 3.20*						
BTE (%)	23.64	16.52	22.52	23.79	16.67	22.95	*0.63*	*0.90*	*1.90*
Diesel saving (%)	30.07	28.86	46.33	31.97	29.96	46.97	*6.31*	*3.81*	*1.38*
CO (%vol.)	0.067	0.022	0.06	0.07	0.023	0.063	*4.47*	*4.54*	*5*
HC (ppm)	14.95	6.60	16.73	15.4	6.67	17	*3.01*	*1.06*	*1.61*
CO_2 (%vol.)	1.37	1.14	1.51	1.4	1.16	1.53	2.18	1.75	1.32
NO_x (ppm)	7.97	128.08	8.19	8.5	130	6	*6.6*	*1.4*	*3.7*

4.1.9 Conclusions

Hence, present study investigated the comparative performance and emission characteristics of VCR diesel engine (DF) running on producer gas obtained through briquette, mahua wood, and coconut shell biomass gasification. The optimum BTE observed during biomass gasification was 16-23% with maximum diesel savings of 50-57%. Mahua wood based PG-CI engine application has low CO, HC , and CO_2 engine emissions.

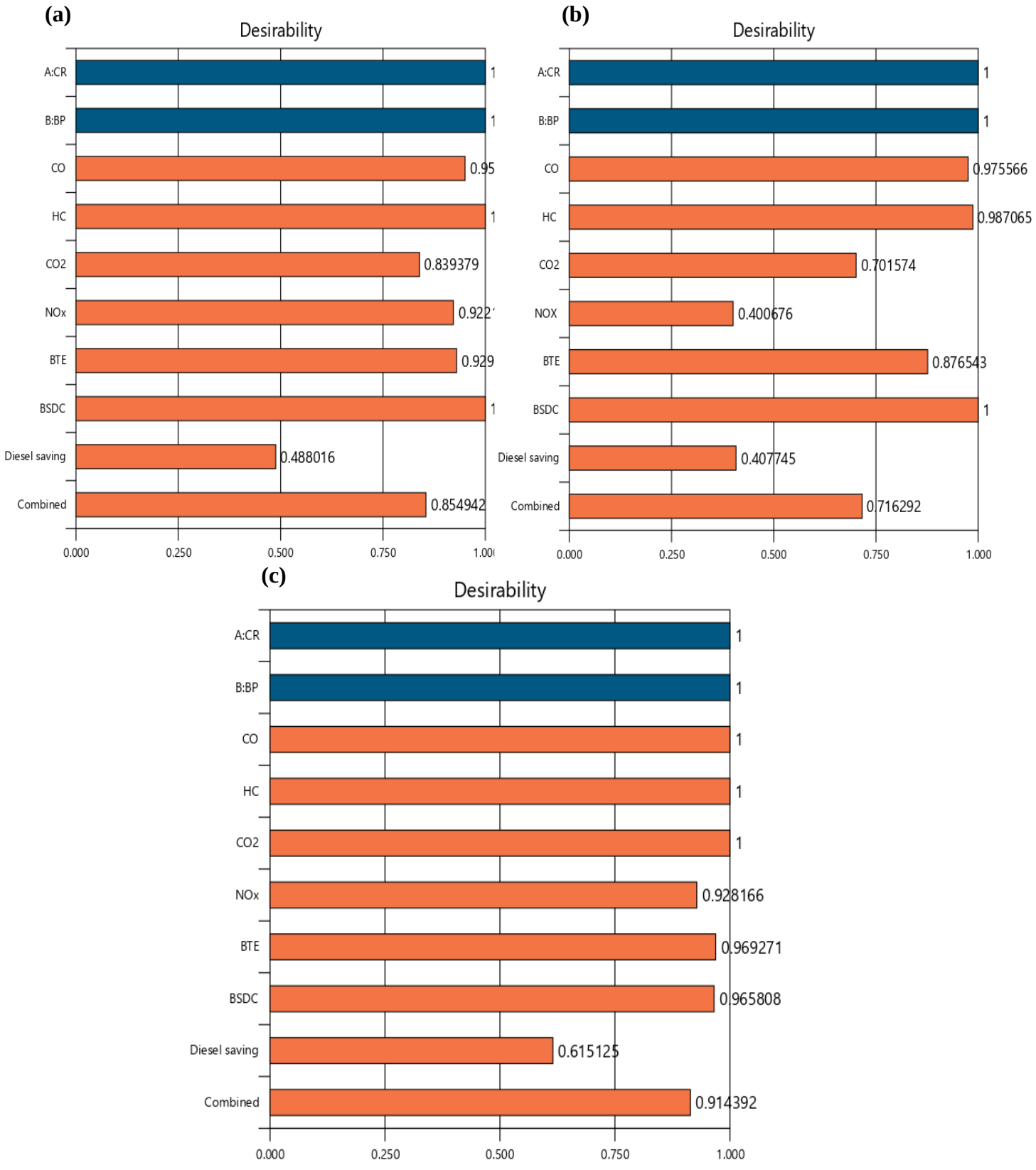

Figure 4.1.13. Desirability plots of input and output parameters for (a) Briquette, (b) Mahua wood, (c) Coconut shell

4.2 Co-gasification of Low-grade Coal with Mahua Biomass and dual-fuelled engine performance

4.2.1 *Introduction*

Increasing energy requirements worldwide have prompted energy generation migration through alternate resources. Gasification is an established thermochemical conversion technology to convert solid fuel into gaseous fuel for alternative decentralized power generation. One of the significant challenges is the sustainable availability of feedstock like coal and biomass, where co-gasification could be the viable option. The present study includes producer gas (PG) generation through co-gasification of low-grade coal and Madhuca longifolia (Mahua) Biomass and PG utilization with the dual-fuelled mode in a compression ignition engine. The influences of biomass-coal percentage, gasification equivalence ratio (GER), engine compression ratio (CR), and engine load variation have been analysed in detail on the performance, emission, and diesel saving during engine run. Finally, multi-objective optimization tool-response surface method (RSM) is applied to optimize gasifier CI engine operating variables. Dual feedstock air-gasifier integrated dual-fuelled compression ignition (CI) engine experimental results show: that the maximum diesel saving achieved 54.16% at GER 0.43, CR 18, and at 100% biomass percentage; the maximum brake thermal efficiency obtained was 27 % at GER 0.1, CR 16, and 0% mahua blend. Engine emission results suggest that the Co-gasification decreases the magnitude of CO engine emission as compared to single feedstock coal gasification. Minimum concentration of CO_2 0.8 vol% is emitted at 75% blending running at 12 kg load, CR16, 0.43 GER. Increasing the percentages of mahua biomass in co-gasification increases the levels of hydrocarbons from 0-25 % blending and 75-100% blending. The minimum 1 ppm HC is observed at 75% blending at CR 18, having 0.43 GER

and running at a full load of 12 kg, and the minimum concentration of NOx content was 40 ppm which is obtained at the GER 0.43, CR 18, load 0 kg and 75% mahua blend. Hence, the co-gasification of the engine system offers a suitable technology for alternative power generation and could be very useful for small-scale industries.

Since, most of research has identified that co-gasification is more beneficial than its application regarding dual feedstock gasification. Moreover, co-gasification could be helpful when non-availability issues of feedstock appear during individual gasification. Apart from these primary advantages and disadvantages, the performance of co-gasification is influenced by several factors, including the type and size of biomass feedstock, the Coal biomass mixing ratio, the gasification medium, reactor design, and operational parameters [42]. It was reported that variation in coal and biomass properties strongly influences the yield of gaseous products (PG) and their quality in co-gasification [23], [20]. Recently, there is numerous works have been reviewed by Kamble et al. [19] concerning individual and co-gasification reports and investigated the co-gasification benefits as- Coal and rice husk [191], sugarcane bagasse and coconut shells [192], petroleum coke, and biomass [193], sewage sludge and pine sawdust [194], sawdust and bituminous coal [195], biomass and poly-ethylene wastes [196]. But, none of them have attempted to study the co-gasification performance of the Coal and Madhuca longifolia (Mahua) biomass blended feedstock. The reason is to select the Mahua biomass (especially waste: branch cut, old furniture waste, wood industries process like off-cuts sizing, trimming, shaving, etc.) was readily available and can easily be transported to the specific location. Mahua longifolia is a deciduous forest tree in the Sapotaceous species that may reach a height of roughly 20 meters [197]. In India, around 62,500-hectare areas have been covered for Mahua cultivation [162]. The particular details of Mahua are depicted in Table 4.2.1. Therefore, concerning the availability of forestry biomass, its gasification

advantages and specific feature of mahua biomass, the first novelty of the present work is to perform downdraft co-gasification using coal and mahua biomass as a feedstock.

Furthermore, in terms of application, challenges to efficient performance and emission of an ic engine for the coupling of the electric generator have been inadequately addressed in the co-gasification studies. Recently, most of the research work associated with either gasification only or single feedstock based gasifier-IC engine coupling such as sawdust and cotton stalks [81], walnut shells-diesel engine [85], grape wood PG-SI engine [198], coconut shell-CI engine[17]. But, very little work has been studied on the dual feedstock gasifier-IC engine integration performance investigation; for example, Awais et al. [38] worked on a 24kW downdraft for co-gasification with wood pellets and corn husk, as well as sugarcane bagasse and coconut shells. Still, they did not place a premium on engine performance.; Indrawan et al. [30] experimented on the gasifier-IC engine using municipal solid waste (MSW) and agriculture waste and revealed that engine CO, CO_2, and NOx emissions were reduced, whereas SO_2 and HC emissions were raised while municipal solid waste fraction and load increased.

Therefore, the second novelty of this experiment is to analyse the co-gasification of feedstocks with low-grade hard coke coal and forest tree mahua biomass and provide the parameters for improved producer gas quality for compression ignition engine run. And, the third novelty is to optimize the dependent and independent operating parameters for maximizing engine performance characteristics, and minimizing engine emissions by employing the advanced data processing tool response surface methodology (RSM) technique. Concerning issues and challenges in terms of the parametric effect of gasification and engine operating variables discussed in the above literature survey, The current study will concentrate on a comprehensive experimental investigation of the performance and emission characteristics of an air gasifier-compression ignition engine employing a percentage variation of coal and

mahua biomass feedstock. As a result, we have attempted to bridge the apparent gap and respective novelty in the current study. The following is an impartial order of the content:

- To generate the producer gas through air agent-based downdraft gasifier form dual feedstock of low-grade Coal and Mahua biomass and use PG with diesel fuel for CI engine run.
- To analyse the impact of variation in low-grade coal and mahua biomass on engine performance, emission, and diesel saving.
- To study the influence of gasification equivalence ratio (GER), engine's CR, and engines' load on the performance rating (power, emission, and diesel consumption) of dual fuel mode engine run.
- To determine optimum ER of the gasifier, CR, and load for the best power response and emission and fuel consumption using the response surface method (RSM).

This study will provide a base for the end-users and researchers to adopt a co-gasification-IC engine integration system as a feasible approach toward utilizing low-grade hard coke coal and biomass waste in air gasification through a downdraft gasifier.

Furthermore, the photograph of coal and mahua wood feedstock is depicted in Figure 4.2.1, and the detailed chemical composition (proximate-ultimate analysis) of coal and mahua biomass is listed in Table 4.2.2.

Table 4.2.1. Particular Mahua tree (Madhuca longifolia)

Mahua plant growth **(A-B-C)** 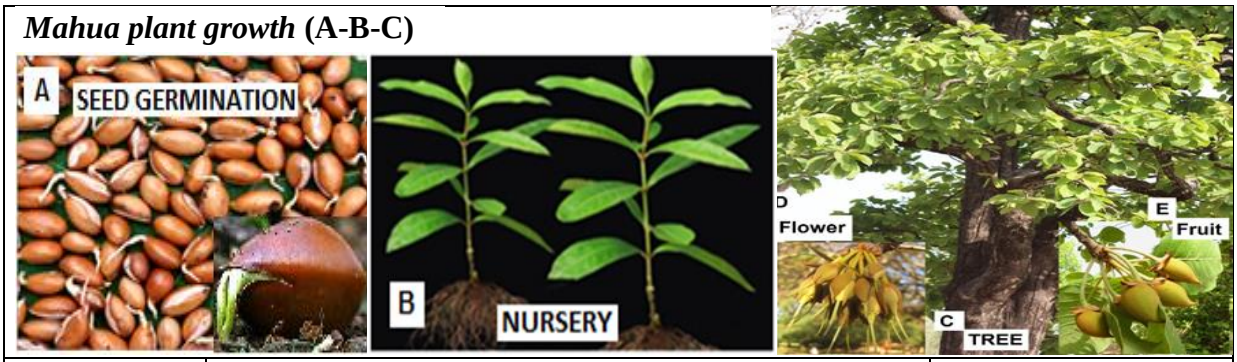		
Particular	**Specification**	**References**
Land	Deep/sandy-loam soil, clayey and calcareous soil	[199] ,[200]
Climate	Mean Temperature: 2-46 ^{o}C, humidity: 40-90 %	[199], [201]
Rain	550-1500 mm annual rainfall	[199],[201]
Period	8-15-year gestation and 9-year maturation	[162], [202, 203]
Spacing	7 m × 7 m plant to plant	[199]
Number	Plants per hectare: 200 no.	[162]
Fruit (kg)	Seed 40-56 %, husk 44-60 %	[204],[205], [206]
Tree size:	Height 21-23 m, stout trunk, 80 cm diameter	[162],[207]

(A) Supply feedstock (before co-gasification)

(B) Coal char + Mahua (after co-gasification)

Figure 4.2.1. Picture of feedstock, before and after gasification

Table. 4.2.2 Chemical property of fuel- coal [208], [209], [210].

Particular	**Value**	
Proximate analysis	*Coal*	*Mahua biomass*
VM	57.5 %	77.05 ± 0.2 %
FC	39.52 %	12.63 ± 0.3 %
Ash	1.31 %	2.08 ± 0.05 %
Moisture content	1.67 %	7.88 ± 0.5 %
Ultimate analysis	*Coal*	*Mahua biomass*
C	58.999 %	47.577 %
H	0.215 %	6.400 %
N	0.546 %	0.722 %
S	0.304 %	0.34 %
CV (MJ/kg)	17.371	25.88 ± 0.18
Cellulose	-	37.92 ± 0.13 %
Hemicellulose	-	27.33 ± 0.13 %
Lignin content	-	14.20 0.11 %

4.2.2 *Experimental uncertainty*

Uncertainty is created well during an experiment due to the experimental metering adjustment. Working environment, equipment selection, test preparation, result calibration, and data processing are critical contributors to practical mistakes and system uncertainty. Table 4.2.3 lists the different apparatus utilized in this experimental run and its operating ranges, resolutions, system accuracies, and percentage uncertainties employed in that system. Frequent and precise mistakes, together with the equipment utilized to gather records and round off inaccuracies while observing data, might all contribute to these uncertainties. The entire experimental uncertainty cost was calculated using the equation below.

Total uncertainty (in %)

$$= [\text{Uncertainty of } \{(\text{B.P})^2 + (\text{Thermocouple})^2 + (\text{Tachometer})^2 + (\text{Dynamometer})^2$$

$$+ (\text{Crank angle sensor})^2 + (\text{Pressure transducer})^2 + (\text{Burette Fuel measurement})^2\}]^{(1/2)}$$

$$= (0.39^2 + 0.16^2 + 0.33^2 + 0.2^2 + 0.2^2 + 0.04^2 + 1.0^2)^{1/2}$$

$$= \pm 1.16\ \%$$

Table 4.2.3. Instrument descriptions and their accompanying uncertainties

S.No	Apparatus	Range	Resolution	Accuracy	Uncertainty (%)
1.	Tachometer	1200-1500 rpm	1 rpm	±5 rpm	± 0.33
2.	Brake power	0 – 3.4 kw	0.1 kw	±0.1 kW	± 0.39
3.	Thermocouple	0-1200^{o}C	1 ^{o}C	±2 ^{o}C	± 0.16
4.	Dynamometer	0-50 kg	0.01 kg	±0.1 kg	± 0.2
5.	Transducer pressure	0-5000 psi	---	±2 psi	± 0.04
6.	Crank angle sensor	0-360^o	1^o	±1^o	± 0.2
7.	Burette fuel measurement	---	---	±0.1 cc	± 1.0

4.2.3 *Engine performance parameters*

The effect of gasifier-diesel engine operating parameters are quite significant on the performance and emission of the engine. In this section, the impact of gasification equivalence ratio (GER), engine compression ratio (CR), and engine load (EL) on the dual fuel mode (diesel/mahua coal-producer gas) engine performance (BTE and diesel saving) and exhaust emissions (NOx, CO_2, UHC, CO) are investigated. In this context, a brief overview of gasifier-engine coupled experimental results has been revealed in the following sections.

4.2.3.1 Brake thermal efficiency

Brake thermal efficiency (BTE) is one of the significant performance parameter for analyzing and evaluating the fuel energy to power conversion [198]. Figure 4.2.2 depicts the simultaneous impact of independent parameters i.e., GER, CR, and Engine load on the Brake thermal efficiency with varying percentages of Mahua wood blending in coal. It was observed in Figure 4.2.2(a), as the blending percentages of Mahua wood in coal increases, on an average the magnitude of BTE decreases for the all gasification equivalence ratios (GER). The reason is that in dual mode (Diesel + PG) engine run, BTE depends on the blended fuel calorific value, which increases while the quality of PG increases [211]. And the quality of PG, especially hydrogen concentration, significantly depends on the gasification equivalence ratio [33]. Also, it was reported that at a higher biomass ratio, H_2 concentration in PG reduces, but increases CO, CO_2, CH_4, and HC [23]. Moreover, at higher temperatures ($\approx 800^0$C), carbon conversion maximizes, increasing the calorific value of producer gas [19]. In the present experiment, the maximum gasification temperature observed was equals to 650^0C. In Figure 4.2.2(c), the magnitude of BTE is maximum at higher load conditions (12 kg i.e., 100% load). The reason is that as the load increases, the temperature inside the cylinder increases, which assists a better combustion efficiency, and hence BTE increases. The similar trends of the performance has

been obtained by [85]. It can also be inferred from Figure 4.2.2(b) that BTE also increases with increasing engine compression ratio. Because as the CR increases, cylinder gas pressure and temperature increases burning rate and thermal efficiency [212]. In the dual fuelled mode engine run, the maximum brake thermal efficiency observed was 27% in DF mode at 0.1 GER with 0% mahua blend gasification, and 18 CR with 12 kg load. However, the comparison is concerned, the maximum BTE has been found to be 21.61% by Sharma et al. [85], 19% by Yaliwal et al. [185], and 26% by Shrivastava et al. [171] in the dual mode with PG fuel. Moreover, in the current study maximum BTE during diesel mode was observed as 28.37%.

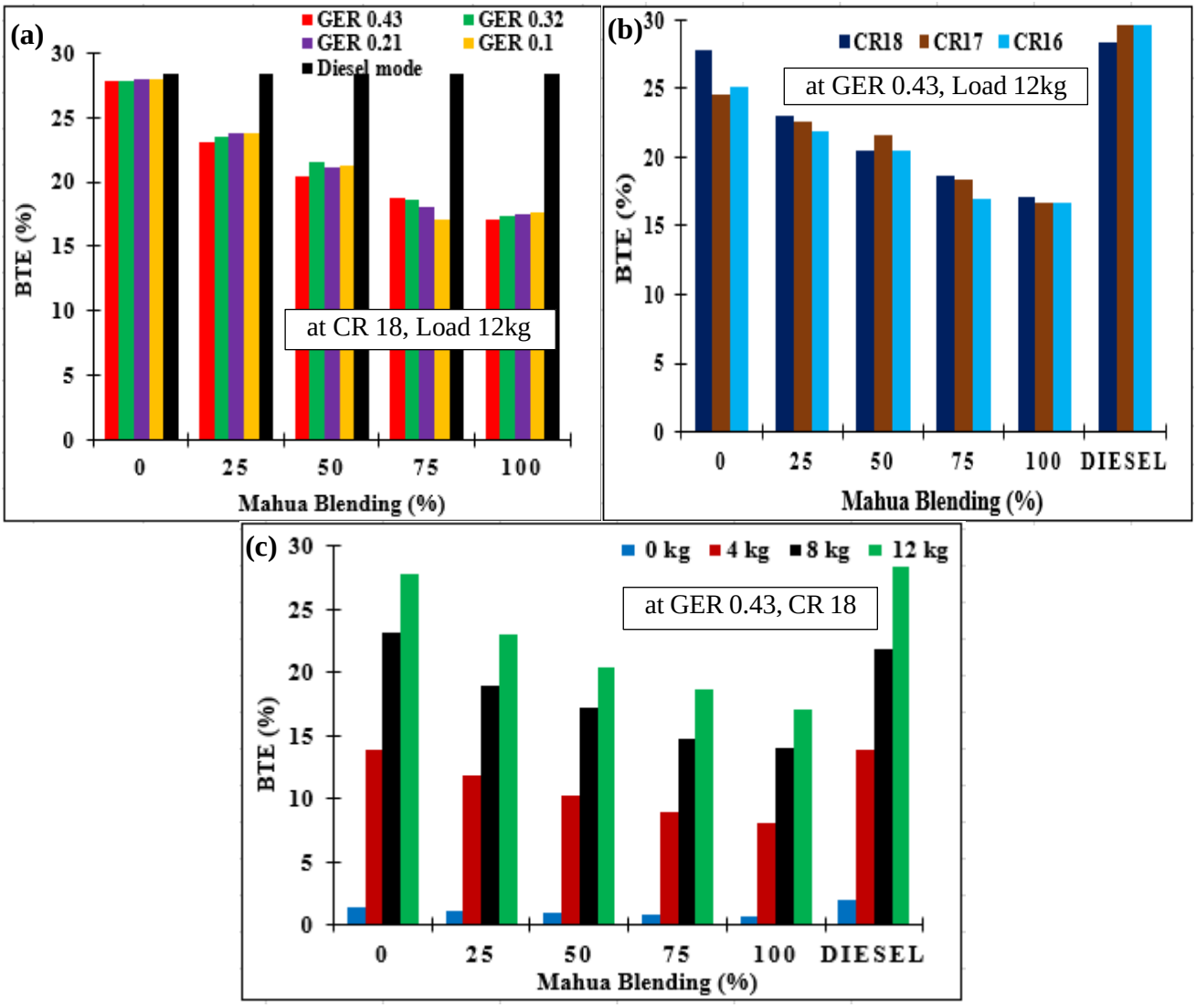

Figure 4.2.2. Variation of (a) GER, (b) CR, and (c) Load on BTE

4.2.3.2 Diesel saving

During gasifier-dual fuel engine operation, diesel savings with respect to engine compression ratio, brake power, and blending percentages of mahua-coal gasification are depicted in Table 4.2.4. Diesel saving varies with the gasification of different blend fractions of mahua wood and coal, that was 49.05 %, 45.25 %, 39.81 %, 39.10 %, and 54.16 %, saving for 0 %, 25 %, 50 %, 75 %, and 100 % mahua blending respectively. Amongst, 54.16 % maximum diesel saving was obtained at higher CR (i.e., 18) and 100 % Mahua Blending percentage. Sharma et al. [85] cited the similar magnitude of the Diesel savings while running the engine at dual fuel mode. It may be accredited to the fact that increasing CR leads to an increase in engine cylinders' pressure and temperature, which improves efficiency and lowers fuel consumption. Also, it was found that at every blending percentage of mahua, as brake power increases with load increment, diesel consumption increases in both single mode and dual mode fuelled CI engines. However, the comparison is concerned, Sharma et al. [85] achieved a maximum diesel replacement of 58.18 % at CR 18 for wallnut gasification, while Singh et al. [233] achieved diesel replacements of 44.44 % and 41.94 % for cotton stalks and wheat straw, respectively.

Table 4.2.4. Comparison of diesel saving at different mahua blending percentage.

CR	Load kg	B.P kw	Diesel mode fuel kg/h	0% mahua blending		25% mahua blending		50% mahua blending		75% mahua blending		100% mahua blending	
				DFM* kg/h	DS** %	DFM kg/h	DS %	DFM kg/h	DS %	DFM kg/h	DS %	DFM kg/h	DS %
16	0	0	0.55	0.27	12.57	0.33	43.51	0.33	39.81	0.36	33.33	0.26	51.85
	4	1.3	0.91	0.48	9.96	0.49	45.25	0.55	39.10	0.55	39.10	0.58	35.75
	8	2.4	1.19	0.67	8.76	0.70	41.88	0.77	35.47	0.75	36.75	0.74	37.17
	12	3.4	1.36	0.87	5.93	0.92	32.95	0.99	26.59	0.97	28.46	0.96	28.83
17	0	0	0.51	0.29	22.48	0.30	39.60	0.34	33.66	0.33	35.64	0.24	51.48
	4	1.3	0.70	0.48	19.60	0.48	31.65	0.55	21.58	0.55	21.58	0.49	30.21
	8	2.4	0.79	0.68	9.72	0.68	14.10	0.73	7.05	0.76	3.846	0.67	14.74
	12	3.4	1.08	0.89	4.29	0.92	18.77	0.94	12.67	1.02	5.633	0.86	20.18
18	0	0	0.48	0.30	21.90	0.28	36.45	0.3	22.91	0.32	33.33	0.22	54.16
	4	1.3	0.80	0.36	37.08	0.47	39.24	0.60	25.31	0.55	31.01	0.47	41.13
	8	2.4	1.00	0.40	49.05	0.68	32.48	0.78	21.82	0.78	22.33	0.66	34.01
	12	3.4	1.23	0.60	34.98	0.87	29.21	1.00	18.51	0.98	20.57	0.89	27.57

DFM* - Dual fuel mode diesel consumption in kg/h

DS** - Diesel saving in %

4.2.4 *Engine emission parameters*

The results of the emission analysis of a dual-mode engine have been shown in this section and the following section also analyzes comparing emission gases at different mahua percentages blending with low-grade coal.

4.2.4.1 NO_X emission

The generation of NOx emissions is predominantly caused by increased combustion temperature and oxygen availability. The combined impacts of engine load, equivalence ratio, and compression ratio on NOx are shown in Figure 4.2.3. Nitrogen gas is treated as inert at an average temperature. When the temperature exceeds 1100^{o}C, it starts reacting [213]. The cylinder pressure and temperature determine the quantity of NOx generated. Increased valance oxygen and nitrogen atoms form due to elevated in-cylinder temperature and pressure, leading to increased NOx emissions at the exhaust. It converts into nitrogen oxide after interacting with oxygen [214]. It can be concluded from Figure 4.2.3 that as the mahua percentages increase from 0 % blending to 25 % blending, the NOx concentration increases. This might be because as the biomass percentage in coal increases, the heating value of PG increases, leading to a rise in engine temperature, and hence NOx increases [215]. The NOx concentration decreases from a further increase of biomass percentage i.e., 25% to 50% blending for every GER and CR value. This might be due to the lowering of intake air that decreases oxygen concentration in the cylinder and eventually reduces NOx emission [216]. From Figure 4.2.3(c), it can be deduced that the magnitude of NOx concentration is lesser in lower load conditions and upsurges with increasing load. This may be due to the fact that at lower load, temperature and pressure inside the cylinder is lower, thus lowering the formation of NOx. Similar characteristics also have been seen in the experiment conducted by Sohan lal et al. [81]. A similar result has also been observed by Chintalal et al. [217]. They found that at a higher biomass blending percentage, the share of H_2 in PG increases, which eventually leads to the

rise in the concentration of NOx emission at high and medium loads while decreasing at low load conditions, respectively. From Figure 4.2.3(b), it can be inferred that the NOx emission is low at low CR, and increases with increased CR. Maximum NOx emitted was 308 ppm at 100 % blending, GER 0.1, CR 18, load 12 kg. In contrast to this, the minimum range of NOx emission can be obtained if gasification performs at 0.43 GER, 12 kg engine load with 16 CR, and without 25% mahua blend.

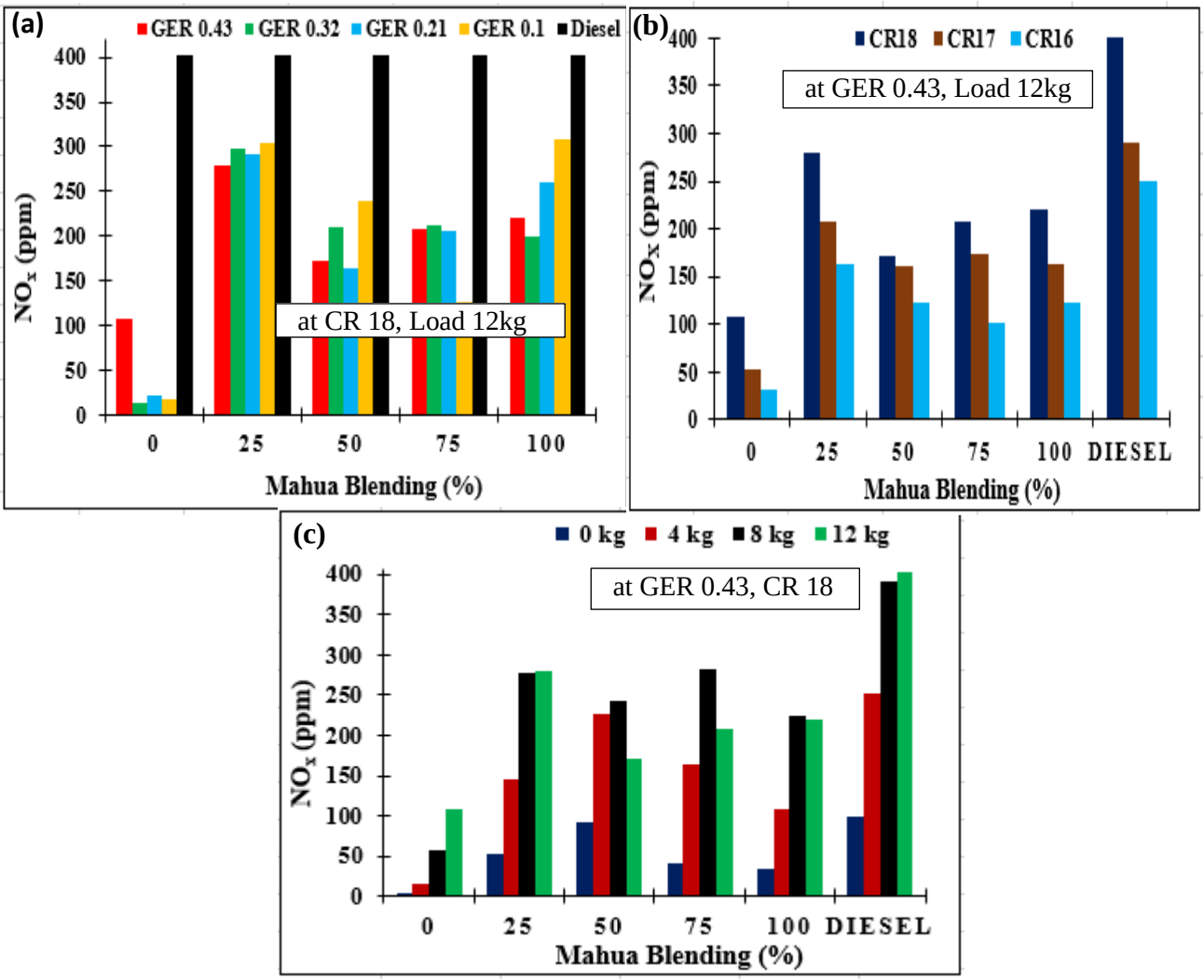

Figure 4.2.3. Variation of (a) GER, (b) CR, and (c) Load on NO_x emission

4.2.4.2 CO_2 emission

Carbon dioxide is the primary contributor to greenhouse gas emissions and global warming [218]. Figure 4.2.4 illustrates the impact of the different operating variables of gasifier-engine on CO_2 emissions. It can be concluded from Figure 4.2.4(a), that as the mahua biomass percentages increases from 0 % to 25 % blending, the CO_2 concentration increases for all GER conditions. This might be due to the higher oxygen contents in biomass based gaseous fuel [23]. Also due to improved combustion process in engine at higher gasifier-ER leads to more CO_2 emission [216] at 0 % to 25 % mahua blending. Further increase in Mahua percentage blending from 25 % to 50 % leads to a decrease in CO_2 emissions, which could be due to its PG consumption in the Boudouard reaction [23]. Figure 4.2.4(c) shows that on an average CO_2 emission of engine initially increases with load up to 4 kg load and later decreases to the full load. Also, as the blending ratio of mahua wood increases in gasification, CO_2 emission decreases. The CO_2 emission in diesel engine indicates the fuel burnt efficiency in the combustion chamber. At elevated combustion chamber temperature, the engine's performance improves by better fuel burning, leading to increased CO_2. A diesel engine works in excess air; at a lower load, cylinder temperature might be too low, which increases with more fuel injection to maintain a constant speed of 1500 rpm with an increment of load. However, at further loading, more fuel is required to led, which may cause more smoke and prevent oxidation of CO to CO_2; consequently CO_2 decreases [219]. The maximum engine CO_2 emission observed was 2.7 % volume at 0 % mahua blending, 4 kg load, GER 0.43, and CR 18. From Figure 4.2.4(b), it can be inferred that CO_2 emission is lower at a lower compression ratio. This is because, at a lower compression ratio, temperature and pressure in the engine cylinder reduces, consequently inefficient combustion of fuel; thus, CO_2 magnitude lowers with the decrease in CR. The maximum CO_2 observed during DF mode was 2.7 %vol which is in a good agreement

with other authors 3.41 %vol [83]. Moreover, in the current study, the CO_2 concentration during diesel mode was observed as 2.1 %vol which is in range of 2.07 %vol by [83].

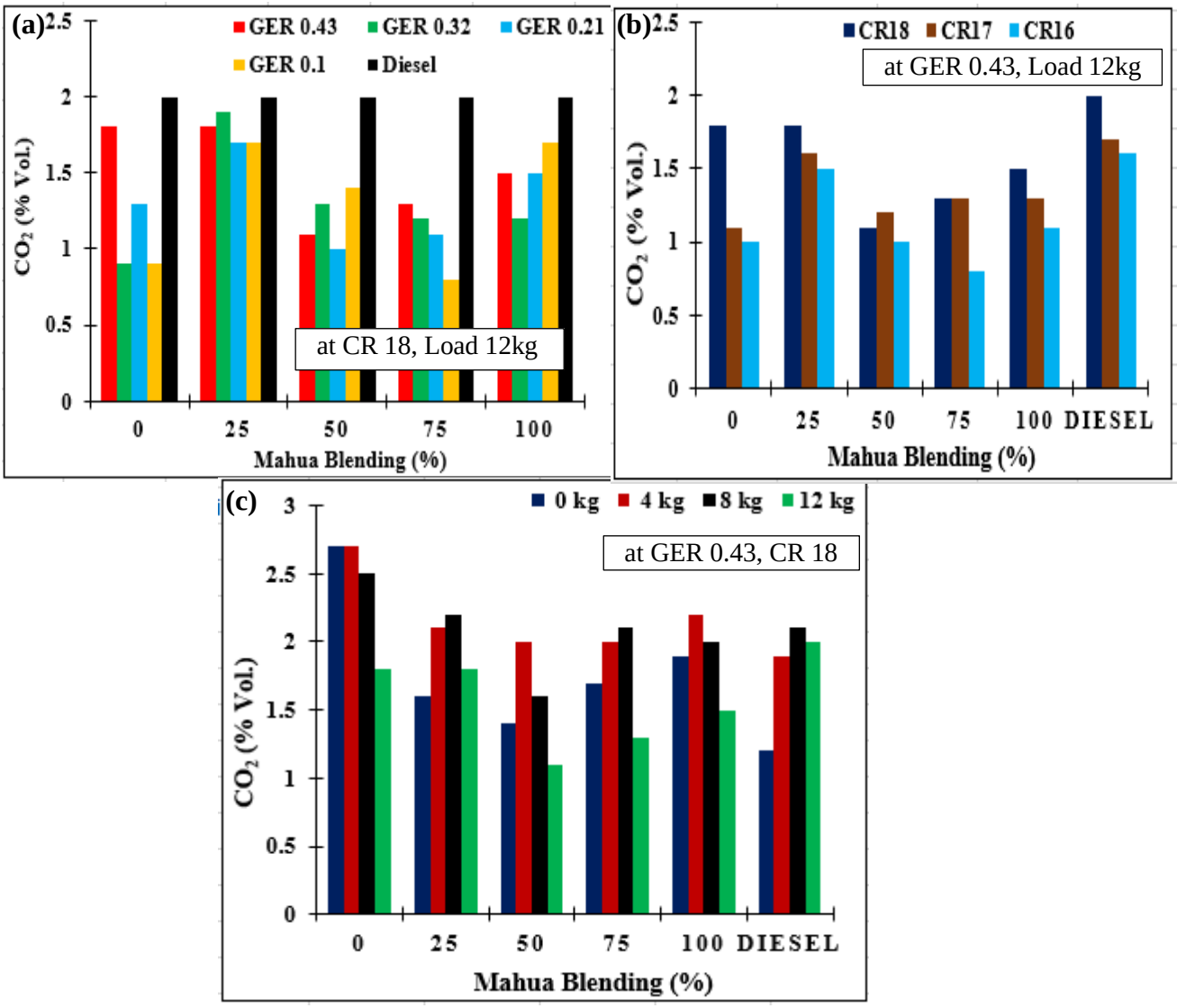

Figure 4.2.4. Variation of (a) GER (b) CR & (c) Load on CO_2 emission

4.2.4.3 Unburnt Hydrocarbon (UHC) emission

The incomplete combustion of the fuels utilized to power the engine results in the emission of unburnt HC. Moreover, the creation of localized over-lean or over-rich mixes, which slow down the reaction rate, and the bulk quenching or extinction of the flame front at the combustion chamber's wallowing to boundary layer formation enhance the generation of HC emission [220]. In the Gasifier-engine operation, operating variables such as GER, engine load, and compression ratio significantly influence HC emission, which is shown in Figure 4.2.5. It can be inferred from Figure 4.2.5 (a and b) that the trend of hydrocarbon concentration increases with an increase in biomass concentration from 0-25 % blending, lowers between 45-65 % blend, and thereafter increases. The maximum HC emission was observed at 100 % Mahua blending at CR 18; however, the HC value is lowest for the blending range 15-90 % in comparison to CR 16 and 17. These results might be due to the variation of the co-gasification product. Because the contents of hydrocarbons from co-gasification processes are higher than coal gasification, and its magnitude increases with biomass fraction in the fuel blends co-gasification [23]. In Figure 4.2.5(c), HC exhaust emission is found to be lower with increasing load. Because, as load increases, elevated combustion chamber temperature leads to better combustion; thus, unburnt hydrocarbon emission reduces. It can be concluded that the favourable operating condition for the lower HC emission could be 45-65 % mahua blend gasification with 0.43 GER and 12 kg load with 18 CR. Maximum HC emission observed during DF engine run was 68 ppm at GER 0.43, CR 18 which is in a good agreement by other authors with 55 ppm [221], 20 ppm [171]. Moreover, during neat diesel run, the HC emission observed was 15 ppm at full load condition.

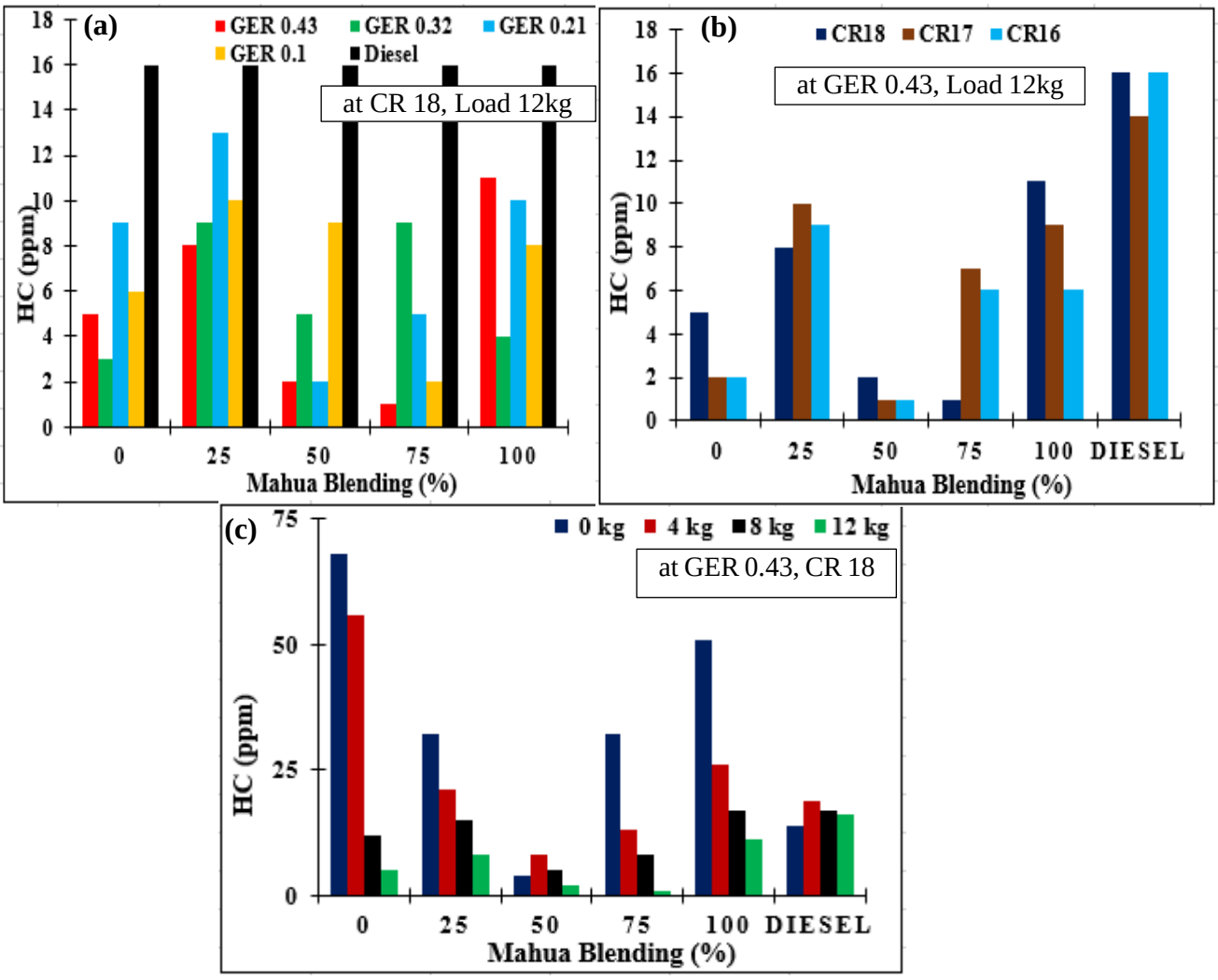

Figure 4.2.5. Variation of (a) GER, (b) CR, and (c) Load on UHC emission

4.2.4.4 CO emission

There are two fundamental reasons for CO emission: incomplete combustion owing to inadequate oxygen supply in the combustion chamber and poor mixture formation**.** Figure 4.2.6 depicts the overall consequence of the load, GER, and CR on CO exhaust emissions. The CO emission decreases as the Mahua percentage increases from 0 % blending to 25 % for every GER, CR, and load conditions. This might be due to the low fixed carbon content of biomass, which causes CO to be decreased as it was consumed in the water gas shift reaction [23]. Maximum CO emission observed was 0.67 % volume at 0 % mahua blending, 0 kg load, GER

0.43, and CR 18. The CO content increases as biomass content increases from 75 % to 100 %. Because there is more oxygen in the sample due to the high biomass concentrations, more carbon dioxide is produced. The Boudouard reaction, which is triggered by high temperature and high CR, consumes CO_2 and increases carbon monoxide production [23]. The maximum CO emission observed during DF mode was 0.47 %vol at GER 0.43, CR 18, 0% mahua blending which is in a good agreement with other authors 0.10 %vol [81], 2.17 %vol [83].

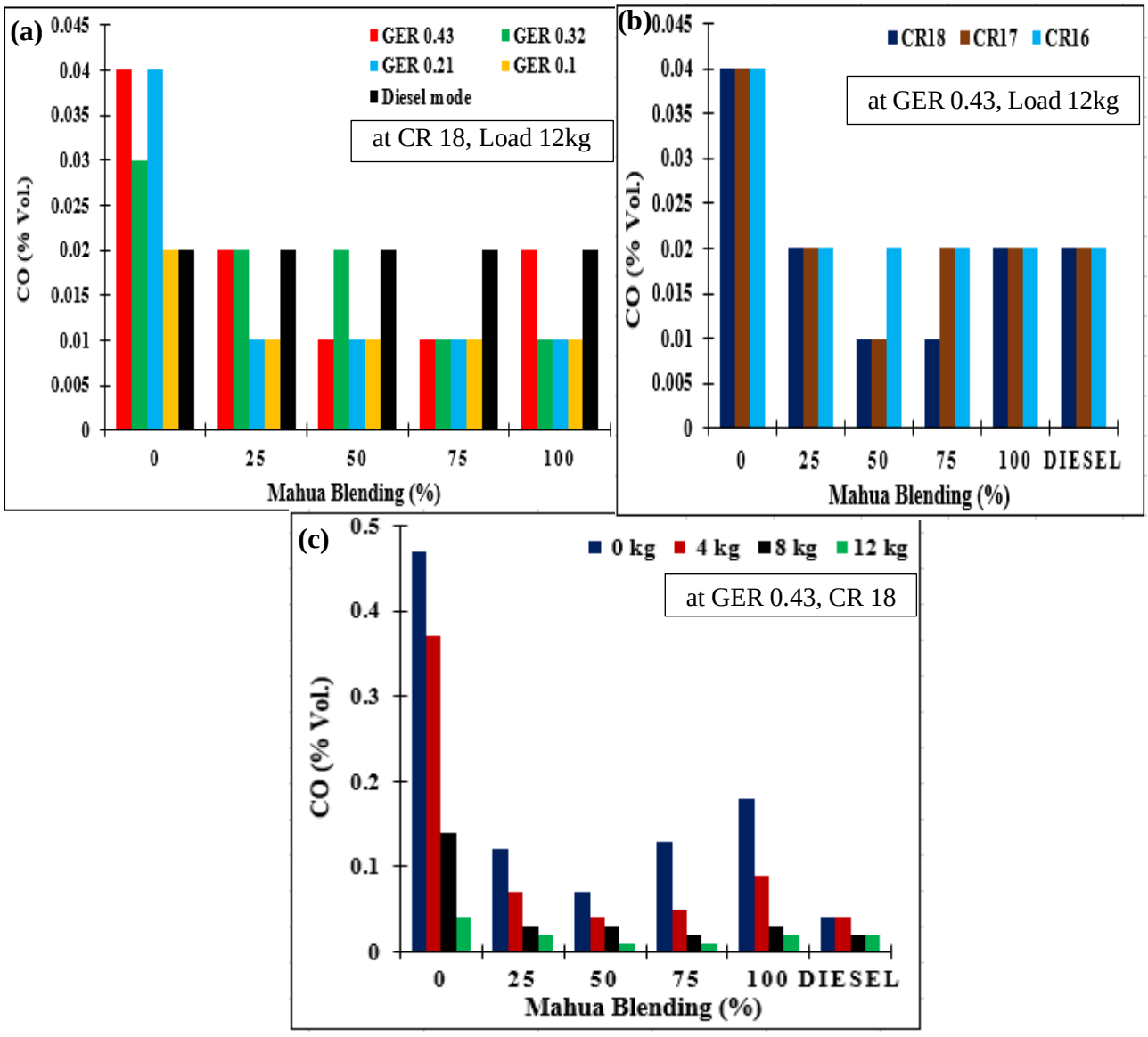

Figure 4.2.6. Variation of (a) GER, (b) CR, and (c) Load on CO emission

4.2.5 *RSM optimisation plot*

In many engineering and industrial applications, there is a need of multiple response optimisation for decision making process. A technique to solve such multifaceted problem is the composite desirability approach. In the current study multiple response output variables, i.e., BP, BTE, CO, HC, CO_2, and NO_X are optimised simultaneously corresponding to the independent input parameters GER, CR, and Engine load using RSM. The combined goals of these parameters is to maximise the performance parameter and minimise the engine emission exhausts. Composite desirability incorporates the shifting of the response variables to a desired value model that lies between 0 to 1 which represents how good the answer resembles its goal values. More the desirability the closer its value to 1 for optimised response variable. Figure 4.2.7 shows the individual composite desirability values, the optimised response output values for maximum engine performance and minimum emissions simultaneously corresponding to optimised input values for every coal-mahua biomass blending percentages. The magnitude of optimised results for input and output responses at every blending percentages are tabulated in Table 4.2.5. The composite desirability value for 0 % mahua blending, 25 % mahua blending, 50 % mahua blending, 75 % mahua blending, and 100 % mahua blending are 0.97, 0.84, 0.87, 0.91, and 0.89 respectively which are very close to 1, Hence the model has high desirability and resembles close to the target value.

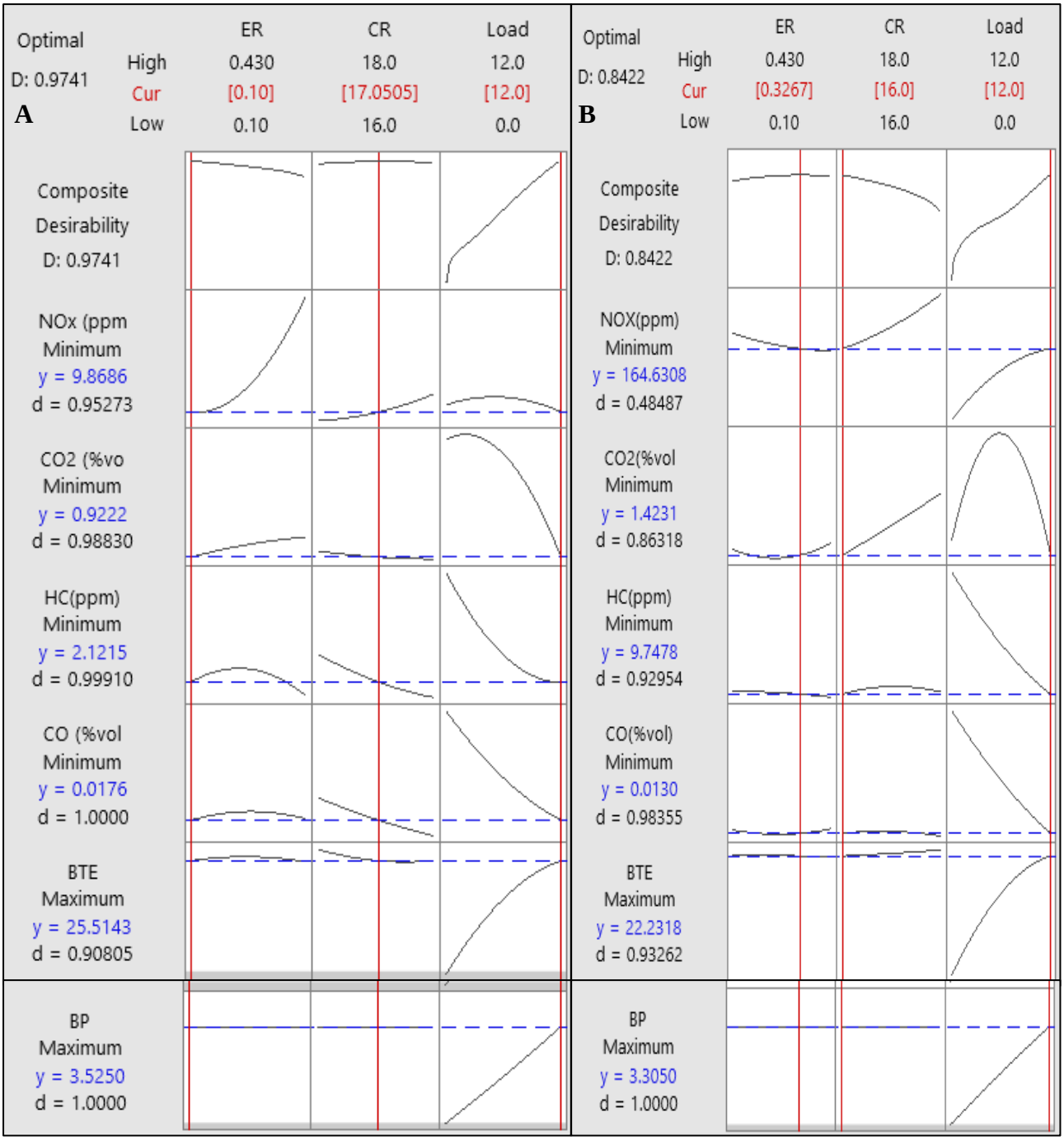

Figure 4.2.7. RSM optimisation plot for (A) 0 % mahua blending, (B) 25 % mahua blending

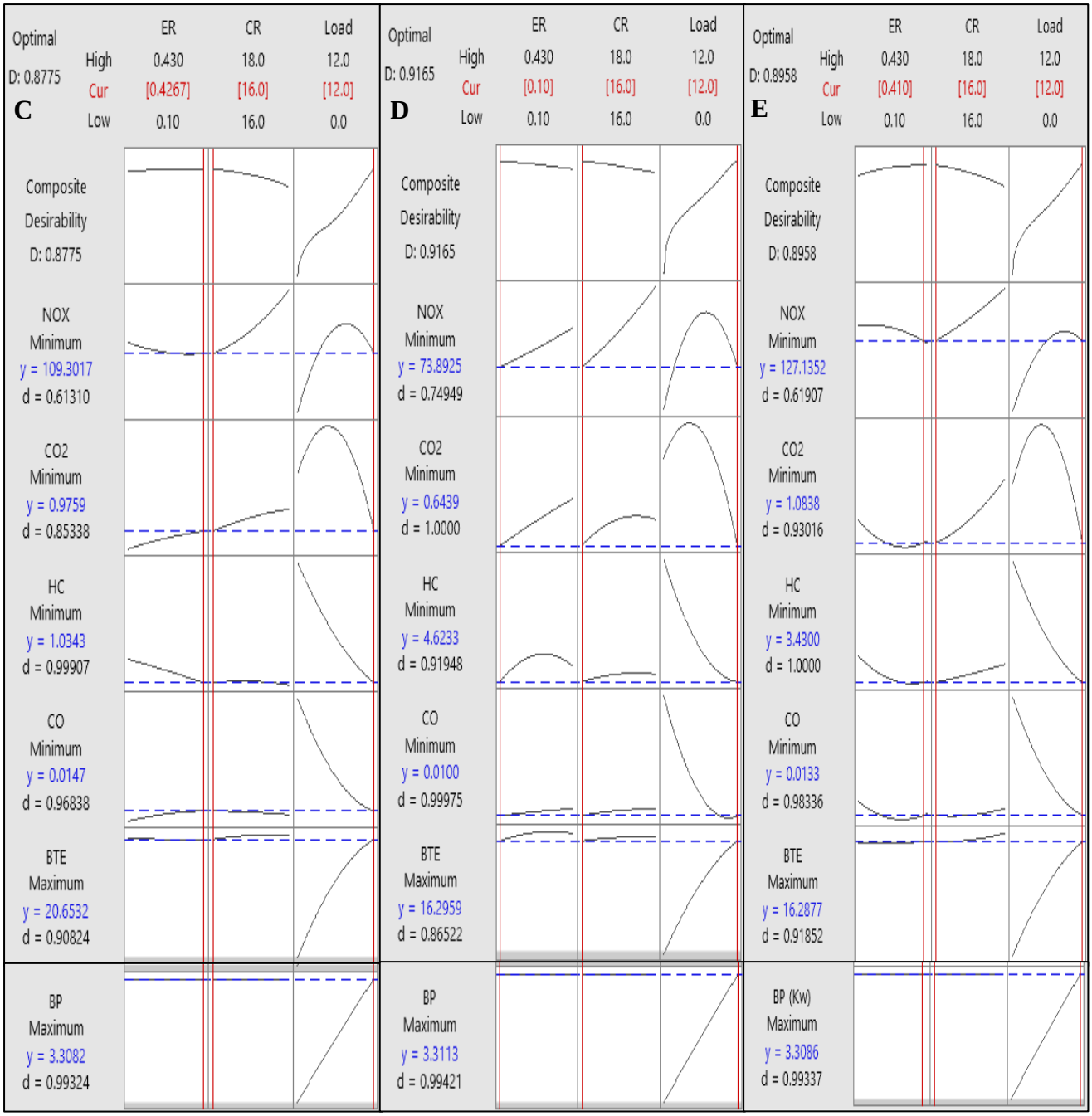

Figure 4.2.7. RSM optimisation plot for (C) 50 % mahua blending, (D) 75 % mahua blending, and (E) 100 % mahua blending

Table 4.2.5. Optimised results for different mahua wood + coal blending

Blending percent	Independent parameters			Optimised Response output					
	GER	CR	Load (kg)	BP (kW)	BTE (%)	CO	HC	CO_2	NO_X
0 % mahua	0.10	17	12	3.52	25.51	0.0176 (% vol.) 0.632 (g/kWh)	2.1215 (ppm) 0.0042 (g/kWh)	0.9222 (% vol.) 0.0585 (g/kWh)	9.8686 (ppm) 0.0654 (g/kWh)
25 % mahua	0.32	16	12	3.305	22.23	0.0130 (% vol.) 0.466 (g/kWh)	9.7478 (ppm) 0.0195 (g/kWh)	1.4231 (% vol.) 0.0903 (g/kWh)	164.6308 (ppm) 1.0924 (g/kWh)
50 % mahua	0.42	16	12	3.308	20.65	0.0147 (% vol.) 0.527 (g/kWh)	1.0343 (ppm) 0.002 (g/kWh)	0.9759 (% vol.) 0.0619 (g/kWh)	109.3017 (ppm) 0.725 (g/kWh)
75 % mahua	0.1	16	12	3.311	16.29	0.01 (% vol.) 0.359 (g/kWh)	4.6233 (ppm) 0.009 (g/kWh)	0.6439 (% vol.) 0.0408 (g/kWh)	73.8925 (ppm) 0.490 (g/kWh)
100 % mahua	0.41	16	12	3.308	16.28	0.0133 (% vol.) 0.477 (g/kWh)	3.43 (ppm) 0.006 (g/kWh)	1.0838 (% vol.) 0.0687 (g/kWh)	127.1352 (ppm) 0.8436 (g/kWh)

4.2.6 *Conclusions*

Hence, present study investigated the performance and emission characteristics of VCR diesel engine (DF) running on producer gas obtained through various blends of coal-mahua wood gasification. The optimum BTE observed during coal gasification was 25.51 % with maximum diesel savings obtained for 100 % mahua blending.

4.3 Co-gasification of Mahua Biomass- Saw dust briquette and dual-fuelled engine performance

4.3.1 *Introduction*

The gasifier-compression ignition engine (G-CIE) system has been an attractive alternative power source to generate decentralized electricity and reduce ecological degradation. However, the major challenge of G-CIE system is to deal with the performance-emissions trade-off via operating settings, consequently, low power and efficiency. Hence, this study aims to generate producer gas (PG) from the co-gasification of mahua wood and saw-dust briquette from the downdraft gasifier and to determine the performance of the G-CIE system with dual-fueled diesel and PG. Further, the novelty of this work is to optimize G-CIE's operating variables, such as gasification equivalence ratio (ER), engine compression ratio (CR), and engine Brake power (BP). To this end, a multi-objective optimization tool, RSM, was applied to employ optimization of the operating setting. Results reveal the optimum operational conditions as 0.10 gasification ER, 16 CR, and 3.18 kW engine BP. The corresponding performance responses are Brake specific fuel consumption (BSFC) 0.1654 kg/kWh, Brake thermal efficiency (BTE) 17.41 %, sound intensity 91.74 db, CO 0.017 % vol., HC 3.83 ppm, CO_2 3.11 %vol., and NOx 1.85 ppm. Maximum diesel replacement observed was 44.76 %, 54.28 %, and 62.75 % at CR 16, 17, and 18, respectively. The average values obtained for R^2 were 95-99% and 0.8380 composite desirabilities. Further, predicted performance responses were compared experimentally at optimized input conditions and found to be a 6.07 % maximum error. Thus, using RSM, the proper operating setting can be found, and results will be guided to end users for more diesel substitution and environmental protection.

Since, gasification of single-source feedstock usually has pros and cons, for instance, coal gasification has environmental issues such as emission of CO_2, H_2S, SOx, NOx, and low reactivity of coal. The problem with biomass gasification is the limited availability of biomass during certain seasons and its scattered distribution, which increases transportation costs [20]. These problems can be improved with the use of co-gasification. Additionally, co-gasification has an advantage over individual gasification in terms of producer gas composition and quality by varying feedstock blending [222]. Therefore, the requirement of upgraded energy with a higher density is essential, and it can be achieved either by co-gasification or by operating a dual-fuel model engine [223], [171], [88]. Also, co-gasification (wood and coal, or wood and briquettes/pallets) has advantages in maintaining feedstock availability due to seasonal occurrence because varieties of biomass and its quantity differ with locations, and their collection and processing are significant constraints [19].

In view of waste-to-energy conversion with improved energy density, the novelty of the present work aims to utilize a compressed wooden saw-dust briquette and mahua wood for co-gasification and integration with a compression ignition engine for power generation. All studies above contributed significantly to the up-gradation in the gasification field, gasification systems for different wood fuels, and coupling with ICE for heat-mechanical-electric conversion. For example, on the co-gasification- sugarcane bagasse and coconut shells [192], petroleum coke and biomass [193], sewage sludge and pine saw-dust [194], saw-dust and bituminous coal [195], biomass, and poly-ethylene wastes [196]. One aspect, specifically in the saw-dust briquette gasification and ICE power generation, gasifier-CI engine integrated parametric performance and its optimization has not yet been reported. Concerning this research gap, the first aim of this study was to promote the waste-to-fuel conversion by waste mahua wood and briquette of saw-dust. In this respect, the first novelty of this study is to determine producer gas from the gasification of mahua wood and saw-dust briquette (50:50)

and application to diesel engine, and subsequent performance analysis of Gasifier-engine in terms of power, exhaust and sound emission, and diesel saving. And, second one is to predict optimization of operating variables for maximizing engine power, and minimizing engine emission and fuel consumption using the multi-objective response surface methodology.

To accomplish these objectives, an experiment was conducted to investigate the performance of mahua wood and saw-dust briquette (SDB)-based gasification on different equivalence ratios than of dual fuel mode CI engine on variable compression ratio and load. Finally, optimization was conducted for input operating conditions (50:50 biomass to briquette gasification equivalence ratio, engine CR, BP) of the gasifier and dual fuel mode engine variables for better response on gasification and engine performance as well. Regarding previous work on optimization, Yusri et al. [106] concluded that artificial neural network (ANN) and RSM are better techniques for building the relationship between the output and input variables of spark ignition (SI) and CI engine and optimizing. Although, the RSM model has been considered a better performance technique than the ANN approach [107]. RSM is a combination of detailed statistics and mathematics, as well as modeling and optimization, that corresponds to numerous factors in the response of large data sets. RSM-based optimization has recently been popular owing to its high-level accuracy and sensitivity in reaching collective understanding and reacting, the shortest time to finish the process by reducing the number of data sets, and the capacity to provide a suitable matrix for testing [107], [108], [109]. Further, Table 4.4.1 shows the recent work, where most previous work is associated with modeling and optimization, and few are related to the experimental and respective optimization approaches. However, none of the work has been found related to dual feedstock gasification particularly mahua wood and SDB, and subsequently dual fuel mode engine performance analysis and operational optimization. On the basis of this research gap and novelty, the current study aims

to ensure the suitability of SDB-based PG with diesel in ICE for power generation with the following objectives:

- Compatibility study of the gasifier-engine system with dual-fuelled mode engine operation using mahua wood and SDB-based PG and diesel fuel.
- Comprehensive performance assessment of the dual-fuelled mode on engine power output, exhaust, sound emission, and specific fuel consumption with varying gasification ER, engine CR, and BP.
- Determination of optimum ER of the gasifier, CR, and BP for the best response of power, emission, and fuel consumption using the RSM.

Results of the above analyses provide key insights into the gasifier-engine system for generating producer gas from 50:50 mahua wood waste and saw-dust briquette feedstock and reveal the balanced operating setting for diesel fuel-saving strategy with a balanced between engine power and emission trade-off. Thus, this study will be a substantial reference platform for end-users and researchers with respect to co-gasification and engine application.

Table 4.3.1. Comparative previous work and the present study

Type of engine	Investigation method	Optimization technique	Fuels	Optimization Parameter	Ref.
CI Engine	Simulation-ANN	RSM	Biodiesel-Diesel blend	Biodiesel ratio, Engine load, Injection pressure	[109]
CI Engine	Experimental	RSM	Babool wood PG and Biodiesel	Engine load, pilot fuel injection timing, and pressure	[167]
CI engine	Simulation-ANN	RSM	Diesel blended with Acetylene	Acetylene blend, injection timing, pressure, CR,	[224]
CI Engine	Experimental	RSM	Biodiesel and Producer gas	Load, CR, Injection timing	[168]
CI Engine	Simulation-Fortran	RSM	Babul wood PG and diesel	blending ratios, CR, and Injection timing	[169]
CI Engine	Experimental	RSM	Diesel and cocoa pod husk-PG	Brake power and Compression ratio	[170]
CI Engine	Experimental	RSM	Coal PG and Diesel	Gasification ER, engine load, and CR	[35]
CI Engine	Experimental	RSM	Mahua-Briquette PG and diesel	Gasification ER, CR and BP	**Present work**

4.3.2 *Properties of feed-material*

Briquette and *Madhuca Indica* (Mahua wood) are the chief feedstocks for this experimental analysis. These feedstocks were collected from ghat areas near Varanasi, India, and are primarily grown and transported from the central and northern regions and forests of the Indian subcontinent. The briquette biomass used in the experiment had a diameter of approximately

95 mm and a thickness of 30-35 mm, while the Mahua wood feedstock had dimensions of 40-60 mm in length, 30-40 mm in width, and 20-25 mm in height shown in Figure 4.3.1(a). The gasified biomasses are shown in Figure 4.3.1(b). The chemical properties of briquette biomass and mahua wood are shown in Table 4.3.2. Typical moisture contents of freshly cut mahua wood and saw-dust briquette range from 30–60%, whereas most gasification systems use dry-fed biomass with 10–20% moisture content to generate a reasonably high product gas heating value [225]. In the current study, the moisture content of briquette and mahua wood dropped to around 7-9wt% after drying (Table 4.3.2). The moisture content influences the heating values of feedstocks. The studies suggested that an increase of the moisture content by approximately 5–50% leads to a large decrease of gasification efficiency as suggested by [225].

Figure 4.3.1. Briquette & Mahua wood feedstock: (a) Before gasification (b) After gasification

Table 4.3.2. Properties of feedstocks [178, 226, 227].

Characteristics	**Value**	
	Briquette	**Mahua Wood**
***By Proximate analysis, (wt.%)*:**		
Ash content	3.11	2.08
Fixed carbon	9.41	12.63
Moisture content	8.85	7.88
Volatile matter	78.63	77.05
***By Ultimate analysis (dry basis wt.%)*:**		
Carbon	40.52	47.57
Hydrogen	8.61	6.4
Oxygen	38.90	44.96
CV (MJ/kg)	19.10	25.88
Cellulose (wt%)	43.6	37.92
Hemicellulose (wt%)	27.4	27.33
Lignin (wt%)	29.0	14.20
Mass analysis		
Feedstock Input (kg)	20	20
Char residual left (kg)	8.95	9.30
After gasification- Residual CV (MJ/kg)	82.97	116.80
Producer gas composition		
CH_4 (%)	1.535	
CO (%)	20.38	
CO_2 (%)	12.94	
H_2 (%)	14.77	
N_2 (%)	50.36	
PG calorific value (MJ/Nm^3)	3.21	
Tar content (g/Nm^3)	~0.02-4	

4.3.3 *RSM normal probability plots and Pareto chart*

RSM is a valuable tool for the design of experiments and can save time and resources by reducing the need for actual experimental runs. The flow chart representing the techniques of

RSM is depicted in Figure 4.3.2. In the present study, the independent parameters are ER, CR, and engine BP, and corresponding output responses are analyzed using the RSM tool. Moreover, the Normal probability plots and Pareto charts are used to analyze the impacts and efficiency of a model using the RSM technique. Normal probability plots use standardized residuals and normal percentage probability values to illustrate the significance of the model. At the same time, Pareto charts show critical values of standardized significances and statistically significant input parameters. Horizontal bars crossing the reference line on the Pareto chart indicate impactful input parameters.

4.3.3.1 Normal probability and Pareto curve for performance responses

The normally distributed experimental data and most significant input parameter for engine output responses are well analyzed from normal probability plots and Pareto charts, as shown in Figure 4.3.3. All output response points are scattered across a normal, theoretically distributed straight line. The closeness of these response points from a normally distributed line predicted an efficient model with less error in exact value and predicted value. Figure 4.3.3 shows that all normal probability curves of engine response, i.e., (a) BSFC, (b) BTE, and (c) Sound, lie close to the normally distributed center line. Hence the errors are normally distributed, and the model is efficient as predicted by a normal probability plot. Also, Figure 4.3.3 shows the Pareto charts of BSFC, BTE, and sound intensity, respectively, for encountering the most influential independent parameter terms in predicting the engine output responses. In the BSFC Pareto chart, the bars that influence the variables most are linear terms (C) and square terms (CC, BC), as these bars cross the vertical reference line 2.02. Thus, from the Pareto plot of BSFC, the most significant term for predicting the model is BP. Similarly, the BTE Pareto chart's horizontal bars influencing the variables are C, CC, and AC, as these

terms cross the vertical reference line at 2.02. The current model terms indicate that these parameters are statistically significant at the $\alpha = 0.05$ level. In the Pareto chart of sound intensity, the most significant term is linear term C which is BP, as the bar C crosses the maximum reference line at 2.02. Hence, this variable is statistically significant at $\alpha = 0.05$ level for the existing model. This is attributed to the fact that the experiment was conducted with varied BP at a constant speed of 1500 rpm. And, as engine BP increases, the fuel supply of the diesel engine increases to maintain 1500 rpm through the governor mechanism, resulting in the enrichment of fuel in the air-fuel mixture inside the cylinder, producing more sensible heat to generate piston work with mass of fuel along with its calorific value (i.e., MJ/kg). Moreover, corresponding to BP change, the variation in the amount of heat generated during combustion (MJ) is higher than that of ER and CR.

4.3.3.2 Normal probability and Pareto curve for emission response

Figure 4.3.4 shows the normal probability plots and Pareto charts for engine emissions CO, HC, CO_2, and NO_X. The x-axis of normal probability plots shows the residuals and the y-axis shows the normal percentage probability plots of the dependent parameters. Figure 4.3.4 shows that CO, HC, CO_2, and NO_X emissions residuals are normally distributed across a straight line, which implies that errors are distributed normally. The figure also shows the Pareto charts for engine emissions depicting that the linear term BP is the most significant deciding input variable for CO emission, HC emission, and CO_2 emission, but for NO_X emission, the square term, AC, that is, ER*BP is the most significant term as the bar crosses the reference line at 2.02. Hence the experimental trials are in good agreement with the model predicted by these plots at $\alpha = 0.05$.

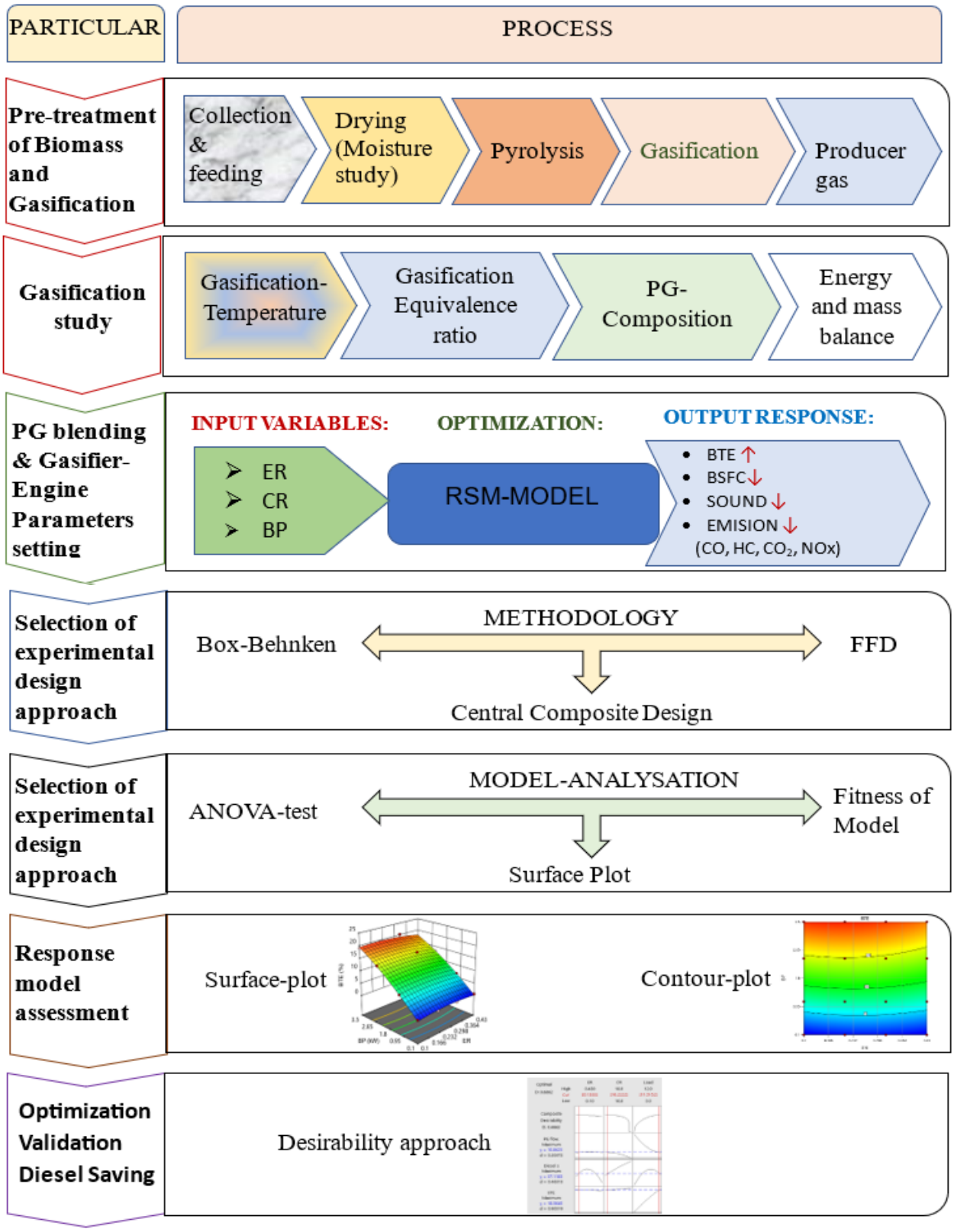

Figure 4.3.2. Flow chart of the gasification-engine study with RSM

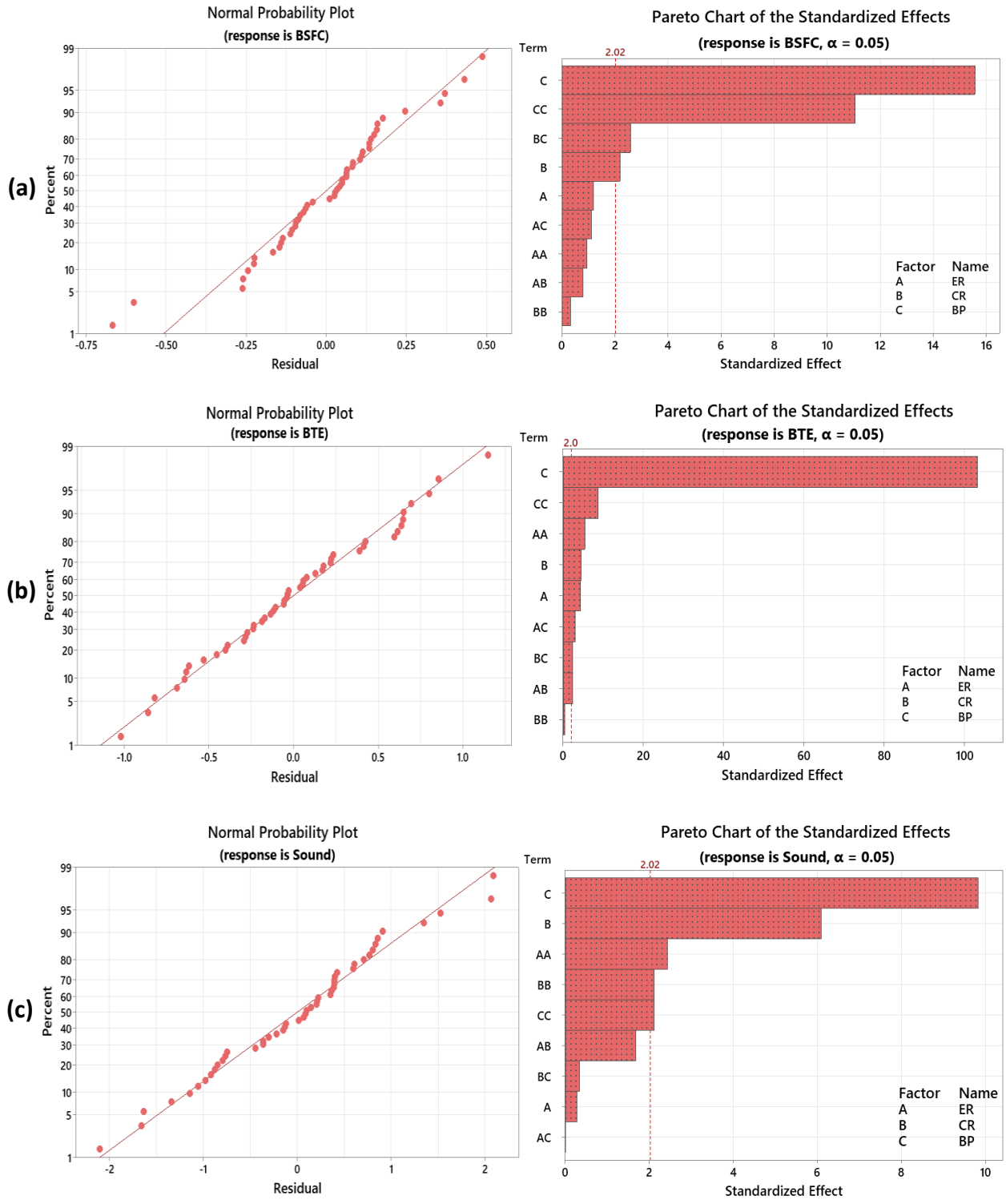

Figure 4.3.3. Normal probability plot and Pareto chart of engine responses: (a) BSFC, (b) BTE, and (c) Sound

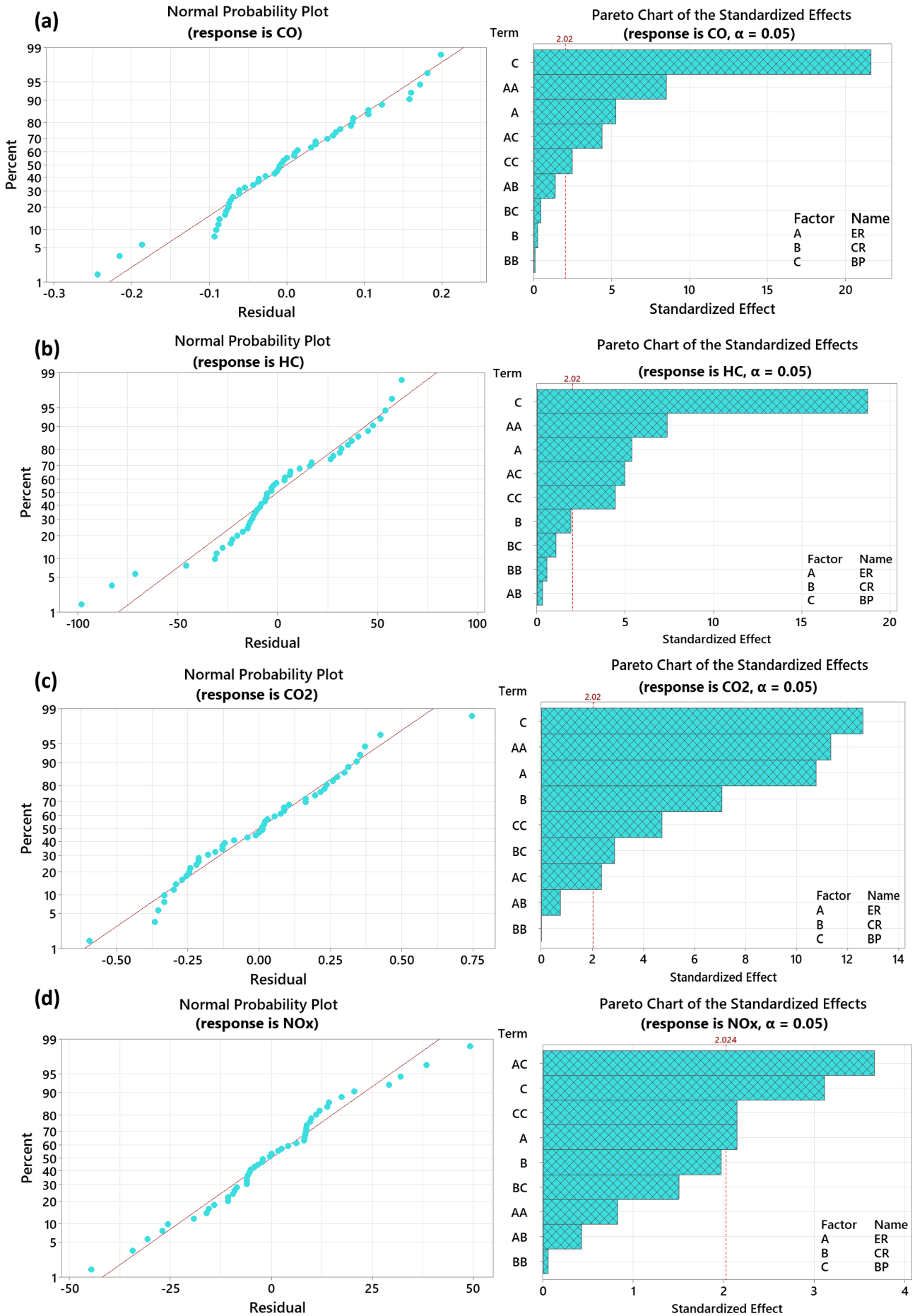

Figure 4.3.4. Normal probability plot and Pareto chart of emission responses: (a) CO, (b) HC, (c) CO_2, (d) NO_X

4.3.4 *RSM regression analysis*

The engine output responses are decided by three independent parameters: ER, CR, and BP. A regression equation was developed from these input variables that have linear terms, 2-way interaction terms, and quadratic terms. These regression equations use first-order response surface models to predict the equations of responses. The response models are well depicted from equations (4.3.1) - (4.3.7).

BSFC, (kg/kWh) = 21.9 - 8.20 ER - 1.76 CR - 4.530 BP + 4.21 ER*ER + 0.037 CR*CR + 0.4810 BP*BP + 0.422 ER*CR - 0.380 ER*BP + 0.1323 CR*BP (4.3.1)

BTE, (%) = 8.5 + 42.6 ER - 1.73 CR + 4.88 BP - 30.31 ER*ER + 0.066 CR*CR - 0.4830 BP*BP - 1.560 ER*CR - 1.305 ER*BP + 0.1562 CR*BP (4.3.2)

Sound (db) = 265.2 + 28.6 ER - 22.3 CR - 0.64 BP + 31.7 ER*ER + 0.709 CR*CR + 0.270 BP*BP - 2.65 ER*CR + 0.001 ER*BP + 0.051 CR*BP (4.3.3)

CO, (% vol) = -1.08 + 6.65 ER + 0.147 CR - 0.309 BP - 9.14 ER*ER - 0.0025 CR*CR + 0.0262 BP*BP - 0.177 ER*CR + 0.3610 ER*BP - 0.0059 CR*BP (4.3.4)

HC, (ppm) = -1030 + 1182 ER + 162 CR - 226.9 BP - 2603 ER*ER - 5.19 CR*CR + 15.33 BP*BP - 13.6 ER*CR + 134.9 ER*BP + 4.33 CR*BP (4.3.5)

CO_2, (% vol) = 2.6 + 9.27 ER + 0.06 CR - 1.689 BP - 34.09 ER*ER + 0.0000 CR*CR - 0.1391 BP*BP + 0.273 ER*CR + 0.544 ER*BP + 0.0994 CR*BP (4.3.6)

NO_X (ppm) = 207 - 152 ER - 14 CR - 98.8 BP - 172 ER*ER + 0.31 CR*CR + 4.39 BP*BP + 10.7 ER*CR + 58.5 ER*BP + 3.61 CR*BP (4.3.7)

4.3.5 *Performance parameter*

4.3.5.1 Brake-specific fuel consumption

The fuel consumption relying on brake power is known as brake-specific fuel consumption. The BSFC gives an approach to determining fuel usage. Figure 4.3.5a shows the simultaneous effect of independent variables on the BSFC. Results obtained from surface plots suggest that BSFC drops as the BP increases. At higher loads, combustion efficiency improves, reducing the fuel required per unit of brake power produced. Experiments show that the mass flow rate is higher in dual-mode fuel consumption, leading to higher BSFC than diesel mode. The graph shows that as the CR is increased, the brake-specific fuel consumption reduces slightly. This might be because as CR increases, the mean effective pressure and the mechanical efficiency increase leading to less fuel consumption [228]. From the experiment, it can also be inferred that as the gasifier's ER increases, the producer gas's heating value decreases, increasing thermal efficiency and reducing BSFC accordingly. The minimum and maximum magnitude of BSFC observed from the experiment was 0.1621 kg/kWh at 0.32 ER, 17 CR, and 3.5 kW engine BP and 3.3549 kg/ kWh at ER 0.43, CR 16, and 0.1 kW BP conditions.

4.3.5.2 Brake thermal efficiency

The brake thermal efficiency of an engine is the relative measure of available work at the crankshaft to thermal energy provided by the fuel at the same time. The 3D surface plot of brake thermal efficiency at three independent variables is shown in Figure 4.3.5b. From the experiment, it can be inferred that BTE in dual-fuelled mode is lower than in diesel-run mode. Because of the low fuel mixture strength caused by the short period of diesel spraying in dual mode, the delay times prolong [85]. When the engine BP is increased, the BTE improves. This is due to the increased engine load resulting in higher combustion efficiency. The fuel ignition

delay is reduced as the average temperature rises at higher loads, resulting in an improved BTE. With an increase in CR, there is a slight increase in BTE. This might be because as CR increases, the temperature and the pressure within the cylinder increases, increasing the probability of PG undergoing complete combustion. Experiments show that in dual-fuelled mode, when ER increases, BTE increases up to ER 0.3, then decreases. This is because the heat energy supplied by the PG decreases with the rise in gasifier equivalence ratio up to 0.3, leading to reduced heat input by the fuel inside the cylinder. Thus, thermal efficiency increases up to that point. The maximum BTE observed in diesel mode is 29.64 % and 20.44 % in dual fuel mode at ER 0.21, CR 18, and 3.5kW engine BP running at 1500 rpm, respectively. The maximum BTE in diesel and dual fuel modes, according to Yaliwal et al. [185], was 24 % and 19 %, and 26.9 % and 23.5 % by N. Homdoung [229], respectively, which is in close conformity with the present investigation.

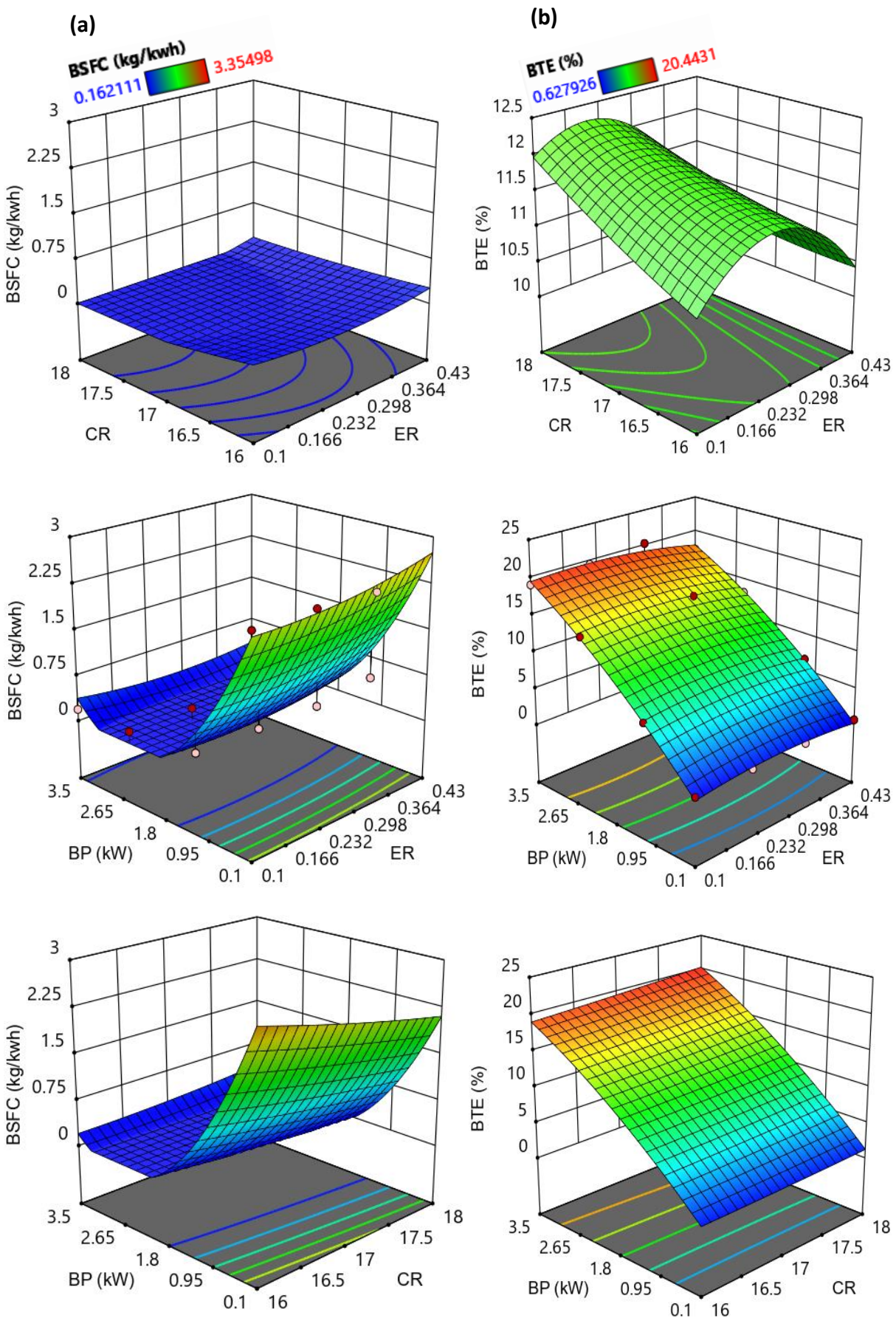

. **Figure 4.3.5.** 3D Surface plots of (a) BSFC (kg/kWh) and (b) BTE (%)

4.3.5.3 Diesel Replacement

The introduction of gaseous fuel, i.e., PG and diesel in dual-fuelled CI engines, reduces diesel fuel consumption. Table 4.3.3 shows the air and fuel flow in diesel and dual modes with percentage saving on diesel. As the CR increases, the expenditure of gaseous fuel PG increases. This might be because as the CR increases, the temperature develops within the cylinder, which assists the combustion of PG fuel. Maximum diesel replacement at CR 16, CR 17, and CR 18 was 44.76%, 54.28%, and 62.75% at a BP of 2.4 kW, 1.1 kW, and 1.1 kW, respectively. At maximum load conditions, the fuel replacement decreases as the engine BP increases. This may happen due to higher load conditions; a rich fuel mixture is required for running the engine at a constant 1500 rpm. The maximum diesel replacement estimated by Sombatwong et al. [230] was 64.21 %. Similarly, Yaliwal et al. [185] recorded a maximum reduction in fuel usage of 65 % while using dual-fuel mode. The present analysis of operating the VCR engine on dual-fuel mode with mahua wood and briquette as the biomass feedstock for co-gasification has a maximum diesel replacement of 62.75%, which is in good agreement with the literature review. Thus, it's economical to use gaseous fuel blended with diesel to upsurge diesel saving in a dual-fuel mode CI engine. This can also be inferred that diesel replacement was maximum at high CR and lower BP conditions, as depicted from the surface plot in Figure 4.3.6(a).

Table 4.3.3. Investigation of Diesel-mode and Dual-mode diesel saving

CR	Load (kg)	BP (kW)	Diesel-mode		Dual-mode		Diesel saving (%)
			Air (kg/h)	Fuel (kg/h)	Air (kg/h)	Fuel (kg/h)	
18	0	0.1	29.43	0.43	17.49	0.18	58.42
	4	1.1	28.23	0.71	17.19	0.26	62.75
	8	2.4	27.83	0.98	17.19	0.38	60.5
	12	3.5	27.43	1.11	16.88	0.57	48.44
17	0	0.1	29.45	0.39	17.49	0.24	38.27
	4	1.1	28.91	0.69	17.19	0.33	52.14
	8	2.4	28.11	0.91	17.19	0.47	48.10
	12	3.5	27.58	1.06	16.88	0.62	40.93
16	0	0.1	29.56	0.39	17.49	0.31	20
	4	1.1	28.92	0.64	17.49	0.39	37.69
	8	2.4	28.13	0.84	17.19	0.48	43.02
	12	3.5	27.85	1.06	16.88	0.65	38.13

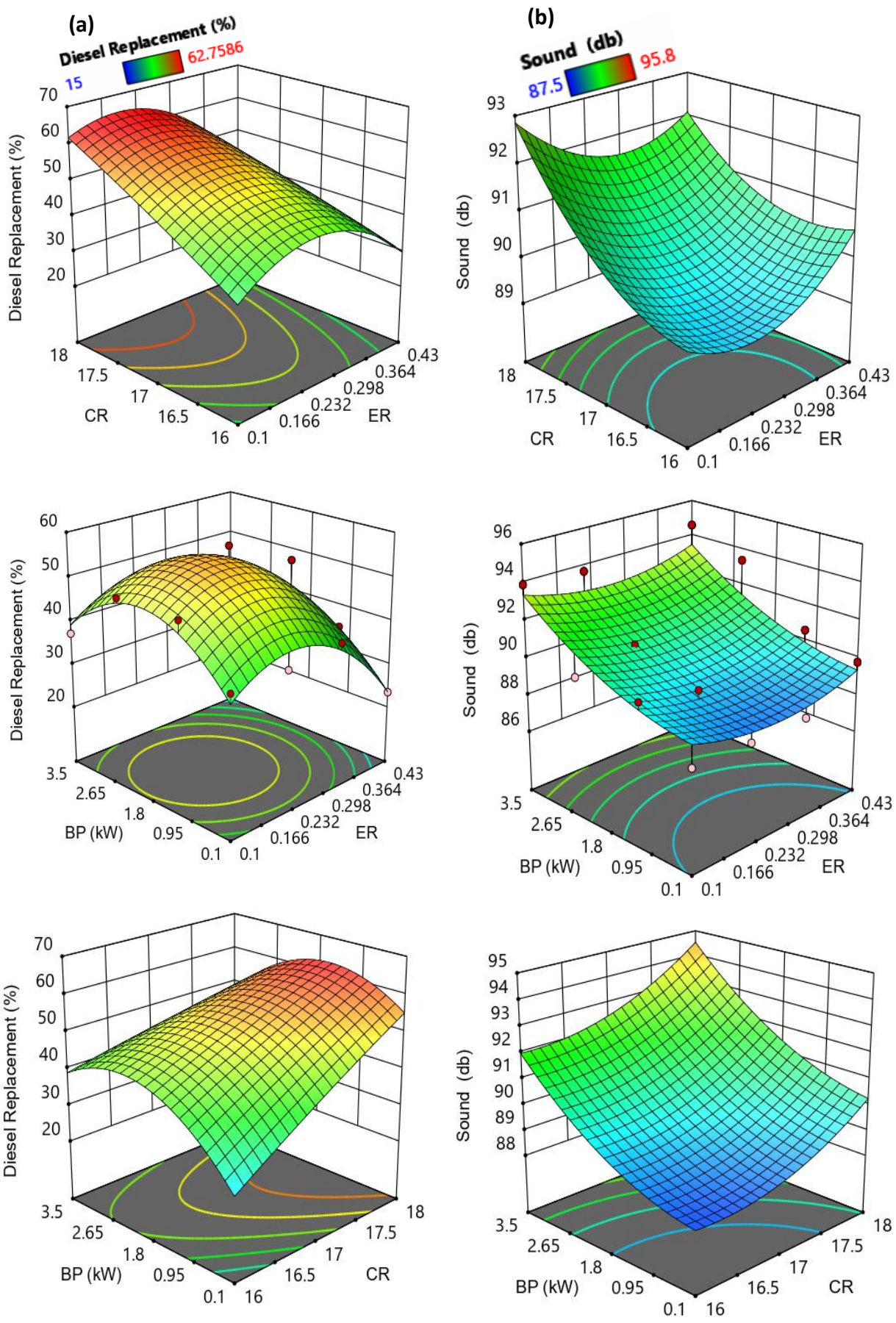

Figure 4.3.6. 3D Surface plots of (a) Diesel replacement (%) and (b) Sound (db)

4.3.5.4 Sound intensity

The primary source of noise in a vehicle is the high sound intensity from an engine. As a result, the sound parameters of the test engine were monitored during the whole experiment. Mechanical processes, gas flow, fuel properties, and combustion are the diesel engine's chief sources of noise generation [231]. Figure 4.3.6(b) shows the simultaneous influence of independent parameters, ER, CR, and BP, on the sound intensity. It can be inferred from the surface plots that the intensity of sound is high at CR 18 and the maximum BP condition. This might be due to the fact that as load increases, the vibration of the engine parts increases. The digital sound level meter (MECO instrument, model – 970P) measures the intensity of sound or noise from the engine. From the experiment, the sound level recorded in the diesel mode lies in the range of 89.2-96.2db, and while operating the VCR engine in dual-fuel mode, the intensity of sound recorded was 87.5-95.8db, respectively. During dual fuel mode, the density and the viscosity of the fuel decrease due to the high temperature of PG admitted inside the combustion chamber, making the engine runs smoothly. Thus, sound intensity reduces marginally while operating the VCR engine in dual-fuel mode. The maximum sound intensity recorded during dual-fuel mode was 95.8 db at CR 18 and, 3.5 kW engine BP. The results obtained from the present experiment agree with environmental norms, i.e., Environment Protection Rules 1986 [232]. According to Singh et al. [233], the noise in diesel mode is 82.7-87.1 db, whereas, in dual-fuel mode, it is 82.9-90.1db. Sharma et al. [85] found that the maximum sound levels measured were 98.90 db for diesel and 98 db for dual fuel modes, respectively.

4.3.6 *Emission analysis*

4.3.6.1 CO emission

When fuels are burnt inefficiently, carbon monoxide (CO) is formed, an odorless and colorless gas. The fuel decomposition and oxidation rate are the primary sources of CO formation. Results from the experiment revealed that the CO emissions from standard diesel mode are less than from dual-fuelled mode engines. This might be because in dual-fuel mode, the oxygen content in PG is comparatively low, making it difficult for complete combustion, and thus CO content increases. The maximum CO emission during diesel mode was 0.02 % volume at 12 kg load, while it was 1.14 % volume at ER 0.21, CR 18, and 0.1-kW load conditions. Figure 4.3.7(a) shows the 3D surface plots of CO emissions with their associated impact on independent parameters. The figure shows that CO content falls with an increase in engine BP. This might be because as load increases, the engine requires a rich fuel mixture that assists complete combustion; hence, CO concentration decreases. The CO contents increase with a rise in gasifier equivalence ratio up to ER 0.3 and then decreases. This is again due to better flame propagation and a rich mixture leading to complete combustion after ER 0.3 [216]. Results from the experiment inferred that though the CO emissions decreased at high ER, the magnitude of CO emissions was still higher than the emissions from standard diesel mode, as shown in Figure 4.3.8. The maximum magnitude of CO emission increased to 10.5 times in dual- mode at CR 18, ER 0.43. The minimum concentration of CO emission observed was 0.05 % volume at ER 0.43, CR 18, and 3.5 kW BP in dual fuel mode.

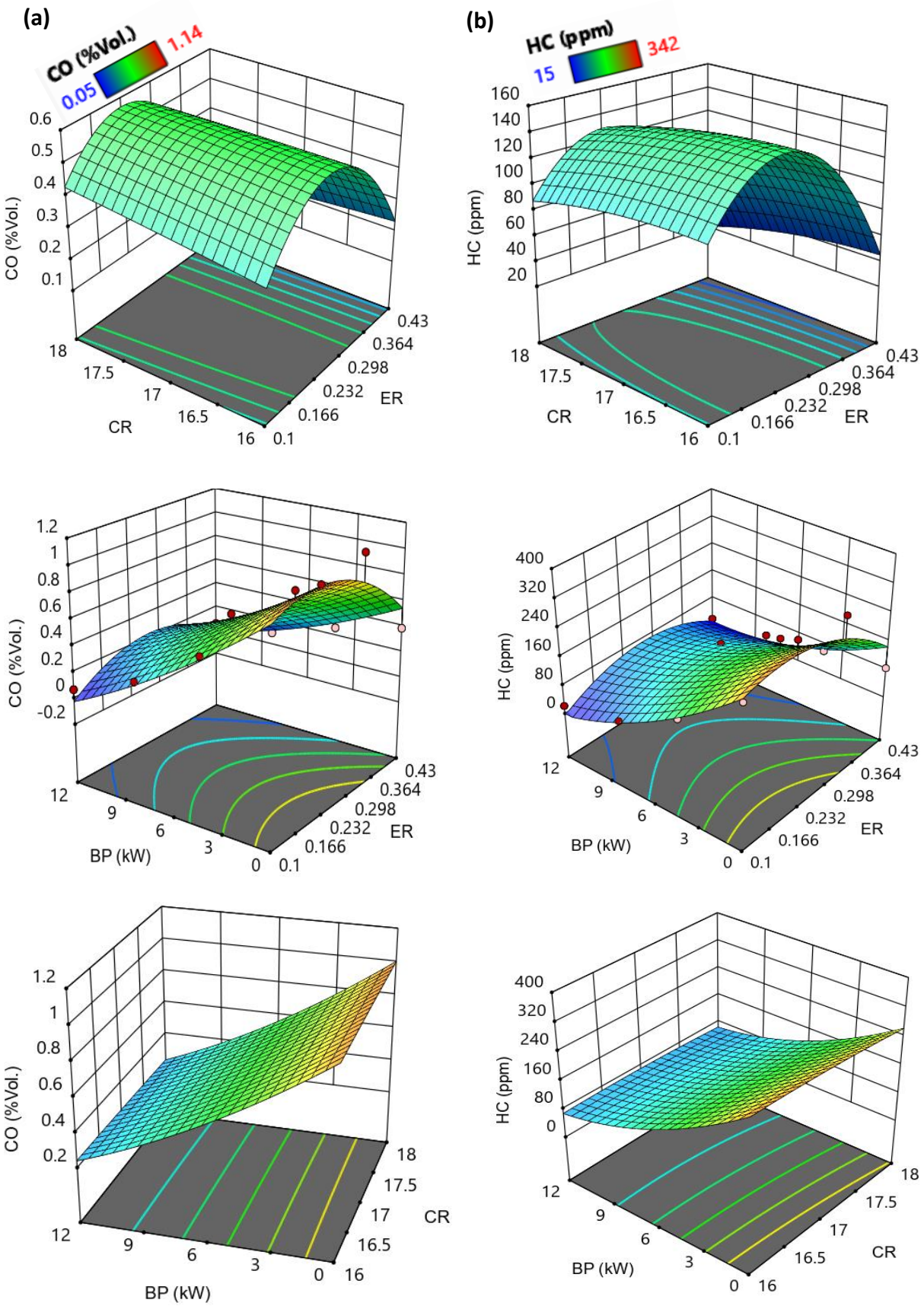

Figure 4.3.7. 3D Surface plots of (a) CO (% vol.) and (b) HC (ppm)

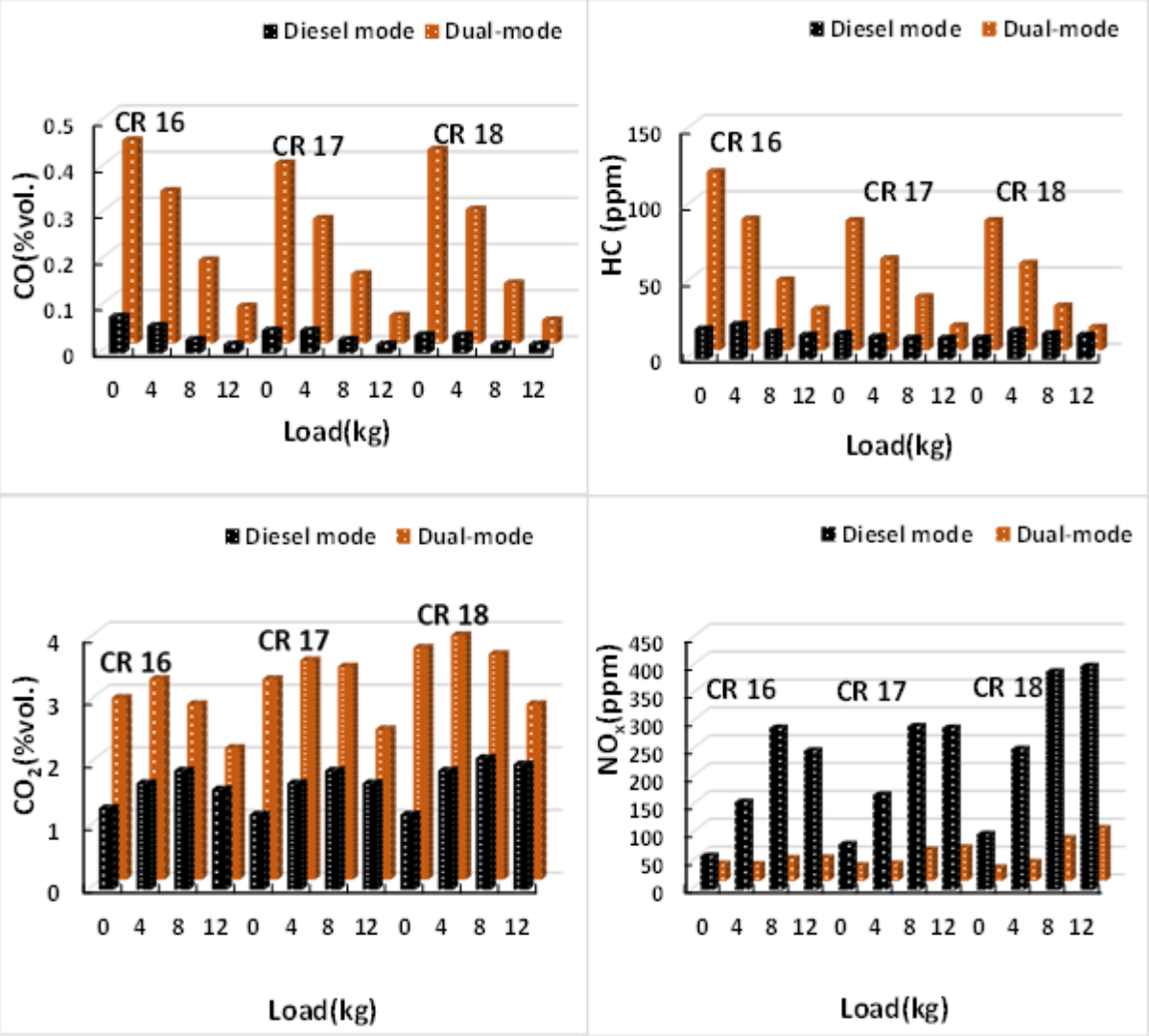

Figure 4.3.8. Engine emissions at diesel-mode and Dual-mode

4.3.6.2 HC emission

Hydrocarbon emissions are the principal pollutant of concern due to unburned or partially burned fuel. The amount of hydrocarbon in the exhaust determines the execution of the combustion process [234]. Figure 4.3.8 depicts the magnitude of unburned HC emissions simultaneously during diesel and dual-fuel modes. From the experiment, it can be inferred that the maximum HC emissions increased to 6.07 times more than a standard diesel fuel mode. This is due to more improper combustion in dual fuel mode. Figure 4.3.7(b) shows the surface plots of HC emission and its impact associated with independent parameters simultaneously. It can be inferred from the graphs that HC decreases as the CR increases. This might be due to,

at a higher CR, the pressure of the fuel mixture and temperature inside the cylinder rises, resulting in an increase in the probability of complete combustion of fuel. In the present work, the maximum HC emissions are a severe problem running the engine at lighter loads in diesel engines as it increases the chances of unburned fuel leading to an increase in HC emission at light loads. During dual-fuel mode, it can be noticed from the surface plot that the HC concentration increases as the gasifier equivalence ratio rises from ER 0.1 to ER 0.43, and then HC emissions decreases. This might be because as the ER increases, the PG fuel flow increases, making the fuel mixture rich and promoting flame propagation leading to the complete combustion of fuel. Consequently, HC emissions decrease significantly at high ER [216]. The maximum magnitude of HC emitted was 342 ppm vol. at ER 0.21, CR 17, and 23 ppm vol. at ER 0.43, CR 16, and 1.1-kW BP in dual fuel and diesel fuel modes, respectively. The minimum magnitude of HC emission is 15 ppm vol. at ER 0.43, CR 18, and 3.5 kW engine BP.

4.3.6.3 CO_2 emission

The prominent reason for global warming, climatic change, and greenhouse gases is the emissions of CO_2 from engine exhausts. Figure 4.3.8 illustrates that CO_2 emission is higher in dual fuel mode than in diesel mode run. This is due to the ample amount of CO_2 in the producer gas that enters the engine cylinder during dual fuel mode. The CO_2 emissions increases with an increase in CR, as observed in Figure 4.3.9(a). The reason being as the CR increases, the temperature and pressure inside the cylinder increases, resulting in complete combustion. From the experiment, it can be inferred that CO_2 increases and then decreases as the ER value grows. This might be due to the improvement of combustion as ER grows. The surface plots illustrate that as the engine BP increases, the CO_2 concentrations decrease accordingly. Efficient fuel combustion in the engine cylinder ensures a low CO_2 component in the exhaust as BP increases. The maximum magnitude of CO_2 observed was 5.50 % vol. at ER 0.21, CR 18, and 1.1-kW BP in dual fuel mode. Similar results have also been observed by Mohit et al. 3.41% [85] and

Sohan lal et al. 11.81% [81]. The CO_2 emissions during dual fuel mode are 1.03 - 3.08 times greater than the diesel mode run, which is in good agreement with different literature reviews [85, 235].

4.3.6.4 NO_x emission

Nitrogen oxides are a family of hazardous gases that are highly reactive. When fuel is burnt at high temperatures, these gases are formed. The rate of NOx production is substantially influenced by the temperature of the gas in the cylinder. As a result, the distribution of fuel inside the cylinder and the combustion process has an impact on NOx production. Figure 4.3.9(b) shows the simultaneous effect of independent parameters on the NOx emissions from the engine exhausts. It can be inferred from the surface plots that at high CR and ER, the engine's NOx emissions have a high magnitude. As the CR rises, the temperature within the cylinder rises, leading to NOx formation at elevated temperatures. Also, introducing producer gas inside the engine cylinder at high ER lowers the air intake through the inlet manifold of the diesel engine, leading to reduced oxygen content; thus, NOx concentration increases and decreases marginally at high ER. Figure 4.3.8 shows the comparative analysis of NOx emission during dual and diesel modes. The experiment revealed that NOx emission during dual fuel mode is lower than during diesel mode run. This might be due to the improper premixed combustion process that occurs during dual fuel mode leading to the increased temperature within the combustion chamber. Also, the oxygen content is low during the dual fuel mode leading to reduced NOx concentration. The maximum reduction of NOx concentration in dual fuel mode observed was 86.95% at ER 0.43, CR 18, and 1.1-kW BP. The maximum magnitude of NOx emitted was 99 ppm at ER 0.21, CR 17 in dual-fuel mode, and 402 ppm vol. in diesel mode at ER 0.43, CR 18, and 3.5kW BP. Shrivastava et al. [171] estimated a maximum NO_X concentration of 180 ppm and 325 ppm in the dual fuel and diesel modes, which agrees with the present study.

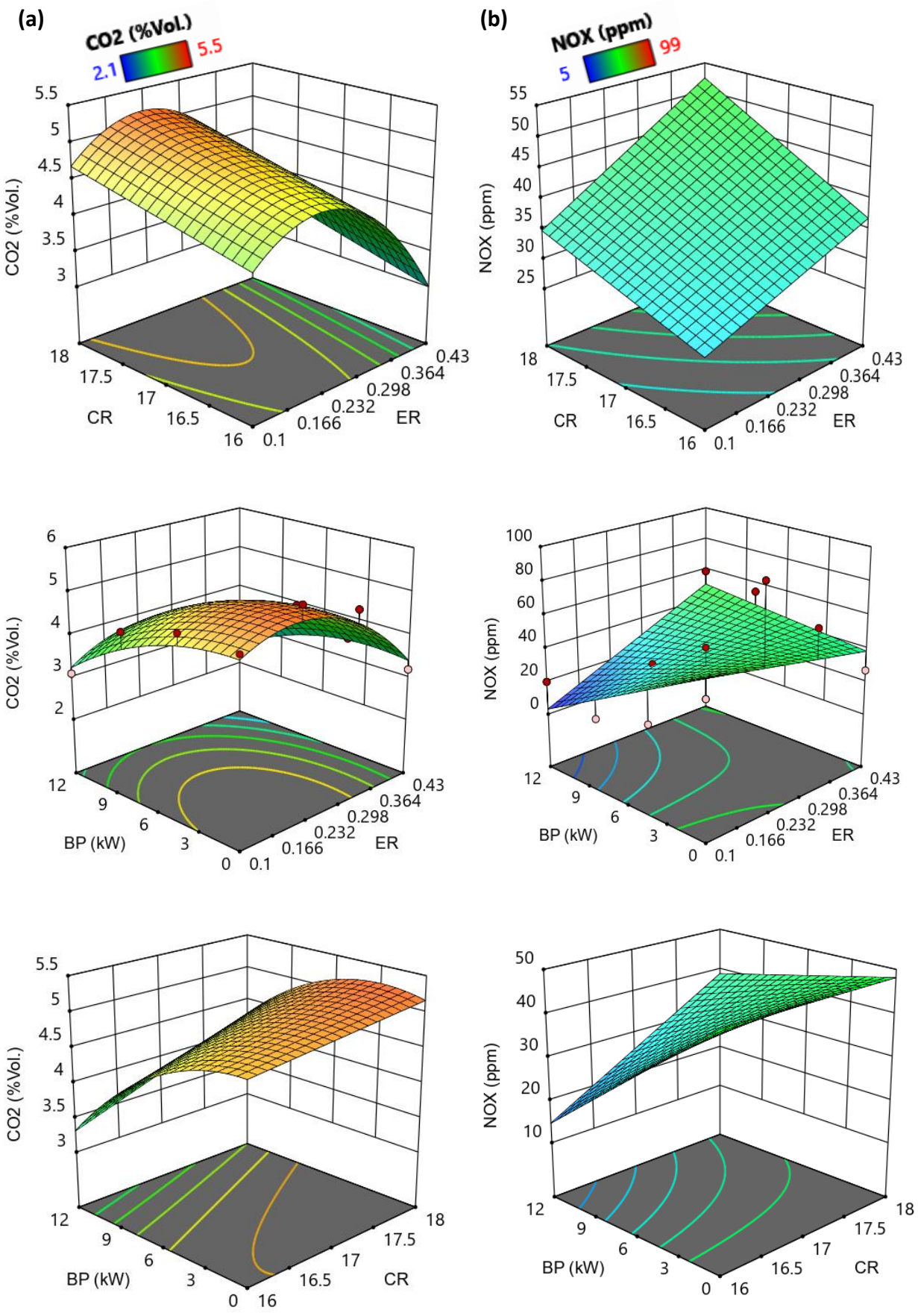

Figure 4.3.9. 3D Surface plot of (a) CO_2 (% vol.) and (b) NO_x (ppm)

4.3.7 *Energy balance in the gasifier*

The performance of the gasifier may be measured by the quality of the PG in terms of heating value. Gas yield, Lower heating value, Cold gas efficiency, and energy distribution are the essential criteria for the analysis of gasification performance [172]. Gas yield mainly depends on the producer gas flow rate to the feedstock consumption rate [178]. The gas yield in the current experiment was observed as 2.5Nm^3/kg of co-feed biomass materials. Moreover, the gas yield, or energy yield of PG, was higher for co-gasification than biomass or coal gasification [21]. Cold gas efficiency is the ratio of the heat energy contained in the producer gas to the heat energy contained in the raw biomass, i.e., (briquette and mahua wood). Figure 4.3.10 shows the Sankey diagram for the energy distribution in the downdraft gasifier. In the current experiment, the total energy content of the feedstocks observed was 899.6MJ, as shown in Figure 4.3.10. The values have been calculated based on the energy-mass allocation method. In the present experiment, the feed material intake was (20kg:20kg) for briquette and mahua wood. Accordingly, based on the LHV of feed materials (Table-4.3.2), the total energy content of feed materials was calculated as 382MJ and 517.6MJ for briquette, and mahua wood, respectively, as shown in Figure 4.3.10. Thus, cumulatively 899.6MJ of energy inputs are attributed to the co-gasification feedstocks. According to reports, 20% of the LHV of the fuels is typically utilized for sensible heat contribution during gasification [180]. Consequently, a sensible heat share has been allocated for co-gasifying feedstock gasification. Using gas yield-energy allocation and the heating values of various materials (Table-4.3.2), the total PG-energy content was calculated as 321.25MJ for blended co-gasifying PG. Table 4.3.2 shows the residual mass left after gasification and the respective CV content for residual energy evaluation. Thus, using the residual mass-energy allocation technique, the energy of residual char content was determined as 199.77MJ for co-gasification feedstocks. The rest percentages of the energy balance are considered unaccountable energy losses, which include

losses from minor gas leakages, circumference of temperature sensors, gasifier lid, and different pipe joints. This value was found to be 22.09% for co-gasification of briquette and mahua wood. Moreover, compared with normal gasification, the percentage of residual chars and tar from co-gasification is low. In the current study, quantity of residual char left after co-gasification was 18.25kg while for gasification of mahua wood was 18.90kg. Other authors had also suggested the similar insights [21, 178, 236].

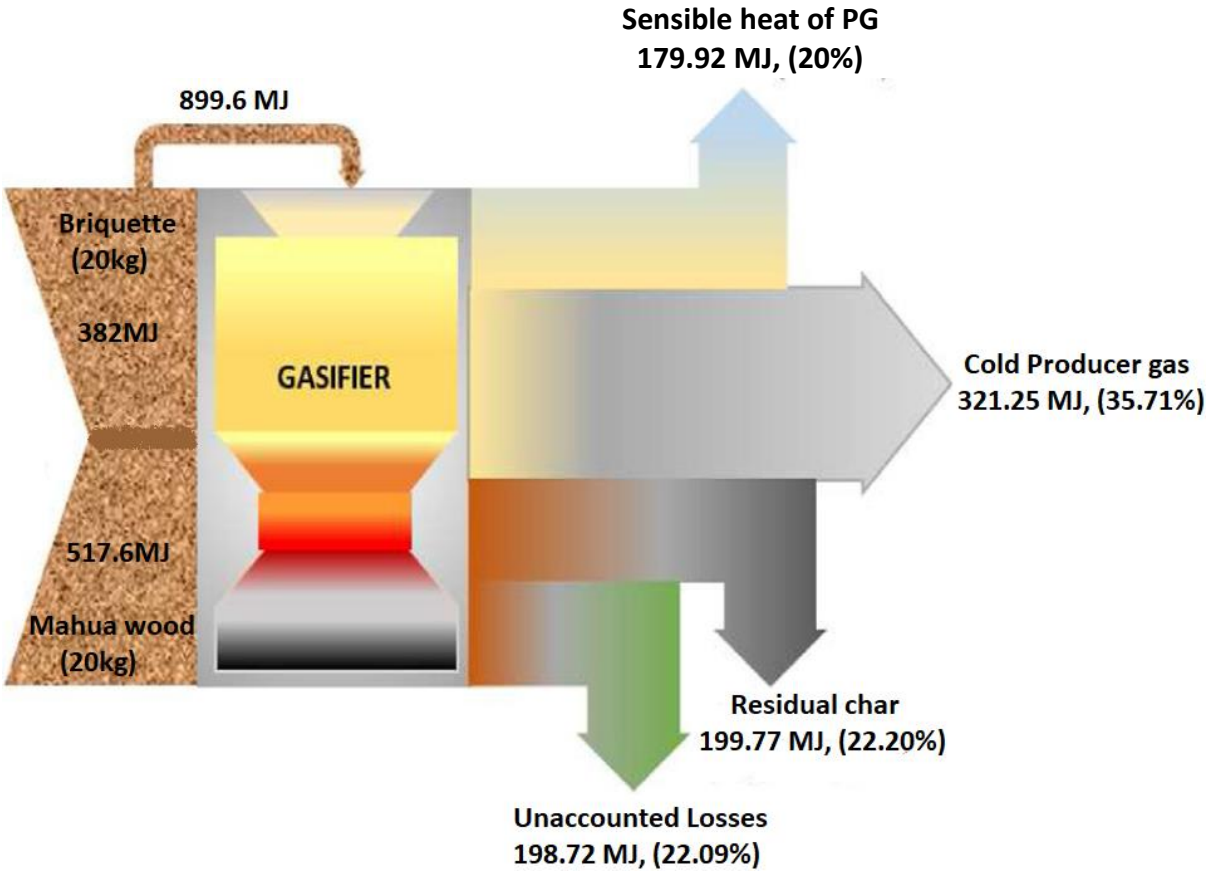

Figure 4.3.10. Sankey diagram representing energy distribution across gasifier

4.3.8 *Analysis of Variance*

Analysis of variance (ANOVA) can be used to determine the statistical significance of the model coefficients. The proportion between the variance across and the variance within the group has been correlated with the F-value. Greater F-values indicate that the equivalent model accounts for greater variability [237]. The F-value will be close to 1 if the null hypothesis is accepted. The p-value, on the other hand, is the probability of getting findings that are closer to the true data. A small p-value (≤ 0.05) indicates that the associated coefficient is significant, and the null hypothesis is rejected. A higher F-value and a lower p-value quantify the significance of factors on response. Table 4.3.1S, provided in the Appendix, depicts the ANOVA results for the engine's performance as the response variable. In the case of sound, the maximum F-value is 96.63 for BP, with its associated P-value found to be 0.00. BP is the most impactful variable, followed by CR, which influences sound as the engine's sound level increases with an increase in BP. According to ANOVA analysis for BSFC, the magnitude of the F-value is highest for BP, followed by CR and ER. The F-value and P-value of the BP are 242.14 and 0.00, respectively. Thus, engine BP is the significant input decision variable for the BSFC output response variable. For BTE, the highest and lowest magnitude of the F-value and P-value are 10663.00 and 0.00, respectively. Hence varying engine BP followed by the CR and ER are the deciding control factors for BTE. The other higher-order terms are not relevant as their F-value is relatively low. Higher-order terms, such as two-way interaction, have a P-value larger than 0.05, therefore, they are insignificant. This indicates that for improving an engine's performance or efficiency, the BP is the significant input parameter for response variables.

Table 4.3.2S, provided in the Appendix, demonstrates the ANOVA analysis of the emissions from the engine. According to the ANOVA study in the case of engine exhaust emissions, the BP is the influential parameter followed by ER and CR as their F-values have maximum magnitude, and their associated P-value lies below 0.05. The CO, HC, CO_2, and NO_x emissions

table show that square terms and the 2-way interaction term of the model are insignificant as their P-values are greater than the prescribed range. For experimental analysis, engine emissions are the important output responses, and variable engine BP has the greatest influence on emissions. The temperature within the cylinder rises as the engine brake power rises, resulting in increased fuel supply and higher NOx and CO_2 concentrations in the exhaust.

4.3.9 *Response optimizer*

Figure 4.3.1S, (as provided in the Appendix), depicts the RSM optimizer setup with its associated responses and goals constraints. To determine the optimum input conditions of the engine for the optimal engine output responses, an optimizer plot by RSM is drawn. Figure 4.3.11 shows the optimization plot generated by Minitab statistical software. The main goal of this analysis is to maximize the engine's performance and minimize exhaust emissions (CO, HC, CO_2, and NOx). In the Minitab RSM optimizer module, each output response is specified by dimensionless desirability value (d), which has a range of 0 to 1. An unacceptable response is represented by 0, and an acceptable, desirable response is depicted by 1. The solution to the acceptability equation has been characterized as "smaller-the-better" (SB) or "larger-the-better" (LB). Optimum engine output response for performance BSFC, BTE, and sound intensity are 0.165 kg/kWh, 17.41%, and 91.74 decibels, respectively, and optimum engine emissions for CO, HC, CO_2, and NO_x are 0.017%vol., 3.83 ppm, 3.11%vol., and 1.85 ppm respectively at the corresponding optimum input variables of gasifier ER 0.10, engine CR 16, and 3.18 kW. The optimal composite desirability found is 0.838. Hence, according to the desirability methodology, it can be inferred that the model is feasible. Thus, the waste mahua wood and briquette biomass can be valuable feedstocks for biomass co-gasification to generate electricity in remote areas.

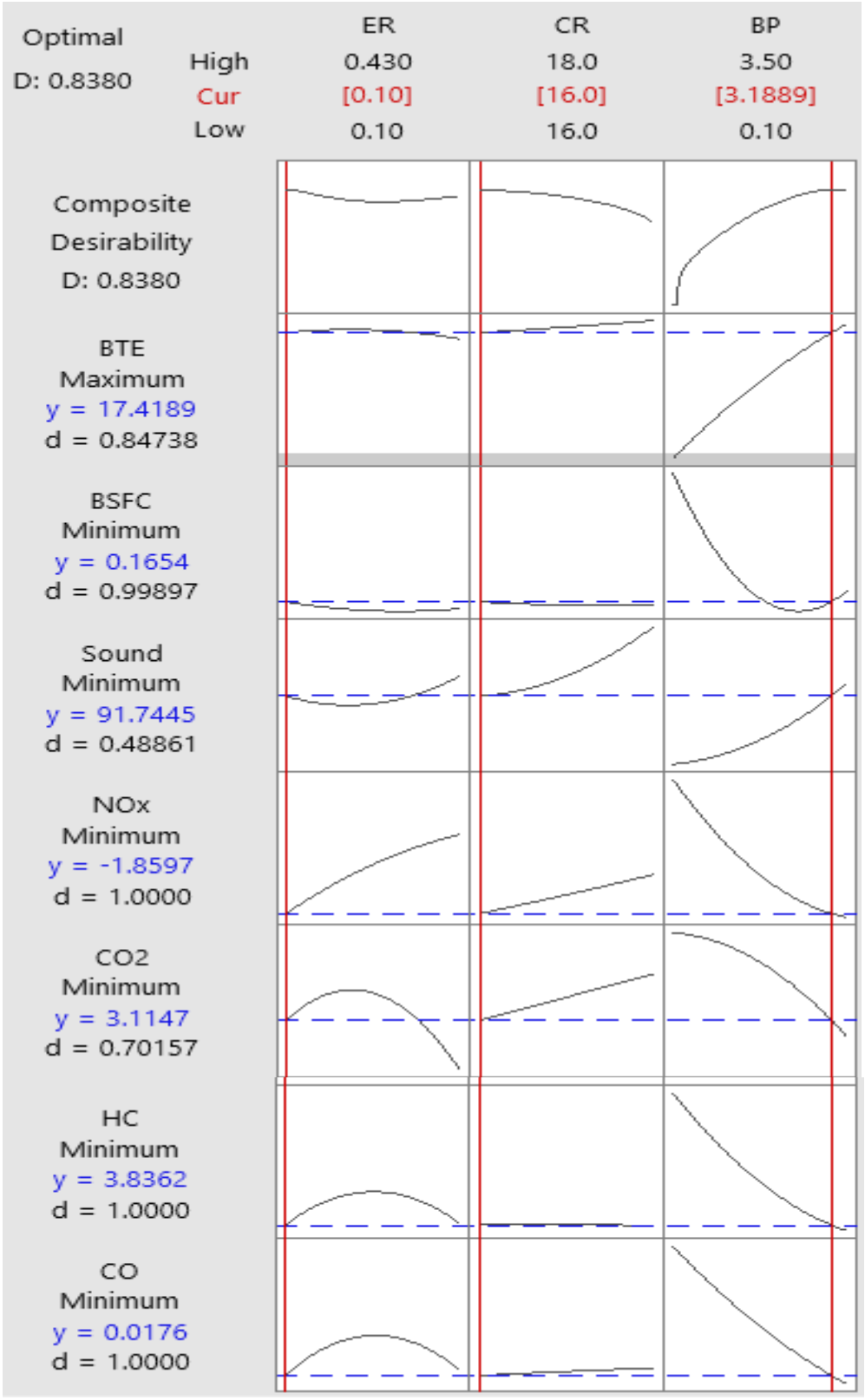

Figure 4.3.11. Optimization results by RSM

4.3.10 *Validation of RSM engine responses*

To verify the results obtained from RSM, the engine experiments were carried out at optimal input conditions of ER 0.10, CR 16, and engine BP of 3.18 kW, having an engine speed of 1500 rpm. Table 4.3.4 depicts the output responses from the experimental trial and the results obtained from optimized RSM. The average error percentages for BSFC, BTE, Sound intensity, CO, HC, CO_2, and NO_x were 5.59, 5.38, 0.16, 6.07, 1.26, 4.14, and 3.76, respectively. Consequently, the RSM findings may be used to optimize the input setting for this Kirloskar diesel engine.

Table 4.3.4. Validation of engine responses

Engine response at optimized value: (ER 0.10, CR 16, BP 3.18 kW)			
Response	***RSM optimized result***	***RSM-based Experimental result***	***% Error***
BSFC (kg/kWh)	0.1654	0.1892	5.59
BTE (%)	17.41	18.4	5.38
Sound intensity (db)	91.74	91.89	0.16
CO (% vol.)	0.017	0.079	6.07
CO (g/kWh)	0.610	2.836	
CO_2 (% vol.)	3.11	3.15	1.26
CO_2 (g/kWh)	0.197	0.199	
NO_X (ppm)	1.85	2.96	4.14
NO_X (g/kWh)	0.012	0.019	
HC (ppm)	3.83	4.52	3.76
HC (g/kWh)	0.007	0.009	

4.3.11 *Uncertainty analysis*

Instruments and measures have common properties, and errors and uncertainties are inherent in the equipment and measurement process. Dependence on a single reading should be avoided; precision depends on a solid program and adequate procedures. Reiterated readings tend to

create a range of results rather than a single point or line. Errors can arise from instrument conditions, selection, calibration, observation and reading, surroundings, and test design. Uncertainty analysis is used to calculate errors in parameter measurements (Table 4.3.5), and the total experimental uncertainty can be determined using a formula that involves the square root of the sum of uncertainties from multiple sources.

Overall uncertainty =

$$\sqrt{(BTE)^2 + (BP)^2 + \left(\frac{Air}{Fuel}\right)^2 + (Tachometer)^2 + (Thermocouple)^2 + (CO)^2 + (CO2)^2 + (HC)^2 + (NOx)^2 + (Engine\ load)^2}$$

$$= \pm \sqrt{(2.76)^2 + (0.39)^2 + (0.56)^2 + (0.33)^2 + (0.160)^2 + (0.1)^2 + (0.2)^2 + (0.2)^2 + (0.5)^2 + (0.2)^2}$$

= ± 3.74

Table 4.3.5. Uncertainties of variables

S.No.	Equipment	Measuring range	Resolution	Accuracy	Uncertainty (%)
1	Tachometer	1200 – 1500 rpm	1 rpm	± 5 rpm	± 0.33
2	Thermocouple	0 – 1200 ^oC	1 ^oC	± 2 ^oC	± 0.16
3	Brake Power	0-3.4 kW	0.1 kW	± 0.1 kW	± 0.39
3	CO	0 – 10% vol.	0.01 %vol.	± 0.1% vol.	± 0.1
4	CO_2	0 – 20% vol.	0.1 %vol.	± 0.3 %vol.	± 0.2
5	HC	0 – 20000 ppm	1 ppm	± 10 ppm	± 0.2
6	NO_x	0 – 5000 ppm	1 ppm	± 20 ppm	± 0.5

4.3.12 *Conclusions*

Results of the above analyses provide key insights into the gasifier-engine system for generating producer gas from 50:50 mahua wood waste and saw-dust briquette feedstock and reveal the balanced operating setting for diesel fuel-saving strategy with a balanced between engine power and emission trade-off.

4.4 Co-gasification of Triple feed materials and dual-fuelled engine performance

4.4.1 *Introduction*

Biomass has promising potential as feed material for gasification and subsequent power generation, whereas these sources are seasonal and scattered in the country. Therefore, the consistency of feed material availability and supply chain may be hard to maintain. Gasification with multiple feedstocks, such as biomass-coal-briquette blends, could be one of the practical solutions to mitigate the availability and supply chain problems. Therefore, the present study aims to experiment on an air-downdraft gasifier and use generated producer gas (PG) (, a mixture of gases such as hydrogen, carbon monoxide, carbon dioxide, and nitrogen produced by incomplete combustion of coal/biomass) for power generation through a dual-fuelled mode CI engine. The three input operating conditions for the gasification-engine experiment were GER (0.1-0.43), engine load (0-100%), and compression ratio (CR) 16-18, with output parameters such as engine brake power (BP), brake thermal efficiency (BTE), brake specific energy consumption (BSEC), gas substitution rate (GSR), engine emission (CO, CO_2, HC, NOx), and sound. Further optimization using Response Surface Methodology (RSM) was used to obtain the optimal operating conditions with the goal of maximizing engine performance while minimizing emissions. Based on 48 experimental data sets, ANOVA analysis and RSM-based optimization has been conducted. RSM optimization showed the optimum operational conditions of 0.43 GER, 16 CR, and 100 % engine load. The respective performance responses were BP 3.52kW, BSEC 34.16 MJ/kWh, BTE 21.02 %, sound intensity 90.21db, CO 0.0918 % vol., HC 17.41 ppm vol., CO_2 2.05 %vol., and NO_x 4.55 ppm. The average values obtained for R^2 were 95-99% and a 0.72 coefficient of determination. Further, the developed model predicted the output response very closely with the experiment, found to be a 4.4% maximum

error. Thus, gasification with triple feed material (biomass-coal-briquette) with engine integration could partially substitute diesel fuel with optimum exhaust emission and noise.

In respect to the above literature review, it was found that there is a certain research gap of triple feed material gasification (especially, Mahua biomass - Coal - Sawdust briquette) to generate producer gas, its application in dual-fuelled mode Diesel engine run, and respective performance characteristics analysis. Concerning these research gaps, the first novel aim of this study is to encourage waste-to-gaseous fuel conversion through a combination of biomass-coal-briquette and its feasibility for gasification. The second is to analyze gasifier-CI engine performance, exhaust and noise emission, and diesel saving. And third is to optimize Gasifier-CI engine operating variables for maximizing engine power, minimizing engine exhaust emission, fuel consumption, and noise level using the multi-objective response surface method (RSM). Furthermore, regarding selecting feeding material for gasification, excluding coal, the Mahua waste biomass (branch cut, old furniture waste, wood industries process: off-cuts sizing, trimming, shaving, etc.) are readily available and can easily be transported. Mahua longifolia is a deciduous forest tree that reaches a height of roughly 20 meters and sustains an average of 60 years of age [197]. In India, around 62,500 hectares have been used for Mahua cultivation [162]. Successive biomass briquettes as feed material and wood briquettes are being significantly used as blending in co-firing power generation in Europe, North America, and Asia (viz., Japan, China, and South Korea)[58]. In India, it was reported [58] that growth in net residue availability for biomass briquette will be from 227 Mt (in 2010/11) to 281 Mt (in 2030/31). Regarding optimization tool as RSM, it was revealed in the literature that it is most compatible with engine applications and is popular due to its capability of high-level accuracy and sensitiveness to reach the collective results with less time and generate a suitable matrix for tests [106],[107], [110], [109]. The recent progress in optimization with gasification-engine application and the associated gap for the present work are shown in Table 4.5.1. Table 4.4.1

shows that the RSM optimization tool is quite common for optimization approaches. However, experiments on the performance and subsequent optimization of PG from biomass-coal-briquette and diesel-fuelled modes have not yet been done. Concerning the accomplishment of mentioned aims, initially, experiments were conducted to generate PG through a downdraft air gasifier using mahua biomass-coal-sawdust briquette (15kg each) as feed material. Gasification ER, engine CR, and engine load have been considered operating variables during the Gasifier-CI Engine runs. Finally, operating variables as inputs were optimized using an RSM optimizer to respond to maximum brake power, minimum engine exhaust emission, fuel consumption, and sound level. Finally, it was summarized that biomass-coal-briquette-based co-gasification is suitable for PG generation and its application for dual-fuelled mode CI engine run. Further, this study will offer a base for the industrialist and researchers for efficient marketing and further research and development. Furthermore, the current study may offer significant benefits and societal implications of co-gasification integrated engine systems. Because, these systems have the ability to convert solid waste and biomass into a cleaner fuel, thus it will tend to reduce the carbon footprint of industries and municipalities. Additionally, the co-gasification study provides a more reliable and sustainable energy alternative that will help reduce waste disposal's environmental impact, conserve natural resources, create new job opportunities within the renewable energy sector, and promote economic growth in the communities. Finally, by increasing public awareness of waste-to-energy technologies, the current co-gasification study will benefit society by supporting a more resilient, sustainable, and prosperous future.

Table 4.4.1. Comparative previous work and the present study

Type of engine	Investigation method	Optimization technique	Fuels	Optimization Parameter	Ref.
CI Engine	Simulation-ANN	RSM	Biodiesel-Diesel blend	Biodiesel ratio, Engine load, Injection pressure	[109]
CI Engine	Experimental	RSM	Babool wood PG and Biodiesel	Engine load, pilot fuel injection timing, and pressure	[167]
CI engine	Simulation-ANN	RSM	Diesel blended with Acetylene	Acetelene blend, injection timing, pressure, CR,	[224]
CI Engine	Experimental	RSM	Biodiesel and Producer gas	Load, CR, Injection timing	[168]
CI Engine	Simulation-Fortran	RSM	Babul wood PG and diesel	blending ratios, CR, and Injection timing	[169]
CI Engine	Experimental	RSM	Diesel and cocoa pod husk-PG	Brake power and Compression ratio	[170]
CI Engine	Experimental	RSM	Coal PG and Diesel	Gasification ER, engine load, and CR	[35]
CI Engine	Experimental	RSM	PG from Biomass-coal-Briquette and diesel	Gasification ER, CR, and load	**Not yet**

4.4.2 *Chemical properties of feed-material*

In the experiment, the gasification was conducted with the feed material of hard coke low-grade coal, mahua wood waste, and briquette blended with a 1:1:1 ratio. These feedstocks were

primarily acquired from Varanasi, Uttar Pradesh, India. The raw and dry coal-biomass were prepared as gasification feedstock by shredding them into pieces, with average lengths and breadths of about 45-60 mm and 25-35 mm and diameter of 90 mm. The chemical composition of the feedstocks is shown in Figure 4.4.1.

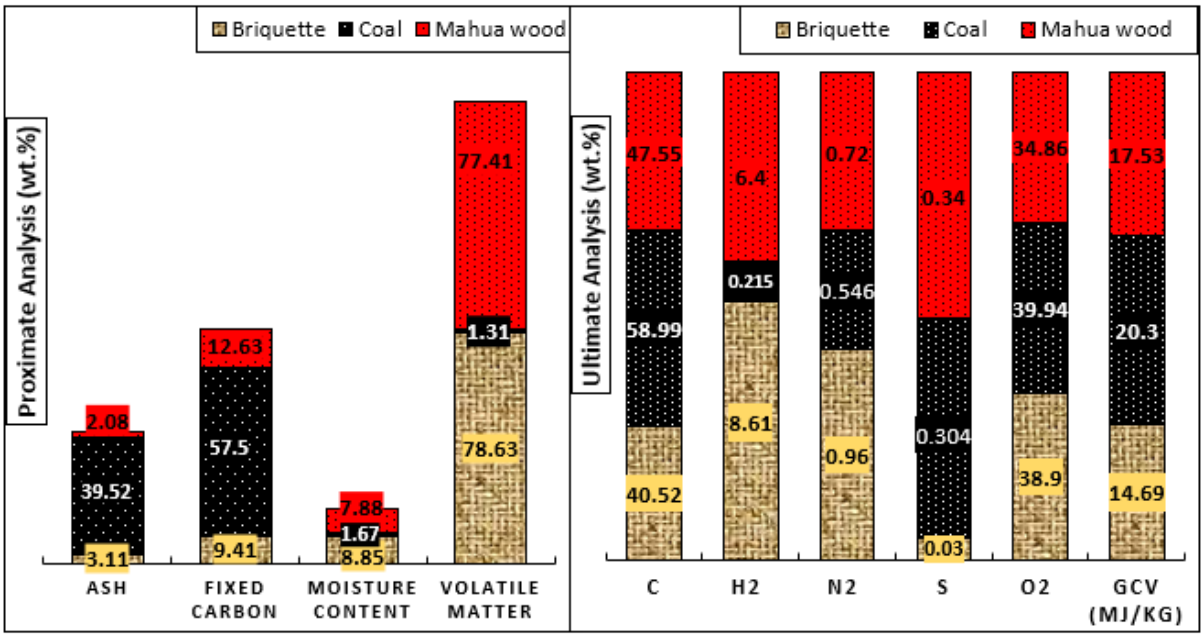

Figure 4.4.1. Chemical properties of feed-materials[226, 227]

4.4.3 *Gasifier performance*

The performance of the gasifier may be measured by the quality of the PG in terms of heating value. In the current experiment, the total energy content of the feedstocks observed was 787.8 MJ, as shown in Figure 4.4.2. The figure shows the Sankey diagram for the energy transfer in the downdraft gasifier. It can be observed that 40.48% of the biomass energy was transferred to cold producer gas. 20% of energy goes into sensible heating of the PG [238]. Cumulative energy losses from tar residues and minor gas leakages from different pipe connections total 39.52%.

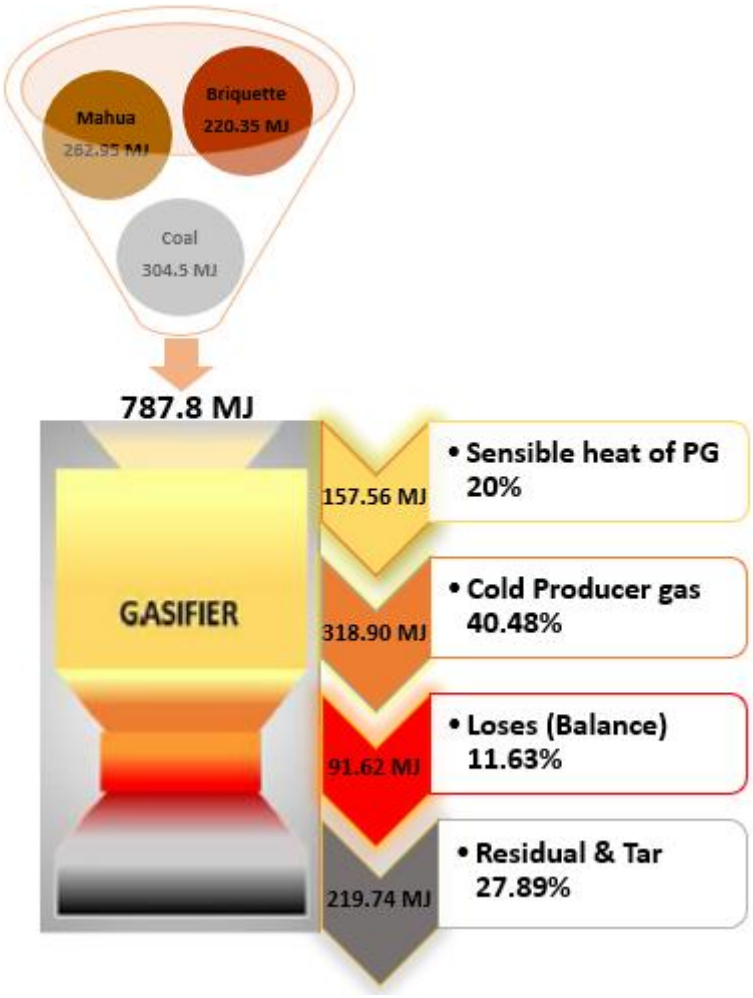

Figure 4.4.2. Sankey diagram for gasifier

4.4.4 *Model fitting and adequacy checking*

Minitab statistical software has been used in our study to generate a regression equation representing an empirical relationship between the independent parameters and the response variables. The polynomial quadratic equation regression model has been developed to fit the experimental results, as shown in equations (4.4.1) - (4.4.9). The proposed model has been examined for adequacy to identify any errors associated with the normality assumptions. The regression equation indicates the effect of different independent variables on the response. The positive sign in the regression equation of each term indicates a synergetic effect, while the

negative sign indicates an antagonistic effect. In RSM, the F-value, P-value, and α-value are statistical measures used to evaluate the significance of a model and its terms. An Analysis of Variance (ANOVA) was performed to discover the significant dependence on the response and factors influencing the process. The F-value is a measure of how well the model fits the data. It is calculated by dividing two mean squares. This calculation determines the ratio of explained variance to unexplained variance. A high F-value indicates a good fit between the model and the data [110]. The P-value is defined as the smallest level of significance that leads to the rejection of the null hypothesis. A low P-value (typically less than 0.05) indicates that the particular term is statistically significant in the model and should be included for further prediction [239]. And the α-value shows the confidence level or the probability of rejecting the null hypothesis when it is actually true. For example, if the α-value is set at 0.05, which indicates a 95 % confidence level of modeling with experimental results, 5 % is considered a null hypothesis. All these values were obtained from (ANOVA) table, which is shown in Tables 4.4.2 and 4.4.3 for performance and emissions, respectively. This table shows that the model results predicted by the regression operation are statistically significant at an α-value of 0.05 (i.e., 95% confidence level). Higher the magnitude of the F-value, the higher the impact of that parameter on the response variable. The desirable P-value of the model has a magnitude ≤ 0.05. From the ANOVA results of engine performance and emission, as shown in Table 4.4.2 and 4.4.3, it can be concluded that the load has the highest impact on all the response variables, i.e., BP, BSEC, BTE, GSR, CO, HC, and CO_2 except NO_x emission. The magnitude of the F-value in linear terms is highest in the case of load, and the corresponding P-value is 0.00, which is less than 0.05. The magnitude of F-value in the case of NO_x emission is highest for gasifier ER, followed by load and CR. This is because oxygen availability increases with the increase in gasifier ER; thus, NO_x concentration rises. The R^2 and R^2 Adj values are also shown in the ANOVA analysis. The model adequacy was checked by the coefficient of correlation (R^2),

adjusted coefficient of determination (R^2 adj), and the predicted coefficient of determination (R^2 pred). The R^2 value expresses the overall response variability and the R^2 Adj value accounts for the number of significant elements in the model. R^2 and R^2 Adj preferred values must be close to 1 or 100%, as the closer to this value suggests a higher level of agreement between the experiment and the predicted value calculated by the regression model. Moreover, if the R^2 and R^2 Adj difference is less than 0.2 or 20%, the RSM-predicted model is likely to be accurate [240]. All the nine models produced in our investigation had R^2 and R^2 Adj differences of less than 0.2. The higher value of R^2 Adj provides a better goodness-of-fit for regression models. The highest R^2 Adj value was found for the BP model, followed by the engine BTE model, the GSR model, the BSEC model, and for engine emissions, the HC model, followed by CO_2, CO, NO_x, and the engine sound models. Thus, the ANOVA results illustrate that the model successfully represents most of the experimental data.

$$\begin{aligned} BP\ (kW) = {} & 0.07 - 0.00\ ER + 0.000\ CR + 0.03226\ LOAD + 0.000\ ER*ER \\ & - 0.0000\ CR*CR + 0.000022\ LOAD*LOAD + 0.0000\ ER*CR \\ & + 0.00000\ ER*LOAD + 0.000000\ CR*LOAD \end{aligned} \quad (4.4.1)$$

$$\begin{aligned} BTE\ (\%) = {} & 63.8 - 81.9\ ER - 6.36\ CR - 0.0119\ LOAD + 37.0\ ER*ER \\ & + 0.162\ CR*CR - 0.000664\ LOAD*LOAD + 3.64\ ER*CR \\ & + 0.1364\ ER*LOAD + 0.01422\ CR*LOAD \end{aligned} \quad (4.4.2)$$

$$\begin{aligned} BSEC\ (MJ/kWh) = {} & 786 + 245\ ER - 22\ CR - 17.67\ LOAD - 110\ ER*ER + 0.2\ CR*CR \\ & + 0.09329\ LOAD*LOAD - 14.0\ ER*CR \\ & + 0.51\ ER*LOAD + 0.242\ CR*LOAD \end{aligned} \quad (4.4.3)$$

$$\begin{aligned} GSR\ (\%) = {} & 60 - 77.3\ ER + 0.7\ CR - 0.388\ LOAD + 46.5\ ER*ER \\ & + 0.014\ CR*CR + 0.000450\ LOAD*LOAD + 2.91\ ER*CR \\ & + 0.2365\ ER*LOAD + 0.00208\ CR*LOAD \end{aligned} \quad (4.4.4)$$

$$\begin{aligned} HC\ (ppm) = {} & 1377 - 1219\ ER - 126\ CR - 2.14\ LOAD + 544\ ER*ER + 2.97\ CR*CR \\ & + 0.01414\ LOAD*LOAD + 85.6\ ER*CR - 5.382\ ER*LOAD \\ & + 0.023\ CR*LOAD \end{aligned} \quad (4.4.5)$$

$$CO\ (\%vol) = -1.23 - 5.41\ ER + 0.222\ CR + 0.00596\ LOAD + 1.860\ ER*ER - 0.0075\ CR*CR + 0.000029\ LOAD*LOAD + 0.3455\ ER*CR - 0.01478\ ER*LOAD - 0.000593\ CR*LOAD \quad (4.4.6)$$

$$CO_2\ (\%vol) = -5.1 - 40.84\ ER + 1.06\ CR + 0.0161\ LOAD + 13.43\ ER*ER - 0.0281\ CR*CR - 0.000225\ LOAD*LOAD + 2.148\ ER*CR + 0.00000\ ER*LOAD - 0.00101\ CR*LOAD \quad (4.4.7)$$

$$NO_X\ (ppm) = 158 - 755\ ER - 13.6\ CR + 0.597\ LOAD + 261.7\ ER*ER + 0.28\ CR*CR + 0.000675\ LOAD*LOAD + 43.30\ ER*CR - 0.955\ ER*LOAD - 0.0341\ CR*LOAD \quad (4.4.8)$$

$$Sound\ (db) = 80.1 + 16.0\ ER - 0.01\ CR + 0.0532\ LOAD - 2.8\ ER*ER + 0.028\ CR*CR + 0.000360\ LOAD*LOAD - 0.90\ ER*CR - 0.0653\ ER*LOAD - 0.00199\ CR*LOAD \quad (4.4.9)$$

The Pareto chart for variable impact on engine performance and emission is shown in Figure 4.4.3 and Figure 4.4.4, respectively. It is observed that all the bars do not cross the reference line of 2.02, which implies that all the factors are not statistically important. The effect of two-way interaction coded AB and square interaction AA and BB are not substantial on the response variable. C, i.e., Load, has the highest significance on the response variables. In the case of NO_x emission, gasifier ER has the highest importance compared to other linear, two-way interaction, or square terms.

The comparison of experimental and RSM-predicted results of engine performance and emission parameters is shown in Figure 4.4.5 and Figure 4.4.6, respectively. From the graph, it can be concluded that the prediction error in the model was below 4.4%. Hence the model is feasible.

Table 4.4.2. Analysis of variance for engine performance

Source	**DF**	**BP**		**BTE**		**BSEC**		**GSR**	
		F-Value	**P-Value**	**F-Value**	**P-Value**	**F-Value**	**P-Value**	**F-Value**	**P-Value**
Model	9	2231.11	0.000	363.24	0.000	79.28	0.000	178.97	0.000
Linear	3	6690.82	0.000	1062.22	0.000	162.57	0.000	525.84	0.000
ER	1	0.00	1.000	34.55	0.000	0.21	0.646	20.29	0.000
CR	1	0.00	1.000	25.93	0.000	0.99	0.326	51.57	0.000
Load	1	20072.46	0.000	3126.16	0.000	486.49	0.000	1505.66	0.000
Square	3	2.51	0.073	14.12	0.000	74.87	0.000	3.43	0.027
ER*ER	1	0.00	1.000	11.31	0.002	0.04	0.848	5.74	0.022
CR*CR	1	0.00	1.000	0.33	0.569	0.00	0.991	0.00	0.978
Load*Load	1	7.53	0.009	30.72	0.000	224.56	0.000	4.55	0.040
2-Way Interaction	3	0.00	1.000	13.39	0.000	0.43	0.733	7.65	0.000
ER*CR	1	0.00	1.000	7.53	0.009	0.04	0.840	1.55	0.221
ER*Load	1	0.00	1.000	22.08	0.000	0.12	0.736	21.33	0.000
CR*Load	1	0.00	1.000	10.57	0.002	1.13	0.294	0.07	0.788
Error	38								
Total	47								
Summary of Fits									
R^2		99.81%		98.85%		94.94%		97.70%	
R^2 Adj		99.71%		98.58%		93.75%		97.15%	
R^2 Pred		99.72%		98.06%		92.53%		95.83%	

Table 4.4.3. Analysis of variance for engine emissions

Source	DF	CO		HC		CO_2		NO_X		Sound	
		F-Value	P-Value	F-Value	P-Value	F-Value	P-Value	F-Value	P-Value	F-Value	P-Value
Model	9	62.37	0.000	70.41	0.000	69.34	0.000	34.73	0.000	20.00	0.000
Linear	3	159.81	0.000	178.56	0.000	185.92	0.000	76.83	0.000	54.30	0.000
ER	1	81.57	0.000	99.10	0.000	57.07	0.000	129.36	0.000	15.77	0.000
CR	1	5.89	0.020	0.11	0.742	125.16	0.000	36.00	0.000	16.13	0.000
Load	1	391.95	0.000	436.46	0.000	375.54	0.000	65.12	0.000	131.00	0.000
Square	3	5.52	0.003	9.79	0.000	14.41	0.000	5.84	0.002	3.50	0.025
ER*ER	1	5.41	0.025	4.36	0.044	12.82	0.001	16.56	0.000	0.07	0.789
CR*CR	1	0.13	0.717	0.20	0.660	0.09	0.772	0.03	0.866	0.01	0.915
Load*Load	1	11.01	0.002	24.82	0.000	30.33	0.000	0.93	0.341	10.42	0.003
2-Way Interaction	3	21.79	0.000	22.88	0.000	7.68	0.000	21.53	0.000	2.20	0.104
ER*CR	1	12.85	0.001	7.42	0.010	22.58	0.000	31.21	0.000	0.53	0.471
ER*Load	1	49.03	0.000	61.17	0.000	0.00	1.000	31.61	0.000	5.83	0.021
CR*Load	1	3.47	0.070	0.05	0.827	0.46	0.501	1.78	0.190	0.24	0.628
Error	38										
Total	47										
Summary of FITS											
R^2		93.66%		94.34%		94.26%		89.16%		82.57%	
R^2 Adj		92.16%		93.00%		92.90%		86.59%		78.44%	
R^2 Pred		88.20%		89.34%		89.11%		80.54%		71.46%	

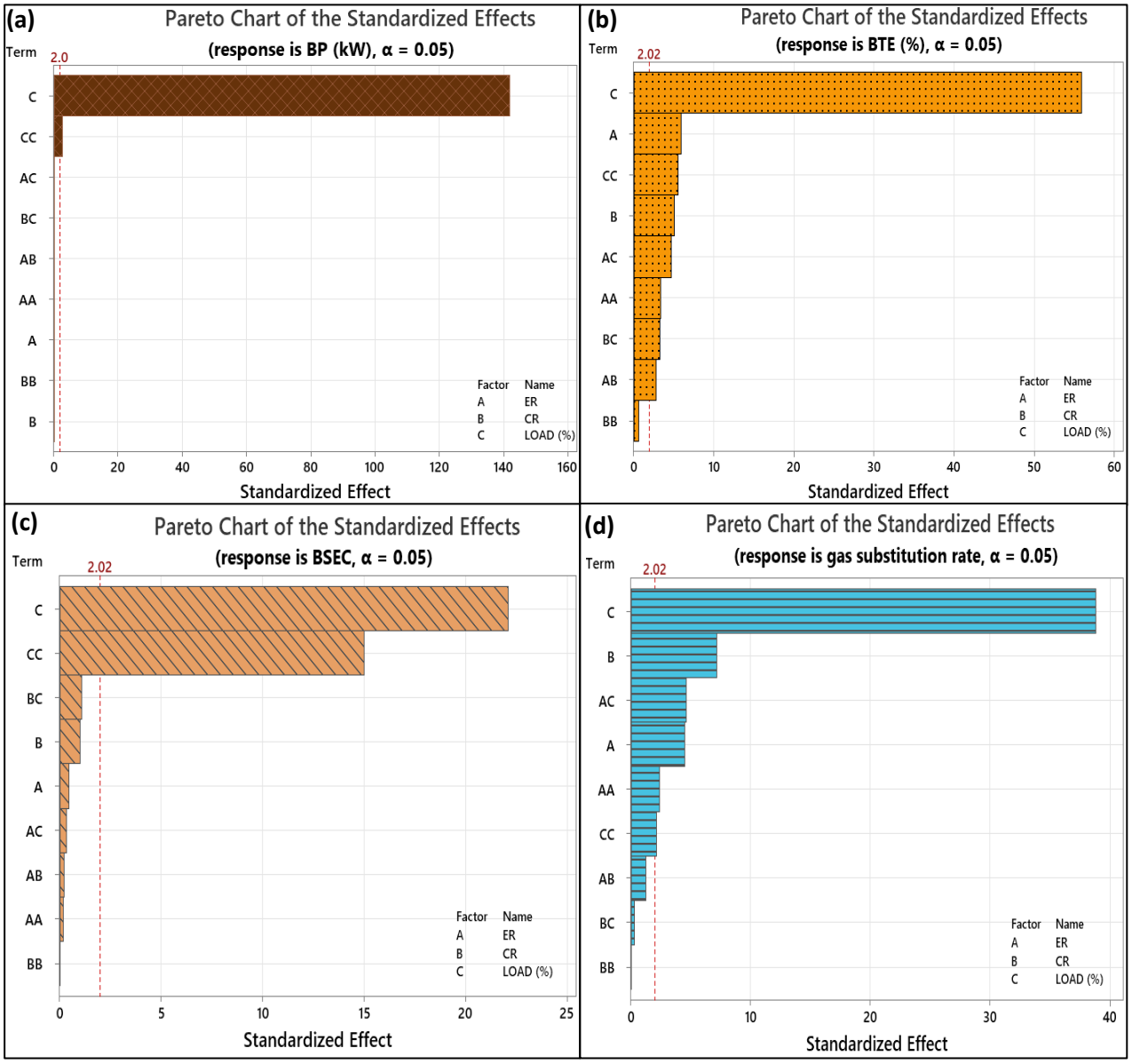

Figure 4.4.3. Pareto chart of engine performances for (a) BP, (b) BTE, (c) BSEC, and (d) GSR

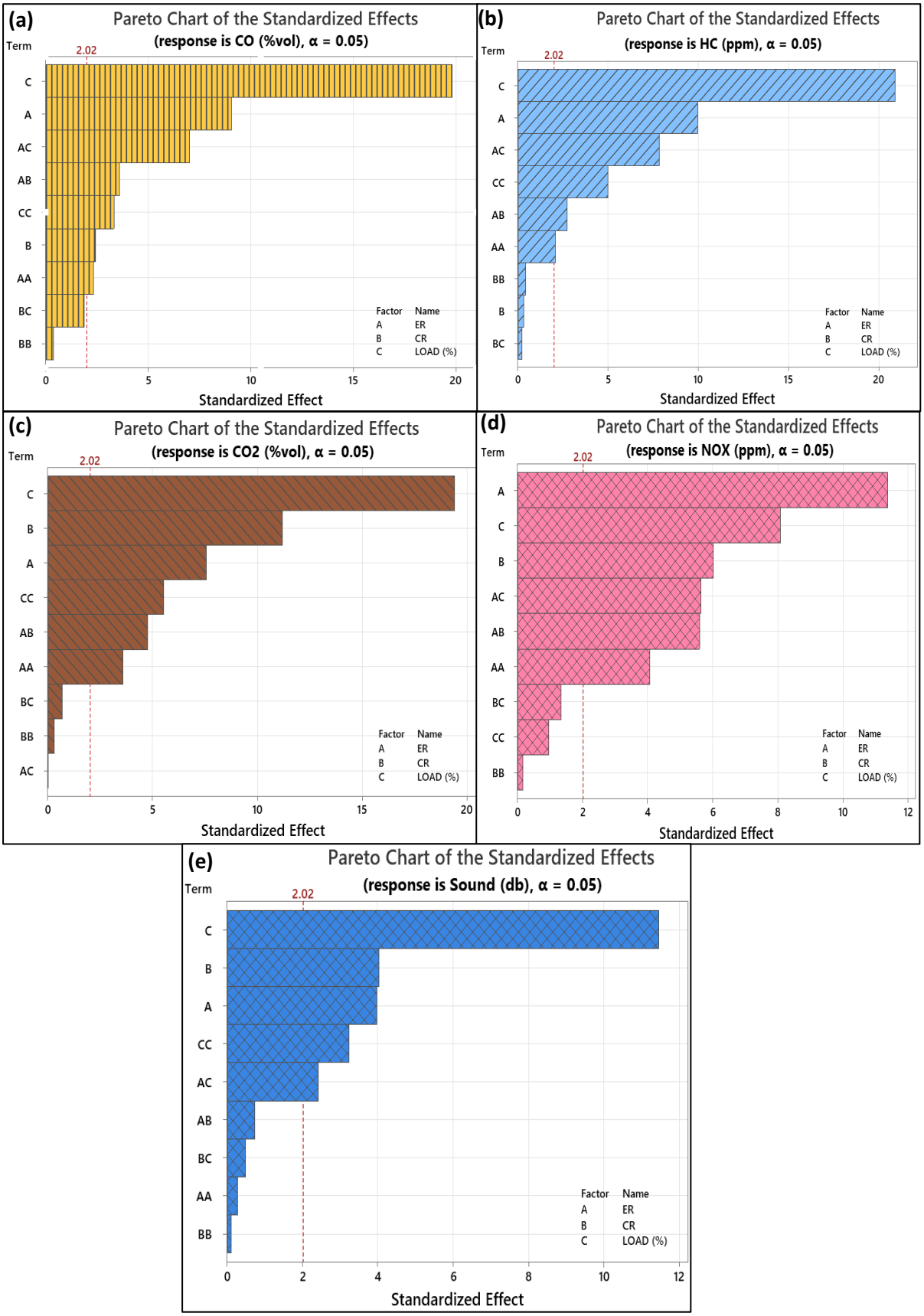

Figure 4.4.4. Pareto chart of engine emissions for (a) CO, (b) HC, (c) CO_2, (d) NOx, and (e) Sound

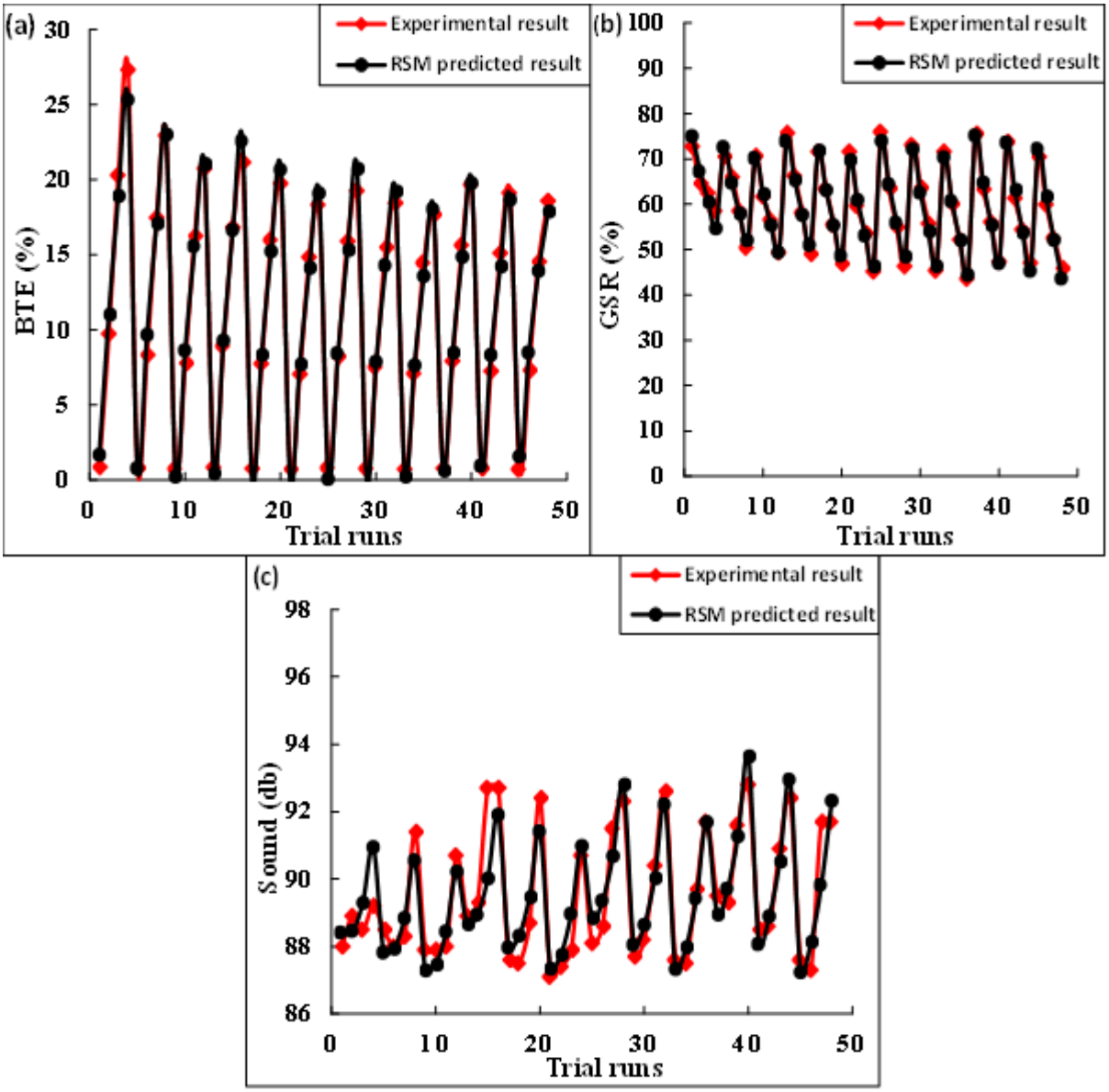

Figure 4.4.5. Experimental and RSM predicted models of Engine performances for (a) BTE, (b) GSR, (c) Sound

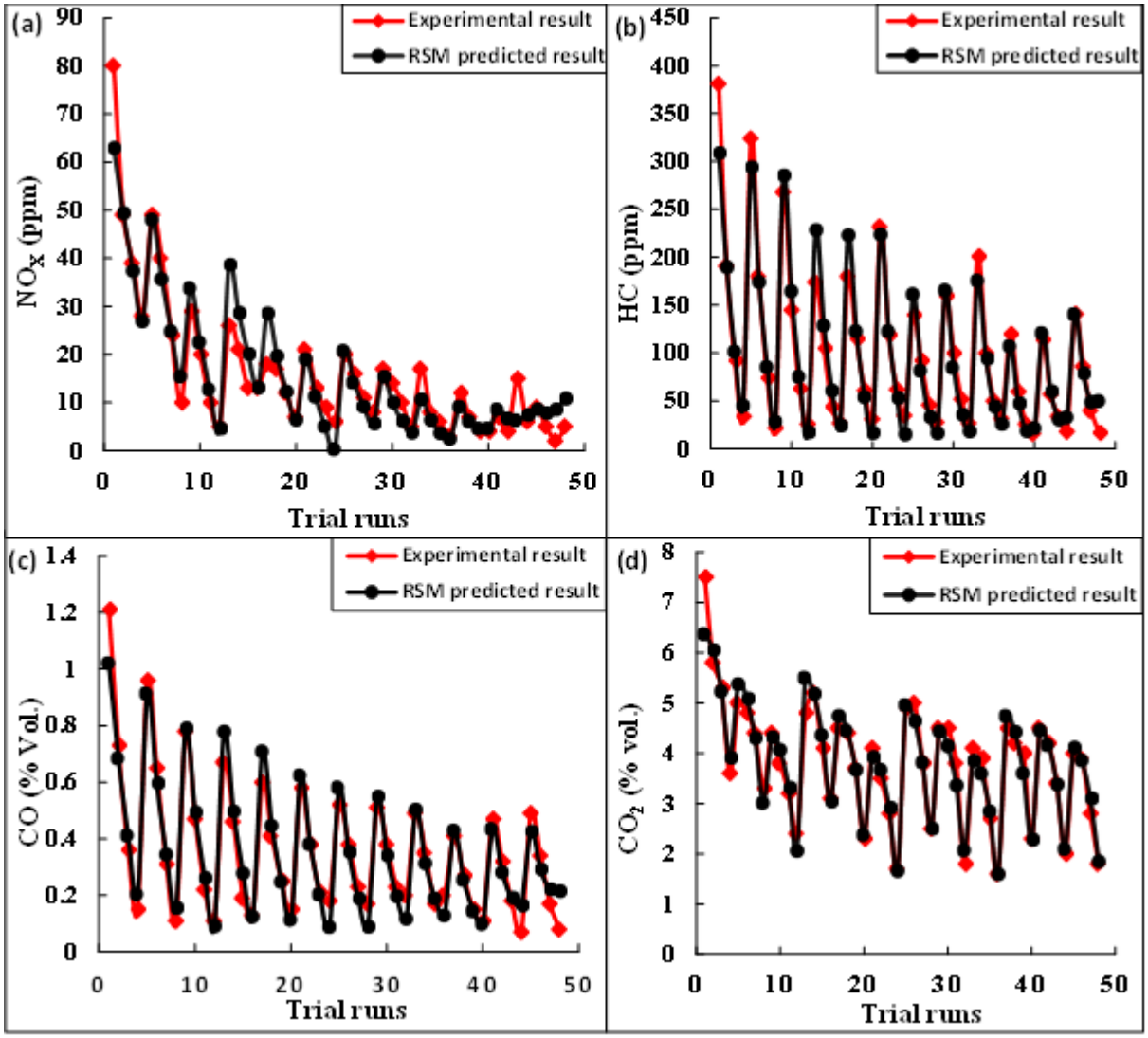

Figure 4.4.6. Experimental and RSM predicted models of Engine Emissions for (a) NO_x, (b) HC, (c) CO, and (d) CO_2

4.4.5 *Surface and Contour plots of the developed models*

The 3-D surface plots and 2-D contour plots are presented to investigate the impact of process parameters (ER, CR, and Load) on engine performance and emission responses.

4.4.5.1 Engine performance

The simultaneous impact of independent parameters (Gasifier ER, CR, and load) on engine performance (BP, BSEC, BTE, and GSR) are shown in Figure 4.4.7.

Brake power is the net output power from the engine that is available at the crankshaft after countering the internal frictional and other thermal losses. It can be concluded from the surface and contour plots of Figure 4.4.7(a) that as the engine load increases, the BP increases. This might be because as the load increases at a constant 1500 rpm, the governor will lead to more fuel combustion, producing more output power at the crankshaft. Surface plots also reveal that the BP remains almost constant with the gasifier ER and CR. The maximum BP developed at the crankshaft was 3.5 kW at a 12 kg load. Girish et al. [241] found that the BP in diesel and dual-mode engine runs are identical.

Brake-specific energy consumption (BSEC) measures engine performance based on energy utilization. BSEC is the ratio of energy released during fuel combustion to the power produced by the engine [242].

$$\text{BSEC} = \frac{\sum(m_{total\ fuel} \times LHV_{total\ fuel})}{BP} \tag{4.4.10}$$

where, $m_{total\ fuel}$ and $LHV_{total\ fuel}$ are the mass and lower calorific value of the total amount of fuel, respectively.

It can be observed from Figure 4.4.7(b) that BSEC is lower at full load conditions in (PG- diesel) dual-fuel engines due to improved combustions by enriching producer gas with air [241]. The surface and contour plots of BSEC show that BSEC is lower at higher CR due to improved fuel combustion at a higher compression ratio [243]. The impact of gasifier ER on BSEC can be seen from the figure that as ER increases, the magnitude of brake-specific energy consumption in dual mode decreases. The possible reason is that at higher ER, the LHV of volatile compounds in PG reduces, leading to a decreased BSEC [244]. At 100% load condition, the minimum BSEC observed was 13.18 MJ/kWh with a PG flow rate of 6.12 kg/h at CR 18. It was observed from the experiment that the energy consumption in diesel mode is lower than the (PG-diesel) dual mode engine run. This might be due to the availability of CO_2 in PG and lower volumetric

efficiency which reduces the burning velocity [245]. Similar results are also being found by [241, 246].

Brake thermal efficiency (BTE) represents the engine's overall efficiency, and it is the ratio of obtained brake power to the calorific value of consumed fuel. Therefore, it signifies the mechanical performance of the overall engine. The simultaneous effects of independent parameters over BTE have been observed from surface and contour plots in Figure 4.4.7(c). It was found that the BTE increases with an increase in load due to better combustion with the enhanced temperature at higher loads [178]. The BTE increases with the gasifier ER, which might be due to the lower heating value of producer gas at a higher ER, which improves the thermal performance of the engine at a higher ER [244]. It can also be observed that there was a marginal enhancement in BTE with an increase in CR due to the improved combustion at higher pressure and temperature. At full operating conditions, i.e., ER 0.43, CR 18, and load 12kg, the maximum BTE of 27.30% was observed while running the engine in dual fuel mode, which is lower than conventional diesel (i.e., 29.69%) fuel at all engine loads, as shown in Figure 4.4.8(a). This result is quite good, with higher BTE in comparison with other findings reported a maximum BTE of 19% [185], 21.61% [85], and 26% [171].

The energy of the gaseous fuel over the total fuel energy input is defined as the gas substitution rate (GSR) [247].

$$GSR = \frac{m_{gas} \times LHV_{gas}}{(m_{gas} \times LHV_{gas}) + (m_{diesel} \times LHV_{diesel})} \times 100\ \% \qquad (4.4.11)$$

Where m is fuel mass, and LHV is the lower heating value.

Figure 4.4.7(d) shows that the percentage of gas substitution is less at higher loads. This might be because the diesel fuel supply will be higher at a higher load, resulting in less gaseous fuel substitution. From the contour plot, it can be observed that maximum GSR was found at high

CR and low load conditions. At gasifier, ER 0.21, i.e., 50 % nozzle opening condition, a maximum producer gas substitution of 75.96 % was observed. This might be due to more fuel combustion at higher CR and ER values.

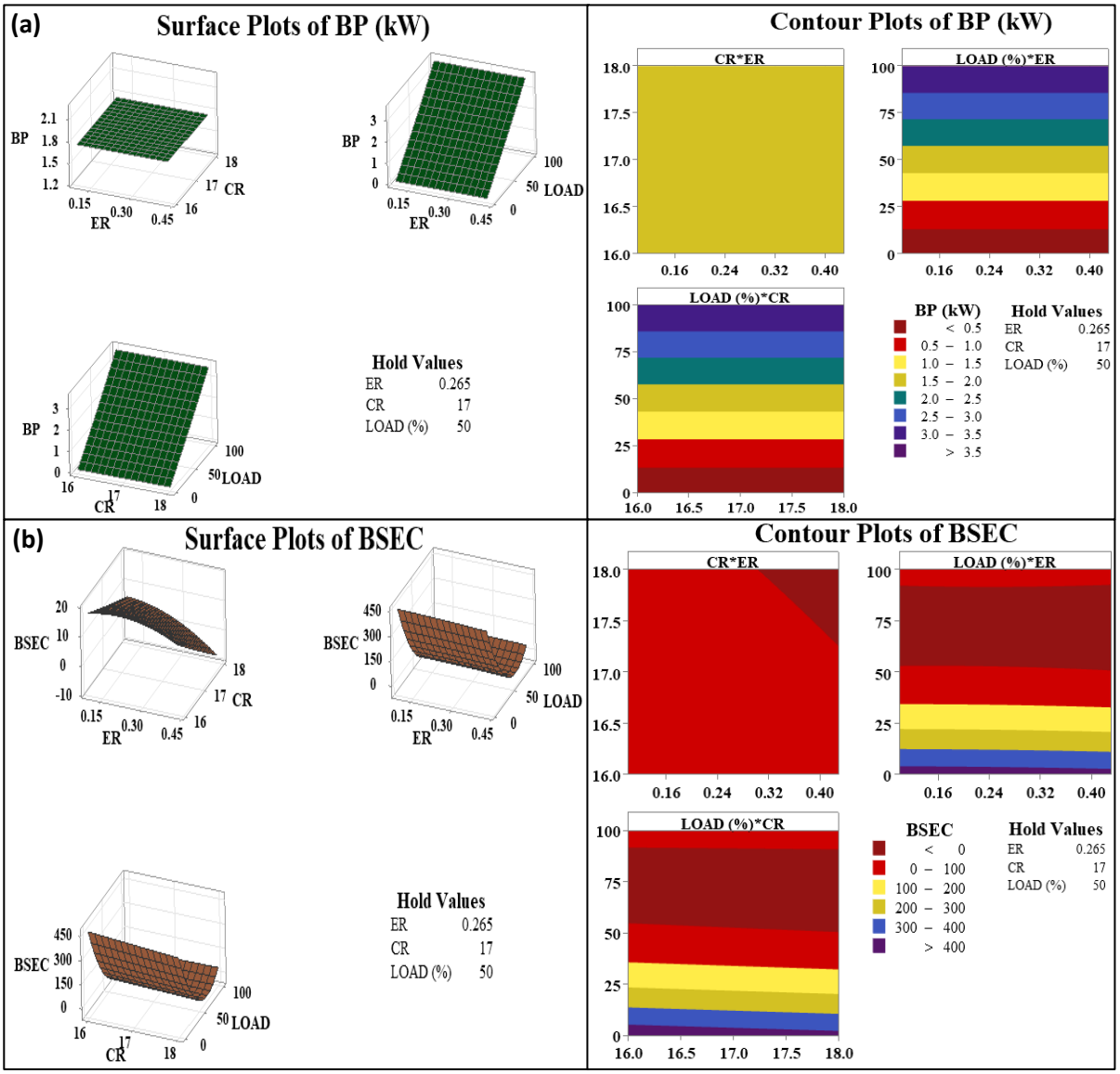

Figure 4.4.7. Surface & Contour plots of engine performance parameter (a) BP (b) BSEC

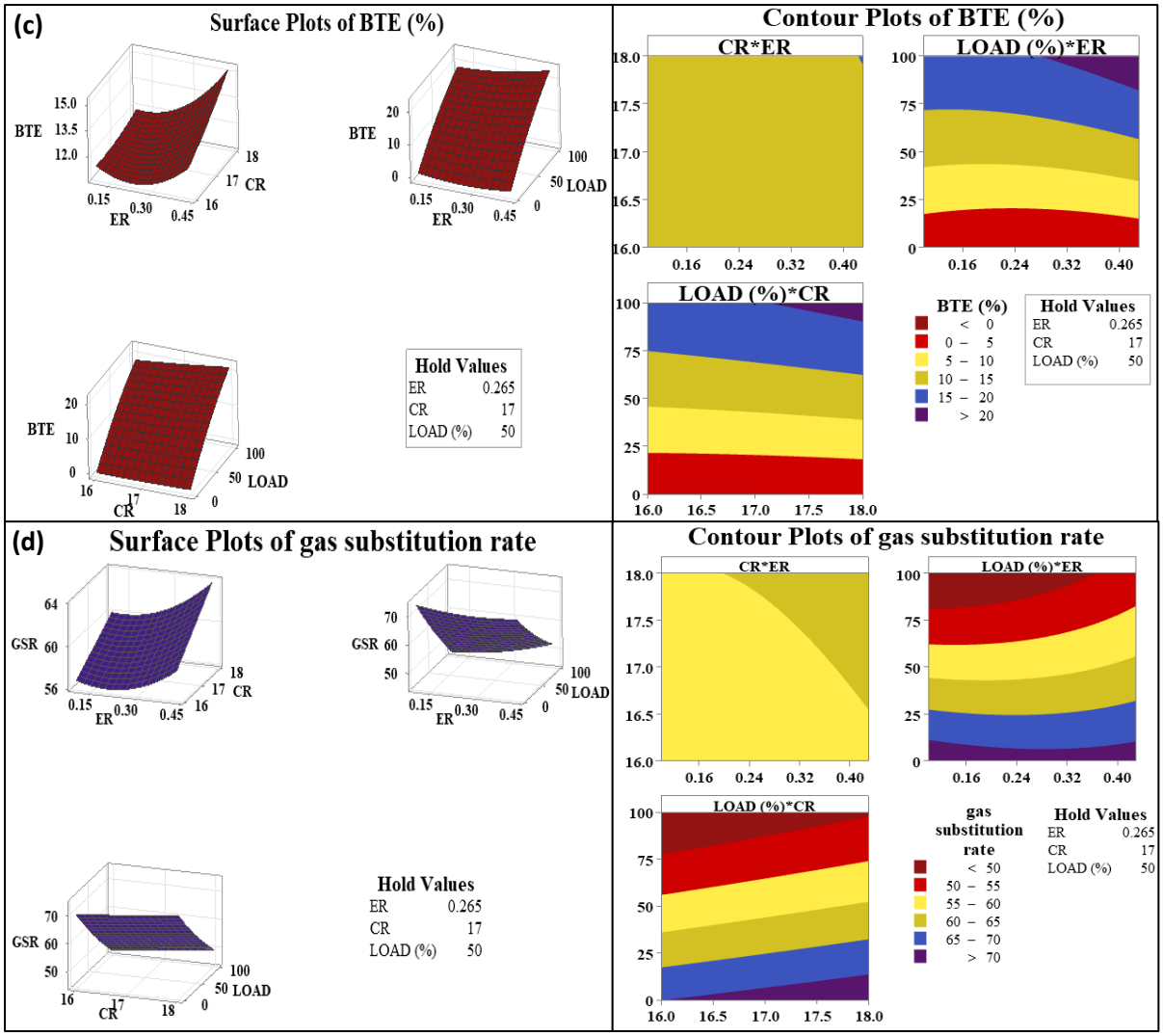

Figure 4.4.7. Surface & Contour plots of engine performance parameter (c) BTE (d) GSR

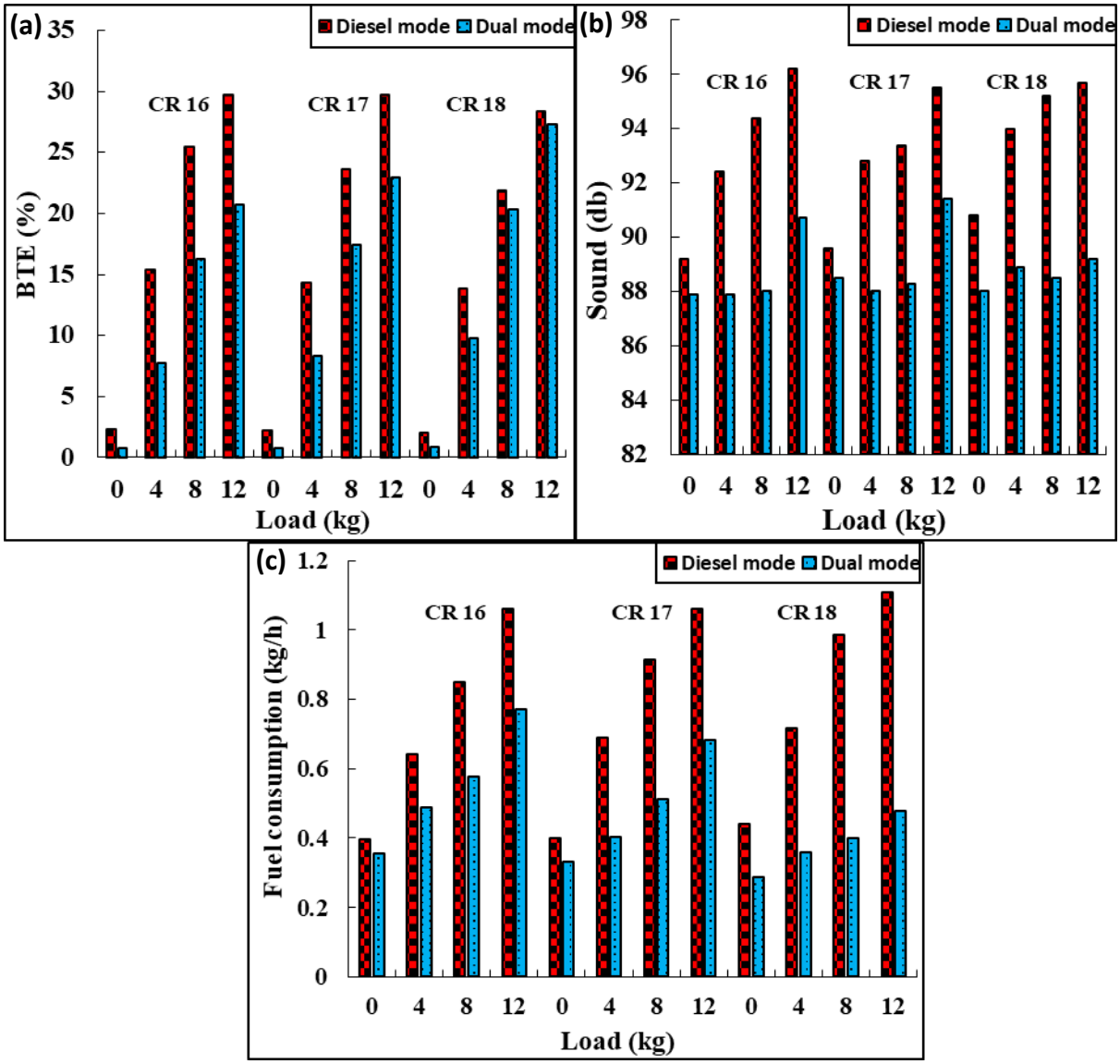

Figure 4.4.8. Comparison of diesel and dual mode engine performances for (a) BTE, (b) Sound, (c) fuel consumption

4.4.5.2 Engine emission characteristics

In this experimental investigation, the effects of the independent operating parameters, namely gasifier ER, compression ratio (CR), and engine load, on the engine emissions, namely CO, HC, CO_2, and NOx, are analyzed simultaneously. The study lets us interpret the engine's emissions characteristics in a more detailed manner.

The presence of carbon monoxide (CO) in the emissions is mainly characterized due to incomplete combustion [248], the existence of a local-lean mixture, and insufficient residence time for complete combustion [249]. Figure 4.4.9(a) shows the simultaneous impact of ER, CR, and load on the CO emissions. As the load increases, the magnitude of CO emission decreases. This is because, at a higher load, the temperature inside the cylinder rises, which assists in better combustion and decreases carbon monoxide concentrations [250]. It can be further noticed that CO emission increases at high ER and CR values. This might be due to the poor flame propagation leading to incomplete combustion due to the lean mixture at higher ER and CR values [216]. However, it can also be observed from Figure 4.4.10(a) that the maximum CO emission concentration in (diesel + PG) mode is 30.25 times more than in the pure diesel mode. The minimum magnitude of CO emission in dual mode engine run observed was 0.07% vol at ER 0.1, CR 17, and load 12 kg.

By interacting with nitrogen oxide in the vicinity of sunrays, hydrocarbon (HC) emissions produce ground-level ozone, which significantly negatively influences environmental degradation. It usually forms due to the incomplete combustion of unburned hydrocarbons. It is typically located in low-temperature regions, such as the cylinder wall, where the temperature is lower than in the middle. Figure 4.4.9(b) infers that the HC reduces with an enhancement in the load. This is due to the improved combustion at high cylinder pressure and temperature [241]. It can be further observed from the contour plot that a higher CR leads to a reduction in HC emission below 50 ppm. This results from short ignition delay leading to improved combustion and reduced HC emissions [241]. However, the HC emitted is more while running the engine on dual mode than in conventional diesel mode, as shown in Figure 4.4.10(b). It was further discovered that HC emission increases with gasifier ER. This is due to the availability of oxygen at higher ER [17]. The minimum magnitude of HC emitted in dual fuel mode was 16 ppm vol. at ER 0.1, CR 18, and 12 kg load.

The emission of carbon dioxide (CO_2) content characterizes due to the occurrence of complete combustion in IC Engines [248]. It is favored by lean charge, which is predominant in CI engines [251]. Figure 4.4.9(c) simultaneously shows the surface and contour plots of CO_2 emission versus three independent operating parameters (ER, CR, and load). It can be inferred that the magnitude of CO_2 increases as the gasifier ER and CR value increases. This is illustrated by the enhancement in the combustion process with the rise in ER [216, 252]. From the contour plot, it can be well inferred that CO_2 concentration decreases as the engine load increases. However, the concentration of CO_2 was 1 to 6.25 times more than the diesel mode run, as shown in Figure 4.4.10(c). The lowest CO_2 of 1.6 % vol was observed at ER 0.21, CR 16, and 12 kg load.

NOx is produced due to the availability of oxygen in the atmosphere and the existence of N_2 in the fuel. Figure 4.4.9(d) shows that the concentration of NO_x is high at high ER and CR values. This might be due to the availability of oxygen and higher temperature at high CR values [253]. It can also be observed that the NOx concentration decreases as the load increases; similar outcomes were also found by Mahla et al. [246]. However, inert gases, such as CO_2, with more significant specific heat dilute the cylinder charge. It remarkably lowers the peak combustion temperature and oxygen availability in the PG-fueled dual-fuel operation [254]. This is the primary factor that reduces NOx production while using PG dual fuel engines compared to diesel engines, shown in Figure 4.4.10(d). The minimum magnitude of NOx from the engine observed was 2 ppm at ER 0.1, CR 16, and 8 kg load.

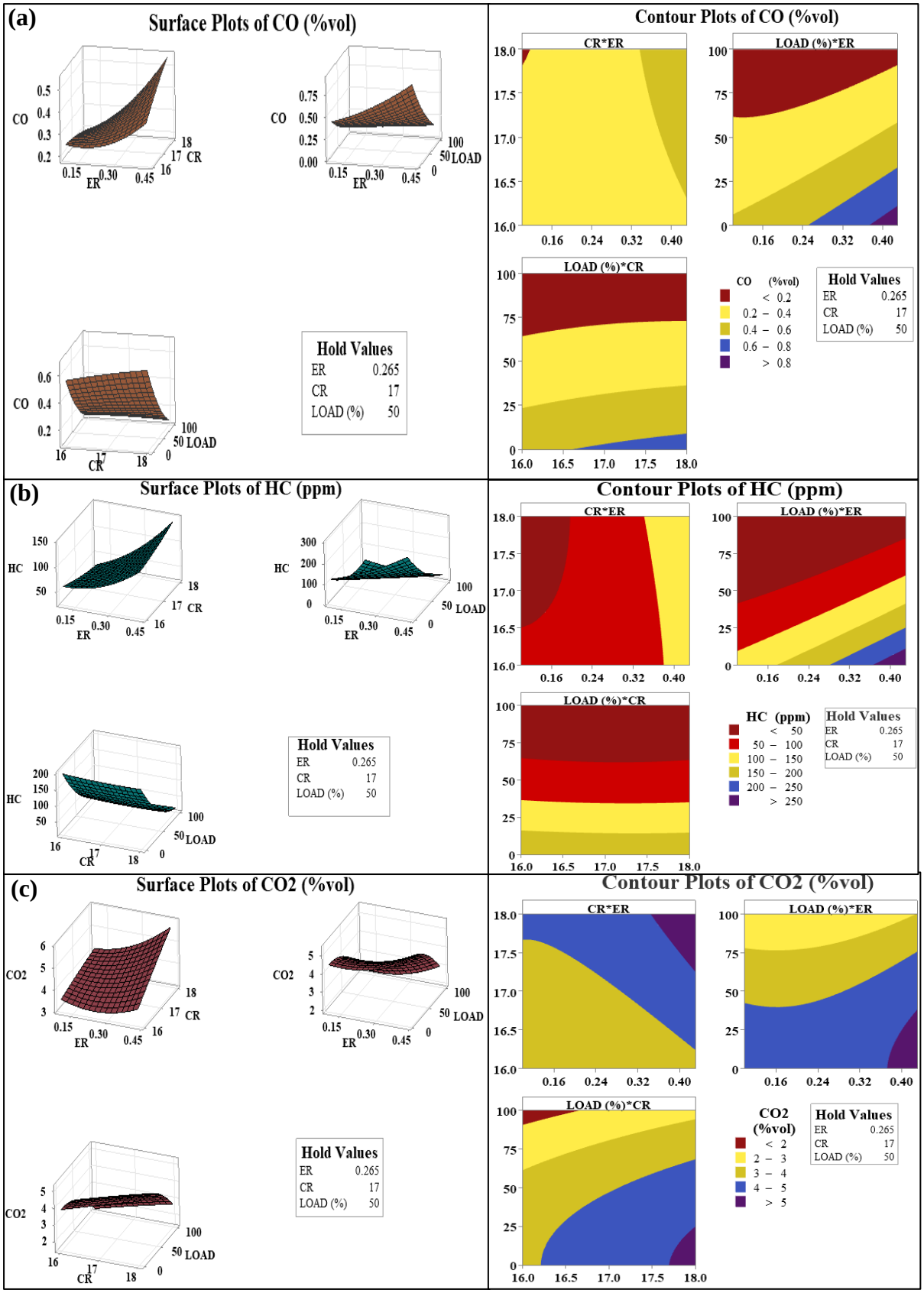

Figure 4.4.9. Surface & Contour plots of engine emission parameters (a) CO, (b) HC, (c) CO_2

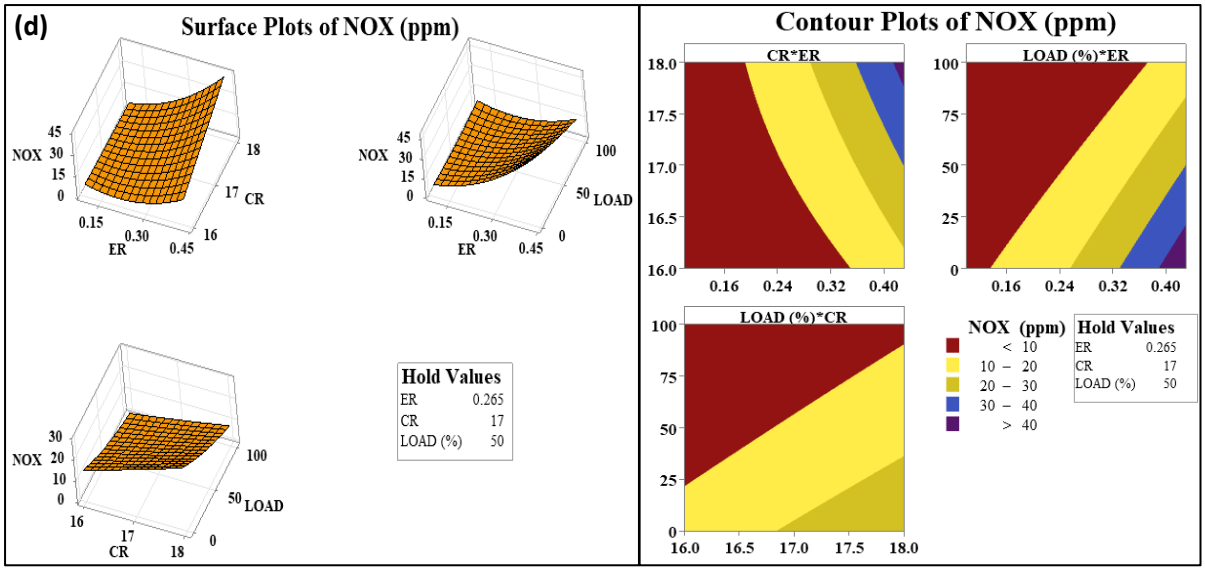

Figure 4.4.9. Surface & Contour plots of engine emission parameters (d) NO_x

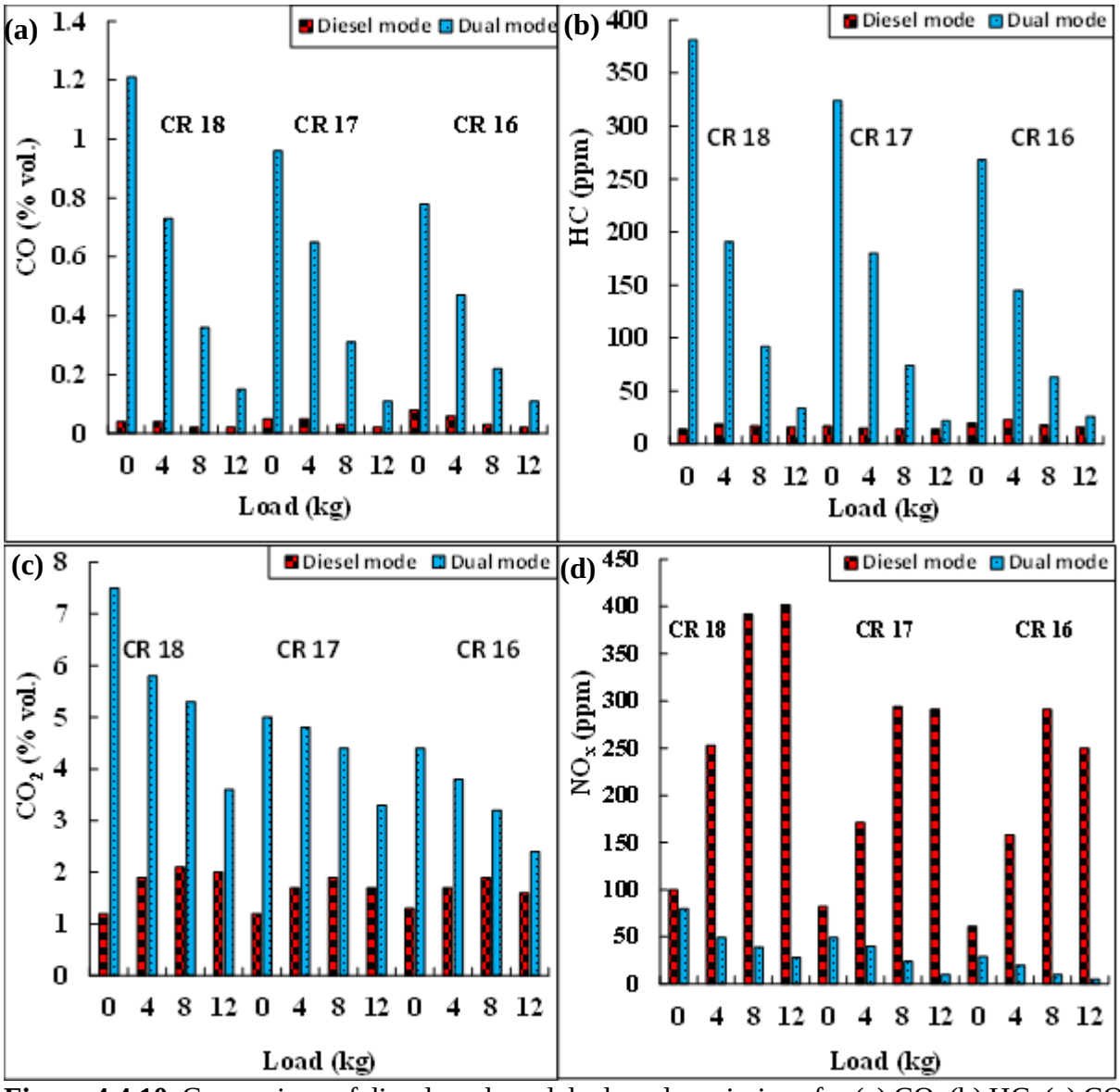

Figure 4.4.10. Comparison of diesel mode and dual mode emissions for (a) CO, (b) HC, (c) CO_2, and (d) NO_x

4.4.6 *Engine sound and Diesel savings*

The intensity of sound coming out of the engine was recorded using a digital sound meter Meco 970P in both diesel and dual mode engine run. Figure 4.4.11(a) shows the impact of ER, CR, and load on the sound coming from the engine. It can be observed that as the CR and load increases, the sound intensity also increases. This might be due to increased vibration at higher loads. At the higher gasifier ER, the noise from the engine was low. It was also observed from the Figure 4.4.8(b) that running the engine on (diesel + PG) had less sound intensity than conventional diesel mode engine run. The maximum sound level recorded from a dual-fuelled engine was 92.8 db at ER 0.1, CR 18, and 12 kg load, which falls under the acceptable limit as per the environment protection act [232]. The sound intensity recorded was 1.22-6.88 % less than the diesel mode engine run. The maximum sound intensity noted by other authors during dual-fuel mode engine runs was 98.90 db [85] and 89.6 db [81].

From the experiment, it was observed that running the CI engine on dual mode (Diesel + PG) saves a significant percentage of non-renewable diesel fuel. Figure 4.4.11(b) shows that the maximum diesel saving can be achieved at higher compression ratios. This is because, at higher CR values, the engine's thermal efficiency improves, leading to lower fuel consumption [35]. The diesel saving increases with the load; however, there needs to be a richer mixture for maintaining the engine at a constant 1500 rpm at maximum loading conditions. Thus diesel saving has a slight decrement [35]. Table 4.4.4 compares airflow, diesel, and PG flow during diesel and dual fuel mode engine run. The table shows that diesel fuel consumption increases in both modes as load increases. However, the fuel flow decreases as the CR increases. During the experiment, the maximum diesel saving of 59.5% was achieved at CR 18, load 8 kg. Other authors predicted diesel saving of 49.05% [35] and 58.18% [85].

Table 4.4.4. Comparison of diesel and dual mode diesel saving

CR	Load (kg)	BP (kW)	Diesel-mode Air (kg/h)	Diesel-mode Fuel (kg/h)	Dual-mode Air (kg/h)	Dual-mode Fuel (kg/h)	Dual-mode PG (kg/h)	Diesel saving (%)
16	0	0.1	29.56	0.39	21.79	0.35	7.76	9.87
	4	1.1	28.92	0.64	21.79	0.48	7.12	23.84
	8	2.4	28.13	0.84	21.30	0.57	6.83	31.97
	12	3.5	27.85	1.06	21.05	0.76	6.79	27.44
17	0	0.1	29.45	0.39	22.27	0.33	7.18	17.28
	4	1.1	28.91	0.69	21.79	0.40	7.11	41.42
	8	2.4	28.11	0.91	21.55	0.51	6.56	43.78
	12	3.5	27.58	1.06	21.30	0.68	6.28	35.81
18	0	0.1	29.43	0.43	22.51	0.28	6.92	34.83
	4	1.1	28.23	0.71	22.27	0.36	5.95	49.65
	8	2.4	27.83	0.98	21.79	0.39	6.04	59.5
	12	3.5	27.43	1.11	21.30	0.47	6.12	56.88

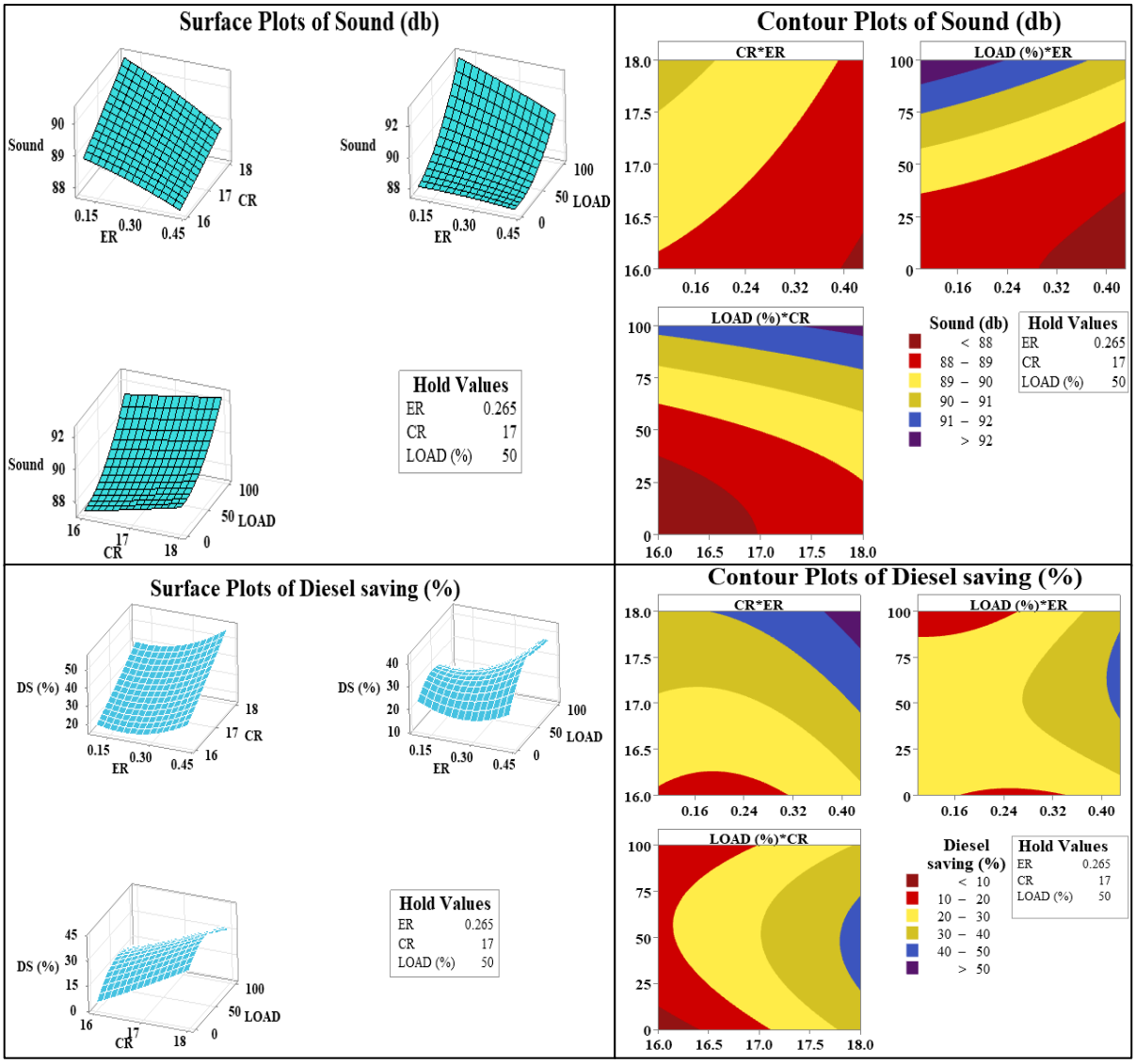

Figure 4.4.11. Surface & Contour plots of (a) Sound intensity and (b) Diesel saving

4.4.7 *Response optimizer*

To determine the best input setting of the gasifier and engine at which output responses are optimally analysed. The fundamental goal of this study is to minimize engine emissions (CO, HC, CO_2, and NOx) while maximizing engine responses (BP, BSEC, BTE, and GSR). The overall desirability function D is defined as the weighted geometric average of the individual desirability (d_i) [110, 159]. Here the overall composite desirability of the model is 0.7201, as shown in Figure 4.4.12, which is close to 1. Hence the model is feasible according to the desired approach. Figure 4.5.13 shows the RSM optimizer plot generated by Minitab. Optimum values

of engine performances (BP, BSEC, BTE, and GSR) were found as 3.52 kW, 34.16 MJ/kWh, 21.02 %, and 49.39 %, respectively. Also, the optimum values of engine emissions for CO, HC, CO_2, NOx, and sound intensity were found as 0.0918 %vol., 17.4144 ppm, 2.0575 %vol., 4.5538 ppm, and 90.21 db, respectively, with the corresponding values of input parameters as ER 0.43, CR 16, and, engine load 100% (i.e.,12 kg). Regarding model confirmatory tests, the result indicates 99 % of the population's findings are within the 95% confidence interval, as described in Table 4.4.5. A similar trend of test results was observed in reference [110]. Additionally, the confirmation of the RSM-based result with experimental value was performed, and respective comparative error values are mentioned in Table 4.4.6. The highest error proportion of 4.45% and lowest error proportion of 0.16 % were achieved. The overall engine performance and exhaust emission error rate are less than 5%. Thus, the values optimized by RSM are feasible.

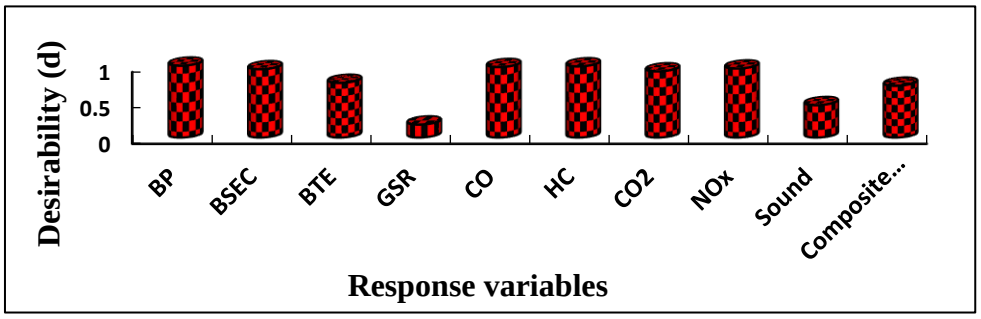

Figure 4.4.12. Desirability 'd' value of engine response variables

Table 4.4.5. Confirmatory test of a predicted optimum set of operation

Analysis	Predicted Mean	Predicted Median	Std Dev	n	SE Pred	95% PI low	95% PI high
BP	1.77509	1.77509	0.0639603	1	0.0646231	1.64485	1.90533
BTE	11.5021	11.5021	0.922099	1	0.979164	9.51992	13.4843
BSEC	9.9081	9.9081	47.9236	1	50.8894	-93.1121	112.928

Analysis	Predicted Mean	Predicted Median	Std Dev	n	SE Pred	95% PI low	95% PI high
GSR	58.4926	58.4926	1.62626	1	1.72691	54.9966	61.9885
CO	0.294242	0.294242	0.0670342	1	0.0711826	0.15014	0.438344
HC	68.9389	68.9389	21.8504	1	23.2026	21.9676	115.91
CO_2	3.92798	3.92798	0.314444	1	0.333903	3.25203	4.60393
NO_X	11.0408	11.0408	5.39141	1	5.72507	-0.548995	22.6306
Sound	89.0232	89.0232	0.858387	1	0.911509	87.1779	90.8684

Table 4.4.6. Validation tests for optimized and experimental values

Engine response at optimized input setting: (ER 0.43, CR 16, Load 100%)			
Response	***Optimized result***	***Experimental result***	***% Error***
BP (kW)	3.5	3.4	2.94
BSEC (MJ/kWh)	34.16	35	2.4
BTE (%)	21.02	22	4.45
GSR (%)	49.39	49.31	0.16
Sound (db)	90.21	90.7	0.54
CO (% vol.)	0.091	0.094	3.19
CO (g/kWh)	3.267	3.375	
CO_2 (% vol.)	2.05	2.13	3.75
CO_2 (g/kWh)	0.130	0.135	
NO_X (ppm)	4.55	4.75	4.21
NO_X (g/kWh)	0.030	0.031	
HC (ppm)	17.41	18	3.27
HC (g/kWh)	0.034	0.036	

4.4.8 *Uncertainty analysis*

Every measuring equipment or device has some inaccuracy caused by factors such as operating conditions, calibration, inspection, trial planning, and environment. As a result, the complete experiment was run so that the values were duplicated three times, and then the arithmetic mean of all the weights was computed to arrive at a good result. Table 4.4.7 shows the list of different variables and their associated variables for calculating the errors. The overall experimental uncertainty is calculated as follows:

Overall Uncertainty =

$$\sqrt{(BP)^2 + (Thermocouple)^2 + (Dynometer)^2 + (Burette\ Fuel\ measurement)^2 + (CO)^2 + (HC)^2 + (CO2)^2 + (NOx)^2}$$

$= \pm \sqrt{(0.39)^2 + (0.16)^2 + (0.2)^2 + (1)^2 + (0.1)^2 + (0.2)^2 + (0.2)^2 + (0.5)^2} = \pm 1.55$

Table 4.4.7. Uncertainties of variables

S.No.	Equipment name	Measuring range	Resolution	Accuracy	Uncertainty (%)
1	Thermocouple	0 – 1200 ^oC	1 ^oC	± 2 ^oC	± 0.16
2	Dynometer	0-50kg	0.01 kg	± 0.1 kg	±0.2
3	Burette fuel meas.	-	-	± 0.1 cm^3	± 1
4	CO	0 – 10 vol.%	0.01 vol.%	± 0.1 vol.%	± 0.1
5	HC	0 – 20000 ppm	1 ppm	± 10 ppm	± 0.2
6	CO_2	0 – 20 vol.%	0.1 vol.%	± 0.3 vol.%	± 0.2
7	NO_X	0 – 5000 ppm	1 ppm	± 20 ppm	± 0.5

4.4.9 *Conclusions*

Present study investigated the performance and emission characteristics of VCR diesel engine (DF) running on PG obtained through triple feedstock gasification. 90-95% reduction in NO_x emission was achieved during DF with a maximum BTE of 27.30% in DF engine run at 12 kg load. A maximum diesel saving of 59.5% was achieved at CR 18.

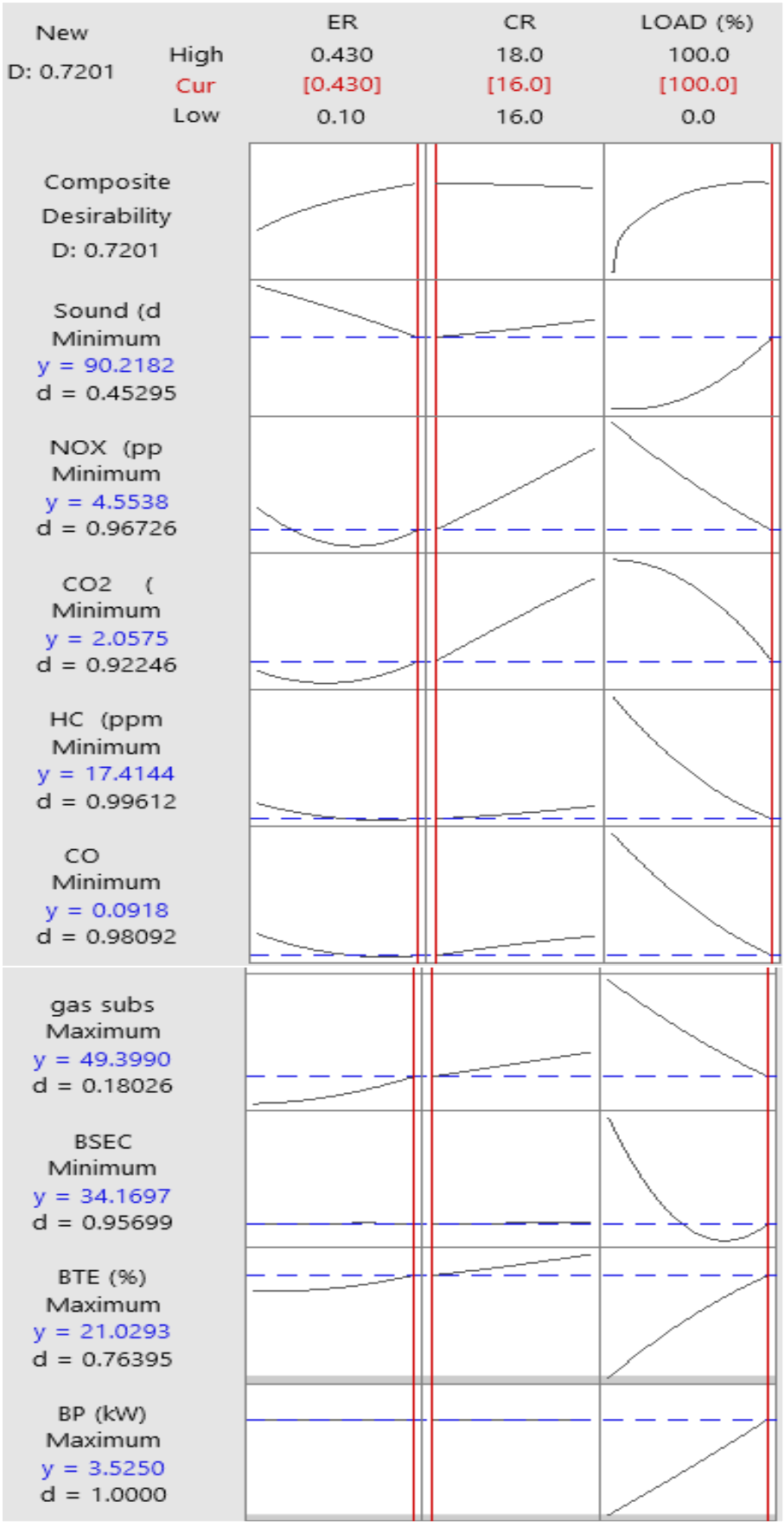

Figure 4.4.13. RSM generated optimisation plot

4.5 Comparative analysis of gasification/co-gasification on CI engine performance

4.5.1 *Introduction*

The key challenges in biomass-based gasification energy extraction are location-based feedstock unavailability and subsequent unstable power generation. However, it is solvable through energy-efficient technology innovation with alternate biomass utilisation and blending. Thus, in order to recommend multiple feedstocks for sustainable gasification and power generation via engine integration, a comparative study is required, which is rarely conducted at same platform. Therefore, in this study, gasifier-dual fuelled engine (G-DFE) performance was conducted and compared together with gasification of individual feedstock (i.e., Mahua wood waste, coconut shell, sawdust briquette) and their blends with low grade coal. Additionally, the performance of different set of feedstock gasification and in engine utilization were compared with optimal operating setting and output response using RSM. The operating setting of G-DFE include gasification equivalence ratio (GER), and engine load percentage at a compression ratio of 18. The G-DFE performance includes engine brake thermal efficiency (BTE), diesel saving (DS), gasification efficiency, emission of CO, CO_2, HC, and NO_X. Results showed that the biomass co-gasification blends presented higher engine performance than the single feedstock gasification. The (briquette+ mahua wood) producer gas (PG) based dual fuel (DF) engine offers maximum brake thermal efficiency (BTE) of 27.6%. The maximum DS of 63.44 % was obtained for coconut shell G-DFE at input condition of GER 0.24, and 33.33 % load. Regarding optimum emission, the maximum CO, and HC, belongs to the setting of GER 0.10, 100% load for briquette G-DFE. The maximum CO_2 and NO_X, belongs to the setting of GER 0.20, 80.80 % load for (coal+ briquette), and GER 0.43, 100% load for mahua wood G-DFE respectively. Further, the

various experimental results and optimisation in this study can be used to guide G-DFE management for optimal operation and environmental footprint reduction.

As the citation mentioned in literature review unit, CI engines have been employed with producer gas, which is generated from a variety of feedstocks utilizing both solo and co-gasification. It can be seen that gasifier engine performance varies with feedstock type, its blending ratio, the calorific value of feed material, and the quality of PG. Moreover, there are a number of other types of biomasses that are also available in rural areas, and their waste-to-energy conversion and utilization are still lacking, and their versatility in terms of reports is still limited. It was discussed above that scarcity of feedstock availability due to a seasonal boundary can be solved mainly by co-gasification. Therefore, to determine the viability of effective utilization and wider applications, the performance of the gasifier-engine integration system must be studied in relation to the newly identified feedstock at various load conditions and with variable operating conditions. Simultaneously, it must be a comparative assessment and analysis of the optimum operating setting to obtain the optimal results in terms of power output and emissions. Consequently, the primary goal of this research was to investigate the impact of different feedstock-PG on gasifier-engine performance with parametric operating variation. So far as the literature gap is concerned, there is a paucity of information on the comparison of different feedstock in terms of purely and co-gasification comparison in a similar platform. Furthermore, no previous research has attempted a comparison of the sole and co-gasification performance of coal-mahua-coconut shell-briquette feedstock and its blends in the same gasifier-engine experimental setup. So far as sole feedstock and dual feedstock co-gasification coupled engine performance is concerned, due to composition and heating value variation, there will definitely be variations in power generation and trade-offs among power, efficiency, and emission parameters. Therefore, to achieve the best performance response, its operating variables

must be optimized. However, there is a research gap in the literature regarding comparative optimization performance measuring.

The selection of mahua, coconut shell, and briquette is due to their abundance in India, an agricultural country. Mahua tree (madhuca-indica) cultivation is widespread in India, a forest-based tree-borne non-edible oil, and around 62,463 hectares have been allocated to plant this species [255]. It was reported that around 45% of waste biomass (trims, sawdust, off-cuts, shavings, etc.) is produced by the wood processing industries like plywood mills, sawmills, craft industries, carpentry shops, etc. [256]. Similarly, over 11.7 million metric tonnes of coconuts were produced in India in 2018, producing approximately 15% solid waste [257]. Regarding the production of sawdust base briquettes, approximately 18.91 million tons of sawdust are generated in India each year, of which about 5.5 million tonnes remain unused [164]. Hence, due to the accessibility of these feedstocks, it is therefore feasible to ensure that feedstock supply interruption can be resolved and sustainable power generation could be achieved.

Taking into account the literature review, existing perspectives, and research gap, the first objective of this study is to approve the utilization of feedstock available (mahua tree, coconut shell, sawdust briquette, and blends with low-grade coal) at the Indian rural region for sustainable distributed power generation experimentally. The novelty of the work is to investigate the comparative assessment of gasifier-engine performance in terms of gasification efficiency, engine power, diesel saving, and emission with sole feedstock gasification and dual feedstock co-gasification. A further novelty involves comparing the optimization outcomes of the gasifier-engine operating settings for the best power and emission-balanced performance in the single and co-gasification modes utilizing the RSM optimizer tool. Considering these aspects, this study was composed with the following order: initially, it carried out an experimental investigation on individual feedstock (mahua tree, coconut shell, and sawdust briquette) gasification to make PG and utilized as secondary fuel with diesel/biodiesel in the CI engine. Thereafter, co-gasification

of these feed materials was conducted with a 50:50 ratio of biomass and coal, and generated PG was utilized in a dual mode CI engine. In both conditions, gasifier-engine performance (power and emission) was experimentally investigated with varying operating settings as GER, and engine load at CR 18. Finally, to optimize the trade-off between power and emission in relation to operating variables, an RSM optimizer was conducted to achieve control strategies for the best gasifier engine performance response. Although several feedstock blend gasifications have recently been proposed with RSM-based optimization, as shown in Table 4.5.1, comparisons of such blends with single ones in the same platform are rarely investigated. The performance of the gasifier-engine coupled system deals with brake thermal efficiency, DS, and the engine emissions. Further, optimization is concerned with balancing the maximization of engine power with the minimization of exhaust emission. Conclusively, it was found that all three feed materials have significant potential to generate PG, and its utilization successively generates power by CI engine, while co-gasification with coal blend offers better performance results. Thus, these findings can be used as guidelines in gasifier-engine applications and platforms for further improvement.

Table 4.5.1. Comparison between prior research and current study

Feedstocks	Experiment on Engine	Optimization tool	Input variable	Ref.
Coconut shell, rice husk coir pith, rubber wood, and rubber seed kernel shell-PG and diesel	CI	RSM	Engine load and calorific value	[82]
Coconut shell, rice husk, rubber shell-based PG and diesel	CI	RSM	CR and load	[166]
Vachellia nilotica-PG and biodiesel	CI	RSM	Pressure, injection timing (IT), and load	[167]
PG and biodiesel	CI	RSM	CR, engine load, and IT	[168]
Vachellia nilotica-PG and diesel	CI	RSM	CR, blending ratios, and IT	[169]
Cocoa pod husk-PG and diesel	CI	RSM	Brake power and CR	[170]
Coal PG and Diesel	CI	RSM	GER, engine load and CR	[178]
Current Work				
PG of coal/ briquette/ coconut shell/ mahua wood and its blend with diesel/biodiesel fuelled engine	CI Engine	RSM	GER, and load percentage	Not yet

4.5.2 *Characteristics of feedstocks*

In this study, producer gas derived from the coal, biomass (briquette, coconut shell, mahua wood), its 1:1 blend (coal + briquette, coal + coconut shell, coal + mahua wood, briquette + mahua wood), 1:1:1 blend (coal + briquette + mahua wood), and (mahua wood PG + B20 safflower biodiesel) was used as inducted fuel. Biodiesel was produced from safflower oil through a transesterification process. In this process, 20% methyl alcohol and 0.4% NaOH were mixed together. This mixture was added to safflower oil in a glass borosil container. The combined mixture was heated to 55–65°C and stirred within a transesterification reactor for a duration of 120 minutes at around 1000 rpm. After 2 hours, the mixture was left in a separation funnel for 24 hours to let methyl ester and glycerine separate. The biodiesel that had been separated was subjected to three rounds of washing in order to eliminate any impurities. Subsequently, the biodiesel was heated to a temperature of 110°C in order to remove any residual moisture. The resultant biodiesel was blended with conventional diesel fuel in a proportion of 20% by volume, yielding fuel blends known as B20. The proximate and ultimate analysis results of different feed materials are depicted in Figure 4.5.1(a)-(b) in terms of weight% dry basis. The values of ash, moisture, volatiles, and fixed carbon present are based on weight percentage. The oxygen content in the feedstocks varies in the range of 39.49-44.96%. Moreover, the PG compositions from different gasification/ co-gasification-based feedstocks are also shown in Figure 4.5.1(c), along with the LHV of respective fuels. Hydrogen content in the PG varies in the range of 10-17%, and the LHV of gaseous fuels varies in the range of 2.62-5.18MJ/Nm^3 for different feedstocks. Thus, the choice of biomass feedstock has a profound impact on the gasification process and subsequent performance in IC engine applications. Different biomass feedstocks have different chemical compositions, including its moisture content, lignin, cellulose, and hemicellulose content that releases different amounts of tar, ash, and other contaminants during gasification, influencing the gasification efficiency, PG quality, and overall

engine performance. Lower moisture and tar content-based feedstocks are preferable for IC engine applications. Feedstocks with higher energy content, such as mahua wood, coconut shell result in PG with higher heating value, contributing to higher engine performance (i.e., Brake power, and BTE). Moreover, the choice of biomass feedstock determines the composition of the PG. The PG composition influences combustion characteristics, flame stability, and emissions in the IC engine. Higher energy content biomass led to higher combustion temperatures and potentially increased NOx emissions. A biomass feedstock with a higher HHV generally results in more efficient combustion, as it provides more energy per unit mass. This can lead to improved overall combustion efficiency in the CI engine. However, when compared to neat diesel operation, DF CI engine run experiences cyclic variability and a slight reduction in power as PG has lower energy content compared to diesel fuel. Additionally, a significant reduction in engine NOx emissions and diesel savings are also experienced in DF engine run. The block diagram of the whole experimental setup, along with different feedstocks, is shown in Figure 4.5.2.

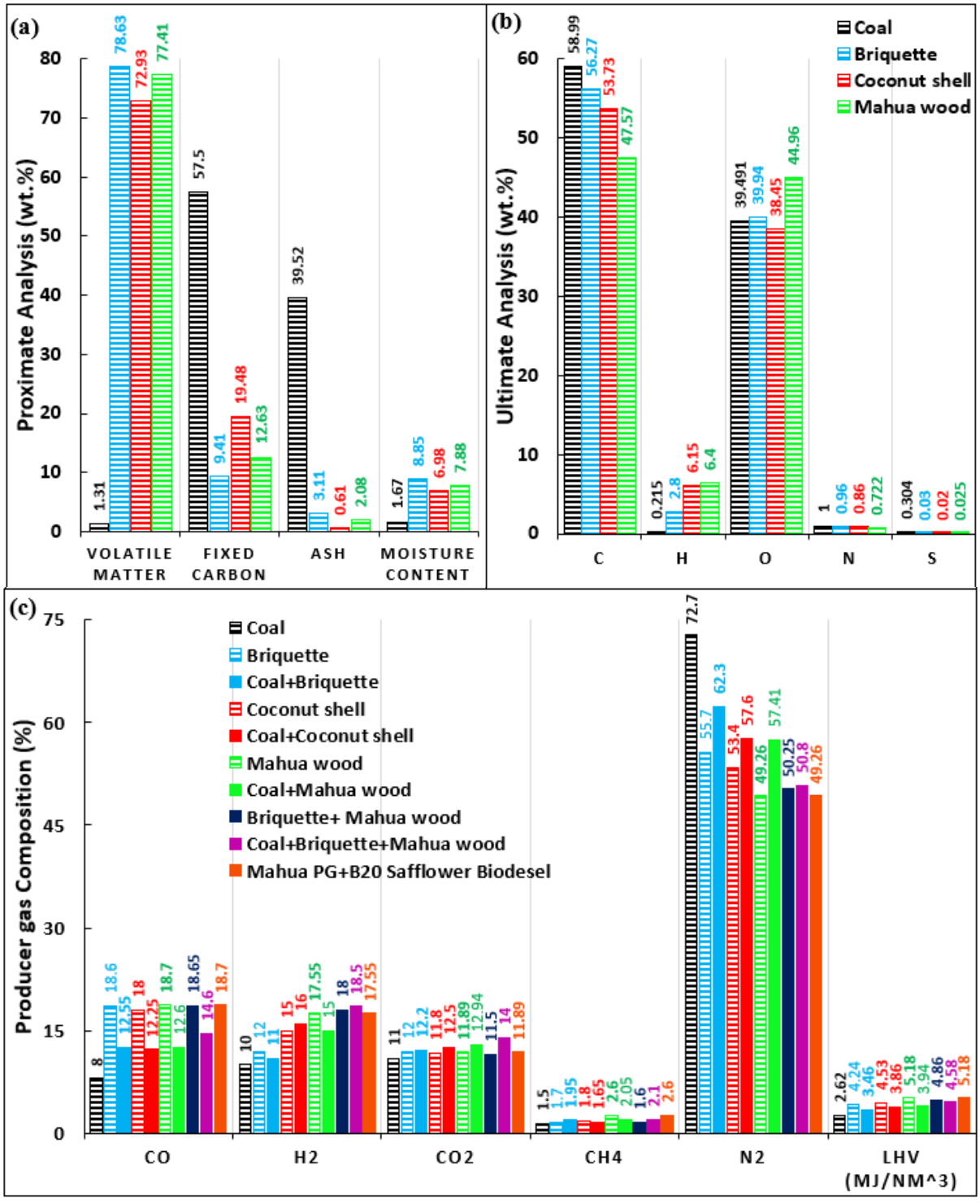

Figure 4.5.1. Proximate-Ultimate and PG composition of fuels used during experimentation

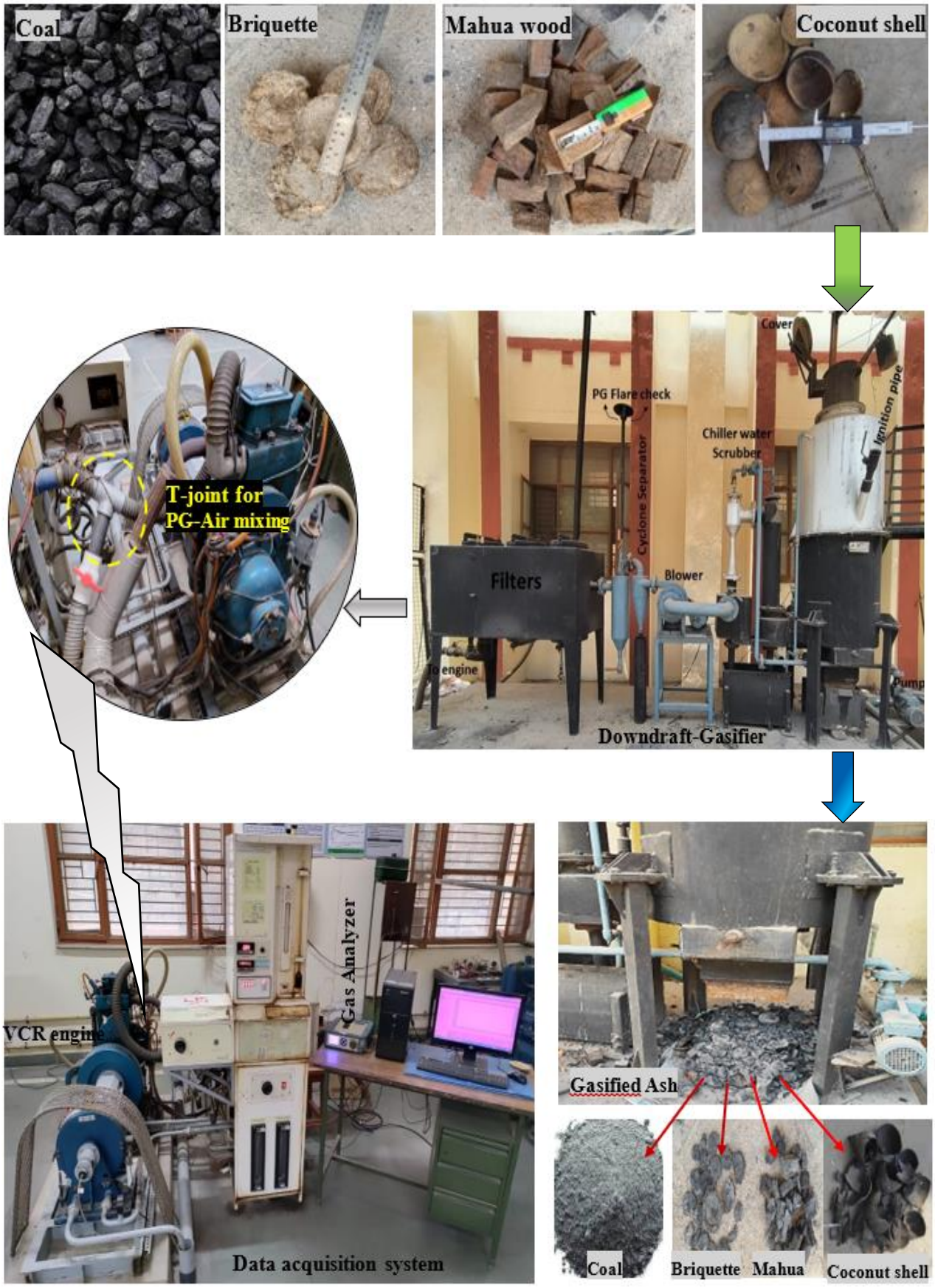

Figure 4.5.2. Block diagram of gasification/co-gasification experimentations performed

4.5.3 *Gasification performance*

Gasification performance refers to the efficiency and effectiveness of a gasification process. Gasification performance is influenced by several key factors like temperature, gas yield, residual char, LHV of PG, gasification efficiency, carbon conversion efficiency, and energy distribution. Close to the oxidation zone, the maximum gasification temperature reached approximately 700°C on the inner surface of the gasifier shell. Figure 4.5.3 displays the temperature distribution averaged along the vertical axis of the gasifier, observed across distinct gasification reaction zones (T1-T2: drying; T3: pyrolysis; T4: oxidation; T5: reduction; T6: grate). The temperatures were recorded with the six thermocouples placed at six different positions of the downdraft gasifier. It can be noticed from figure that the temperature attained during gasification is more than the co-gasification. The temperature attained during co-gasification was marginally reduced due to high ash content in coal [258]. The temperatures measured in this study are attributed to different feedstock properties and operating conditions. The experimental findings indicated that the gasification temperatures remained consistent within the temperature range of 600-700ºC. Coal gasification has the maximum, and (coal+ briquette+ mahua wood) feedstock has the minimum temperature obtained in the reduction zone.

LHV of PG holds crucial significance in the context of decentralized power generation, and exhaust emissions through internal combustion (IC) engines. The LHV of PG obtained from different feed materials is shown in Figure 4.5.1(c). Gas yield (GY) primarily relies on the flow rate of PG to the consumption rate of feed material. In the current experiments, the GY observed was 2.5Nm^3/kg of biomass. Cold gas efficiency (CGE) is determined as the ratio of energy contained in PG to the energy contained in the fuel (coal, briquette, coconut shell, mahua wood, or mixtures) [22]. CGE is calculated as per equation (4.5.1).

$$\eta = \frac{\text{LHVof gas (MJ/Nm}^3) \times \text{gasyield (Nm}^3/\text{kg})}{\text{LHVof fuel (MJ/kg)}} \times 100\% \quad (4.5.1)$$

The measure of gasification's effectiveness is determined by the carbon conversion efficiency (CCE), which is expressed as the ratio of carbon moles from solid biomass transformed into carbon-containing gases [259]. Figure 4.5.4 illustrates the impacts of gasification/co-gasification on CCE and gasification efficiency. The mahua wood gasification leads to the maximum carbon conversion and cold gas efficiency of 95.42% and 85.24%, respectively. Experimental analysis shows that the co-gasification (coal + biomass) has less CGE and CCE than its respective gasification. Several factors lead to decreased efficiency when coal is used as the feed material, including heat loss from elevated reactor temperatures, fuel loss through residue, and clinker formation due to high ash content of coal. On the other hand, biomass achieves higher efficiency due to contrasting reactivity, with increased volatiles and the catalytic impact of elements like potassium causing faster reactions and resulting in higher calorific value gas [22].

Figure 4.5.5 illustrates the Sankey diagram energy distribution for different feed materials integrating downdraft gasifier. The study employed the energy-mass allocation methodology to determine values based on a 40 kg feed material intake in a gasification experiment. Energy content for coal, briquette, coconut shell, mahua wood, and its mixtures are shown in Figure 4.5.5. According to reports, around 20% of the lower heating value (LHV) of the fuels is commonly used to provide sensible heat during the process of gasification [180]. As a result, this sensible heat was assigned for the gasification of the respective feedstock and its blends. In case of coal, an elevated temperature results in increased radiative heat losses from the gasifier's surface to the surrounding atmosphere. The greater gas outlet temperatures in coal lead to higher sensible heat for PG compared to other situations. Utilizing the energy allocation method and the LHVs from different feedstocks, the total energy contained of the produced gas was

computed as shown in the figure. The energy content of residual chars was determined by considering the remaining char mass after gasification and the heating value of residual char. Coal results in increased residue formation, leading to the loss of some energy associated with these residues. The co-gasification experiments led to higher residual char than biomass gasification, as the energy content of feedstocks for gasification was higher. The remaining proportion of energy balance represents unaccounted energy losses, including small gas leaks, various piping connections. This figure varied between 4.15-15.48% for the co-gasification (briquette+ mahua wood)- coal feed materials respectively.

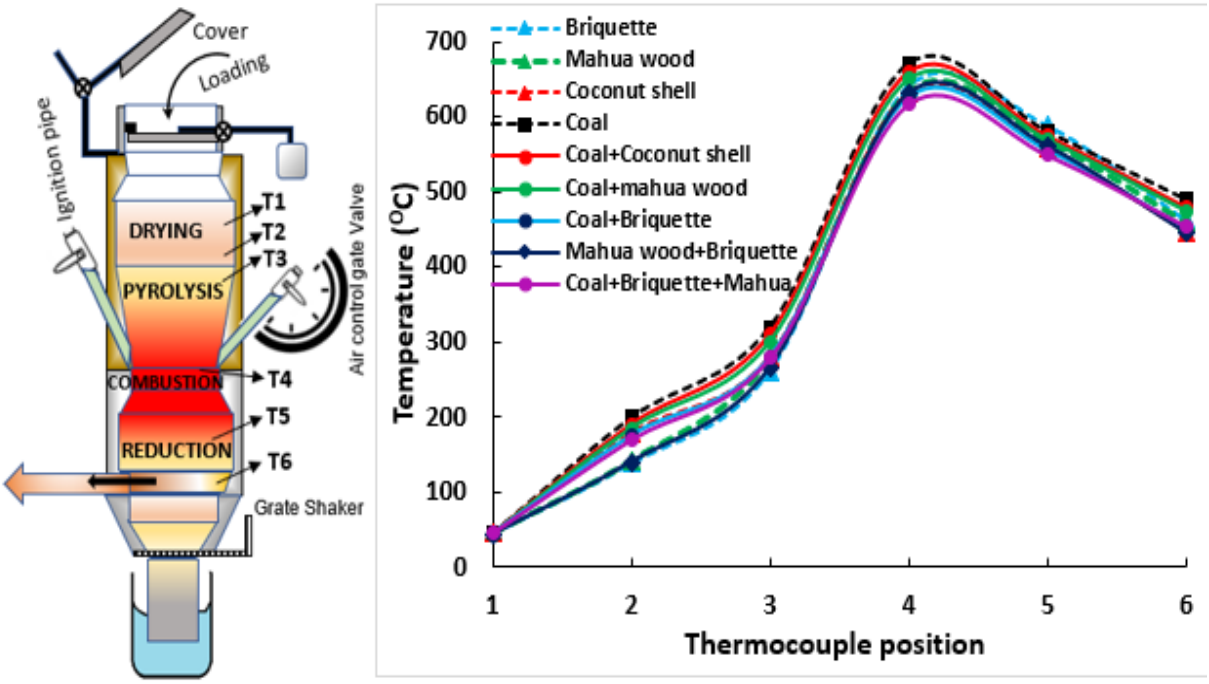

Figure 4.5.3. Temperature profile at different thermocouple position of the downdraft gasifier for different biomass feed-materials

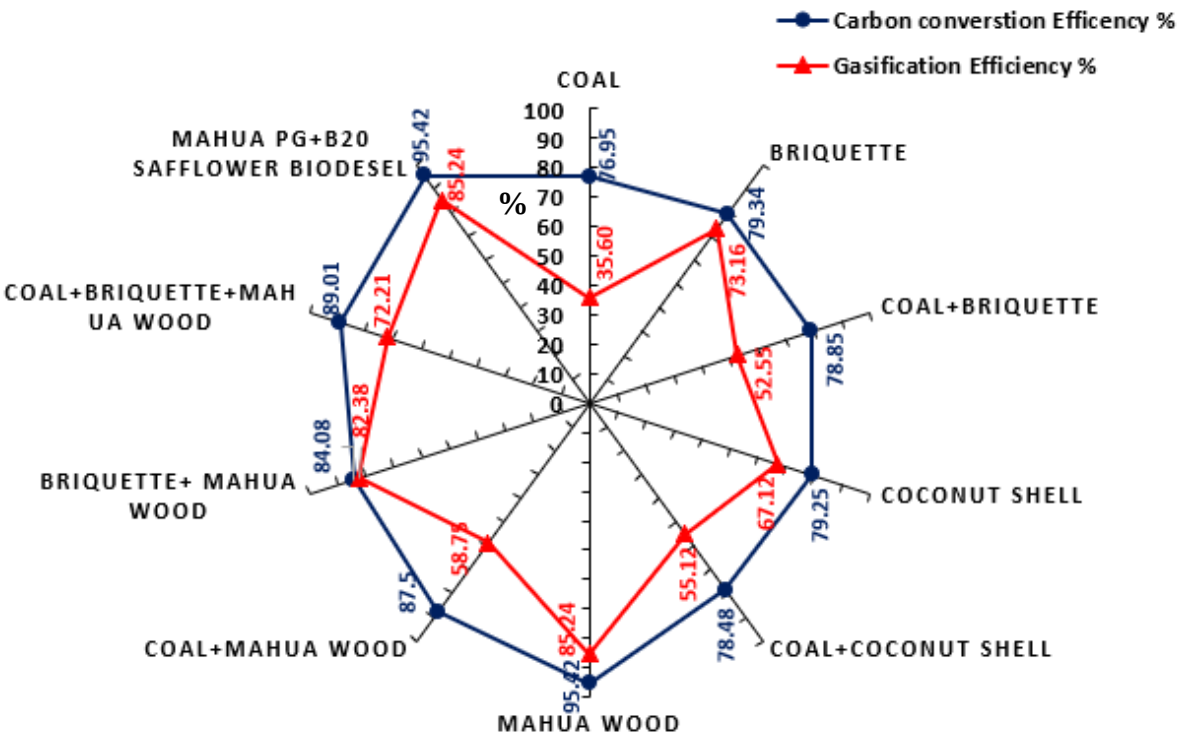

Figure 4.5.4. Carbon conversion and Cold gas efficiency for different feedstocks of downdraft gasifier

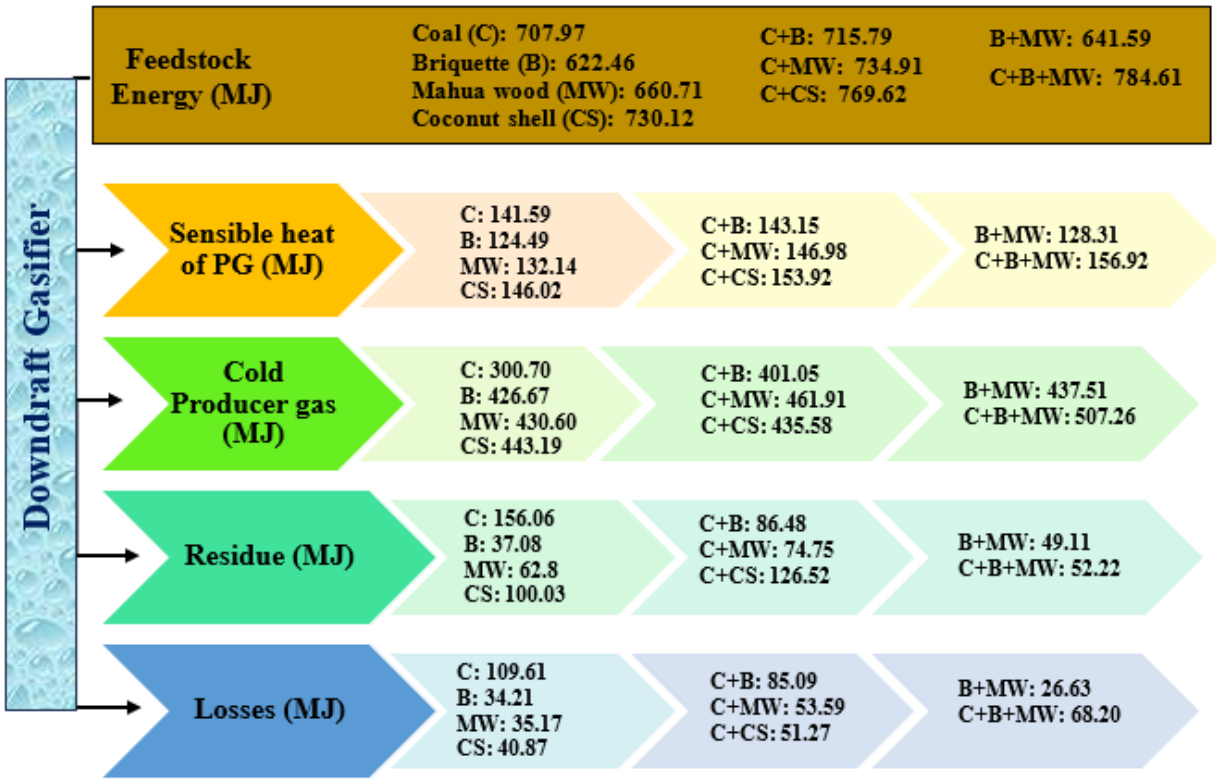

Figure 4.5.5. Sankey diagram for energy balance of different feedstocks in downdraft gasifier

4.5.4 *Engine performance and emissions*

4.5.4.1 BTE with engine load at different GER

Figure 4.5.6 shows how the BTE varies with the engine load percentage at different GERs. The figure shows a continuous increase in BTE for all tested fuels as the engine load increases in both operating modes. This improvement in BTE can be attributed to the higher intake air temperature during fuel injection in diesel engines, which leads to enhanced combustion. Diesel exhibits the highest BTE, followed by DF mode. However, the mahua-based PG+B20 biodiesel blend exhibits lowest BTE with respect to mahua-based PG dual fuel mode operation. This difference may be due to biodiesel's higher viscosity, which hampers proper fuel atomization and leads to incomplete combustion. Additionally, biodiesel has a reduced oxygen content, which further lowers the engine's combustion efficiency. From the experiment on different biomass-based gasification, co-gasification integrated CI engine, it can be concluded that biomass co-gasification (briquette + mahua wood) based PG exhibits maximum BTE, followed by triple feedstock-based co-gasification. Moreover, the experiment suggests that BTE of co-gasification integrated CI engine was less as compared to respective biomass gasification with the minimum BTE being observed for coal gasification. This was due to the lower heating value of PG, which results in a higher proportion of combusted mixture entering the engine [78]. Furthermore, it was observed that at higher GER and engine load, biomass co-gasification possesses maximum BTE due to the enriched PG quality at higher GER. The maximum BTE observed during neat diesel mode was 28.37 %, which was 2.17 % higher than the maximum BTE observed for biomass co-gasification based CI engine operation at GER 0.43 and 100% engine load.

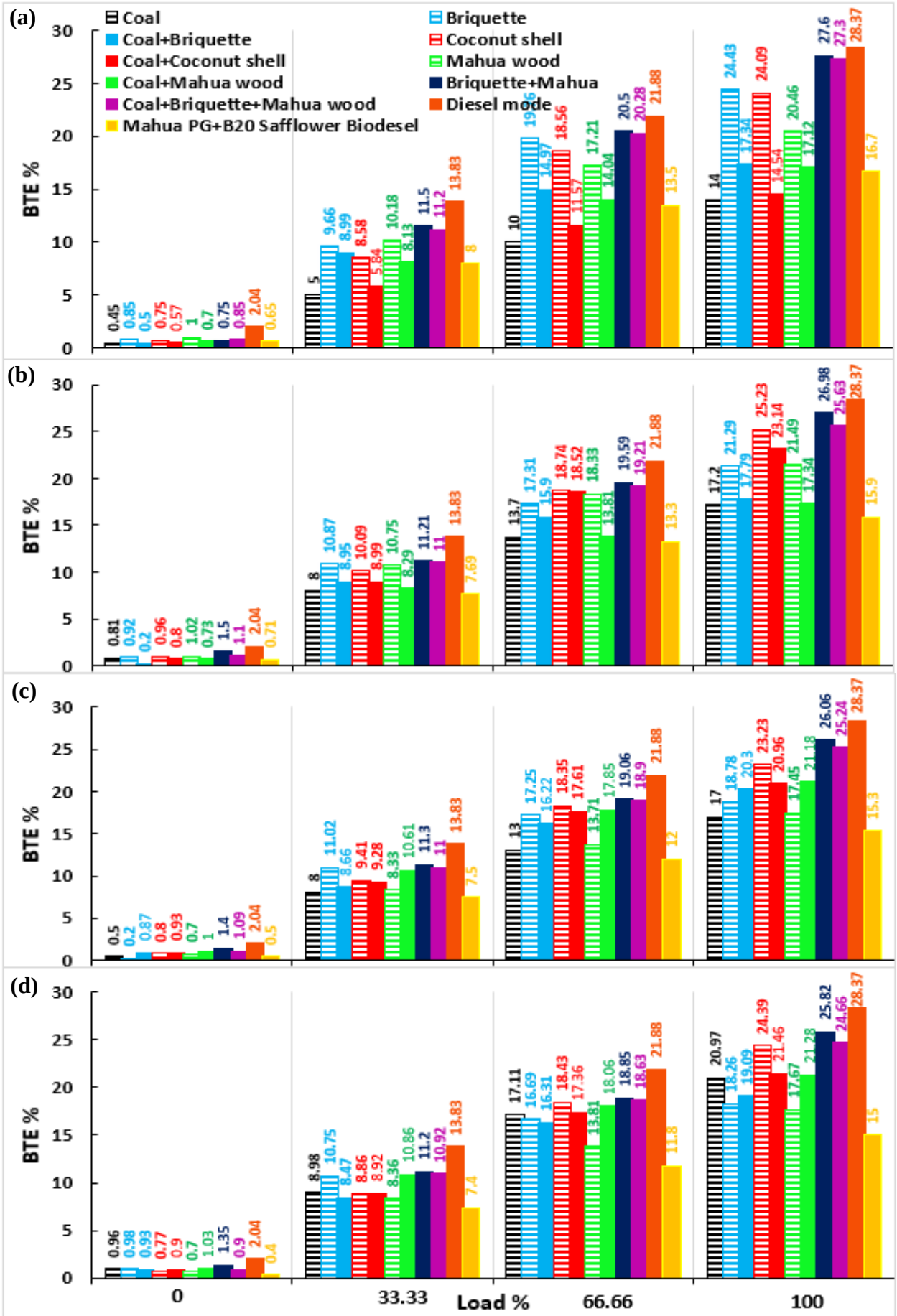

Figure 4.5.6. Variation of BTE with engine load at (a) GER 0.43, (b) GER 0.36, (c) GER 0.24, (d) GER 0.12

4.5.4.2 Diesel saving with engine load at different GER

Combining diesel fuel with PG in an IC engine minimizes usage of diesel fuel [238]. Figure 4.5.7 shows the interaction of engine loads on the diesel fuel savings at different GER for gasification/co-gasification based CI engines. It is noted that biomass co-gasification, and triple feedstock co-gasification integrated CI engine results show an increase in DS with an increase in load, but DS decreases at higher loads. This might be due to the lower calorific value of the fuel blend and its incomplete combustion at high loads that result in reduced pilot fuel substitution [260]. However, the trade-off nature of DS with varying GER can be attributed to the varying PG composition and specific PG fuel consumption inside the engine cylinder. However, the mahua wood PG + B20 biodiesel blend fuel exhibits lower DS as compared to the respective mahua gasification/co-gasification based DF engine run. From the experiment, it was observed that coconut shell based PG integrated CI engine achieved a maximum of 62% diesel saving at GER 0.36 and 66.66% engine load. In comparison to other authors of the PG fuelled diesel engine, a significant DS was obtained, for example, 26.47 % from rice husk PG, 27.15 % from coconut PG and 49.95 % DS from rubber shell PG with 15.38-19.44 % BTE [78], 56% DS from redgram stalk PG [79], 45.7% at CR 18 by SB and carpentry waste-PG [80], 64.3 % at CR 18 by wheat-paddy PG [81], 49.05 % at 18 CR by low-grade coal-PG [35], and 59.04 % DS from biomass PG of 6.57 MJ/Nm^3 CV [82].

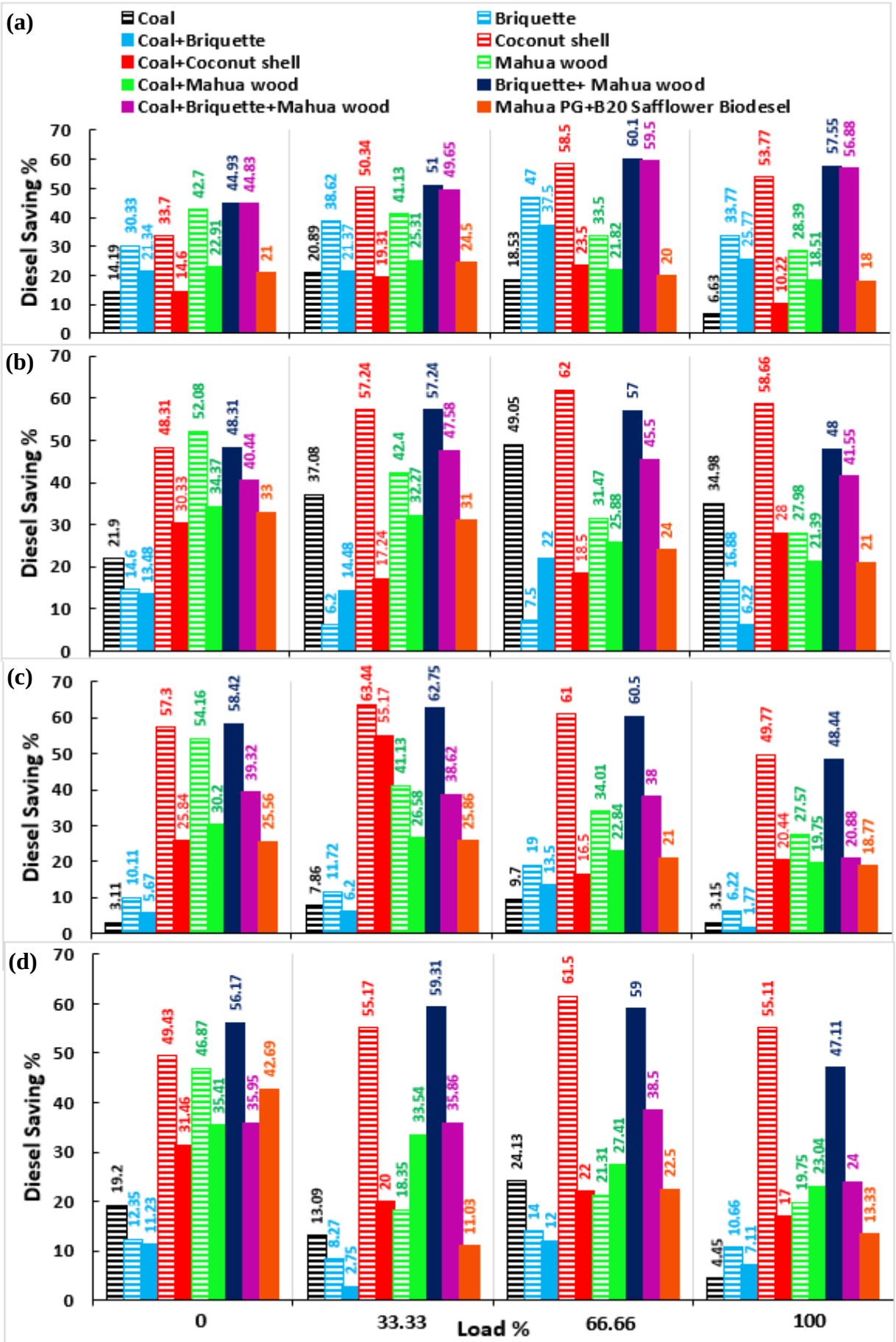

Figure 4.5.7. Variation of DS with engine load at (a) GER 0.43, (b) GER 0.36, (c) GER 0.24, (d) GER 0.12

4.5.4.3 CO emissions with engine load at different GER

Carbon monoxide (CO) emissions in engines can occur mainly due to incomplete combustion of the fuel-air mixture. From Figure 4.5.8, it can be concluded that at higher GER 0.43 (fuel-rich conditions), the combustion process tends to produce higher CO emissions. This is because there is an excess of fuel relative to the available oxygen for complete combustion, leading to the formation of CO. However, at lower GER 0.12 (fuel-lean conditions), the combustion process tends to be more complete, resulting in lower CO emissions. Moreover, at higher engine loads (100%), the combustion process is more efficient, resulting in a more complete burning of fuel. This increased combustion efficiency often leads to lower CO emissions. Additionally, CO emission is greater in the DF mode (PG + Diesel) compared to the single-liquid fuel mode across all test fuels at varying load conditions. This might be due to higher ignition delay and the presence of CO in PG that leads to incomplete combustion. Moreover, the biomass co-gasification (Briquette + Mahua wood) integrated CI engine emits more CO emissions at lower GERs as compared to coal, biomass gasification/co-gasification. At higher loads and lower GER, the blends of diesel with liquid fuels emit lower CO due to the oxygen content present in the biodiesel. Among all the fuel blends tested in the DF mode, mahua wood exhibits the lowest CO emissions, measuring at 0.01% volume.

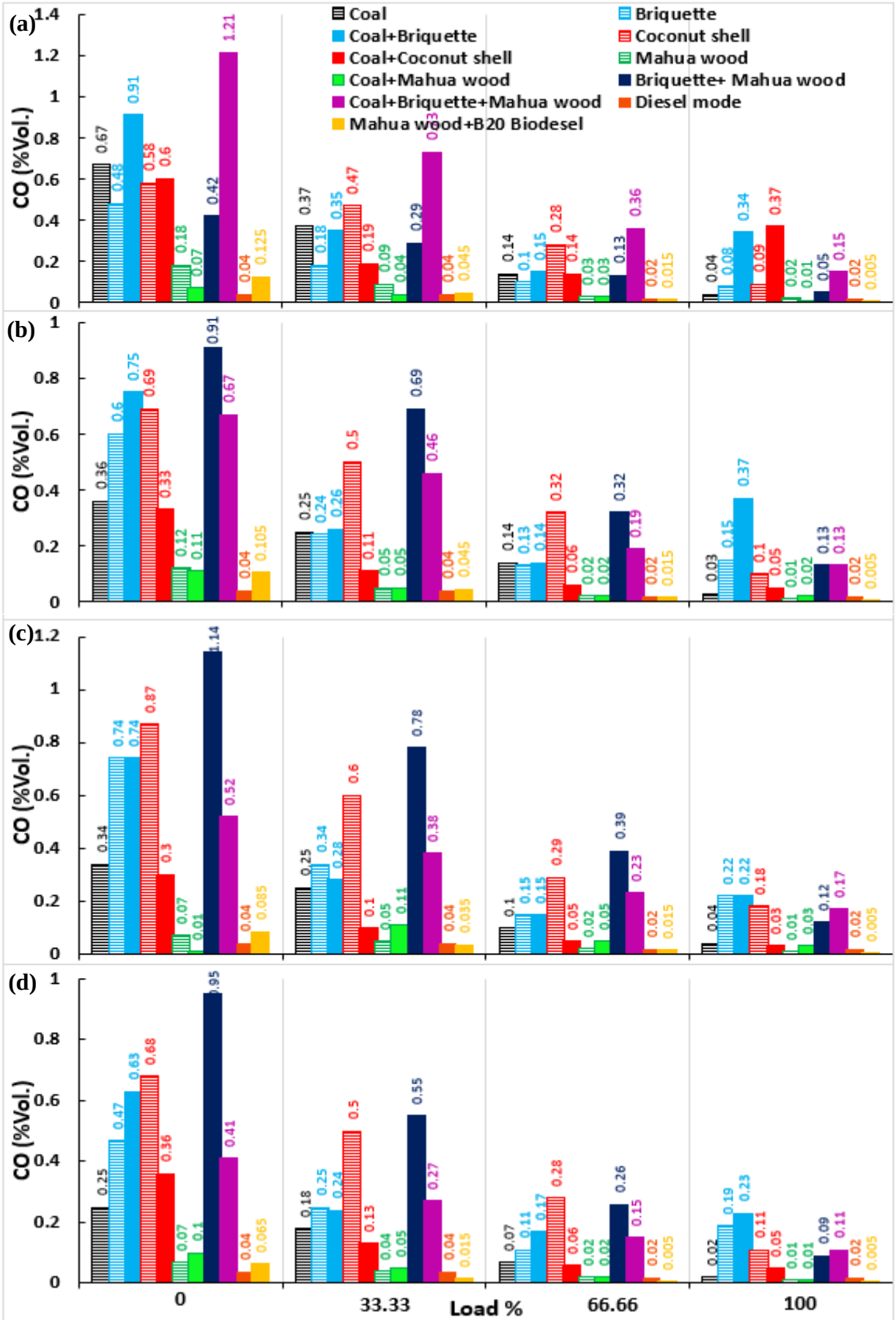

Figure 4.5.8. Variation of CO with engine load at (a) GER 0.43, (b) GER 0.36, (c) GER 0.24, (d) GER 0.12

4.5.4.4 HC emissions with engine load at different GER

Hydrocarbon (HC) emissions in engines can occur primarily due to incomplete combustion, inadequate air-fuel mixing, and the presence of oxygenated compounds in the fuel. The variation of HC emission of the engine with different dual fuel modes (including gasification and co-gasification integrated CI engine) and diesel mode is shown in Figure 4.5.9. Under different GERs, the HC emissions can exhibit varying trends with engine load. Generally, at higher GER, the HC emissions tend to decrease with increasing engine load. This might be due to the improved combustion efficiency achieved at higher GER, leading to more complete combustion of the fuel and lower HC emissions. However, for (coal + briquette and coal + coconut shell) based PG, the HC emissions initially decrease with increasing engine load and then start to increase beyond 66.66% load condition at GER 0.36 and GER 0.12, respectively. This might be due to the incomplete combustion caused by fuel-rich conditions at lower GER. Additionally, it can be concluded that biomass co-gasification based PG emits more engine HCs due to the presence of hydrocarbon in PG. Moreover, diesel or diesel-biodiesel based PG mode have lower HC emissions than DF mode at different engine loads. Coal + Mahua wood based PG emits less HC emissions among different feed materials for gasification/co-gasification operations at various engine load. The minimum HC emission observed was 0.3 ppm at GER 0.43 and 100% engine load condition for mahua wood+B20 based PG.

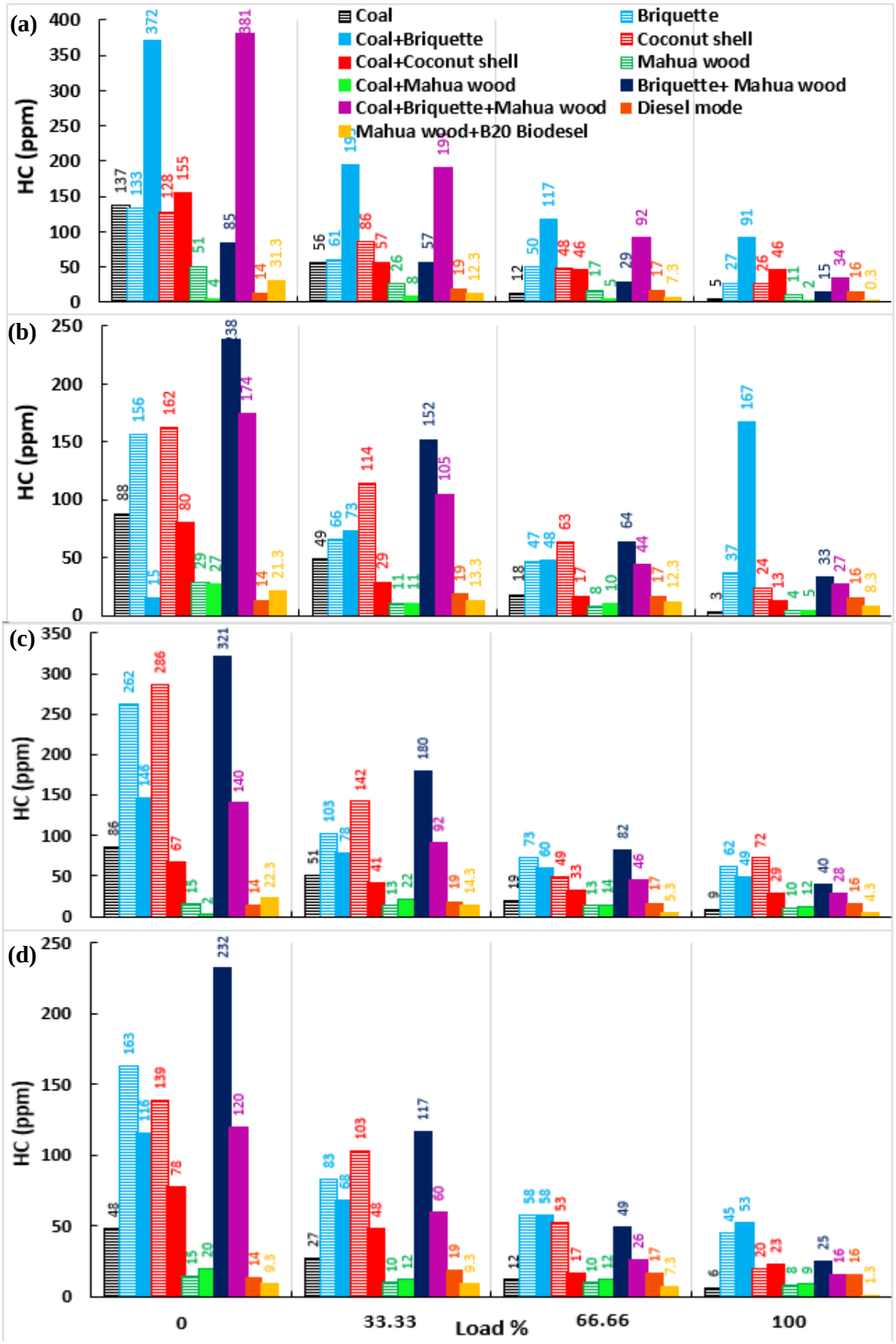

Figure 4.5.9. Variation of HC with engine load at (a) GER 0.43, (b) GER 0.36, (c) GER 0.24, (d) GER 0.12

4.5.4.5 CO_2 emissions with engine load at different GER

Figure 4.5.10 illustrates the relationship between the percentage loading of the engine and CO_2 content present in the engine exhaust at different GERs. It can be seen from the figure that as the load increases, there is an increase in CO_2 emissions. Diesel mode leads to lower CO_2 emission than the DF mode engine run. Since the PG contains CO_2, the combustion of PG also increases CO_2 emissions. Moreover, it is also observed that with an introduction of the B20 biodiesel blend with mahua wood PG, there is a decrease in CO_2 as compared to DF mode (diesel + mahua PG), but higher than neat diesel mode. This occurred due to the higher oxygen content present in biodiesel, which promotes complete combustion and consequently leads to lower CO_2 emissions compared to the DF mode [261]. However, the trade-off variations in engine CO_2 emissions would have been due to the variation in PG compositions with different GER of different feed materials. At 100% engine load, the respective mahua-based PG dual fuel mode has maximum CO_2 emissions, followed by its B20 blend-PG, and the lowest emission in diesel mode. Triple feedstock (coal + briquette + mahua wood) co-gasification based PG integrated CI engine produces the highest CO_2 emission of 7.5%vol at higher GER 0.43, and it decreases with a decrease in GER. This might be due to the less availability of oxygen at lower GER.

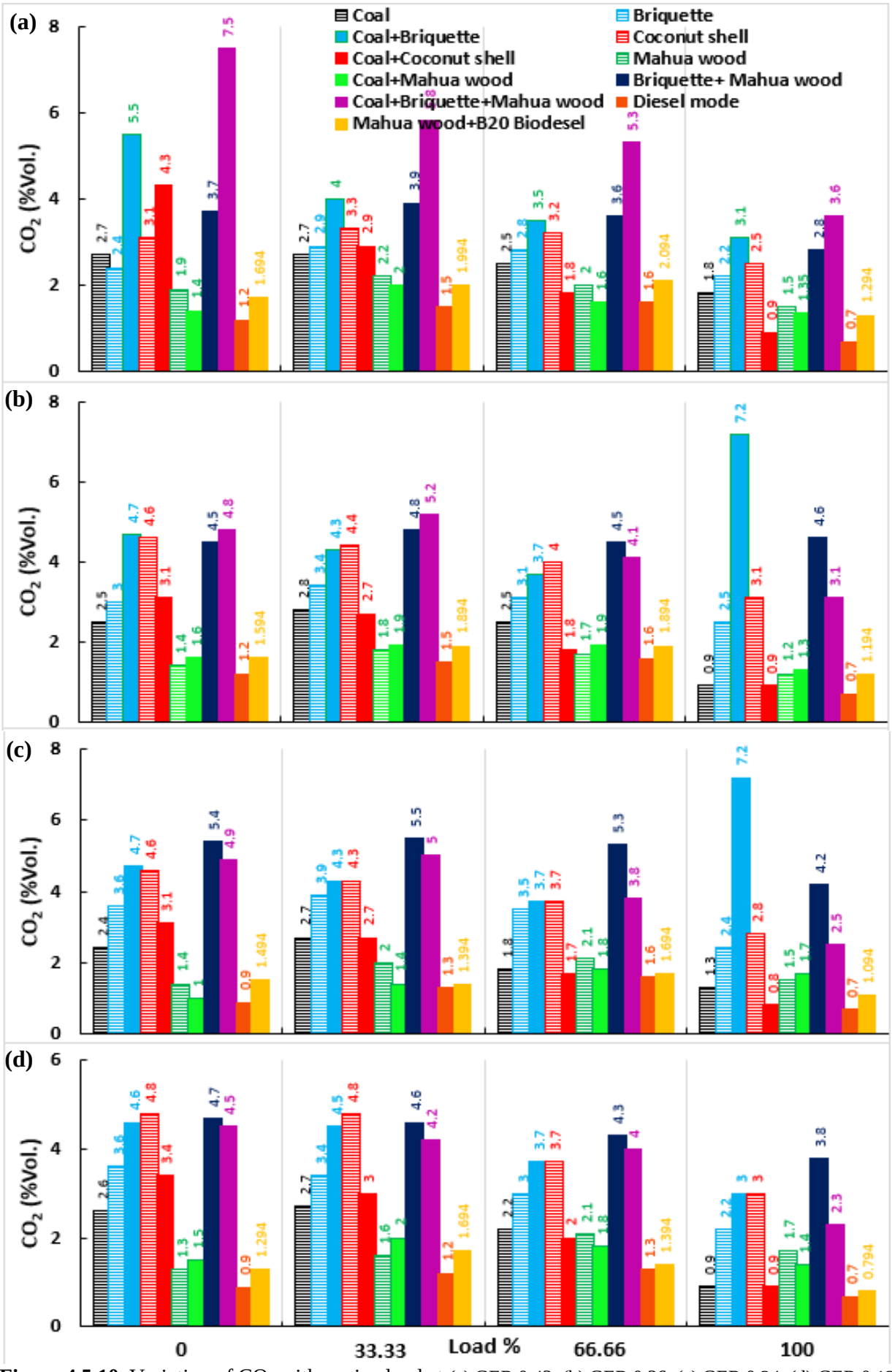

Figure 4.5.10. Variation of CO_2 with engine load at (a) GER 0.43, (b) GER 0.36, (c) GER 0.24, (d) GER 0.12

4.5.4.6 NO_X emissions with engine load at different GER

NOx formation in an engine mainly depends upon combustion conditions, temperature, pressure, oxygen availability, and the fuel composition. The variation of NOx emission from an engine with different dual fuel modes (including gasification and co-gasification integrated CI engine) and diesel mode is depicted in Figure 4.5.11. The relation between NOx emissions and engine load at different GER can vary based on the types of fuel used and their PG compositions. It can be inferred from figure that the NOx emissions are reduced in the DF mode compared to the diesel mode at all loading conditions. Because of PG's low ignition point, the peak temperature during combustion decreases, potentially resulting in a decrease in the formation of NOx. In diesel mode, the NO*x* emission is 402 ppm at GER 0.43 and 100% engine load, and it is 1.82 times higher for DF mode (diesel + mahua wood PG). An increase in engine load leads to higher NOx emissions for all tested fuels in both modes of operation. However, the trade-off nature of NOx emissions may be due to the different PG quality in respective fuel materials. Moreover, with the introduction of biodiesel in the blend, NOx emissions decrease in diesel, and DF (diesel + mahua PG) mode. This decline can be attributed to low-temperature combustion, resulting from the lower energy release during the pre-mixed phase of combustion due to larger droplet sizes of the tested fuel blends [261]. However, the experiment suggests that higher GER conditions generally favors an increase in NOx emissions for biomass co-gasification (briquette + mahua) and triple feedstock co-gasification (coal + briquette + mahua wood). This can be attributed to the higher availability of oxygen in PG and at higher GER. Mahua wood gasification-based PG emits a maximum engine NOx of 311 ppm at GER 0.24 at 66.66% engine load.

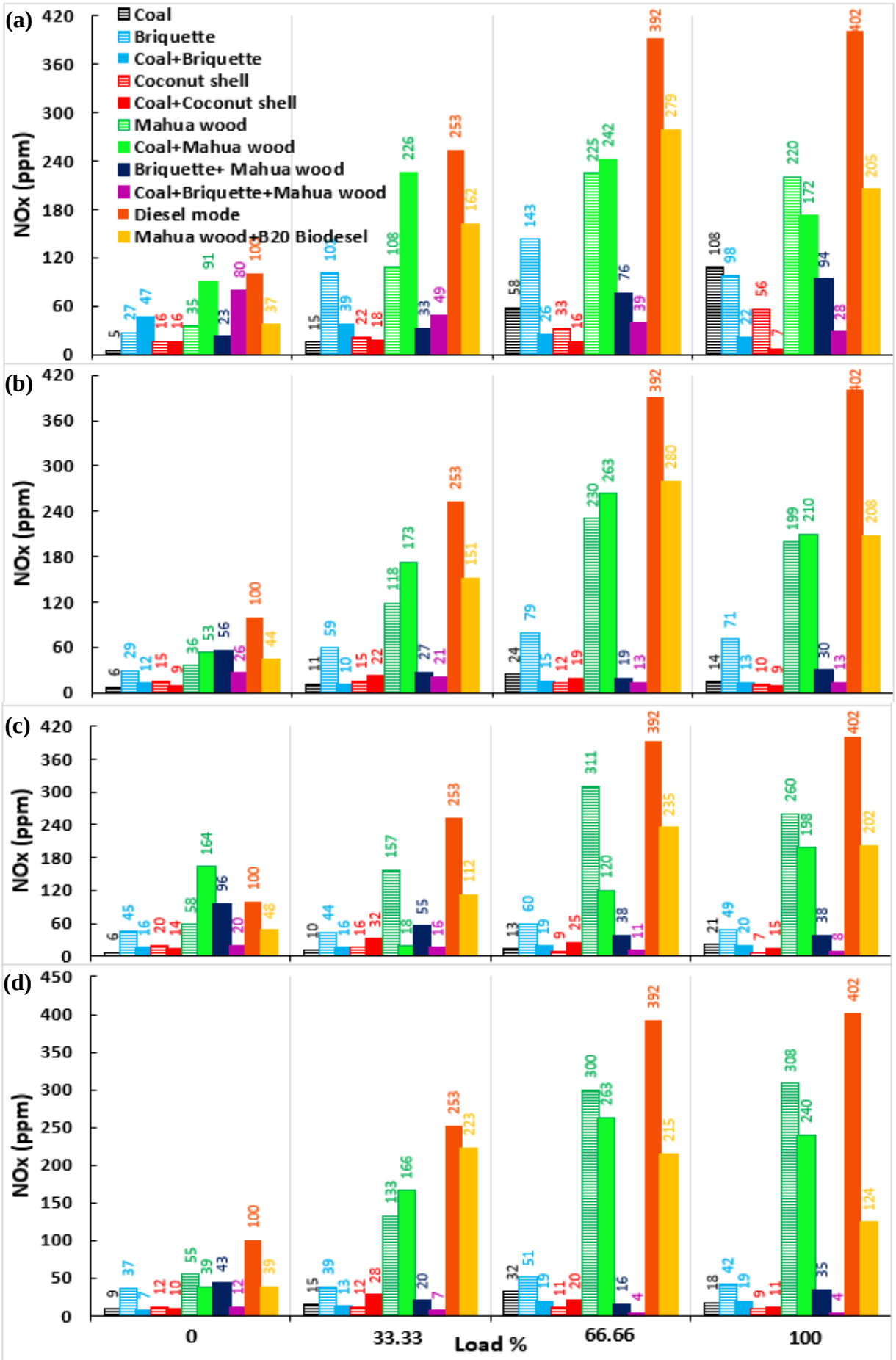

Figure 4.5.11. Variation of NO_x with engine load at (a) GER 0.43, (b) GER 0.36, (c) GER 0.24, (d) GER 0.12

4.5.5 *Optimisation approach*

To conduct the analysis of variance (ANOVA) and achieve the optimal operational condition, the response variables must be simulated using varying input parameter combinations. The range considered for GER and engine load is 0.1-0.43 and 0-100%, respectively. The optimization process aims for maximum engine performance values and minimum engine emission response values. The graphs in Figures 4.5.12 – 4.5.14 demonstrate that the optimal conditions occur at GER values of 0.15, 0.10, 0.12, 0.24, 0.43, 0.43, 0.10, 0.22, 0.10, and an engine load of 100% for coal, briquette, coconut shell, (coal + coconut shell), mahua, (coal + mahua), (briquette + mahua), (coal + briquette + mahua), and (mahua + B20 biodiesel) as feed materials, respectively. The response observed under the optimal conditions is presented in Table 4.5.2. Additionally, model confirmation runs were executed for each type of biomass feed material to validate whether the RSM optimization results align with model simulations with sufficient accuracy. The percentage error between RSM and experimental values is also detailed in Table 4.5.2, with the maximum error remaining below 6%. This indicates that the values optimized by RSM are meaningful and precise. Furthermore, the ANOVA results corroborate the model accuracy, as both the R^2 and R^2_{adj} for all models exceeded 90%.

A desirability test was conducted to validate the accuracy of the model. The desirability value of a model or response ranges from 0 to 1, with higher values indicating better accuracy. It is evident from Figures 4.5.12 – 4.5.14 that the composite desirability of the model (D) and the individual desirability values (d) for all response variables are nearly equal to 1. This suggests that the developed model is proficient in accurately predicting responses and optimal operational conditions. The composite desirability for various feedstocks is as follows: coal (0.94), briquette (0.90), coal + briquette (0.88), coconut shell (0.97), coal + coconut shell (0.93), mahua (0.76), coal+mahua (0.75), briquette + mahua (0.90), coal + briquette+mahua (0.98), and mahua + B20 biodiesel (0.83). The optimal operating conditions and responses for all considered feedstocks

are depicted in Figures 4.5.12 – 4.5.14. The gasification-integrated CI engine process is executed under these optimized conditions, and the key findings are outlined in Table 4.5.2. The response variables obtained at the optimal operating conditions for all considered feedstocks indicate that the developed RSM model achieves a maximum value of 25.60 % BTE for biomass co-gasification (briquette + mahua wood). This high BTE value is attributed to the enriched quality of PG when operated within the optimum conditions. Consequently, it can be deduced that maintaining operating conditions within the specified range is crucial for obtaining the most favorable outcomes as predicted by the developed model. The RSM optimized results can contribute to the advancement of gasification-engine technology. In this regrad, further modifiaction in engine design with different operation setting, the application of RSM optimization tool can be significantely used for guiding and enhancing the overall efficiency with less emissions.

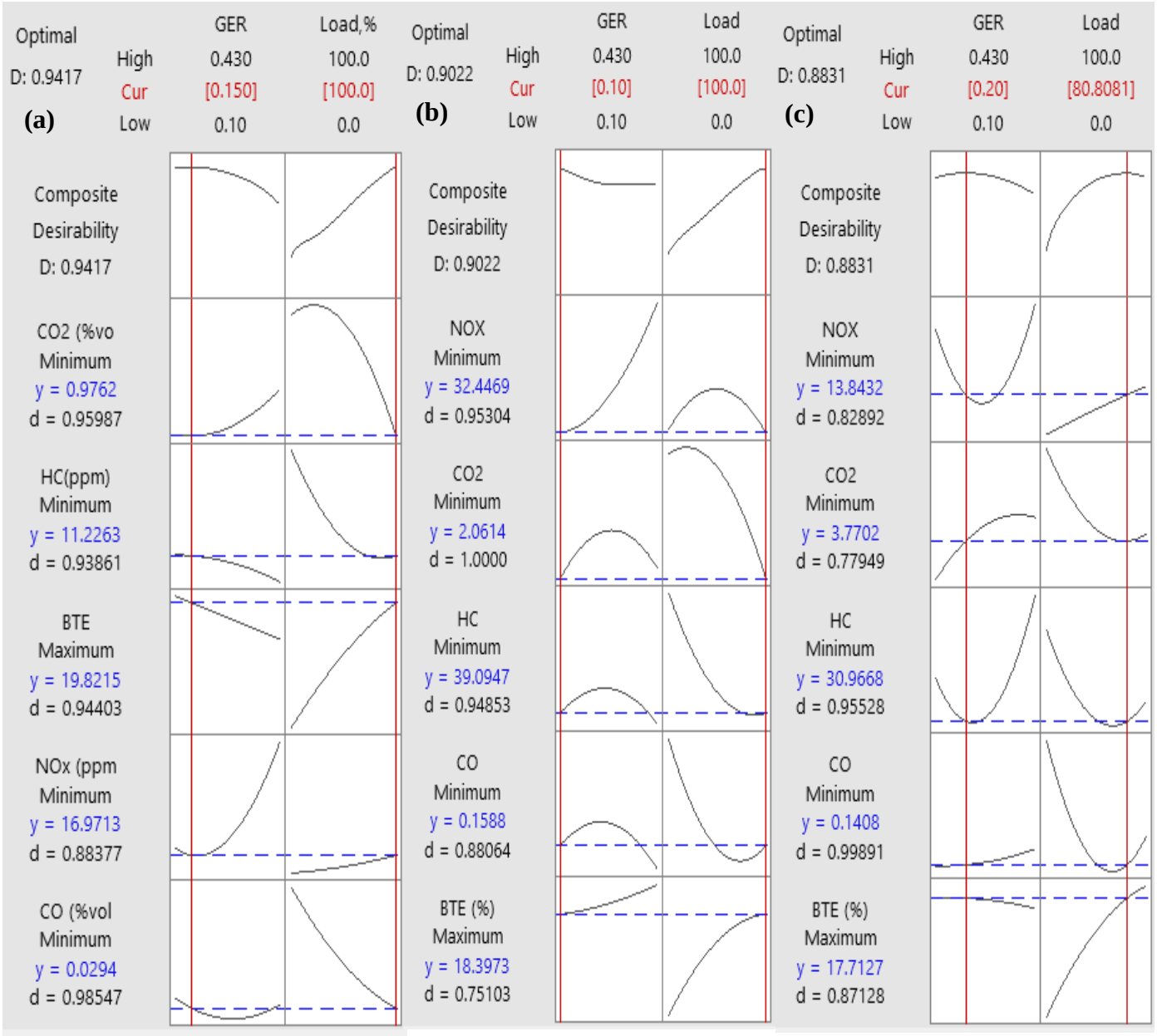

Figure 4.5.12. Response Optimisation plots for (a) Coal, (b) Briquette, (c) Coal + Briquette

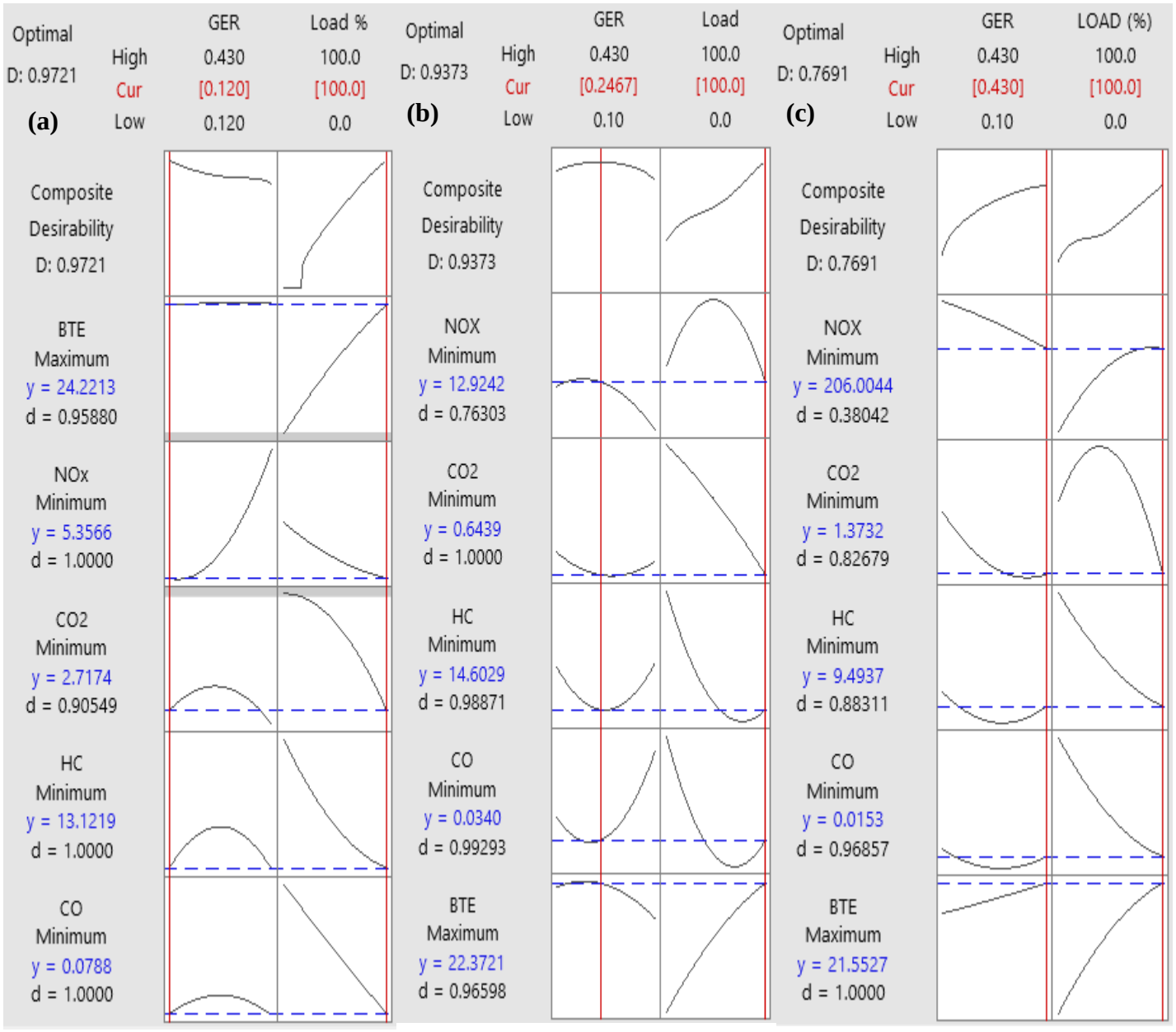

Figure 4.5.13. Response Optimisation plots for (a) Coconut shell (b) Coal + Coconut shell (c) Mahua wood

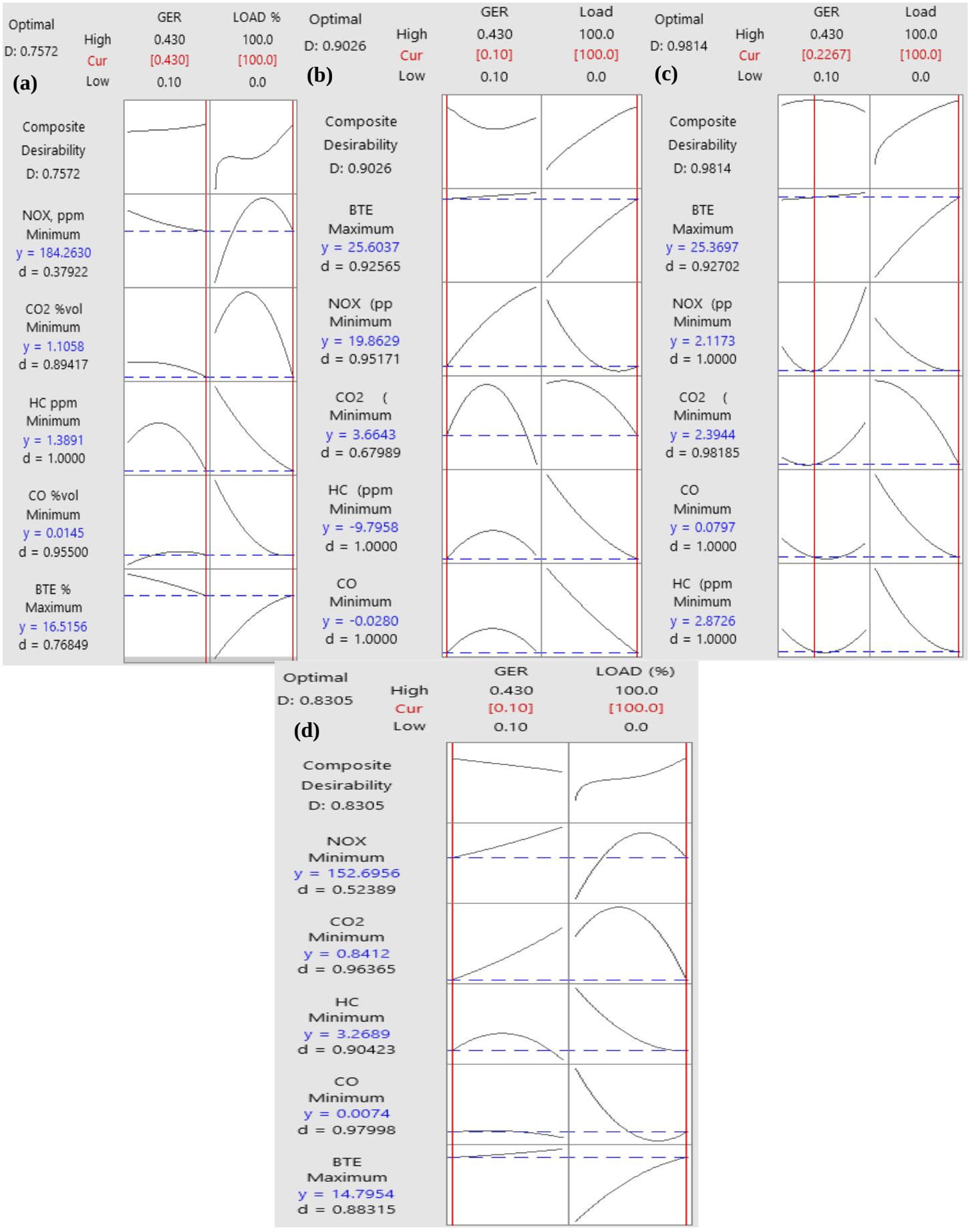

Figure 4.5.14. Response Optimisation plots for (a) Coal + Mahua wood (b) Briquette + Mahua wood (c) Coal+ Briquette + Mahua (d) Mahua wood + B20 Biodiesel

Table 4.5.2. Key findings and Validation tests for RSM and experimental results

Feed	Optimum GER	Optimum engine load (%)	Value	BTE (%)	CO (%vol)	HC (ppm)	CO_2 (%vol)	NO_X (ppm)
Coal	0.15	100	RSM optimized	19.82	0.02	11.22	0.97	16.97
			Experimental	20.97	0.03	11	0.95	17.5
			Error (%)	5.48	2	-2	-2.10	3.02
			R^2	0.97	0.92	0.94	0.91	0.69
			R^2_{adj}	0.96	0.88	0.91	0.87	0.54
Briquette	0.10	100	RSM optimized	18.39	0.150	39.09	2.06	32.44
			Experimental	18.46	0.155	40	2.1	33.2
			Error (%)	0.37	3.22	2.27	1.90	2.28
			R^2	0.99	0.95	0.88	0.97	0.79
			R^2_{adj}	0.98	0.93	0.82	0.96	0.69
Coal+ Briquette	0.20	80.80	RSM optimized	17.71	0.14	30.96	3.77	13.84
			Experimental	18.09	0.144	32.4	3.87	14.34

			Error (%)	2.10	2.77	4.44	2.58	3.48
			R^2	0.99	0.96	0.46	0.24	0.61
			R^2_{adj}	0.99	0.94	0.19	0	0.42
Coconut Shell	0.12	100	RSM optimized	24.22	0.07	13.12	2.71	5.35
			Experimental	24.39	0.073	13.8	2.82	5.47
			Error (%)	0.69	4.10	4.92	3.90	2.19
			R^2	0.99	0.96	0.84	0.9	0.62
			R^2_{adj}	0.99	0.95	0.76	0.85	0.44
Coal+ Coconut	0.24	100	RSM optimized	22.37	0.03	14.60	0.64	12.92
			Experimental	21.46	0.031	15.3	0.66	12.4
			Error (%)	4.24	3.22	4.57	3.03	4.19
			R^2	0.95	0.86	0.82	0.96	0.8
			R^2_{adj}	0.93	0.79	0.73	0.94	0.7
	0.43	100	RSM optimized	21.55	0.01	9.49	1.37	206

Mahua wood			Experimental	21.46	0.0105	9.95	1.42	215
			Error (%)	-0.41	4.76	4.62	3.52	4.18
			R^2	0.98	0.94	0.85	0.78	0.91
			R^2_{adj}	0.98	0.92	0.78	0.67	0.87
Coal+ Mahua wood	0.43	100	RSM optimized	16.51	0.01	1.38	1.10	184.26
			Experimental	17.12	0.0104	2	1.12	176
			Error (%)	3.56	3.84	31	1.78	4.69
			R^2	0.99	0.95	0.68	0.87	0.93
			R^2_{adj}	0.99	0.93	0.53	0.81	0.89
Briquette + Mahua wood	0.10	100	RSM optimized	25.60	0.02	9.79	3.66	19.86
			Experimental	25.82	0.021	10	3.8	20
			Error (%)	0.85	4.76	2.1	3.68	0.7
			R^2	0.99	0.95	0.92	0.91	0.37
			R^2_{adj}	0.99	0.92	0.89	0.87	0.05

Coal+ Briquette + Mahua wood	0.22	100	RSM optimized	25.36	0.07	2.87	2.39	2.11
			Experimental	25.24	0.0743	3	2.5	2
			Error (%)	0.47	5.78	4.33	4.4	5.5
			R^2	0.99	0.92	0.89	0.89	0.85
			R^2_{adj}	0.99	0.88	0.84	0.84	0.77
Mahua wood+ B20 Biodiesel	0.10	100	RSM optimized	14.79	0.007	3.26	0.84	152.69
			Experimental	15	0.0073	3.4	0.87	160
			Error (%)	1.4	4.10	4.11	3.44	4.56
			R^2	0.99	0.98	0.85	0.89	0.88
			R^2_{adj}	0.99	0.98	0.78	0.84	0.82

4.5.6 *Conclusions*

Present study investigated the performance and emission characteristics of VCR diesel engine (DF) running on producer gas obtained through gasification/ co-gasification of different feedstocks. It could be concluded that co-gasification-based PG is suitable for minimizing engine emission. On other hand, BTE of CI engine can be enhanced if PG derives from briquette+Mahua blend gasification.

4.6 Economic analysis of sugarcane bagasse pith briquette production and its application in gasifier-engine system

4.6.1 *Introduction*

Utilizing agriculture co-products and agricultural residues directly leads to Energy, Economic, and Environmental sustainability. Sugar production industries produce a considerable amount of sugarcane bagasse (SB) as a co-product, whereas SB is used in paper-mill sectors, which have a large amount of waste as sugarcane bagasse pith (SBP). In this view, the novelty of the present study aims to ensure the economic viability of the SBP briquette production plant, after that, briquette-based producer gas (PG) generation and application to compression ignition (CI) engine for diesel substitution. The economic analysis includes the Net Present Value (NPV) and Profitability Index (PI) for the feasibility check. And gasifier-engine analysis includes the effect of gasification equivalence ratio (GER), engine compression ratio (CR), and load on engine brake thermal efficiency (BTE), diesel saving, Sound, Exhaust gas temperature (EGT), and emissions (CO, HC, CO_2, NOx). Further, operating variables were optimized with the desirability approach of Response surface methodology (RSM). In the result, NPV and PI values were found to be Rs 49,64,379.5 (≈0.06 million USD) and 1.98, respectively. However, the economic feasibility of the plant is sensitive to capital cost, briquette market price, and discount percentages. Regarding gasifier-engine performance, the maximum diesel substitution was found to be 66.15% at dual fuel (DF) mode engine run. RSM-based optimization result showed the optimum operating setting of 0.10 GER, 16 CR, and 9.93kg load at 1500 rpm with a composite desirability of 0.798. Accordingly, at optimal input parameters, the magnitudes of engine performance as BTE, Sound, CO, HC, CO_2, and NOx were found to be 27.18%, 91.21db, 0.10%vol., 53.19ppm, 2.33%vol., and 8.43ppm respectively. Thus, the higher value

of the economic index and substantial amount of diesel fuel saving through the gasifier-engine system ensures the economic feasibility of briquetting and power generation technology.

So far as briquetting from SBP is considered for waste-to-wealth conversion, it must be confirmed sustainability aspect with respect to feasibilty of sound economic. The details of sugarcane processing to pith briquette to gasification are shown in Figure 4.6.1. Moreover, regarding the present study, some recent work is mentioned in Table 4.6.1. Concerning this research gap, the first novel work aims to study the economic viability of the small-scale briquette manufacturing plant in order to promote waste-to-fuel conversion through sugarcane bagasse pith briquette. The second is to determine the experimental-based briquette gasification with engine-integrated performance, exhaust emission, sound levels, and diesel saving. Moreover, experimental results show that GER, engine CR, and load parameters have trade-off relations to BTE, power, and emissions. Hence, RSM-based optimization is performed to predict the balanced form of emissions and power for appropriate utilization with optimized input operating conditions. And the third one is the comparative analysis of engine performance and emission with diesel to diesel-PG run CI engine. In order to accomplish these objectives, economic indicator methods and sensitivity analysis are performed to achieve the feasibility of the briquette production business. Thereafter, experiments were carried out on a gasifier-engine employing sugarcane pith briquette as a gasifier feed material with varying gasification equivalence ratios and engine load with varying compression ratios. The experimental results suggests that the optimum GER, compression ratio, and load-related input parameters significantly improve power and low emissions. Hence, SBP-producer gas may be considered a gaseous fuel for diesel substitutes. Overall, since sugarcane bagasse pith is available abundantly worldwide, the use of PG derived from SBP as IC engine gaseous fuel can play an important role for developing countries to mimimize power scarcity and pollution of fossil fuels. Moreover, this work will help as a significant reference material for the relevant experts and technologists.

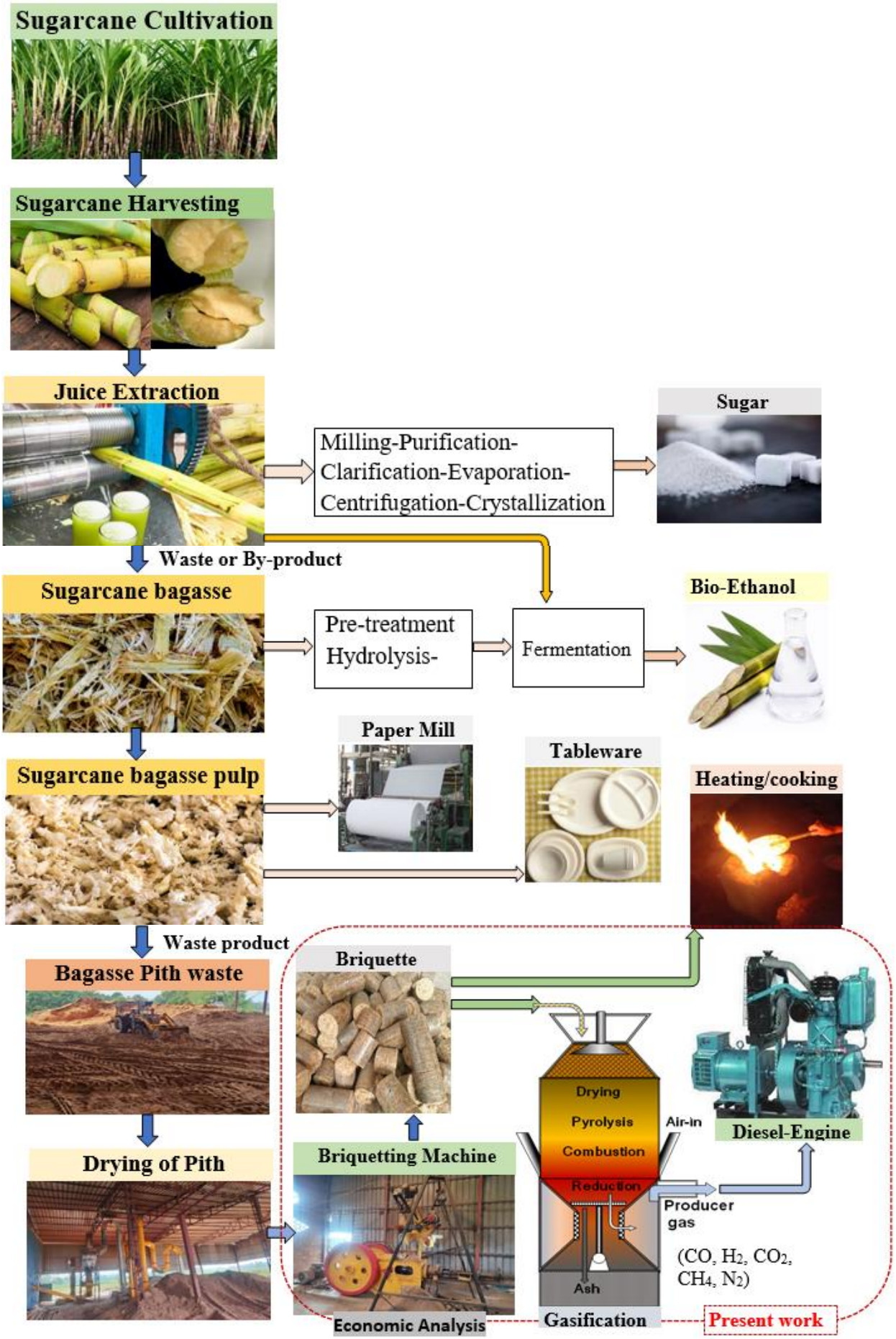

Figure 4.6.1 Processing and respective product from sugarcane-pith briquette to gasification

Table 4.6.1. Comparative previous literature and the current study

Engine	Investigation method	Fuels	Operating Variable	Ref.
CI Engine	Simulation-ANN	Biodiesel-Diesel blend	Injection pressure, Load, Biodiesel ratio	[109]
CI engine	Simulation-ANN	Diesel blended with Acetylene	CR, pressure, injection timing, Acetylene blend	[224]
CI Engine	Experimental	Biodiesel, and Babool wood PG	Load, Pressure, and pilot fuel injection timing	[167]
CI Engine	Simulation-Fortran	Diesel, and Babul wood PG	CR, blending ratios, and Injection timing	[169]
CI Engine	Experimental	Biodiesel and PG	CR, Load, and Injection timing	[168]
CI Engine	Experimental	Diesel and Briquette, Coconut shell, Mahua-PG	Engine Brake power, and CR	[238]
CI Engine	Experimental	Diesel and cocoa pod husk-PG	CR, and Brake power	[170]
CI Engine	Experimental	Bagasse Pith briquette PG and diesel	Gasification ER, CR, and load	**Not yet**

4.6.2 Properties of sugarcane bagasse pith briquette

Sugarcane bagasse pith-derived Briquette (SBP) is the chief feedstock for gasification-Engine experimental analysis. The experiment utilized an SBP-briquette with a diameter of approx 95 mm and a thickness ranging from 30 to 35 mm, as shown in Figure 4.6.2(a). The briquettes left as ash after gasification is shown in Figure 4.6.2(b). The initial 40kg mass of briquette lefts with 17.9kg of residual char after gasification. The chemical properties (proximate/ultimate and producer gas composition) of SBP-briquette biomass are shown in Figure 4.6.3. A proximate analysis was performed to determine the average percentages of volatile matter, ash content, moisture, and fixed carbon in the briquette derived from SBP. Additionally, the ultimate analysis was conducted to ascertain the elemental composition of the briquette, including carbon, hydrogen, nitrogen, oxygen, and sulfur. The ultimate analysis results showed the following percentages: carbon 56.27%, hydrogen 2.8%, nitrogen 0.96%, oxygen 39.94%, and sulfur 0.03%. The gross calorific value (GCV) of the formed briquette was found to be 19.10 MJ/kg. Furthermore, Figure 3 illustrates the composition of the PG, indicating a lower heating value (LHV) of 2.44 MJ/Nm^3.

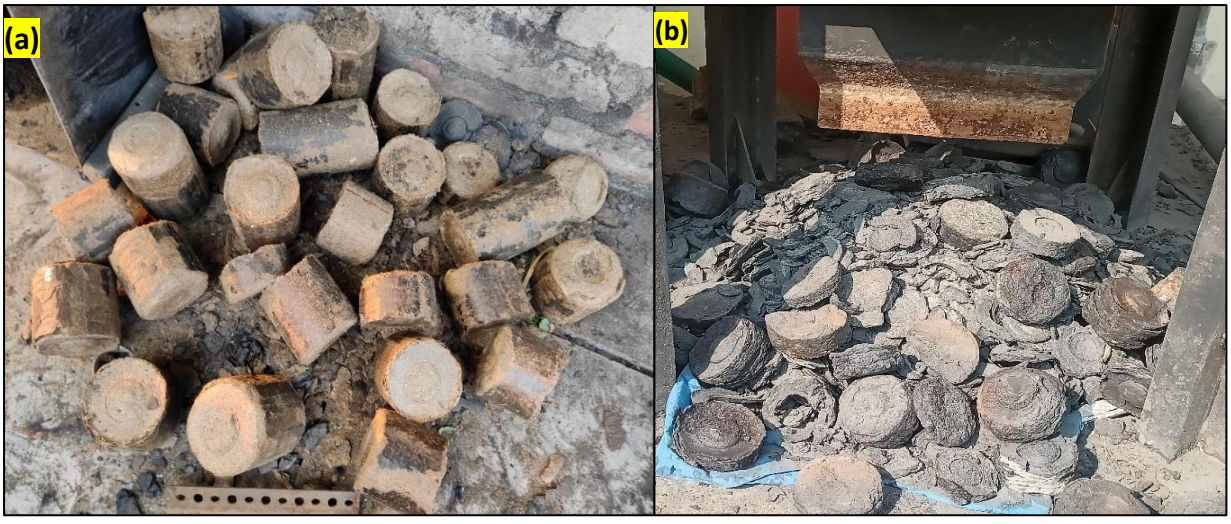

Figure 4.6.2. Briquette feed-material: (a) Before gasification (b) After gasification

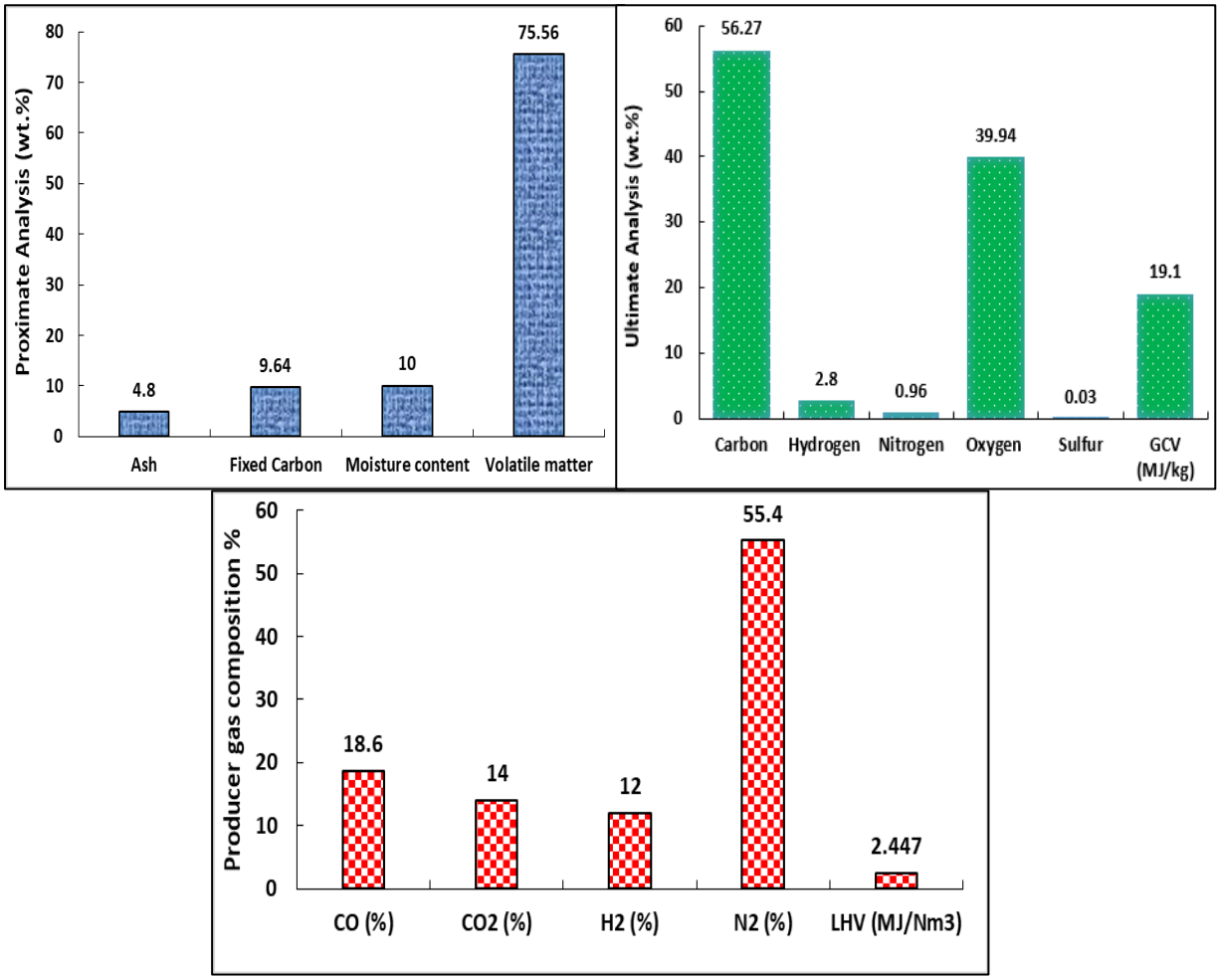

Figure 4.6.3. Properties of Sugarcane bagasse pith-Briquette

The study utilized an air-based fixed bed and batch-type downdraft gasifier to generate PG. This gas was then carefully filtered and employed in an ICE. The gasifier, made of mild steel material, featured a down-draught heating system, and its configuration is depicted in Figure 3.1.2. Technical details of the gasifier can be seen in Table 3.1.1a, while additional information on the integrations made to the gasifier is presented in Table 3.1.1b. Prior to its use in the engine, the PG underwent three stages of filtration. The engine itself was equipped with specific technical features, and its exhaust emissions were analyzed using a dedicated apparatus. The engine specification has been tabulated in Table 3.1.2 and Figure 3.1.3 depicts the engine setup with (air + PG) mixing junction. Throughout the experiment, both the air and PG flow rates were carefully measured, and noise levels were also recorded. The sound level

meter's specifications are listed in Table 3.1.3. As per the sound level standards, the sound level meter was positioned 1.5 m above ground level and 1 m to the rear sides of the variable compression ratio (VCR) engine exhaust, as depicted in Figure 3.1.4.

4.6.3 *Costs analysis*

This section is categorised into two sub-section. First section discusses the cost associated with briquette production system. The second sub-section discusses the cost associated with gasification-engine system.

4.6.3.1 Costs associated with Briquette production system

Figure 4.6.4 shows the percentage contribution of different cost segments associated with the briquetting of SBP over a period of 20 years. It comes into sight that the fixed capital cost contributes 24%, and the diesel cost contributes 43%. The high cost of diesel is attributed to the motorized trucks or tractors that were used to collect the sugarcane bagasse raw items and different stages of briquetting. The maintenance costs represent 1%, property taxes (PT) are 2% (1.1% of cash flow benefits plus Rs.120000 annual rent), and electricity costs represent 13% of the total investment. The other manufacturing costs contain packaging costs, operators' salaries, and briquette binder costs, representing 17% of total expenses.

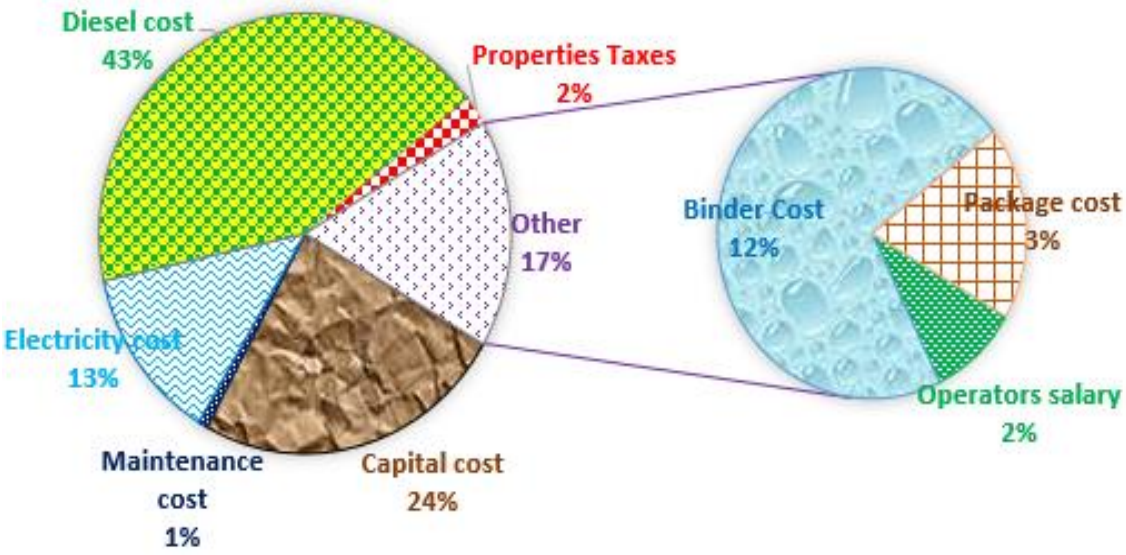

Figure 4.6.4. Contribution of different costs of SBP briquette production plant (0-20 years)

Figure 4.6.5 shows the progression of unit production cost and the market price of SBP-briquette over 20 years. The production costs for SBP briquettes increased slightly during the first five years, indicating that the production process may have required additional investment or incurred higher operating costs during the initial phase. In the figure, the briquette production costs include different operating costs such as maintenance costs, electrical energy costs, gasoil costs, property insurance taxes, binder costs, packaging costs, site rent, and operators' salaries per unit annual briquettes produced, which increases with successive year. However, the production costs dropped considerably in the sixth year, likely due to the reimbursement of the bank loan that was taken to fund the project, which ended in the fifth year. Over the 20 years of market study, the unit production cost of SBP briquettes remains below the market price after the fifth year. Consequently, the sale of SBP briquettes was financially viable and profitable over the long term. Moreover, the briquette production cost can be decreased by reducing different operating costs for the enhancement of benefit.

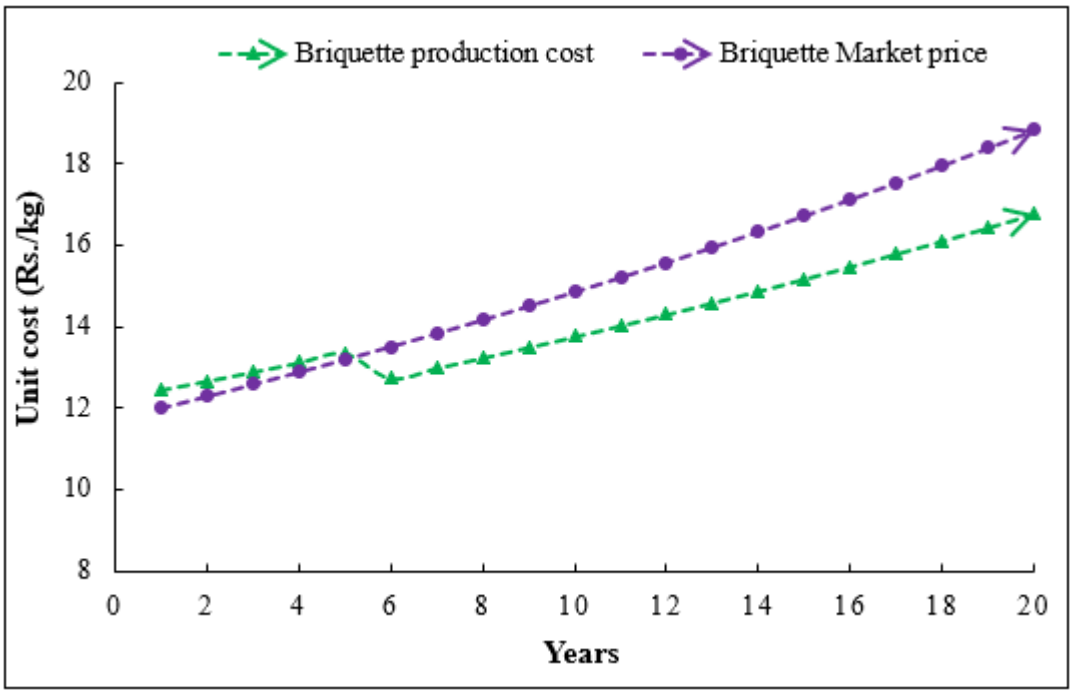

Figure 4.6.5. Evolvement of unit costs of SBP briquette

4.6.3.2 Costs associated with Gasification-engine system

The input parameters, their values and the cost associated used in the economic analysis of gasification-engine system are illustrated in Table 4.6.2.

Table 4.6.2. Economic parameters of gasification-engine system

Parameters	**Value**
14 kW Downdraft gasifier	Rs. 600000
Engine generator set	Rs. 75341.89
Engine modification	Rs. 8610.27
Civil works	
Engine shed	Rs. 21525.67
Engine foundation and earthing	Rs. 16144.05
Drain system	Rs. 1075.67
Low tension electricity distribution network (2 Km)	Rs. 269078.65

Parameters	Value
Total capital investment, or Overall cost of the system,	Rs. 991776.2
Useful life of civil work	20 years
Useful life of engine-generator set with diesel as pilot fuel	20,000 hours
Useful life of gasifier	20 years
Useful life of electricity distribution network	20 years
Annual maintenance cost of the gasifier plant as a fraction of capital cost	0.05
Annual maintenance cost of civil work as a fraction of capital cost	0.02
Annual maintenance cost of engine- generator set as a fraction of capital cost	0.1
Annual maintenance cost of the local distribution network as a fraction of capital cost	0.03
Capacity Utilisation Factor	0.35
Daily manpower wage	Rs.16.0 1/hr
Price of diesel	Rs. 90/l
Specific diesel consumption in a typical DF engine- gasifier plant at rated capacity	0.11 L/kWh
Specific biomass consumption in a typical DF engine Gasifier-engine plant at rated capacity	1.1 kg/kWh
Engine-generator rated output capacity	3.5 kW
Fraction of generated power consumed by the auxiliaries of the plant	0.12
Fraction of electrical losses in the local distribution network	0.1

4.6.4 *Economic Sensitive Analysis*

Table 4.6.3 represents the economic evaluation indicators that show whether the production unit is economically viable or not. The Net present value (NPV) and Profitability index (PI) are the important economic indicators that appeal to the business's profitability. A positive value of NPV and PI suggests the project is considered accepted. Table 4.6.3 shows the NPV of SBP-briquette is Rs. 4964379.5 (≈0.06 million USD) and PI is 1.98, respectively. Based on the figures presented, the production of SBP briquettes appears to be a profitable and financially feasible option for the plant. Various studies in the literature have also reported

positive net positive value for briquetting projects using other raw materials. Studies have shown that other residues, such as grass, cashew shells, and rice husks, can be economically viable for briquette production. Sengar et al. [262] obtained the NPV of these residues to be $30,117.20, $25,831.88, and $8,434.78, respectively. Additionally, studies by Hakizimana and Kim [263] demonstrated an NPV of $17.2 million for peat briquettes and approved their commercialization. Moreover, Net Present Value of cashew shell, grass and rice husk briquettes were Rs. 1935370.8, Rs. 2256434.38 and Rs. 631948.8 respectively [264]. Agro waste pellet plant showed acceptable economics with NPV of Rs.9.35 million [265]. Thus, the results of current economic analysis are compatible with the literature.

Table 4.6.3 Economic evaluation indicators

Economic parameters	***SBP-Briquette***
Net Present Value in Rs. (≈USD)	4964379.5 (≈0.06 million USD) *
Profitability Index	1.98

** 1.0 USD =82.12 INR.*

A sensitivity analysis was performed to assess the consequences of various factors on the economic feasibility of a small-scale plant producing biomass briquettes. The analysis highlighted the various significant factors, including the briquette market price, capital cost, discount rate, and operator's salaries. The discount rate was found to be subject to uncertainty and could significantly impact the economic feasibility of the project. The sensitivity analysis aimed to examine the effect of variations in the discount rate on the NPV of the briquetting systems to determine if the investment would be economically viable.

Figure 4.6.6(a) shows that the NPV and profitability index of the systems decreases as the discount percentage increases. However, the NPV and profitability index remains positive at

all discount percentages, indicating that the briquette production systems are economically viable. The results suggest that the plant can supply the briquettes produced by the systems and still generate a profit. The economic evaluation parameters would be more significant at a lower discount rate, suggesting a more economically viable production unit and vice versa.

The economic viability of briquette production systems is shown in Figure 4.6.6(b). The systems become more financially attractive as the briquette market price increases, with a profitability threshold of Rs. 11.452 per kg for SBP. A current market value of Rs.12/kg would result in an NPV of about Rs. 4964379.5 (≈0.0604 million USD).

Similar conclusions of NPV with market briquette price variation were obtained from authors [66, 67]. Figure 4.6.6(c) shows the NPV and cash flow benefits increases with the years. The negative NPV is attributed to the bank loan debt that will be paid off by the end of the fifth year. A positive NPV implies a positive surplus, and the company's financial position is economically accepted for an increasing cash flow benefit. At the end of 20 years, the SBP-briquette production unit has an NPV of Rs. 383869.5 with a cash flow benefit of Rs. 13558539.7, respectively.

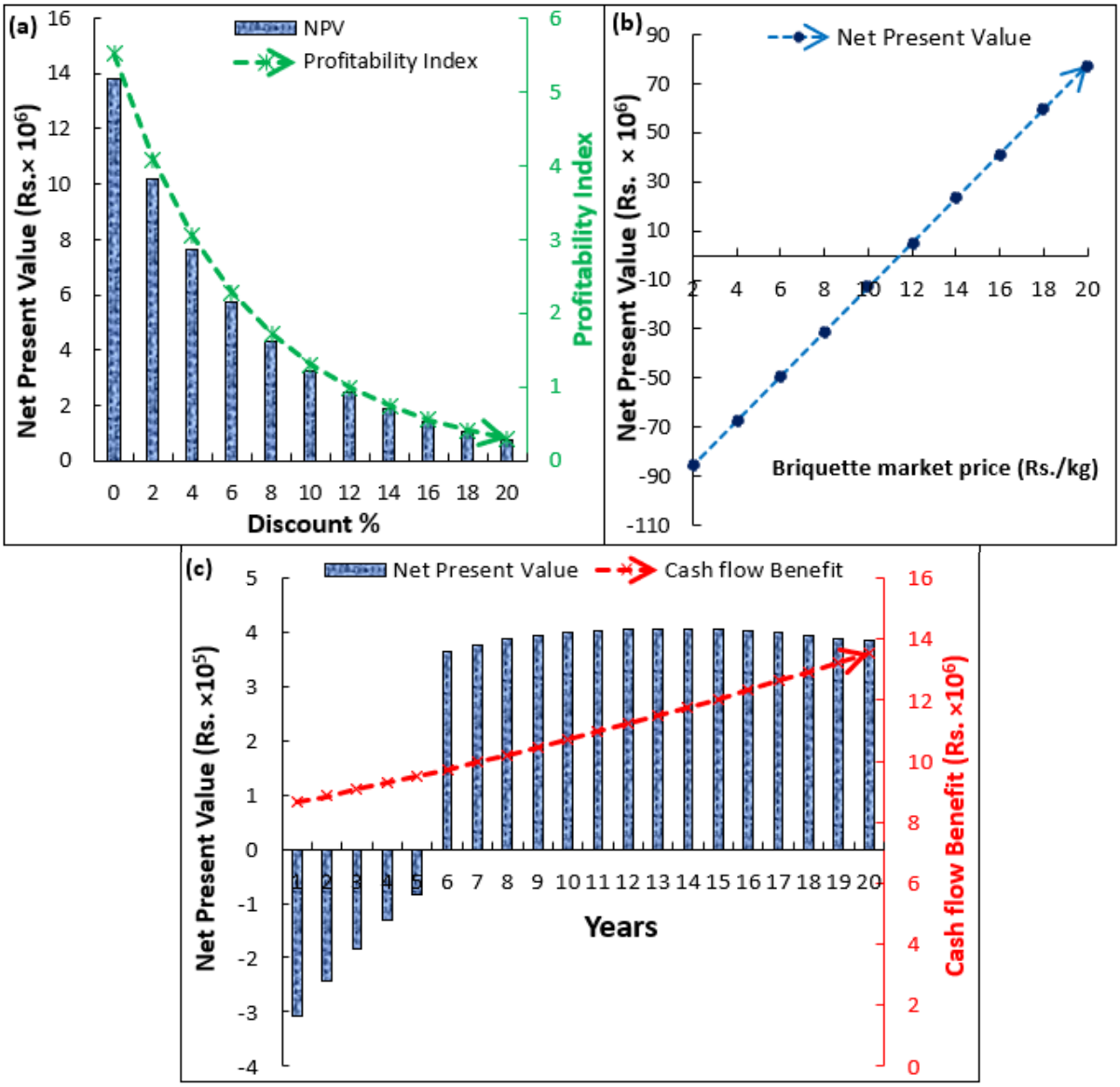

Figure 4.6.6. Relationship between NPV with (a) discount% (b) briquette unit market price (c) years

Moreover, the cost analysis of gasification-engine system and the annual fuel saving while using DF engine is listed in Table 4.6.4. The financial evaluation of the gasification-engine system operating at optimum condition was conducted based on with and without the inclusion of the cost of the line distribution network. From the analysis, it was evident that the per-unit cost of electricity is still on the higher side, which may be due to a number of factors such as CUF, price of diesel, the capacity of the engine. Figure 4.6.7 shows the relationship between NPV with discount% and capital cost of gasification-engine system. From the Figure 4.6.7(a),

it is revealed that NPV decreases with increase in discount percent for both with and without electricity line distribution. However, after 9 % discount, the NPV has negative value (with electricity line distribution) which creates non-profitable business. Moreover, the NPV also decreases with increase in capital cost as shown in Figure 4.6.7(b). Without transmission line distribution generates more NPV as compared to with transmission line distribution as it includes the cost of 2 km low tension electricity distribution network. In conclusion, the economic viability and feasibility of biomass gasification systems for widespread implementation depend on a careful consideration of various factors related to scale, including economies of scale, capital costs, operational efficiency, feedstock availability, flexibility, infrastructure requirements, grid integration, policy support, technology maturity, and risk mitigation strategies. A balanced approach that considers the specific characteristics and needs of the target region or application is essential for successful implementation. Generally, larger biomass gasification systems benefit from economies of scale. As the scale increases, the cost per unit of energy produced tends to decrease. This is because certain fixed costs, such as infrastructure and equipment, can be spread over a larger output. Moreover, Larger systems often achieve higher operational efficiencies. This can result in more energy output per unit of biomass input and better overall performance.

Table 4.6.4. Cost analysis of gasification-engine system

Cost Parameters	**Results (with electricity distribution charge)**	**Results (without electricity distribution charge)**
Total Annualized Capital Cost, (Rs.)	124430.52	92824.65
Total annualized O&M cost (Rs.)	96298.48	88226.12
Total annualized fuel cost (Rs.)	106331.33	106331.33
Total annualized cost, (Rs.)	327060.34	287382.10
Annual electricity delivered, (kWh)	8498.95	9443.28
Net cash flow (Rs.)	124430.52	528140.09
LUCE, (Rs./kWh)	38.43	30.43
NPV (Rs.) (at 7% discount)	14290.43	370203.86
PI	0.014	0.512

CO_2 emission reduction and Fuel saved

Parameters	**Specific fuel consumption (l/kWh)**	**Energy generated per day**	**kg of CO_2 in per litre of diesel**	**Tonnes of CO_2 released per year**	**Annual Fuel Cost (Rs.)**
Diesel	0.30	17.5 kWh	2.68 kg/l	5.13	172462.5
Dual fuel	0.11			1.88	63236.25
Annual Saving				3.25	109226.25
Annual Saving %				68.22	63.33

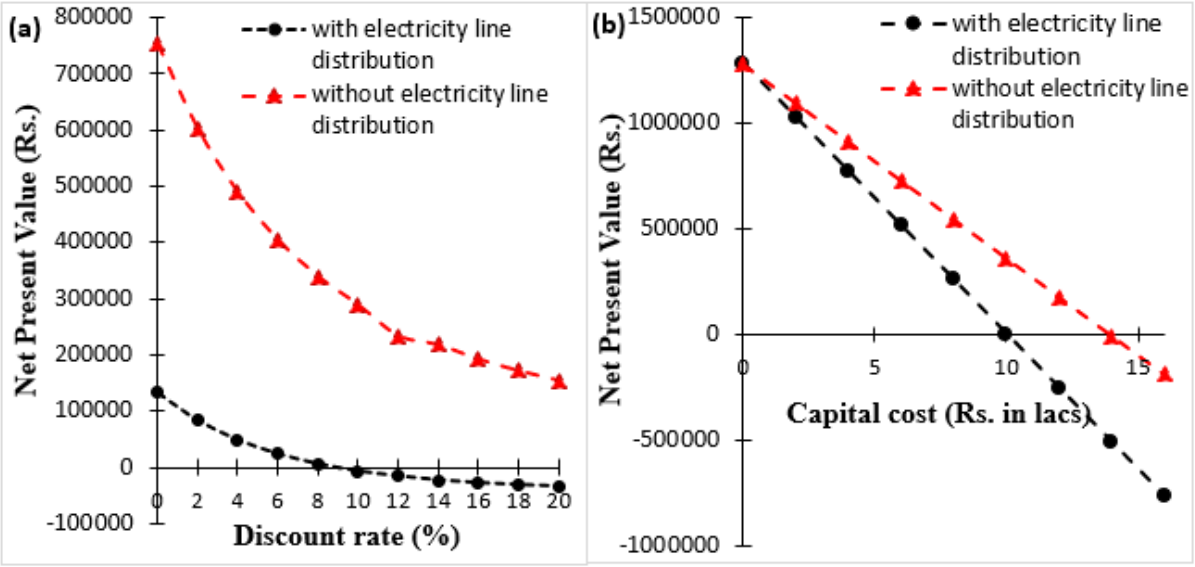

Figure 4.6.7. Relationship between NPV with (a) discount%, (b) capital cost of gasification-engine system

4.6.5 *Gasification energy balance*

The gasifier's performance can be assessed based on the quality of the PG, measured in terms of its heating value. Essential criteria for analyzing gasification performance include gas yield, lower heating value, cold gas efficiency (CGE), and energy distribution [266]. CGE is determined by comparing the heat energy in the PG to that in the raw biomass. In the current experiment, the total energy content of the feedstocks was observed to be 588 MJ for the briquette, as illustrated in Figure 4.6.8 through a Sankey diagram representing the energy transfer in the downdraft gasifier. The diagram reveals that 41.61 % of the biomass energy was converted into cold producer gas. An additional 39.49 % of energy was lost due to cumulative losses from tar residues and minor gas leakages through different pipe connections. The remaining 18.9 % of energy was utilized for sensible heating of the PG.

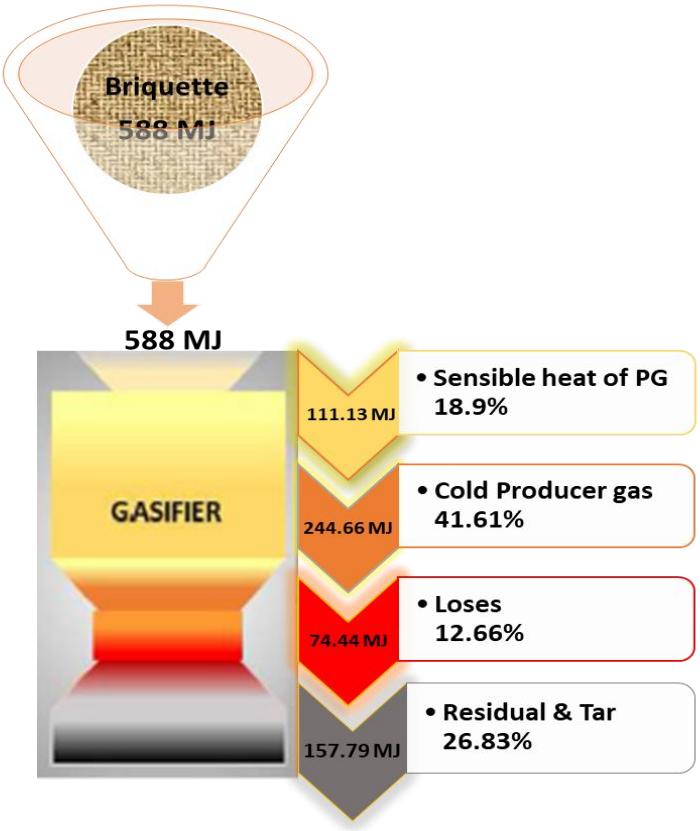

Figure 4.6.8. Sankey diagram for briquette gasification process

4.6.6 *Combustion Analysis*

The current research examined the combustion process by reviewing the pressure versus crank angle data from 10 engine cycles. The prediction of heat energy release rate was made utilizing the 1st law of thermodynamics as,

$$\frac{dQ}{dt} = \frac{\gamma}{\gamma-1}\, p\, \frac{dv}{dt} + \frac{1}{\gamma-1}\, v\, \frac{dp}{dt} \qquad (4.6.1)$$

where γ equals a specific heat ratio of 1.3-1.35 for diesel.

The dual fuel (DF) mode combustion process is more intricate than the standard diesel mode as the fuel mixture ignites before the compression stroke. This pre-ignition affects the combustion of diesel fuel. In DF mode, the ignition delay period is longer due to lower diesel spray and slow burning characteristics of PG. Experimental findings indicate that increasing the CR results in higher cylinder pressure and temperature, which eventually reduces the

ignition delay period of diesel fuel. Figure 4.6.9 shows the variation of 10 number of cycles of maximum cyclinder pressure with crank angle for CR16, CR 17, and CR 18 observed at respective GER 0.43, GER 0.1, and GER 0.1 respectively. Additionally, cylinder pressure increases with engine load during both DF and diesel modes as more fuel is admitted into the engine cylinder. According to the experimental findings, during the diesel mode operation, the maximum cylinder pressure (averaged over 10 number of cycles) observed was at CR 16, 17, and 18, which were 58.99, 62.76, and 70.71 bar, respectively, as shown in Figure 4.6.10(a). On the other hand, in dual mode, the values were 57.47, 58.22, and 64.08 bar (averaged over 10 number of cycles) at the same CR levels. The cylinder pressure in both modes was also observed with respect to crank angles. In diesel mode, the pressure was observed at 9°, 8°, and 7° after TDC, while in DF mode, the pressure was observed at 5°, 6°, and 4° after TDC at CR 16, 17 and 18. The P-V diagram (averaged over 10 number of cycles) of the engine under varying CR and GER conditions at a speed of 1500 rpm is shown in Figure 4.6.10(b). All the respective graphs of engine performance and emissions are drawn keeping in view of averaged of 10 running cycles. The experimental results indicate that increasing the CR leads to an increase in peak pressure for diesel and DF operations. The higher the area under the P-V diagram, the greater the work output. Advancing the ignition causes the combustion process to start at the end of the compression stroke and finishes in the expansion stroke at the beginning of the top dead centre.

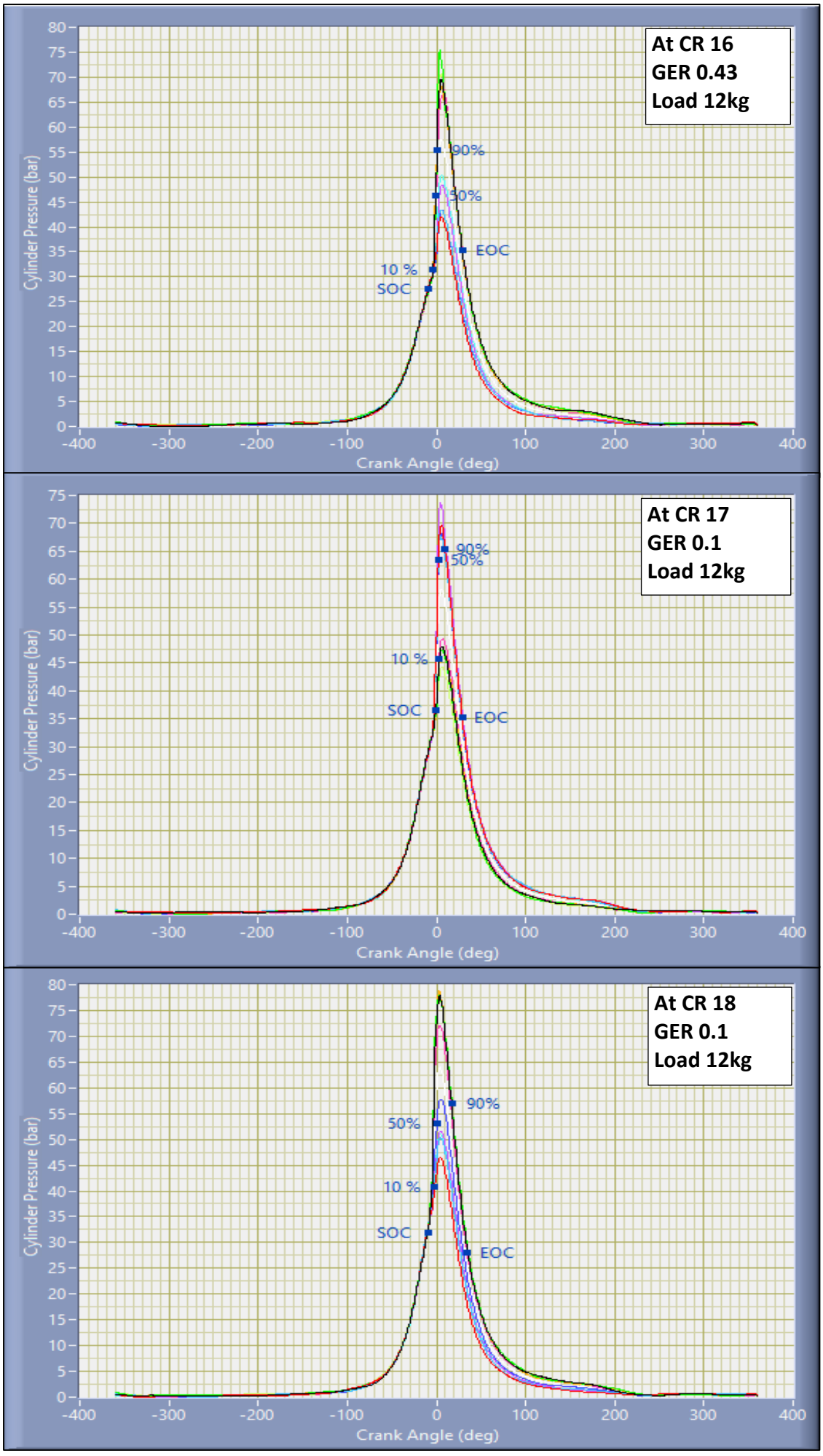

Figure 4.6.9. Variation of max P-theta with 10 number of cycles for different engine CR

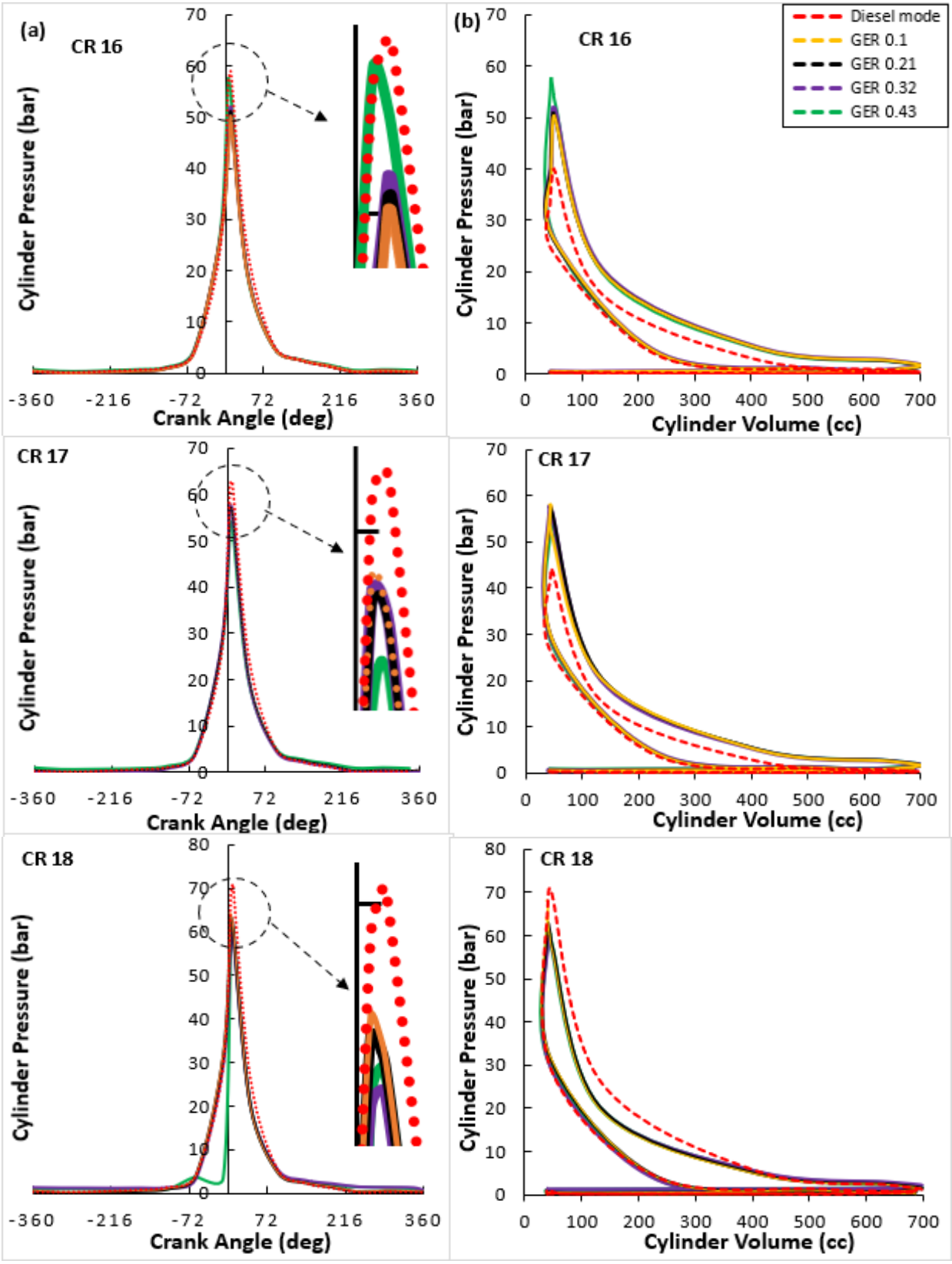

Figure 4.6.10. Variation of (a) P-theta and (b) P-V with maximum engine load at different CR & GER

4.6.7 *Performance Analysis*

4.6.7.1 Brake thermal efficiency

Figure 4.6.11(a) depicts the calculation of Brake Thermal Efficiency (BTE) for diesel and DF mode engine runs concerning compression ratio. BTE is a useful metric for estimating the energy associated with brake power and can be determined through equation (4.6.2).

$$\text{BTE} = \frac{Brake\ Power}{Fuel\ consumption \times Calorific\ value} \quad (4.6.2)$$

The results indicated that the BTE for DF mode was consistently lesser than that of diesel mode across all CR. This was due to the longer ignition delay period in DF mode, caused by poor mixing properties of the fuel mixture resulting from a decrease in the duration of diesel spray. However, BTE showed improvement with increased engine load and lower GER values, as better fuel combustion occurred under enhanced load conditions. The maximum BTE values observed in the experiment were 29.69% for diesel mode and 27.40% for DF mode. Singh et al. [233] concluded similar trends in efficiency, with a maximum BTE of 35.89% for diesel and 26.19% for DF mode, respectively. Sharma et al. [85] reported a maximum BTE of 25.6% and 21.61% for diesel and dual fuel modes, respectively. Thus, the experimental results are compatible with the previous literature.

4.6.7.2 Diesel saving

Diesel consumption is lower when an engine runs on DF mode compared to when it runs on pure diesel, as shown in Figure 4.6.11(b). The percentage of diesel savings is calculated via equation (4.6.3),

$$\text{Diesel saving\%} = \frac{\text{Diesel mode fuel consumption} - \text{Dual mode diesel fuel consumption}}{\text{Diesel mode fuel consumption}} \times 100 \quad (4.6.3)$$

The study has shown that diesel consumption in DF mode decreases as the compression ratio increases, leading to higher specific energy associated with the fuel mixture and a reduced necessity for pilot fuel. The highest diesel savings were observed at CR 16, with savings of 66.15%, followed by 26.97% and 30.33% at CR 17 and 18, respectively. At maximum load conditions, diesel fuel savings are reduced due to the need for a richer fuel mixture to maintain a constant RPM of 1500. Sharma et al. [85] achieved a maximum diesel replacement of 58.18% at CR 18, while Singh et al. [233] achieved diesel replacements of 44.44% and 41.94% for cotton stalks and wheat straw, respectively. Thus, blending producer gas with diesel is economically beneficial, increasing diesel savings by up to 66%.

4.6.7.3 Exhaust Gas Temperature

Figure 4.6.12(a) illustrates that the engine exhaust gas temperature is higher in DF mode than the diesel mode for every compression ratio. This is because excessive heat energy is delivered to the engine in DF mode since the gasification process retains a significant amount of heat energy within the gas. As the CR increases from 16 to 17, the exhaust gas temperature decreases in both modes. The EGT gradually increases as the load increases, reaching its maximum value at full load for all CR. In the DF mode, the EGT at full load is 16.27% higher than the diesel mode for a 16 CR. The maximum exhaust gas temperature for diesel and dual fuel modes are 215°C and 250°C, respectively. The exhaust gas temperature is lower at higher GER values due to the lower calorific value of producer gas, resulting in cooler combustion [267]. Moreover, the results of the experiment conducted by Lal et al. [81] and Singh et al. [233] found that the maximum exhaust temperature in DF mode was 15.15% and 17.5% higher than in diesel mode operation, respectively. Thus, their results were found to be consistent with the current experiment.

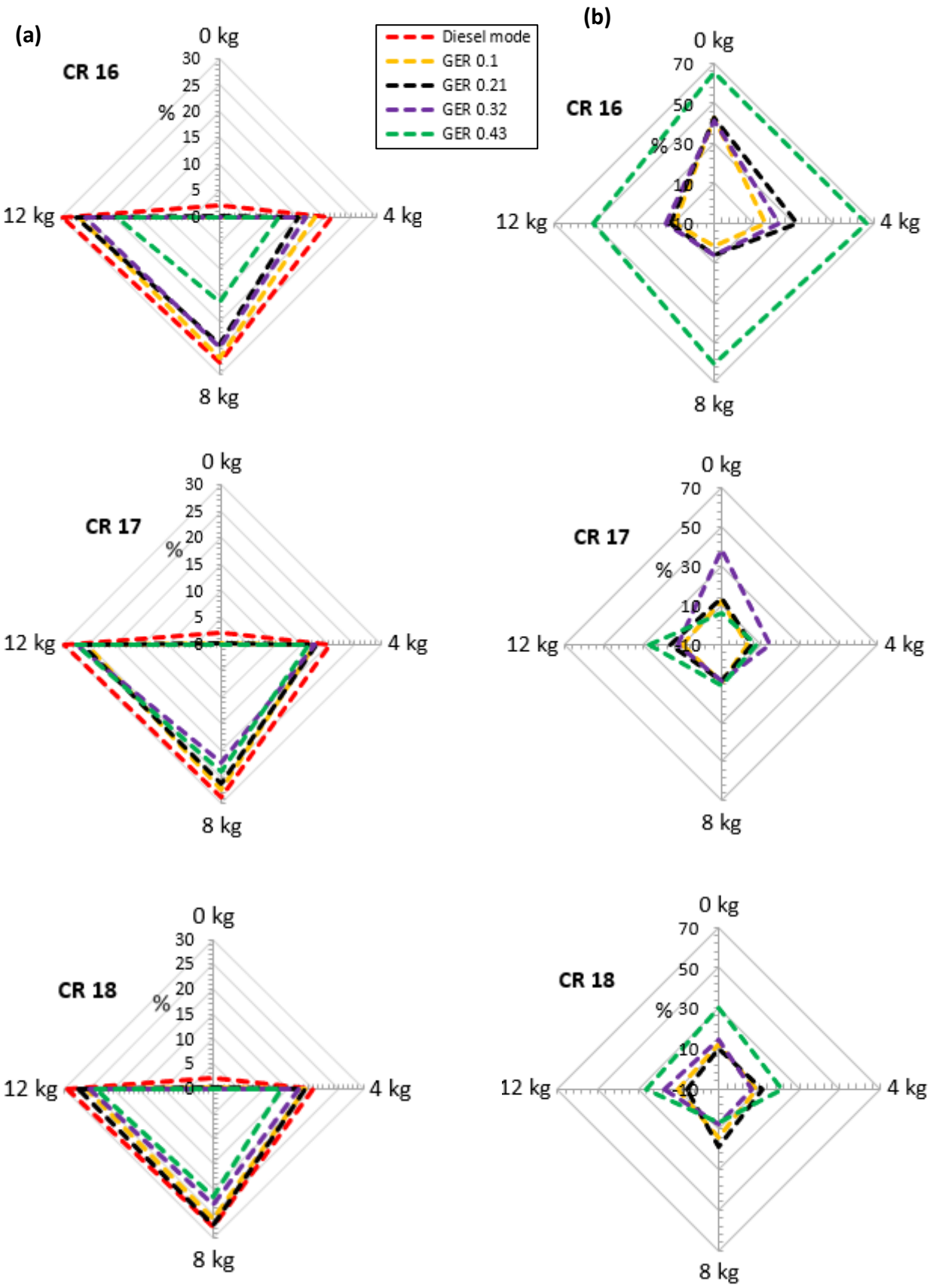

Figure 4.6.11. Variation of (a) BTE %, and (b) Diesel saving % with engine load at different CR & GER.

4.6.7.4 Engine Sound intensity

The sound caused by an engine is influenced by the characteristics of the fuel, including its viscosity and density. When running in DF operation, the high-temperature producer gas introduced into the combustion chamber causes a reduction in fuel viscosity and density, resulting in lower engine noise levels, as shown in Figure 4.6.12(b). A digital sound level meter (MECO instruments, model: 970P) was utilized to measure sound levels. The study found that the recorded sound intensity for diesel mode was between 89.2-96.2 decibels, while it was 86.2-95.7 for DF mode. The range of results obtained in the study is per the Environment Protection Rules of 1986 [34]. Sharma et al. [85] concluded that at CR 18, the highest sound levels recorded were 98.90 db for diesel mode and 98 db for DF mode. Singh et al. [233] showed that in diesel mode, the sound levels ranged from 82.7 to 87.1 db, while in DF mode, they ranged from 82.9 to 90.1 db.

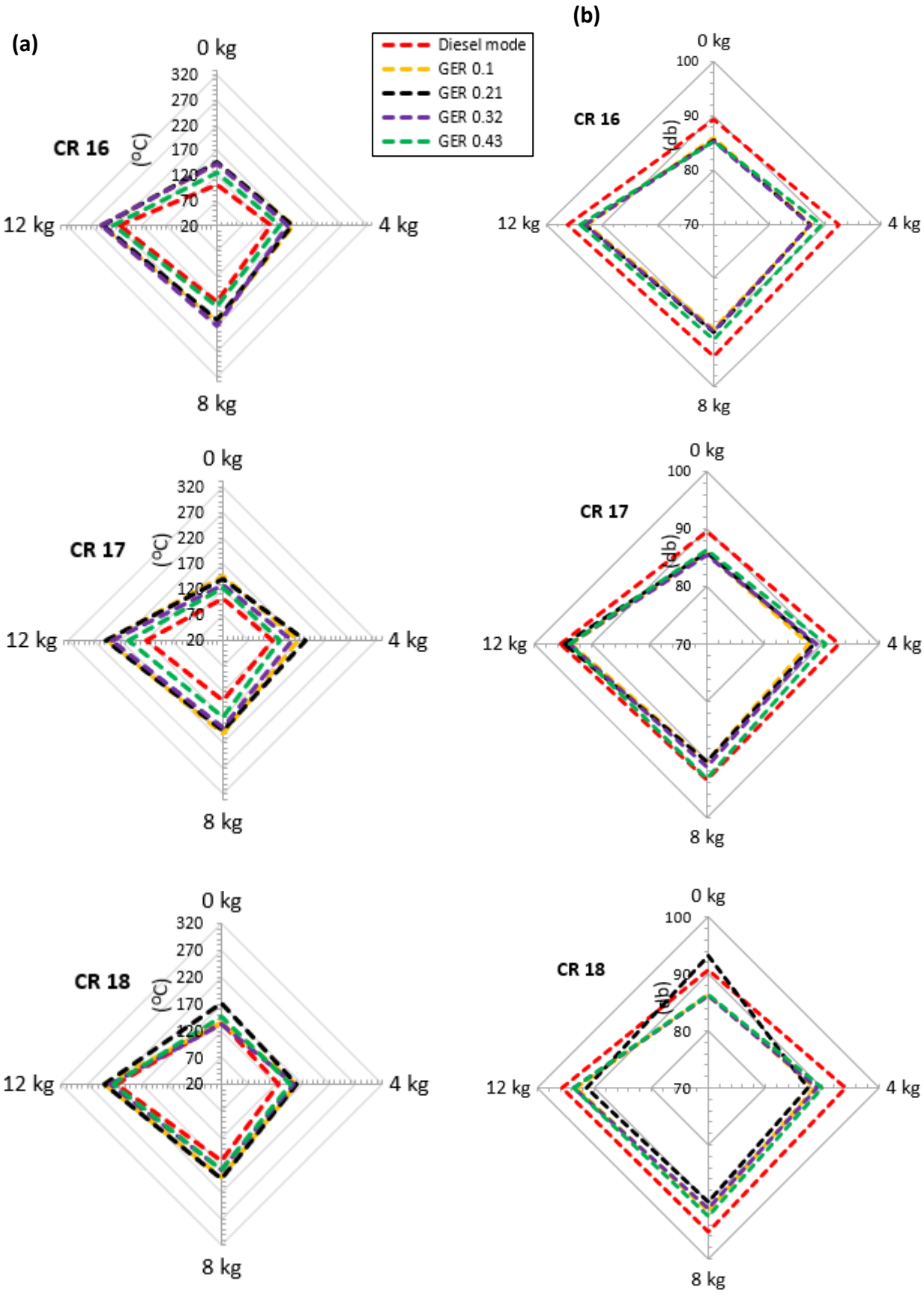

Figure 4.6.12. Variation of (a) EGT °C, and (b) Sound level db with engine load at different CR & GER.

4.6.8 *Emissions analysis*

4.6.8.1 CO emissions

Figure 4.6.13(a) in the study shows the difference in carbon monoxide (CO) emissions between a standard diesel and DF modes at different CR and GER with engine loads. CO is a harmful gas formed by the incomplete combustion of fuel, and its emission levels are affected by the rate of fuel oxidation and decomposition [268]. The CO emissions in standard diesel mode are observed to be lower than in DF mode because PG has a low oxygen fraction that is not conducive to complete combustion. As engine load increases, CO emissions decrease because the engine needs a rich mixture that helps in complete combustion. Research suggests that at a 12 kg engine load, CO emissions in diesel mode were 3-11.5 % lower than in DF mode. Higher GER results in a lower calorific value of PG in the cylinder, ultimately leading to decreased CO emissions. In diesel mode, CO emissions decrease with increased CR because this results in a higher cylinder temperature, which aids in complete combustion. The minimum CO emission recorded was 0.06 % vol. at a 12 kg load, CR 17, and GER 0.43.

4.6.8.2 HC emission

Figure 4.6.13(b) illustrates the discharge of HCs in both dual fuel and diesel modes at varying CR, GER, and engine loads. The findings indicate that the HC emissions in briquette-derived producer gas DF mode exceed those in diesel mode. The HC emissions in dual fuel mode escalated by around 325% during maximum loading conditions compared to standard diesel operation. The data shows that HC emission decreases as the load increases because incomplete combustion occurs at lower loads. However, as the load increases, a richer fuel mixture is supplied to the combustion chamber, resulting in better combustion and reduced HC emissions [269]. Increasing the CR from 16 to 18 resulted in a decrease in hydrocarbon emissions. This is because higher CR values increase the temperature and pressure of the fuel

mixture during the compression process, which in turn increases the possibility of complete fuel combustion during the combustion process. The maximum HC emission observed from the experiment was 318 ppm at 0.21 GER, CR 17, and 0kg load during dual fuel mode operation. The present study's results are consistent with previous literature. Singh et al. [233] found a 300% increase in HC emissions in DF mode as compared to diesel mode. Shrivastava et al.[171] discovered that the maximum HC emissions were 20 ppm for DF and 15 ppm for the diesel-run engine.

4.6.8.3 CO_2 emission

The complete combustion of fuel in engine cylinders is essential for ensuring low levels of CO_2 emissions in the exhaust. Figure 4.6.14(a) illustrates that CO_2 emissions are higher in DF mode than diesel mode because a significant fraction of CO_2 is allied with the alternative fuel PG, which is introduced into the engine cylinder during dual fuel engine run. Additionally, it has been observed that an increase in CR leads to a rise in CO_2 emissions for both running modes, as higher CR results in higher cylinder pressure and temperature. A GER of 0.43 results in lower CO_2 emissions at all CRs, possibly due to its consumption of PG in Boudard reactions [178]. The CO_2 emissions in DF mode were higher than in diesel mode by 10-37.5% at an engine load of 12 kg. In the current study, the maximum CO_2 emissions were 2.1%vol. and 3.9%vol. for diesel and DF modes, respectively, at CR 18. According to Sharma et al. [85], the CO_2 emissions in DF engines were 13.02-39.29 % higher than those of diesel engines. Singh et al. [233] reported that the maximum CO_2 emission from diesel mode was 7.76 % and 3.63 % for DF mode subsequently.

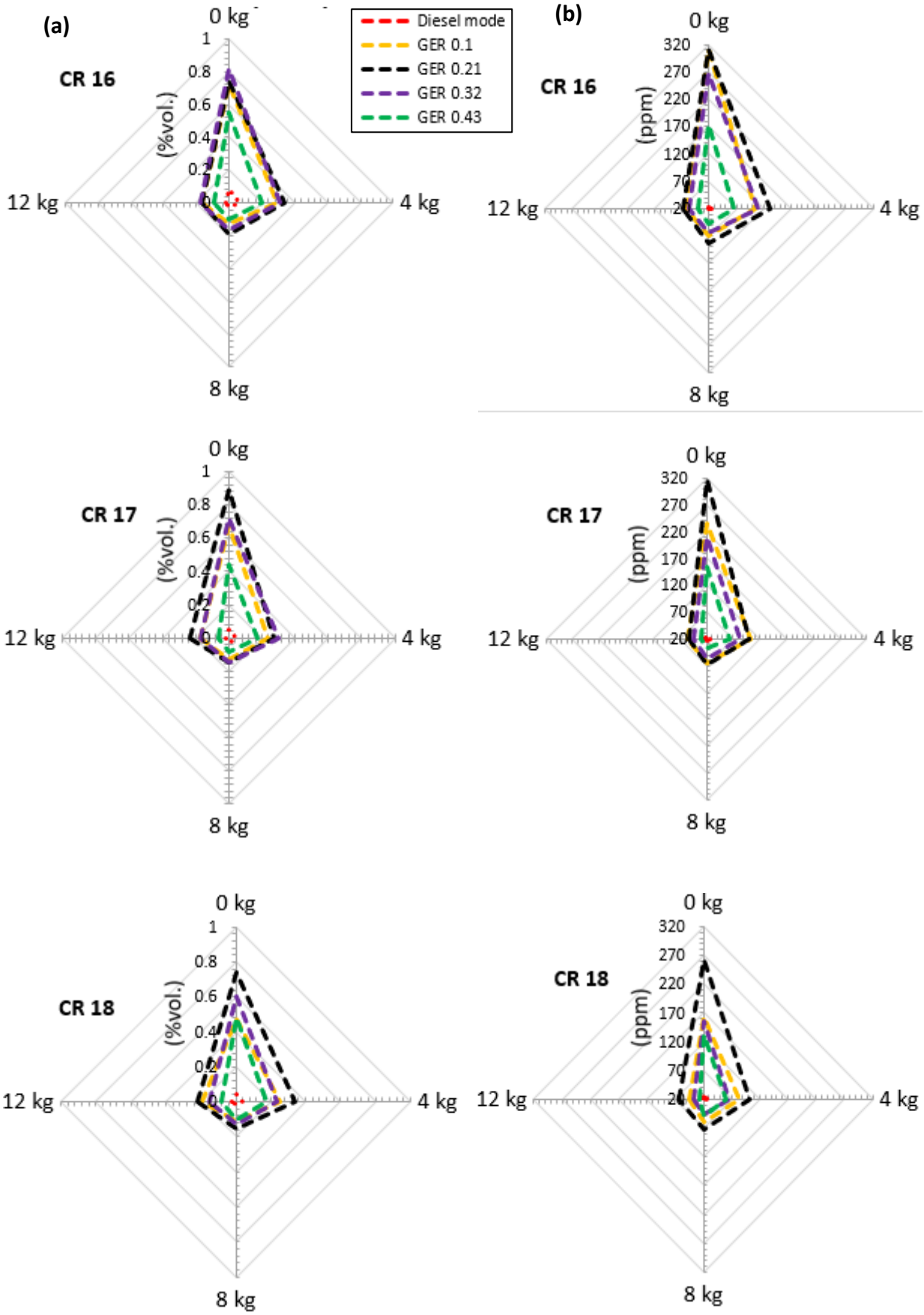

Figure 4.6.12. Variation of (a) CO %vol., and (b) HC ppm emissions with engine load at different CR & GER.

4.6.8.4 NO_X emissions

Nitrogen oxides (NOx) are formed in CI engines primarily due to high temperatures and oxygen. Figure 4.6.14(b) shows NOx emissions increase as the engine load increases in diesel and dual fuel modes. This might be due to the higher combustion chamber temperature at higher loads. There is little difference in NOx emissions at lower loads between diesel and DF modes. Diesel operation results in higher NOx emissions than DF mode, regardless of compression ratio, because the combustion chamber temperature decreases during DF mode due to improper premixed combustion and the lower oxygen content in the fuel mixture. NOx emissions are higher at a higher gasification equivalence ratio (GER) of 0.43, likely because of higher O_2 concentration in the cylinder, which increases NOx emissions [33]. The current study found that the NOx emission during DF mode was about 38.30 % lower than when the engine was running on diesel fuel. The maximum NO_x observed was 402 ppm and 248 ppm during diesel and dual fuel modes, respectively. Shrivastava et al. [171] estimated similar findings of higher NO_x emission (325 ppm) in diesel mode as compared to (180 ppm) in DF mode, respectively.

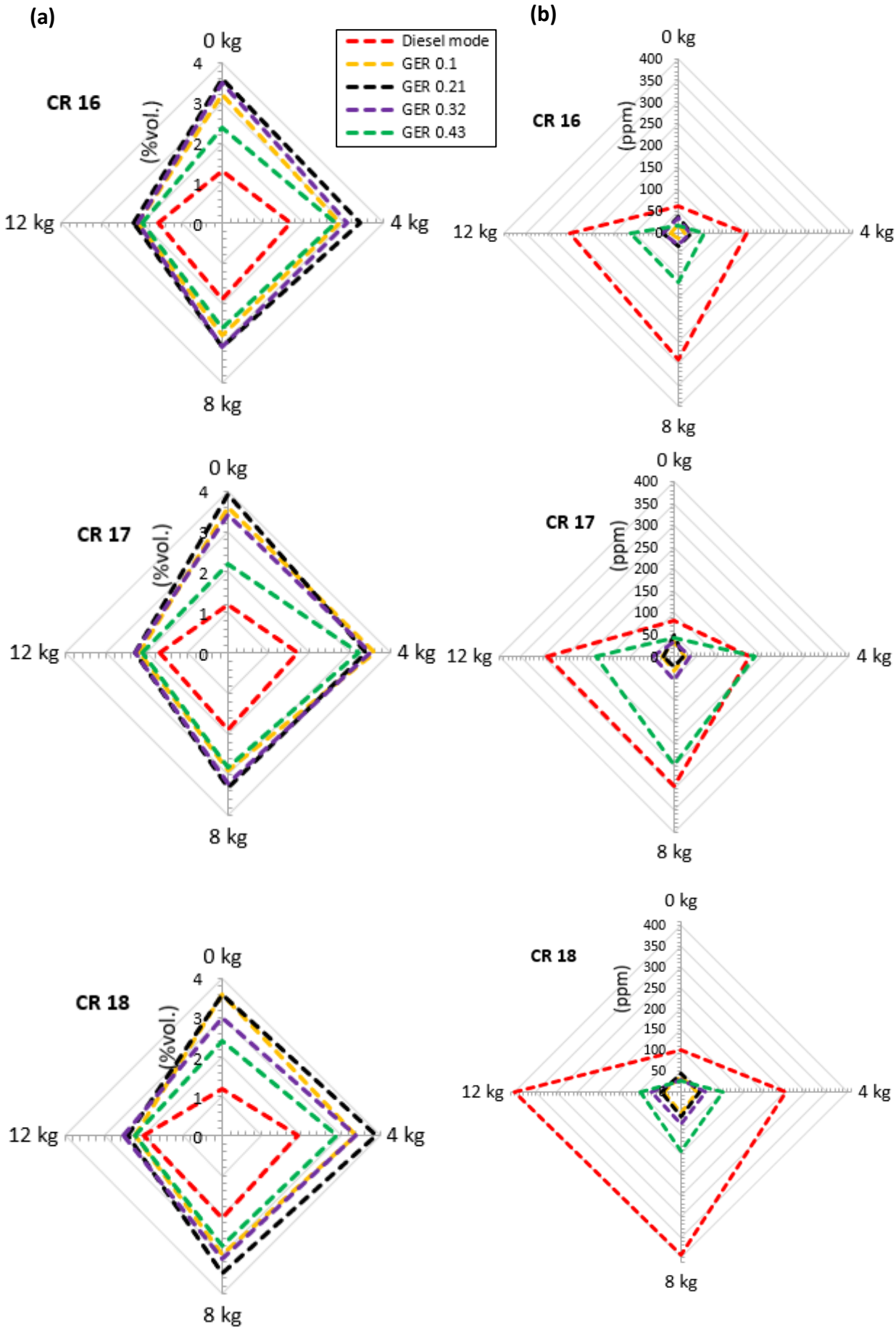

Figure 4.6.14. Variation of (a) CO_2 %vol., and (b) NO_x ppm emissions with engine load at different CR & GER

4.6.9 *Optimum Performance and emission results*

This study focuses on the use of RSM as a popular and effective tool for optimizing engineering systems, particularly in the field of energy systems. The objective of this study is to employ RSM to optimize output parameters. The input parameter ranges considered for the design of experiments and economic analysis are the briquette production capacity (250-400 kg/h), discount rate (0-20%), plant life span (1-20 years), and plant running time (6-12 hours/day). The response parameters selected for evaluation are Net Present Value (NPV), Profitability Index (PI), and Briquette Production Cost (BPC). The ANOVA (Analysis of variance) test and Fit-statistics of the RSM model for the engine performance and emissions have been shown in Table 4.6.1S-4.6.2S (as attached in Appendix). Figure 4.6.15(a) displays an RSM-generated response optimization plot for the economic analysis of briquette plant. The plant offers optimal (maximized NPV, PI, and minimized unit production cost) performance at a production capacity of 400 kg/h; discount of 0%; life span of 14.47 years; and Plant run time of 12 h/day. Corresponding values of NPV, PI, and BPC are Rs.29423596, 11.77, and 14.59 Rs./kg, respectively. A composite desirability value of 0.79, as shown in Figure 4.6.15(b), displays the optimized response output values for maximum engine performance and minimum emissions and the optimized input values for SBP-briquette gasification integrated with an IC engine. In order to analyze the results of an experiment, non-linear quadratic equations are developed for the output responses, which are dependent on the input responses. Response regression is used to develop second-order polynomial models, and the models are designed based on the user's desired outputs. Figure 4.6.16(a) displays the RSM-optimized output parameters validated with the simulated economic analysis model at optimum running conditions of the plant with a percentage error value. Figure 4.6.16(b) shows the RSM optimized output parameters validated with experimental results at an optimum input value of GER 0.10, CR 16, and Load 9.93 kg with percentage

error values. The maximum percentage error between optimized and experimental results at optimized input conditions is 6.68.

4.6.10 *Comparison of performance and emission characteristics*

Various authors have investigated diesel and dual-fuel engines' performance and exhaust characteristics under different experimental conditions, including biomass type, CR range, and engine load. Sharma et al. [85] provide valuable insights into the potential use of PG obtained from walnut shells under similar experimental conditions for VCR engines. Lal et al. [81] provide insights into the consequence of CR and Brake power on engine performance and emissions for both diesel and DF mode operation at a constant 1500rpm engine speed. Shrivastava et al. [171] experimented with different BP (0-4.4kW) at CR 18 and concluded similar BTE and emission characteristics trends. Singh et al. [233] and Sombatwong et al. [230] also experimented on VCR engines at different loads and CR conditions and obtained a maximum BTE in diesel mode engine run with similar trends in engine sound and CO emissions. The present study has been affirmed by comparing its results with previous research works conducted under similar conditions. Table 4.6.5 shows the comparison of present experimental work with the previous works on engine performance and emissions of several authors.

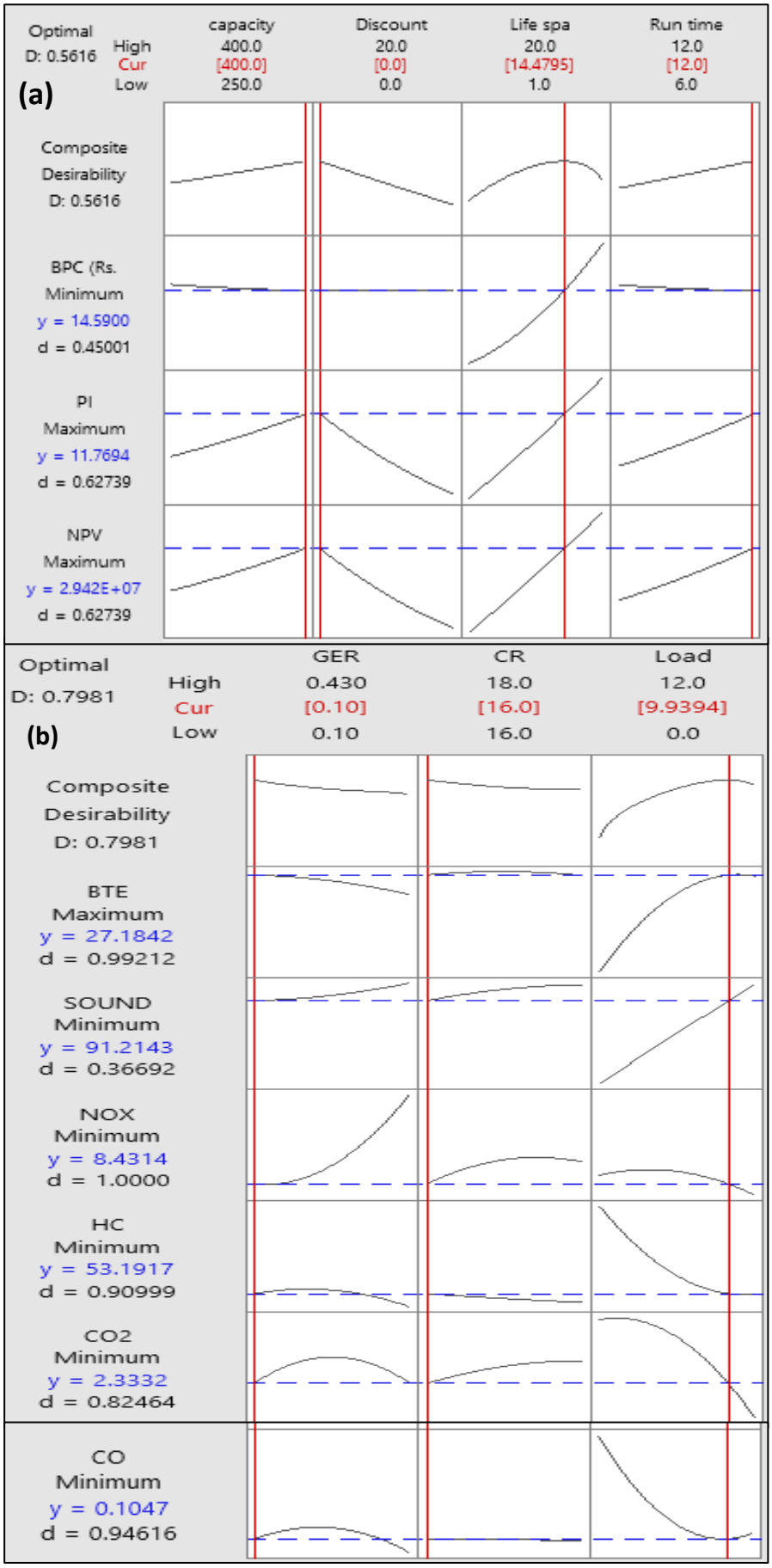

Figure 4.6.15. RSM optimization plot (a) Economic analysis (b) Performance analysis

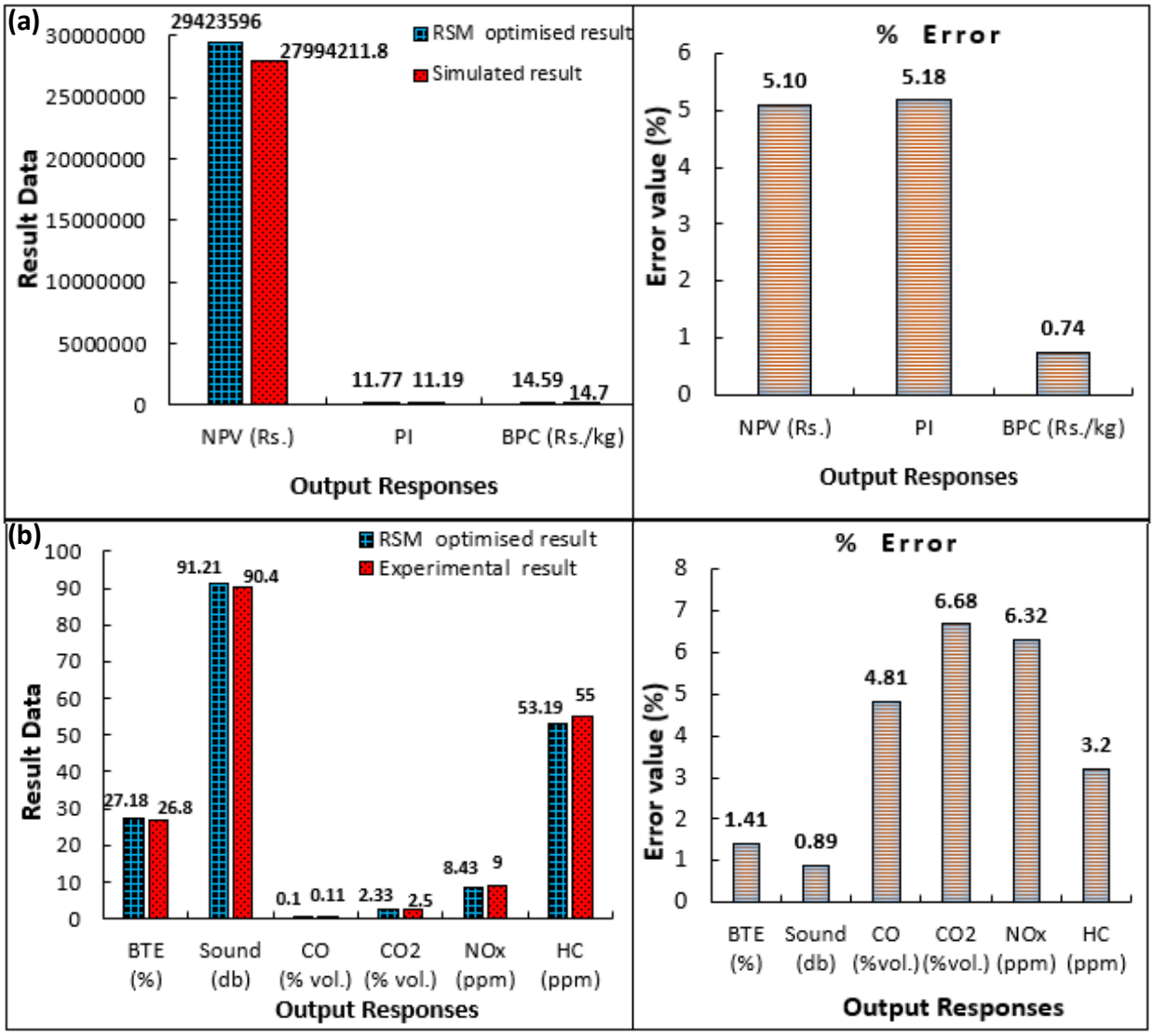

Figure 4.6.16. Validation test for optimized and experimental results with % error values for (a) Economic analysis, (b) Performance analysis

Table 4.6.5. Comparison of experimental findings with the current study [85] [81] [171, 230, 233].

Authors	**Diesel mode**							**Dual fuel mode**							
	BTE (%)	**EGT (º C)**	**Engine Sound (db)**	**HC (ppm)**	**CO (%vol.)**	**CO_2 (%vol.)**	**NO_x (ppm)**	**BTE (%)**	**Diesel saving (%)**	**EGT (º C)**	**Engine Sound (db)**	**HC (ppm)**	**CO (%vol.)**	**CO_2 (%vol)**	**NO_x (ppm)**
Previous works															
Lal et al.	-	330	89	480	0.03	8.62	200	-	64.30	380	89.6	1250	0.10	11.41	80
Singh et al.	35.89	-	87.1	-	-	-	-	26.19	44.44	-	90.1	-	-	-	-
Sombatwong et al.	33.4	260	-	-	0.01	-	-	26.65	64.21	320	-	-	0.05	-	-
Shrivastava et al.	27.5	250	-	15	0.00	-	325	26	-	300	-	20	0.02	-	180
Sharma et al.	25.63	348	102.7	178	0.82	2.07	234	21.61	58.18	453	99.84	1269	2.17	3.41	173
Yaliwalet al.	24	-	-	-	-	-	-	19	65	-	-	-	0.02	-	110
Present study (at 16CR, 8kg)	27.66	170	94.4	18	0.03	1.9	291	23.0	60.46	179	91.3	47	0.1	2.6	113

4.6.11 *Conclusions*

Present study investigated the performance, emission and economic feasibility characteristics of gasification-CI engine obtained through SBP briquette gasification. Maximum DS observed was 66.15% with BTE of 27.4% in DF mode. NPV and PI are positive for briquette manufacturing plant and gasification-CI engine plant over a 20 year timeframe.

(B) Numerical Simulation analysis

In this section, SI engine performance and emission have been simulated through a comprehensive quasi-dimensional thermodynamic model.

4.7 Performance Simulation and Optimization of SI engine using Peach biomass producer gas and propane blend

4.7.1 *Introduction*

Biomass and agricultural waste can be used to generate electricity in remote areas through a Gasifier-engine-generator set. However, producer gas-fueled engines have low power and thermal efficiency. In this view, the objective of this study is to determine optimum operation setting of a spark ignition (SI) engine with improved efficiency, reduced emissions, and fuel consumption. Hence, in the present study, initially, SI engine performance and emission have been simulated through a comprehensive quasi-dimensional thermodynamic model. Thereafter, parametric optimization has been performed to improve the performance of SI engines fueled with peach-based producer gas (PG) and propane blend. The effect of blending percentage, equivalence ratio, and start of ignition (SOI) timing has been considered to analyze the engine performance using response surface methodology (RSM). The experiments were designed according to the design of experiment (DOE) tool based on RSM and optimized using the desirability approach. The use of ANOVA to form regression models resulted high accuracy in forecasting output response variables with a 95% confidence interval. RSM results depict, optimum input parameters to be 90 blend percentage, 1.002 equivalence ratio (ER), and 33.83 SOI at 1500rpm. Corresponding to these optimal inputs, response output performances were found to be 2.41 kW, 0.3003 kg/kW-hr, 27.19 %, 0.809 (vol.%), 2026.05 (ppm) for brake power

(BP), Brake specific fuel consumption (BSFC), Brake thermal efficiency (BTE), CO, and NO respectively, with a composite desirability of 0.868. Thus, RSM has the potential to optimize the performance and emission characteristics of engines fuelled with propane and PG.

Considering the literature survey and subsequent gap mentioned in chapter 1, it was found that the introduction of peach-based producer gas with propane blend in SI engine is not seen with a comprehensive approach to the optimization level. The peach (Prunus persica) is a deciduous tree. Worldwide, Peach-tree cultivation occurs in an area of around 1.54 million hectares, produces approximately 20-22 million tonnes of peach fruit [104], [105], thus its waste biomass could be one of the energy resources. The technical details of peach biomass as a test fuel are depicted in Table 4.7.1. This study aims to promote peach-based PG fuel generation through gasification by an assurance of simulated results of engine performance and emission assessment. Thereafter, to obtain improved performance with low emission of dual fuelled SI engine, conduction of parametric analysis and optimization of operating variable. In the present study, two simulation approaches have been used: engine simulation through FORTRAN Code and optimization through the multi-objective functional response surface method (RSM). In the simulation part, initially, previous experimental peach-based PG compositions were taken as an input fuel for simulation, then engine performance was simulated by a quasi-dimensional model (burned and unburned zone combustion) model, validated with literature experimental results. Further, based on the validation, predicted the engine power, emission, and fuel consumption against the operating variable of PG-propane blend, equivalence ratio, and spark timing. It was reported that the Quasi-dimensional model is better than the thermodynamic zero-dimensional model wherein execution is possible quickly to a significant range of operating conditions efficiently [23]. In the optimization part, firstly RSM based simulated result data has been prepared, then optimized the impact of engine operating variables on the desired response of performance by maximizing the power and minimizing the emission and fuel consumption.

RSM incorporates a series of mathematical/statistical procedures for making an empirical model and exploitation such that the response approaches a desired minimum or maximum value. Recently, RSM-based optimization has become very significant, due to its effectiveness to mitigate the cumulative understanding and to reduce time-consuming experimental work on performance and emission parameters [107]. Some recent progress in the experimental and simulation of the IC engine performance is mentioned in Table 4.7.2. In table, some works have been conducted through Taguchi optimization. Despite the growing interest in SI engines that are integrated with biomass gasification at present, very few publications have been reported in the scientific literature on the quasi-dimensional numerical modeling and simultaneously optimizing engine performance and emission parameters using producer gas from peach-based producer gas blending with propane. In this work, the novelty lies simulation of Peach-Propane fuelled SI engine performance and RSM an optimizing tool to predict the optimization of engine operating parameters for a balanced response of engine power and emission. Subsequently, an analysis of variance (ANOVA) has been conducted to analyze the impact of input variables on the respective response. Concerning this, the present study includes the following main objectives:

- To determine the suitability of peach-based PG with propane blend using a quasi-dimensional thermodynamic simulation approach.
- Optimization of operating variables (blend percentage, equivalence ratio, and spark timing) for the optimal performance of dual-fuelled SI engine.

Table 4.7.1. Thermochemical property analysis of Peach fruit, Gasoline, and Propane test fuels [97, 270, 271].

Parameters	**Peach fruit**	**Gasoline**	**Propane**
Proximate analysis (% weight)			
Moisture	8.99	0.00	-
Ash	0.43	0.00	-
Volatiles	67.52	-	-
Fixed Carbon	23.80	-	-
HHV (MJ/kg)	21.88	44	46.40
Ultimate analysis (% weight)			
C	51.95	0.86	1.09
H	5.76	0.128	2.75
N	0.80	0.00	0.78
S	0.01	0.010	-
Cl	0.53	-	-
O	44.11	0.00	0.20
Density (kg/m^3)	1240	750	545
Viscosity (kg/ms)	-	0.005	1.002×10^{-4}
Thermal conductivity (W/mK)	0.462	0.115185	0.017
Research Octane number	100-105	95.8	112
Heat of Vaporization (kJ/kg)	207-434	305	426

Table 4.7.2. Previous study vs. Present investigation

Type of engine	Investigation method	Optimization technique	Fuels	Optimization Parameter	Ref.
Previous Investigation					
SI engine	Experimental	RSM	Gasoline and ethanol blend	Blend % and Engine speed	[272]
SI Engine	Experimental	ANOVA and Taguchi	pure gasoline, ethanol and methanol	Engine speed, CR, and ignition timing	[273]
SI Engine	Experimental and CFD-ANSYS simulation	Taguchi	Gasoline and Methanol blend	Blend % and engine speed	[274]
SI Engine	Experiment	RSM	Secondary butyl alcohol-gasoline blends	Blend and speed	[103]
SI Engine	Experimental and ANN	RSM	Amyl alcohol-gasoline fuel blends	CR, fuel blend and engine speed	[275]
SI Engine	Experimental and MCDM	SWARA and ARAS	Pure ethanol and methanol	CR, ignition timing, and air excess coefficient	[276]
SI Engine	Experimental and ANOVA	Particle Swarm Optimization (PSO)	Gasoline blended with Acetone-Butanol-Ethanol	Blend percentage and engine speed	[277]
SI Engine (Turbocharged)	1 D-Simulation	Graphical	Gasoline	fuel injection, and spark timing	[278]
SI Engine	Experimental	ANOVA and Grey relational analysis (GRA)	Methanol and gasoline blends	Load and Compression Ratio	[279]
SI Engine	Experimental	MATLAB/Simulink with Genetic-algorithms (GA)	Butanol and gasoline blends	intake and exhaust valve opening time, Air to Fuel ratio, and spark angle	[280]
Present Investigation					
SI Engine	FORTRAN Code	Design Expert	PG and Propane	Blend %, Equivalence ratio, Spark timing	Not yet

4.7.2 *Model Validation*

The quasi-dimensional thermodynamic computational simulation model was validated with an experiment performed by Tsiakmakis et al. [97], the respective validation corresponding to in-cylinder pressure versus crank angle is depicted in Figures 4.7.1 (A & B) for the assurance of prediction capability. The specification of the engine details being used for simulation is depicted in Table 2.7.1. The validation has been demonstrated for the 100% propane (Figure 4.7.1A) and 55% producer gas blends (Figure 4.7.1B). To assess the error value, Root Mean Square Error (RMSE) has been applied to measure the error of a model in predicting quantitative data. And, The RMSE was found to be 0.4451, which indicates the absolute fit of the model to the data. The respective equation was as follows-

$$\text{RMSE} = \sqrt{\frac{\sum_i^n (Model - Experiment)\text{^}2}{n}}\text{; where n is the count of data point sets.} \quad (4.7.1)$$

For pure propane and blending, the comparison of computation and experiment reveals essentially equivalent trends. The small variation that was found, that could be attributable to the assumptions made by the computer program and cycle-to-cycle variability. At a difference of 10^{o} CA, it was found that the maximum peak pressure errors were -0.4% and +1.33% for 100% propane and 55% producer gas, respectively.

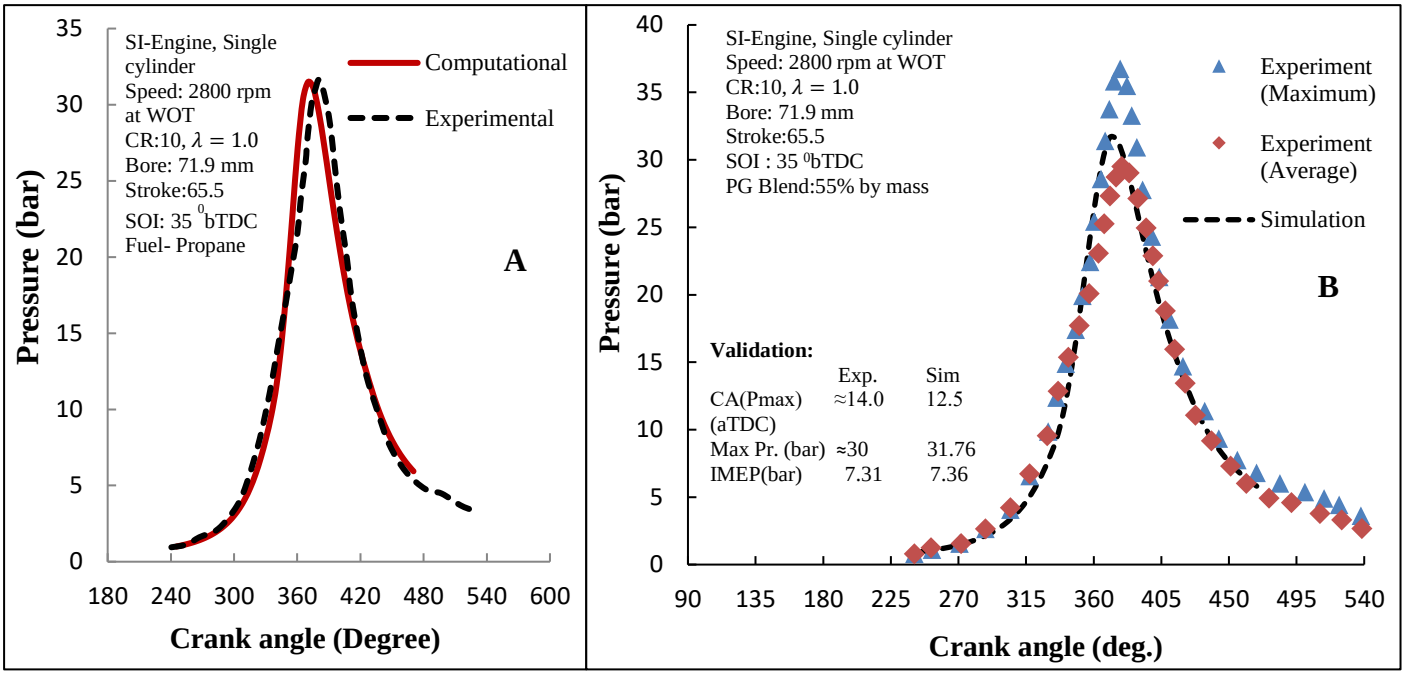

Figure 4.7.1 A & B. Validation of simulation result with experiment.

4.7.3 *RSM approach*

The parameter used for performance analysis in the SI engine was analyzed by standard response surface methodology design called central composite design (CCD). RSM is a collection of mathematical and statistical techniques useful for developing the empirical model building, improving and optimizing processes parameter and it can also be used to find the interaction of several affecting factors [281]. The RSM method is suitable for fitting a quadratic surface and it helps to optimize the process parameters with a minimum number of trials, as well as to analyze the interaction between the parameters. It uses quantitative data from the related experiment to determine a regression model and to optimize a response (output variable) that is influenced by several independent variables (input variables). Optimization by the RSM method involves three major steps; these are firstly statistically designed experiments, secondly, estimating the coefficients in a mathematical model, and finally predicting the response and checking the adequacy of the model [282]. In this study, three independent variables were chosen for the statistical simulation design as follows: Propane Blending in peach PG (vol.%),

Equivalence ratio, and SOI (bTDC). These three parameters are very influential in determining the combustion, performance, and emission characteristics of the engine. The blending ratio affects the fuel property whereas optimizing the Equivalence ratio enhances the combustion characteristics of the engine. SOI decides the magnitude of the performance parameters of the engine. Therefore, there is an utmost need to optimize these independent variables. The range and level of the factors varied accordingly to the simulation design. These three variables together with their respective ranges were found to be important parameters for efficient performance and emission analysis for SI engines. It is assumed in the design, the independent variable in the trials is continuous and regulated with negligible errors. The statistical design aimed to optimize the response variables (Y). It needed to find a suitable correlation between independent variables and response surfaces [283]. The response was used to generate an empirical model, which correlates to the variables using a second-degree polynomial equation.

In this study, FORTRAN-based result data were modeled using the response surface methodology during a process. Table 4.7.3 shows the 126 trial data of the propane + peach PG blended fuel for SI engine performance analysis. In RSM, the model equation is the complete second-order equation. The second-order model can be written in the form of equation (31):

$$Y = C_0 + \sum_{i=1}^{n} C_i X_i + \sum_{i=1}^{n} C_{ii} X_i^2 + \sum_{i<j=1}^{n} C_{ij} X_{ij} + \varphi \quad (4.7.2)$$

where C_0, C_i, C_{ii}, *and* C_{ij} are constant, linear, quadratic, and interaction effects of regression coefficients, respectively. X_i and X_j are independent coded variables.

Based on it, by applying FORTRAN data including independent variables and response outputs to Design expert software, the relationship between the variables was determined and an acceptable prediction was made. The diagnostics of response variables depicted in the graph between predicted versus actual response for BP, BSFC, BTE, CO, and NO is obtained using

the RSM technique as shown in Figure 4.7.2. These graphs are important as they signify the efficiency of the model. The X-axis of the graph represents the actual, and Y-axis represents the predicted values. Actual values are the data sets obtained from FORTRAN and the data sets obtained by regression equation using ANOVA analysis constitute predicted values. The closeness and the linearity of the predicted values from a straight line show that the developed model is fit and efficient. Moreover, the overall perception from the display of the actual and predicted data depicts that the error value is well accepted and that there is no large deviation between them. The statistical significance of the regression models for each response was established at a 95% level of confidence. The margin of error of the response surface methodology defines the width of the confidence interval and is determined by the observed variability in the sample, the sample size, and the confidence level. Accordingly, based on RSM, the margin of error was found to be 0.0011, 0.0008, 0.0198, and 0.0075 for BP, BSFC, BTE, and CO respectively. Optimization was performed and verified with the predicted and simulation test results having a high level of agreement with a margin of error of less than 5%.

Table 4.7.3. Data on the performance of blended fueled for RSM optimization.

S.No.	ER	Propane Blend in Peach PG (V%)	SOI (bTDC)	BP (kW)	BSFC (kg/kWh)	BTE (%)	CO (V%)	NO (ppm)
1	0.8	10	50	1.734	0.986	26.90	0.21	4297.1
2			45	1.73	0.98	26.80	0.17	2601.7
3			40	1.68	1.01	26.07	0.14	1441.7
4			35	1.566	1.09	24.33	0.12	742.6
5			30	1.41	1.21	21.87	0.1	416
6		25	50	1.819	0.617	26.76	0.19	4491.2
7			45	1.83	0.613	26.97	0.15	2772.7
8			40	1.78	0.629	26.26	0.13	1538.4
9			35	1.67	0.672	24.60	0.1	797.8
10			30	1.516	0.741	22.27	0.08	406.7
11		50	50	1.88	0.414	26.85	0.18	4835.8
12			45	1.9	0.407	27.21	0.15	2989.5

S.No.	ER	Propane Blend in Peach PG (V%)	SOI (bTDC)	BP (kW)	BSFC (kg/kWh)	BTE (%)	CO (V%)	NO (ppm)
13			40	1.86	0.417	26.65	0.12	1678.4
14			35	1.766	0.441	25.14	0.1	891.6
15			30	1.615	0.483	23.01	0.08	480.4
16		75	50	1.92	0.33	27.03	0.17	5073
17			45	1.948	0.326	27.40	0.15	3237.9
18			40	1.92	0.33	27.04	0.12	1845.9
19			35	1.83	0.346	25.76	0.1	986.8
20			30	1.68	0.376	23.70	0.08	529.9
21		90	50	1.93	0.3	27.14	0.17	5259.2
22			45	1.97	0.295	27.60	0.15	3396.4
23			40	1.95	0.298	27.33	0.12	1954.8
24			35	1.866	0.311	26.14	0.1	1050
25			30	1.718	0.338	24.07	0.08	552.4
26	0.9	10	50	1.89	0.995	26.66	0.55	5125.2
27			45	1.936	0.973	27.27	0.48	4071.9
28			40	1.919	0.982	27.06	0.41	2933.3
29			35	1.84	1.02	25.91	0.35	1934.5
30			30	1.7	1.1	23.97	0.3	1179.5
31		25	50	1.99	0.627	26.35	0.5	5413.1
32			45	2.04	0.61	27.10	0.44	4327.9
33			40	2.04	0.6119	26.99	0.38	3202.3
34			35	1.97	0.633	26.07	0.32	2148.2
35			30	1.84	0.678	24.32	0.27	1321.7
36		50	50	2.06	0.422	26.32	0.48	5720.3
37			45	2.13	0.409	27.21	0.43	4695.2
38			40	2.138	0.407	27.30	0.37	3563.2
39			35	2.08	0.418	26.62	0.31	2431.7
40			30	1.96	0.443	25.13	0.27	1549.3
41		75	50	2.09	0.339	26.30	0.48	6030.7
42			45	2.17	0.326	27.37	0.42	5043.6
43			40	2.2	0.323	27.66	0.37	3881.1
44			35	2.16	0.328	27.16	0.31	2748.8
45			30	2.06	0.344	25.91	0.27	1789.7
46		90	50	2.103	0.3099	26.30	0.48	6227.3
47			45	2.19	0.296	27.48	0.43	5274.2
48			40	2.23	0.292	27.90	0.37	4120.2
49			35	2.2	0.296	27.54	0.32	2966.5
50			30	2.11	0.308	26.44	0.27	1959.9
51	1	10	50	2.01	1.024	25.94	1.04	3144.4
52			45	2.08	0.989	26.91	0.96	2659.9
53			40	2.09	0.985	26.93	0.89	2167.4
54			35	2.035	1.012	26.24	0.82	1661.3

S.No.	ER	Propane Blend in Peach PG (V%)	SOI (bTDC)	BP (kW)	BSFC (kg/kWh)	BTE (%)	CO (V%)	NO (ppm)
55			30	1.916	1.074	24.71	0.76	1168.1
56		25	50	2.122	0.648	25.46	0.99	3186.6
57			45	2.2	0.624	26.50	0.92	2738.9
58			40	2.22	0.618	26.70	0.84	2216
59			35	2.18	0.631	26.18	0.78	1758.4
60			30	2.07	0.663	24.90	0.72	1281.6
61		50	50	2.19	0.44	25.26	0.97	3303.3
62			45	2.29	0.4208	26.42	0.9	2889.2
63			40	2.33	0.414	26.86	0.84	2461.3
64			35	2.3	0.418	26.57	0.76	1937.7
65			30	2.21	0.435	25.52	0.7	1459.8
66		75	50	2.217	0.355	25.13	0.96	3423
67			45	2.341	0.336	26.53	0.9	3043.4
68			40	2.394	0.329	27.14	0.83	2596.8
69			37.5	2.397	0.328	27.17	0.8	2370.6
70			30	2.313	0.34	26.21	0.7	1646.6
71		90	50	2.229	0.324	25.11	0.96	3483.2
72			45	2.36	0.3068	26.59	0.9	3158.9
73			40	2.42	0.2985	27.28	0.83	2729.2
74			38	2.43	0.2975	27.39	0.81	2553.3
75			35	2.42	0.298	27.31	0.77	2258.5
76			30	2.36	0.305	26.65	0.71	1777.3
77	1.1	10	50	2.05	1.08	24.61	2.9	1047.5
78			45	2.12	1.04	25.49	2.86	902.5
79			40	2.13	1.03	25.58	2.87	738.6
80			35	2.08	1.06	24.99	2.87	577.5
81			30	1.97	1.12	23.66	2.89	410.2
82		25	50	2.157	0.69	23.77	2.78	897.7
83			45	2.246	0.663	24.92	2.78	775.8
84			40	2.263	0.658	25.12	2.77	644.4
85			35	2.224	0.669	24.67	2.77	513.7
86			30	2.12	0.702	23.54	2.78	368.6
87		50	50	2.23	0.4705	23.63	2.73	864.9
88			45	2.33	0.449	24.76	2.74	736.7
89			40	2.365	0.443	25.09	2.75	631.1
90			35	2.341	0.448	24.79	2.72	491.7
91			30	2.254	0.465	23.87	2.73	368.5
92		75	50	2.25	0.38	23.47	2.7	897
93			45	2.378	0.361	24.75	2.71	781.1
94			40	2.432	0.35	25.30	2.73	627.6
95			32.5	2.392	0.36	24.88	2.71	449.6
96			30	2.35	0.365	24.43	2.71	389.6

S.No.	ER	Propane Blend in Peach PG (V%)	SOI (bTDC)	BP (kW)	BSFC (kg/kWh)	BTE (%)	CO (V%)	NO (ppm)
97		90	50	2.264	0.348	23.39	2.69	915.5
98			45	2.398	0.329	24.77	2.7	813.4
99			40	2.464	0.32	25.46	2.72	664.7
100			38	2.47	0.319	25.50	2.72	604.9
101			30	2.4	0.328	24.8	2.7	409.3
102	1.2	10	50	2.026	1.16	22.75	5.41	476.3
103			45	2.059	1.148	23.12	5.48	344.7
104			40	2.127	1.111	23.88	4.97	319
105			35	2.068	1.143	23.22	5.23	220.2
106			30	1.912	1.236	21.46	5.48	89.8
107		25	50	2.142	0.748	22.06	5.26	393.3
108			45	2.236	0.717	23.03	5.24	329
109			40	2.242	0.715	23.08	5.23	258.8
110			35	2.194	0.731	22.59	5.26	182.3
111			30	2.084	0.769	21.46	5.3	105.9
112		50	50	2.23	0.509	21.84	5.19	377.7
113			45	2.33	0.487	22.82	5.15	325
114			40	2.36	0.481	23.11	5.16	258.6
115			35	2.32	0.488	22.76	5.18	184.7
116			30	2.22	0.5105	21.80	5.21	111
117		75	50	2.264	0.4112	21.73	5.21	367.6
118			45	2.378	0.3915	22.82	5.16	321.8
119			40	2.426	0.383	22.38	5.13	266
120			35	2.405	0.387	23.08	5.13	198.1
121			30	2.32	0.401	22.26	5.16	125.4
122		90	50	2.27	0.376	21.64	5.23	365.8
123			45	2.397	0.357	22.82	5.17	326.1
124			40	2.455	0.348	23.40	5.14	272.9
125			35	2.446	0.35	23.28	5.12	208.2
126			30	2.37	0.361	22.59	5.14	135.8

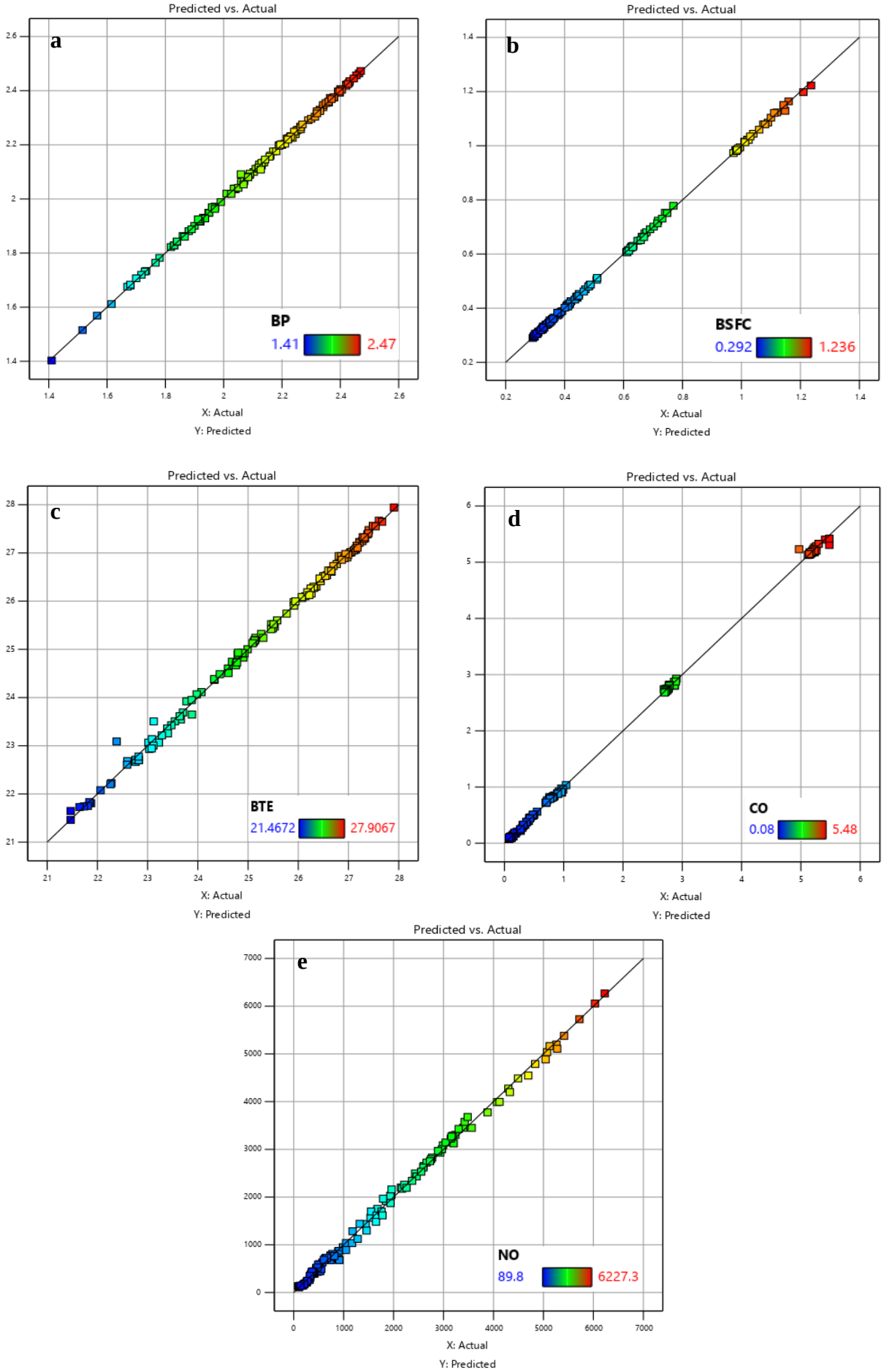

Figure 4.7.2. RSM diagnostic illustration representing the graph between predicted vs actual for response variable (a) BP (b) BSFC (c) BTE (d) CO (e) NO

4.7.4 *Analysis of variance for response model*

By comparing the variation of the actual and predicted value, the statistical concept of a model was examined. Table 4.7.4 shows the ANOVA information about the accuracy of prediction and the importance of respective mathematical model terms. The significance of each response model was observed from the large F-values and small P-values (< 0.05). R^2 should be high, near 1, and reasonable agreement with adjusted R^2 is required. Based on the significant factors, the R^2 number was also performed for the overall variability of responses. In Table 5, higher values of R^2 were observed to the value of0.99, indicating the higher accuracy of the proposed model. Similar higher values of R^2 (0.998) and R^2adj. (0.9967) of the statistical model have been also observed by Zaman et al.[115]. Rith et al. [284] estimated higher R^2 (0.9966) and R^2adj. (0.9949) values for specific energy consumption model. Aparna et al.[285] evaluated the ANOVA model for BP, BTE, NO_x and also observed higher values of Adjusted R^2 (0.9985 to 0.9992) and Predicted R^2 (0.9964 to 0.9993). Simsek et al. [286] determined 0.9919 R^2 for BTE, 0.9967 R^2 for CO [287], and 0.9918 R^2 for BSFC [136].

Table 4.7.4. ANOVA for quartic degree response model

Response	Sum of Squares	df	Mean Square	F-value	P-value	Adjusted R^2	Predicted R^2
BP	6.78	34	0.1993	4720.58	< 0.0001	0.9992	0.9986
BSFC	9.73	34	0.2861	12994.37	< 0.0001	0.9997	0.9994
BTE	394.03	34	11.59	894.20	< 0.0001	0.9959	0.9937
CO	458.06	34	13.47	7175.22	< 0.0001	0.9995	0.9992
NO	3.181E+08	34	9.355E+06	969.23	< 0.0001	0.9962	0.9947

Using the RSM, the nonlinear function of the output response was predicted in terms of three variables: Equivalence ratio, Blending percentage, and SOI timing. The quartic model for

output responses, BP, BSFC, BTE, CO, and NO was generated using RSM-based regression analysis as shown in equations (4.7.3-4.7.7)

BP (Kw) = 49.93961-221.75130 ER -0.101025 Blend +0.033336 SOI +0.300317 ER * Blend
-0.463036ER * SOI+0.000729 Blend*SOI +362.26168 ER^2 -0.000124 $Blend^2$+0.009541SOI^2
-0.002687ER*Blend*SOI-0.222307ER^2*Blend+0.487090 ER^2*SOI-0.000285 ER*$Blend^2$
-0.003758ER * SOI^2+1.22530E-06 $Blend^2$ * SOI+0.000013Blend * SOI^2-253.58290 ER^3
+2.50748E-06$Blend^3$-0.000154SOI^3+0.000093ER^2 * $Blend^2$+0.001163ER^2*Blend*SOI
+0.000254ER^2 * SOI^2-9.62460E-07 ER * $Blend^2$ * SOI+4.39396E-06 ER*Blend*SOI^2
-3.56680E-09$Blend^2$ * SOI^2+0.053390ER^3 * Blend-0.126927ER^3*SOI+6.22540E-07ER*$Blend^3$
+0.000022ER * SOI^3-8.19300E-10 $Blend^3$*SOI -1.45146E-07 Blend*SOI^3
+64.40185 ER^4-1.18443E-08 $Blend^4$+8.82690E-07 SOI^4 (4.7.3)

BSFC (kg/kWh) = +11.55407 -9.63866 ER -0.205515 Blend -0.397238 SOI +0.175286
ER * Blend +0.833836 ER * SOI+0.003886 Blend * SOI-12.86941 ER^2
+0.002063 $Blend^2$ +0.000030 SOI^2 -0.002394 ER*Blend*SOI-0.070057 ER^2*Blend
-0.566174 ER^2*SOI -0.000764 ER*$Blend^2$-0.003368 ER*SOI^2-0.000017 $Blend^2$*SOI
-0.000037 Blend*SOI^2+19.61881 ER^3 -0.000014 $Blend^3$ +0.000053 SOI^3
+0.000346 ER^2*Blend ^{2}+0.000895 ER^2 *Blend*SOI +0.002218 ER^2*SOI^2
+3.20901E-06 ER*$Blend^2$*SOI+1.64330E-06 ER*Blend*SOI^2
+1.23867E-07 $Blend^2$*SOI^2 -0.006235 ER^3*Blend+0.094061ER^3*SOI
-2.37525E-07 ER*$Blend^3$ -0.000010 ER*SOI^3+1.98803E-08 $Blend^3$*SOI
+1.37264E-07 Blend*SOI^3-5.89271ER^4+5.12127E-08 $Blend^4$ -3.26102E-07 SOI^4 (4.7.4)

BTE (%) = +110.07879 -978.01310 ER - 0.730017 Blend +7.63154 SOI +2.55837ER*Blend
-13.38991ER*SOI +0.006281 Blend*SOI +2015.13480 ER^2 -0.002213 $Blend^2$
-0.039911SOI^2-0.032369 ER*Blend*SOI -2.20580 ER^2*Blend+12.81255 ER^2*SOI
+0.003366 ER*$Blend^2$-0.051256 ER*SOI^2+0.000072 $Blend^2$*SOI+0.000089 Blend*SOI^2
-1618.73314 ER^3-0.000014$Blend^3$+0.000736 SOI^3 -0.000664 ER^2*$Blend^2$
+0.011989 ER^2*Blend*SOI+0.009756 ER^2*SOI^2 -0.000013 ER*$Blend^2$*SOI
+0.000126 ER*Blend*SOI^2-4.88853E-07 $Blend^2$*SOI^2 +0.605020 ER^3*Blend
-3.84488 ER^3*SOI -5.89481E-06 ER*$Blend^3$ +0.000299 ER*SOI^3-1.12824E-07 $Blend^3$*SOI
-1.18254E-06 Blend*SOI^3 +450.41777 ER^4+1.06865E-07 $Blend^4$ -6.18104E-06 SOI^4 (4.7.5)

CO (Vol.%) = -775.07810 +3247.96192 ER-0.142661Blend -0.955237 SOI +0.293107 ER*Blend
+6.43037 ER*SOI +0.002489 Blend*SOI -5113.89871 ER^2+0.000469 $Blend^2$
-0.046322 SOI^2 +0.001697 ER*Blend*SOI-0.335566 ER^2*Blend -6.10679 ER^2*SOI
+0.000035 ER*$Blend^2$ -0.008125 ER*SOI^2 -0.000022 $Blend^2$*SOI -0.000053Blend*SOI^2

$$+3525.23377\ ER^3 - 9.72694E{-}07\ Blend^3 + 0.000872\ SOI^3 - 0.000080\ ER^2{*}Blend^2 + 0.001003\ ER^2{*}Blend{*}SOI + 0.014729\ ER^2{*}SOI^2 + 5.32620E{-}06\ ER{*}Blend^2{*}SOI - 0.000051\ ER{*}Blend{*}SOI^2 + 2.35376E{-}07\ Blend^2{*}SOI^2 + 0.099351\ ER^3{*}Blend + 1.56562\ ER^3{*}SOI - 6.75497E{-}08\ ER{*}Blend^3 - 0.000141\ ER{*}SOI^3 - 1.14435E{-}08\ Blend^3{*}SOI + 6.18013E{-}07\ Blend{*}SOI^3 - 891.38977\ ER^4 + 5.71415E{-}09\ Blend^4 - 4.86894E{-}06\ SOI^4 \quad (4.7.6)$$

NO (ppm) =

$$+4.69866E{+}05 - 1.18708E{+}06\ ER - 2037.01862\ Blend - 25146.37373\ SOI + 5802.46007\ ER{*}Blend + 64337.01156\ ER{*}SOI + 9.66416\ Blend{*}SOI + 9.21182E{+}05\ ER^2 - 0.403713\ Blend^2 + 144.08507\ SOI^2 - 19.50352\ ER{*}Blend{*}SOI - 5415.96909\ ER^2{*}Blend - 52346.02413\ ER^2{*}SOI + 0.670646\ ER{*}Blend^2 - 299.64806\ ER{*}SOI^2 - 0.004658\ Blend^2{*}SOI + 0.033090\ Blend{*}SOI^2 - 1.79525E{+}05\ ER^3 + 0.001597\ Blend^3 + 0.283135\ SOI^3 - 0.248504\ ER^2{*}Blend^2 + 7.68975\ ER^2{*}Blend{*}SOI + 132.18444\ ER^2{*}SOI^2 + 0.009285\ ER{*}Blend^2{*}SOI + 0.021996\ ER{*}Blend{*}SOI^2 - 0.000040\ Blend^2{*}SOI^2 + 1681.71923\ ER^3{*}Blend + 13875.97340\ ER^3{*}SOI - 0.002976\ ER{*}Blend^3 + 0.118573\ ER{*}SOI^3 - 0.000010\ Blend^3{*}SOI - 0.000486\ Blend{*}SOI^3 - 32763.47382\ ER^4 + 9.02587E{-}06\ Blend^4 - 0.002603\ SOI^4 \quad (4.7.7)$$

4.7.5 *Performance analysis using 3-D surface plot*

The performance of an SI engine is an important parameter that indicates the degree of success with which the chemical energy contained in the fuel is converted into useful mechanical work. In this view, the degree of success has been considered to analyze with significant parameters such as BP, BSFC, and BTE.

Brake power is the power obtained at the end of the crankshaft [178]. Figure 4.7.3(a) shows the simultaneous impact of ER, blending percentage, and SOI on the brake power. As the SOI timing increases, the BP increases due to an increase in brake mean effective pressure [288]. The increase in the amount of propane blend in peach PG increases the rate of heat release which enhances the brake power [288]. An increase in the equivalence ratio from lean mixture to rich cause an increase in BP. This is due to an increase in cylinder temperature at higher ER [289]. Maximum BP produced was 2.47kW at ER 1.1, blending percentage of 90%, and SOI 38 bTDC. It was also observed that as the blending percentage of PG increases in the blends,

brake power reduces. A similar trend of derating power was also observed while syn gas blends with biogas, which is due to the effect of lower energy density content of PG or syn gas[94].

Brake-specific fuel consumption is a parameter that measures the effectiveness of a combustion engine, which consumes fuel and generates rotational power at the crankshaft. The simultaneous effect of input parameters on BSFC is shown in Figure 4.7.3(b). The aim was to reduce BSFC because it is the "fuel economy" metric, and adding propane blended fuel to the SI engine proved helpful in reducing BSFC. At a particular 1500 rpm speed and CR 10, the amount of fuel consumed increases with increasing ER. The increasing ER is responsible for the rapid boosting of the pressure near TDC; that is, the pressure rise rate increases with ER in the late compression stroke which assists in better combustion [290]. At an SOI timing of 30 bTDC, the magnitude of BSFC is the highest among all blending percentages. BSFC first gradually reduces to the lowest value and then rises slowly with the increase of the spark advance angle. This is because too retarded or too advanced spark timing all lead to reducing brake mean effective pressure and brake power. Thus, the BSFC at the other spark timing is higher than that at the best spark timing. A minimum BSFC of 0.292 kg/kWh was observed at an ER 0.9, propane blend in peach PG 90 vol.%, and SOI 35 bTDC.

Brake thermal efficiency is an important factor to consider when comparing and evaluating an engine's performance. The BTE of the SI engine is the ratio of the brake power at the engine crankshaft to the power generated by the combustion of the fuel. Figure 4.7.3(c) shows the computed results of BTE as a function of ER, blending percentage of propane in PG, and SOI. From the figure, it can be seen that BTE increases with ER and peaks in ER 0.9 to ER 1 region, and then decreases toward the higher ER increment for propane - PG blending as well. This is because, a leaner mixture than a stoichiometric fuel-air ratio produces less sensible heat, which lowers the temperature required for dissociation and the formation of a portion of the exhaust species. Since less energy is used in dissociation, a greater proportion of fuel's energy is instead

used to drive the piston. Efficiency decreases when a mixture is richer than the stoichiometric operating state because there isn't enough oxygen present for complete combustion [198]. As the percentage of propane in PG increases, the BTE of the engine increases. This increment is caused by propane characteristics, as the fast burning of propane enables the combustion phase to release more heat near the top dead center. That could decrease the heat loss generated by the heat release in the expansion stroke. And stratified mixture, which is formed by propane direct injection, can make the fuel burn more completely. The volumetric efficiency is improved by the propane blend. Thus the brake thermal efficiency goes up with the increase of the propane addition fraction [291]. In the figure, it can be seen that BTE increases as the spark timing advance from 30 bTDC to 40 bTDC, the maximum BTE is found to be 27.90% at 40^0 bTDC spark timing. The variation of BTE significantly depends on negative power loss at the compression region and subsequent heat loss and this increases with too much advance in the compression stroke. On the other hand, if spark timing is too retard, combustion prolongs toward the expansion phase and contributes less net work output, thus cumulatively power and efficiency reduces [292]. The brake thermal efficiency of SI-engine fueled with peach-based PG with Propane blend (i.e., 27.90%) is also comparable with the biogas-fueled SI Engine. Huang et al. [293] simulated biogas as fuel for SI engines and observed a maximum BTE of 26% at ER 1.0-1.1. Porpatham et al. [294] analyzed biogas-fuelled SI engines and observed similar trends in brake power and thermal efficiency results as the range of equivalence ratios covered the lean misfire limit on one side to the knock limit on the rich side. On the rich side, there is a drop in power output due to a need to retard the spark timing to prevent knocking. Moreover, Hotta et al. [295] experimented on biogas fuelled SI engine and noticed that BP followed a similar increasing trend till a peak value and then decrease with progressive ignition advance from the TDC.

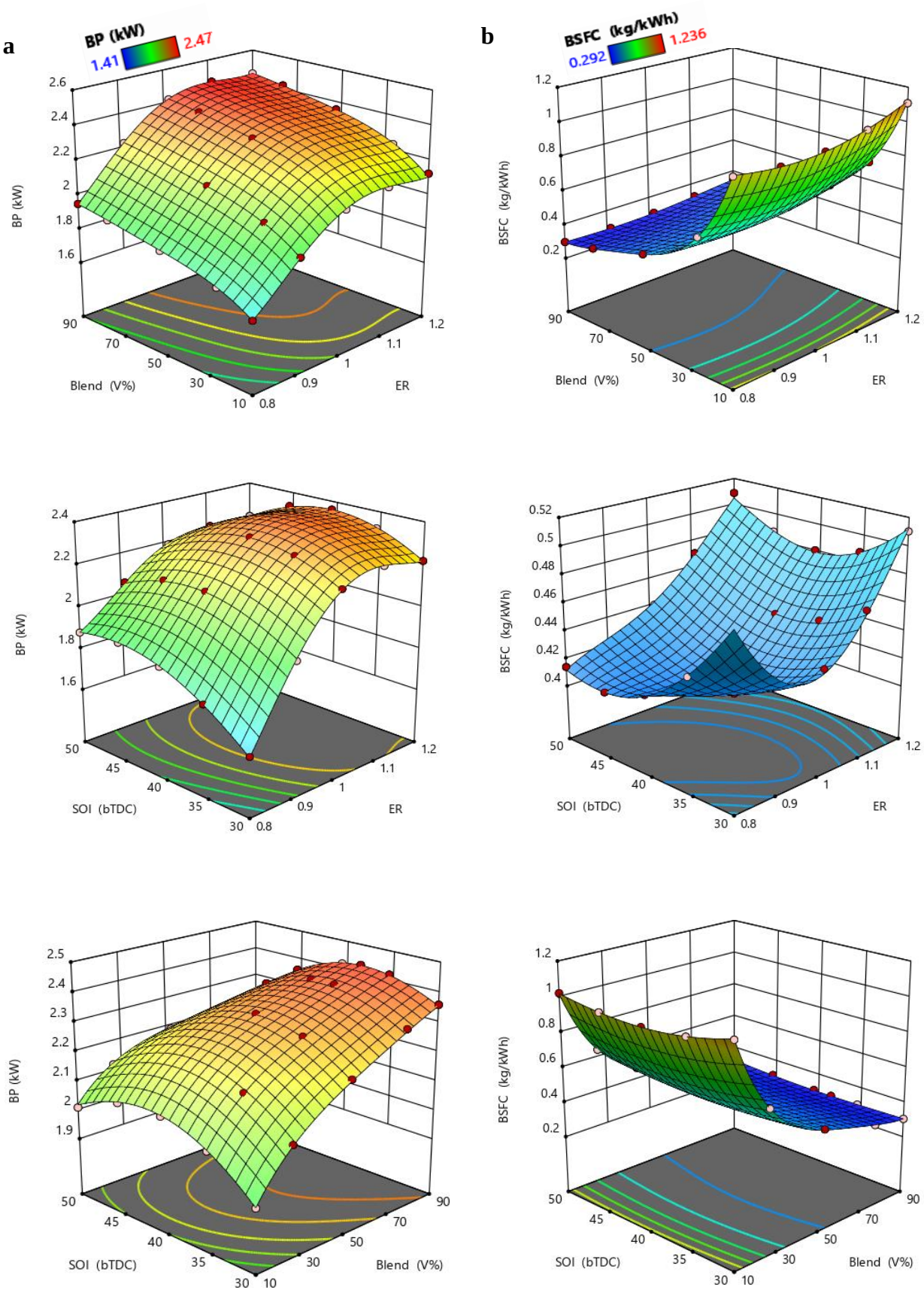

Figure 4.7.3. Simultaneous impact of ER, Propane blend in peach PG, and SOI on (a) BP (b) BSFC

c

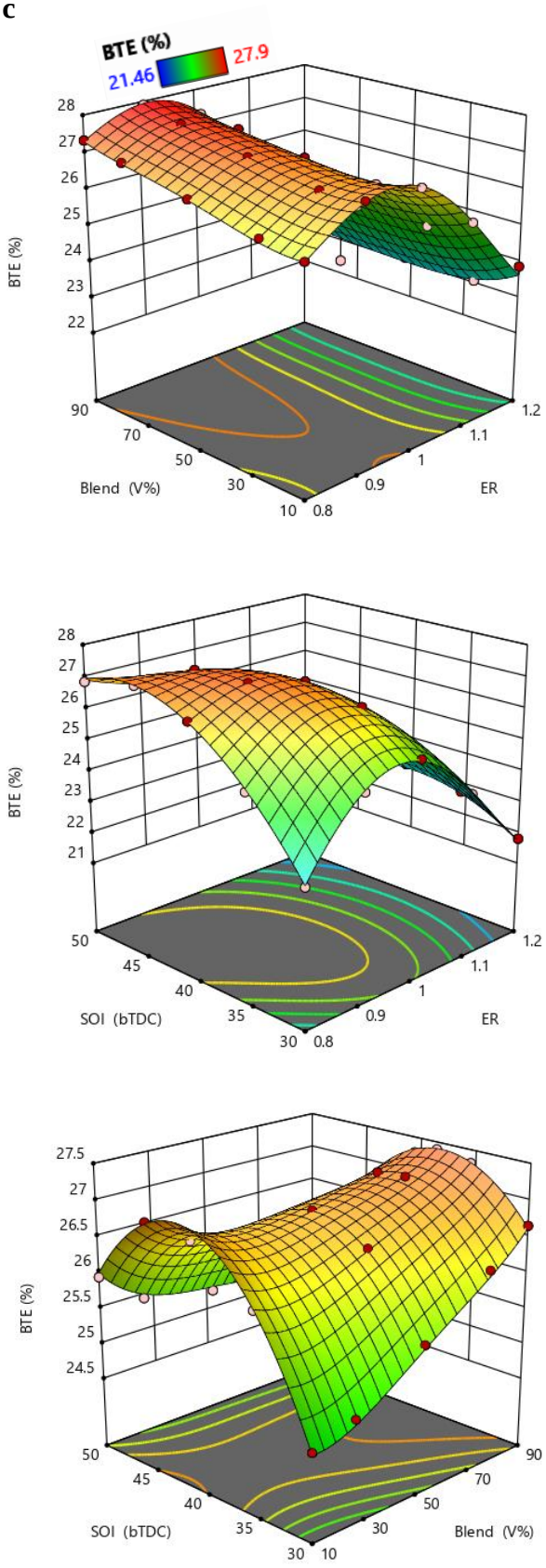

Figure 4.7.3. Simultaneous impact of ER, Propane blend in peach PG, and SOI on (c) BTE

4.7.6 *Emission analysis using 3-D surface plot*

The primary pollutants emitted from SI engines are mainly oxides of nitrogen and carbon monoxide. The rate kinetic technique has been used to determine engine CO and NO concentration.

Carbon monoxide (CO) is a toxic gas released during engine combustion due to an insufficient amount of oxygen. Figure 4.7.4(a) shows CO emissions of blended fuels for the different ER, Propane blending percentages in PG, and SOI. From the figure, it can be seen that CO formation increases with an increase in ER. The favorable condition for less CO emission was observed to be from ER 0.8 to ER 1. The CO formation decreases for all propane blends with PG till ER 1.1. This could be the result of CO being present in the PG fuel, and consequently in the blending. Aside from the possibility of incomplete combustion, the generation of CO can be regulated by the temperature that is present within the cylinder as well as the degree to which CO_2 is dissociated. Retarding the spark has two effects. First, there is more time for mixing so there is a less fuel-rich pocket for CO production. Second, the charge temperature in the expansion stroke is higher so that post-flame oxidation of CO is promoted. Both effects reduce CO emissions. As the SOI timing advances from 30 bTDC to 50 bTDC, the CO formation increases till the stochiometric mixture. Maximum CO formation of 5.48 vol.% was observed at ER 1.2, and 10 vol.% of propane blends with PG.

Nitric oxide (NO) develops in both the flame front and post-flame gases of the SI Engine. The formation of NO is mostly dependent on the temperature of the gas, the concentration of oxygen, and the reaction time during combustion [95]. Figure 4.7.4(b) shows the simultaneous effect of independent parameters on the NO emissions at EVO on a ppm basis. From the figure, it can be noticed that NO concentrations increase with the increase in ER, attains a maximum at ER 0.9, and then starts decreasing in the stochiometric and richer mixture. This could be

because at richer mixture results in a lower maximum temperature in the cylinder as well as lower availability of oxygen [198]. The figure demonstrates that the NO concentration is reduced when lower propane blends are used in conjunction with SOI time. NO emissions increase linearly which is mainly because the advance of the spark timing increases the in-cylinder average temperature. The maximum magnitude of NO observed was 6227.3 ppm at ER 0.9, 90 vol.% propane blend with PG, and SOI 50 bTDC. Porpatham et al. [69] analyzed on biogas fueled SI engine and observed similar trends in CO and NO emissions as the range of equivalence ratios covered from lean to the rich side. In the rich region, the CO level shoots due to incomplete combustion. Jingdang et al. [70] simulated biogas as fuel to SI engines and observed similar trends in CO and NO emissions. The peak value in NO emissions was observed at ER 1.0-1.1. Park et al.[296] investigated biogas blended with hydrogen and observed similar increasing trends in NO emission with blend percentages and ER.

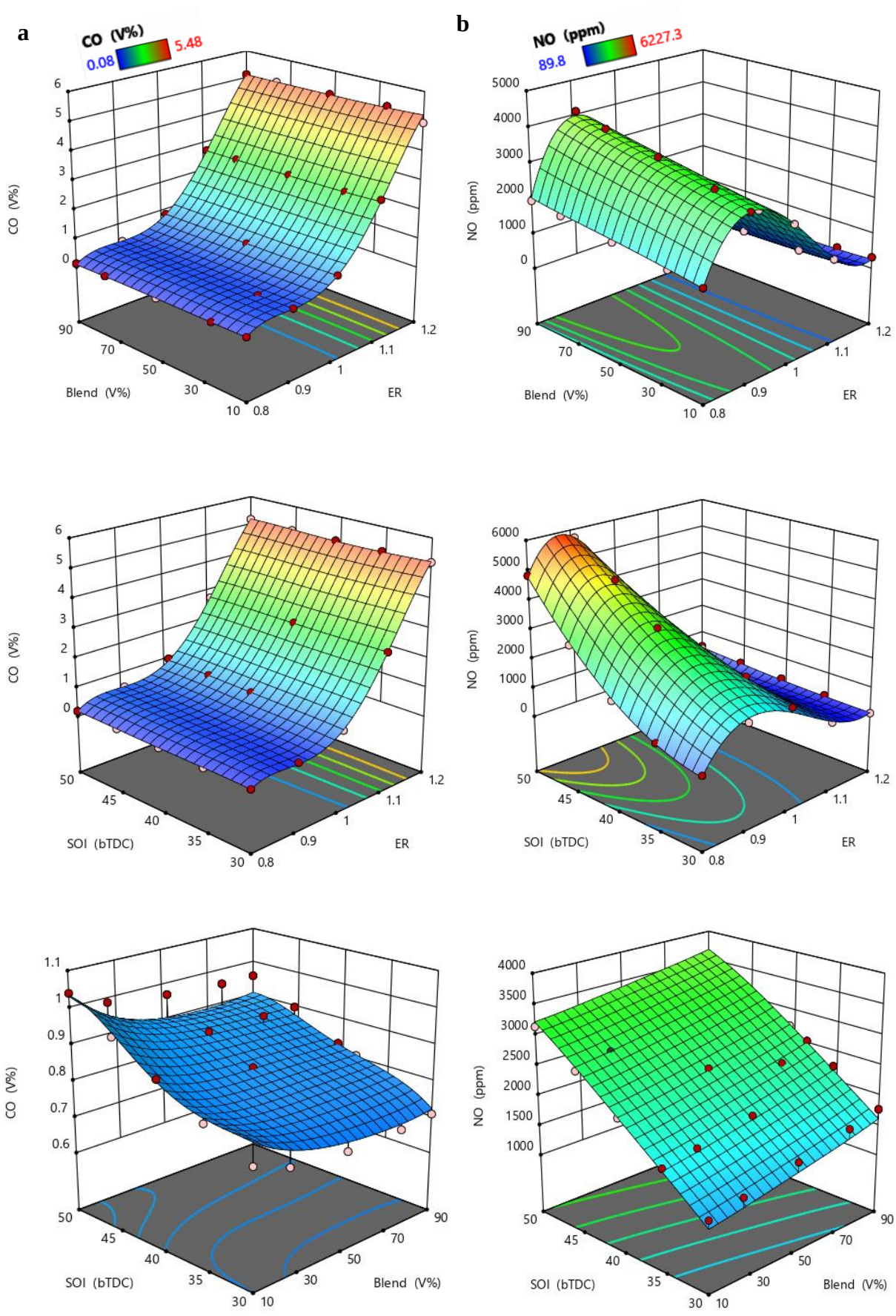

Figure 4.7.4. Simultaneous impact of ER, Propane blend with PG, and SOI on (a) CO (b) NO

4.7.7 *Response optimization*

The desirability function approach was used to obtain the optimum parameters for the multiple responses, as well as to accomplish the goals of maximizing the brake power and brake thermal efficiency, as well as minimizing the brake-specific fuel consumption, CO emission, and NO emission. After computing desirability analysis on the response data using a desire function, a larger value indicated a higher level of desirability, the condition with the highest desirability value was chosen as the ideal one. The outputs of the multi-objective optimization that have desirability values, that are relatively near to one indicate the best possible options. Figure 4.7.5 shows the desirability values of numeric factors and corresponding output responses. The combined desirability obtained was 0.868, indicating that the cumulative multiple parameters tend to produce a favourable result for all of the responses taken together. The best condition of input parameters is equivalence ratio 1.002, propane blend in peach PG 90 vol.%, and SOI 33.83 bTDC as shown in Figure 4.7.6. Also, the predicted optimum values of output responses for BP, BSFC, BTE, CO, and NO are 2.41 kW, 0.3003 kg/kWh, 27.19%, 0.8095 vol.%, and 2026.05 ppm respectively. Table 4.7.5 shows the RSM-optimized values used against the simulated test run for validation and their percentage of error values. All error % were observed to be below 5% and it shows that the confirmation test result and the value of optimal parameters are acceptable and reliable. RMSE value for response output observed was 0.53 which indicates as good ability of the model for the prediction.

After the multi-optimization process, the contour plots of BP, BTE, BSFC, CO, and NO are displayed in Figure 4.7.7. These graphs illustrate the values at which the highest desirability is achieved. The desirability value that is displayed in Figure 4.7.7 (a), is a useful indicator for the values of the parameters that should be optimized for multi-objectives. Figure 4.7.7 (b & d) demonstrates that the BP and BTE increased as the percentage of propane blend increased; hence, the highest blend percentage produced the highest brake power and BTE. The minimum

value of the BSFC was when the highest value of the propane blend as shown in Figure 4.7.7 (c). The minimum value of the CO and NO concentrations were at lean and rich mixture respectively as shown in Figure 4.7.7 (e and f).

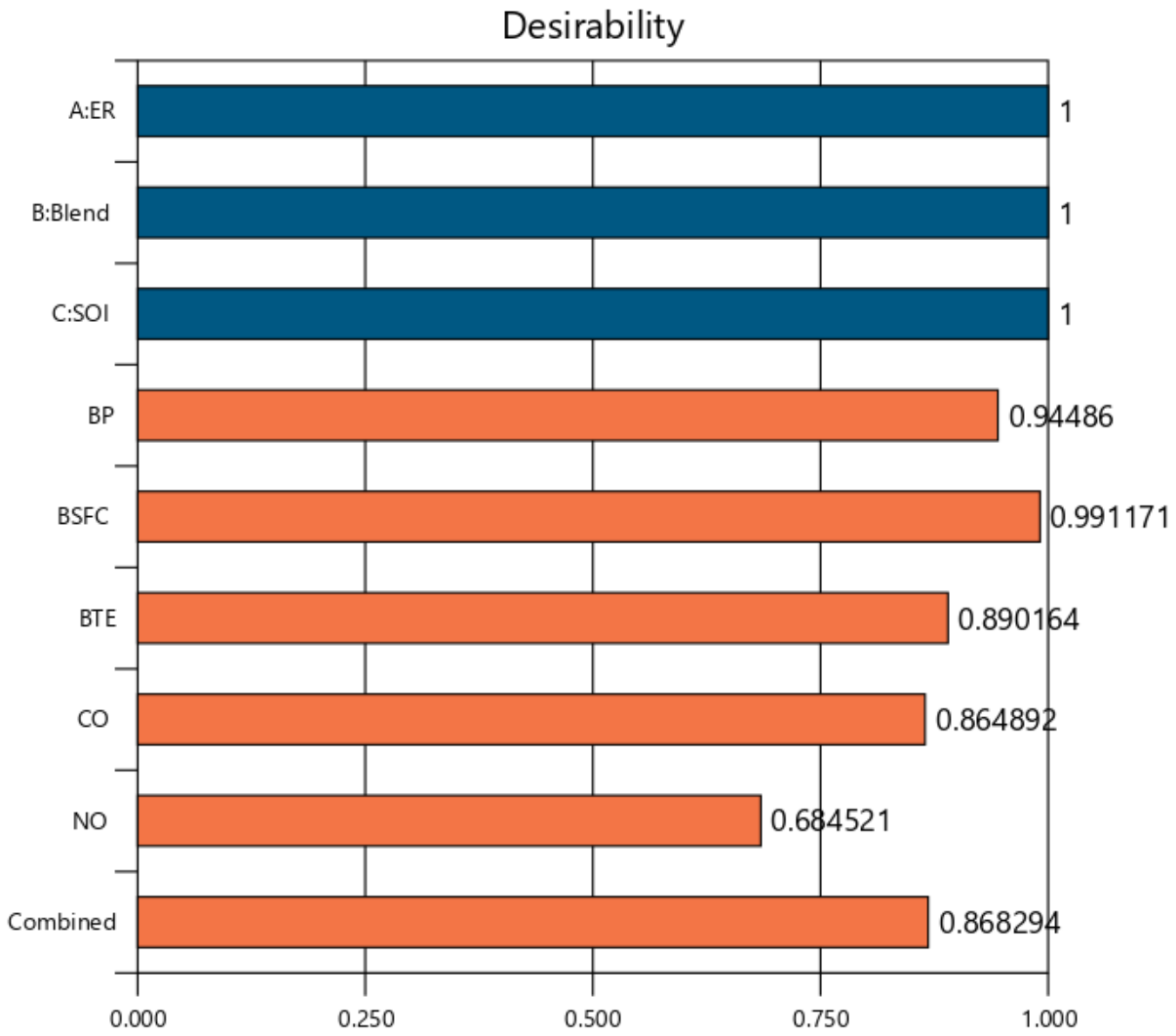

Figure 4.7.5. Composite desirabilities of numeric and response factors

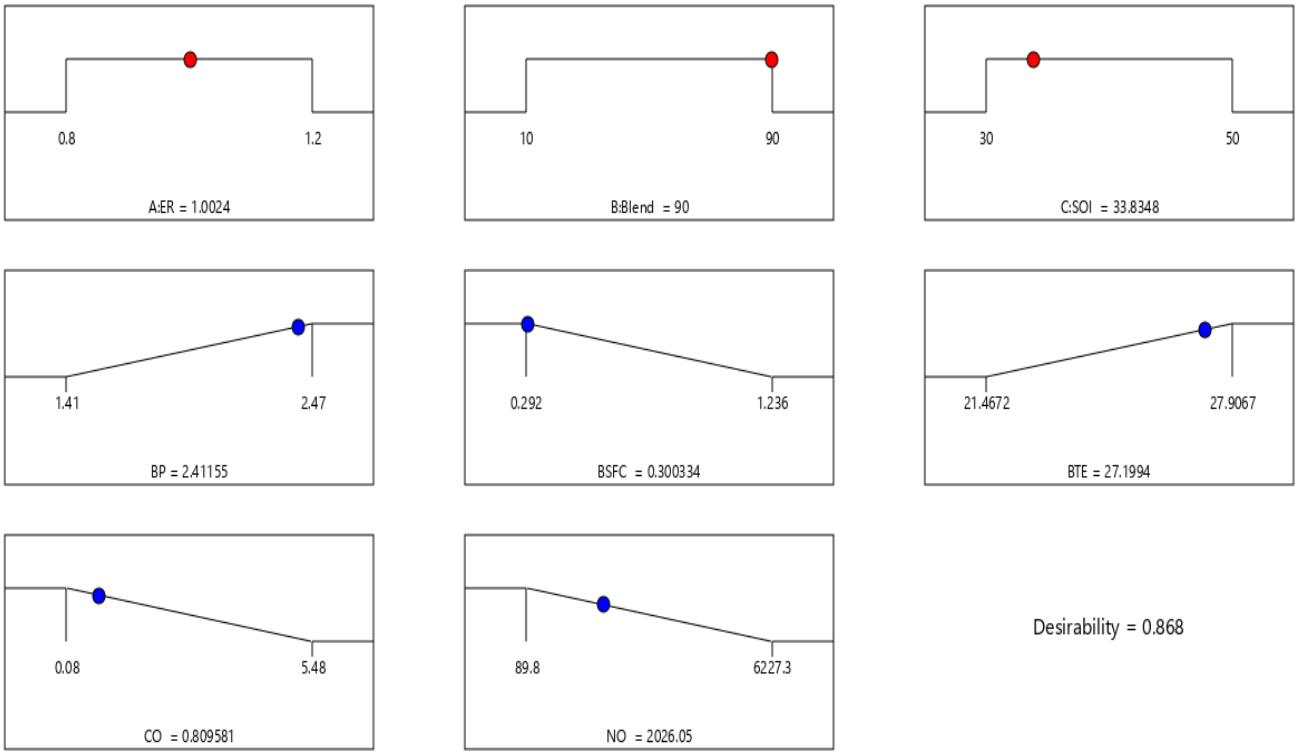

Figure 4.7.6. Optimum values of independent and response parameters

Table 4.7.5. Optimum operating condition and confirmation assessment with error %.

Input parameters				**Response output**				
ER	**Blend (%)**	**SOI-deg (bTDC)**	**Value**	**BP (kW)**	**BSFC (kg/kWh)**	**BTE (%)**	**CO**	**NO**
1.0	90	33.83	*Optimise*	2.411	0.3003	27.199	0.809 (% vol.) 29.051 (g/kWh)	2026.05 (ppm) 13.44 (g/kWh)
			Test run	2.428	0.298	27.354	0.76 (% vol.) 27.29 (g/kWh)	2195.5 (ppm) 14.56 (g/kWh)
			Error %	0.70	-0.77	0.56	-0.06	0.07
			RMSE	0.53				

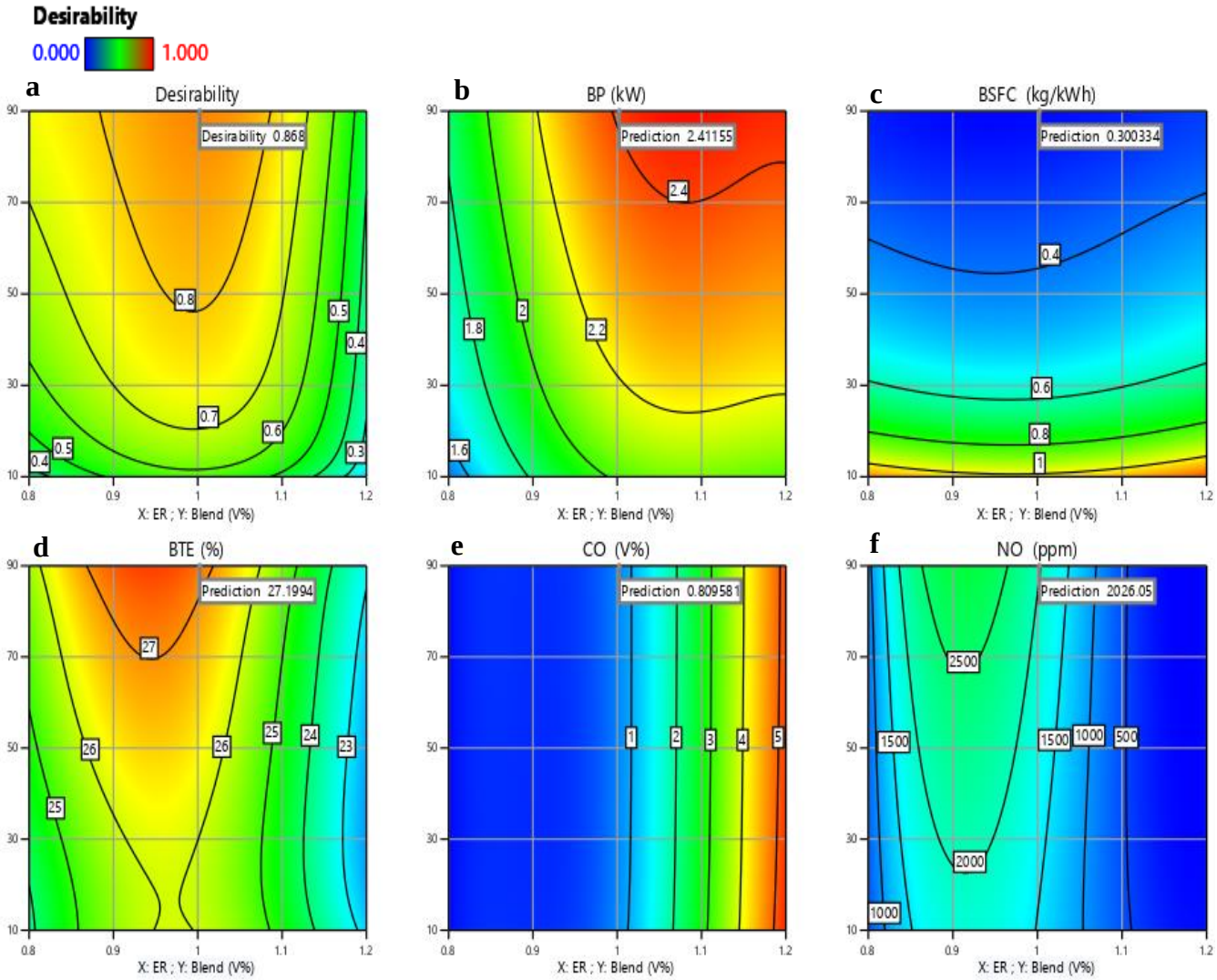

Figure 4.7.7. Desirability of performance and emission parameters

4.7.8 *Conclusions*

Finally, it was concluded that the Peach PG-Propane blend would be an efficient gaseous fuel for the dual-fueled mode SI engine run. Further, this study will offer a suitable platform for researchers and industries for further research and development. The optimum values of dependent parameters i.e., BP, BSFC, BTE, CO, and NO are found to be 2.41 kW, 0.3003 kg/kWh, 27.19 %, 0.809 vol%, and 2026.05 ppm respectively. Regression models created from the ANOVA results were found to be accurate in predicting output response variables.